

---

# **POWERFUL PROTEINS:**

## **Structure and Function of Catalytic Subunits of Electrogenic NADH:Quinone Oxidoreductases**

---

**Dissertation zur Erlangung des Doktorgrades  
der Naturwissenschaften (Dr. rer. nat.)**

**Fakultät Naturwissenschaften  
Universität Hohenheim**

Institut für Mikrobiologie

vorgelegt von  
*Wojtek Roman Steffen*

aus  
*Schlieren ZH, Schweiz*

*Stuttgart, 2013*

Dekan: Prof. Dr. Heinz Breer

1. berichtende Person: Prof. Dr. Julia Fritz-Steuber

2. berichtende Person: Prof. Dr. Andreas Schaller

Eingereicht am: 2. November 2012

Mündliche Prüfung am: 15. März 2013

Die vorliegende Arbeit wurde am 08.01.2013 von der Fakultät Naturwissenschaften der Universität Hohenheim als "Dissertation zur Erlangung des Doktorgrades der Naturwissenschaften" angenommen.

Ich erkläre hiermit, diese Dissertation selbstständig angefertigt zu haben, nur die angegebenen Quellen und Hilfsmittel benutzt und wörtlich oder inhaltlich übernommene Stellen als solche gekennzeichnet zu haben.

Leistungen, die im Rahmen eines Forschungsverbunds in Kollaboration mit anderen Autoren erbracht wurden, sind im Anhang dieser Dissertation aufgelistet.

Wojtek Steffen

*Dedicated to my family*



# Table of contents

Summary .....	1
Zusammenfassung.....	2
Chapter 1	
General introduction .....	3
1.1. The electron transport chain: the electrochemical capacitor of nature .....	4
1.2. NADH:quinone oxidoreductases .....	7
1.2.1. Complex I (NDH I) .....	9
1.2.2. NDH II.....	12
1.2.3. Na <sup>+</sup> -NQR.....	13
1.3. Electron carriers of the NADH:quinone oxidoreductases .....	16
1.3.1. NADH .....	16
1.3.2. Flavins .....	17
1.3.3. Iron-sulfur clusters.....	19
1.3.4. Quinones.....	19
1.4. Inhibitors.....	22
1.5. Scope of the study .....	24
Chapter 2	
Production and functional characterization of the antiporter-like ND5 subunit of complex I from <i>Homo sapiens</i> and <i>Yarrowia lipolytica</i> .....	25
2.1. Introduction.....	26
2.1.1. The structure of respiratory complex I.....	26
2.1.2. Homology to cation/proton antiporters.....	27
2.1.3. Mitochondrially encoded complex I subunits are hotspots for mutations causing muscular and neurodegenerative diseases .....	27
2.1.4. Cation transport of the ND5 subunit of mitochondrial complex I .....	28
2.2. Materials & Methods.....	30
2.2.1. Chemicals and enzymes.....	30
2.2.2. Construction of plasmids .....	30
2.2.3. Bioinformatic tools .....	32
2.2.4. Cell growth, protein expression and purification .....	33
2.2.5. Membrane solubilization and protease protection assay .....	35
2.2.6. Analytical methods .....	35
2.2.7. Preparation and immunostaining of cells for microscopic analysis .....	37
2.2.8. Microscopic imaging .....	38

2.2.9.	Influence of salt on growth of <i>S. cerevisiae</i> .....	38
2.2.10.	Sodium ion transport into ER vesicles .....	38
2.3.	Results.....	40
2.3.1.	Organelle-specific expression of subunit ND5 of human complex I alters cation homeostasis in <i>Saccharomyces cerevisiae</i> .....	40
2.3.2.	Expression, purification and functional characterization of subunit ND5 of complex I from the yeast <i>Yarrowia lipolytica</i> .....	53
2.4.	Discussion .....	64
2.4.1.	Sequence alignment of ND5 and related proteins .....	64
2.4.2.	Expression and localization of ND5 .....	65
2.4.3.	Orientation of GFPND5 <sub>YI</sub> in native ER vesicles.....	65
2.4.4.	ND5 imbalances the cation homeostasis of intracellular organelles .....	66
2.4.5.	A putative role of E144 of the ND5 <sub>YI</sub> subunit of complex I in cation transport .....	67
2.4.6.	Correlation between structure and function of ND5 .....	68
2.4.7.	Model of H <sup>+</sup> /Na <sup>+</sup> Antiport in NuoL (ND5) .....	71
 Chapter 3		
Structure-function analysis of catalytic subunits of the Na <sup>+</sup> -translocating NADH:ubiquinone reductase from <i>Vibrio cholerae</i> .....		
3.1.	Introduction.....	75
3.1.1.	Silver, a potent bactericide and inhibitor of the Na <sup>+</sup> -NQR.....	75
3.1.2.	Structure and function of the NADH oxidizing domain of the Na <sup>+</sup> -NQR, a flavoprotein .....	76
3.1.3.	The catalytic quinone binding site of Na <sup>+</sup> -NQR .....	77
3.2.	Materials and Methods .....	80
3.2.1.	Chemicals and enzymes.....	80
3.2.2.	Construction of plasmids .....	80
3.2.3.	Preparation of FAD domain and its variants .....	80
3.2.4.	Preparation of Na <sup>+</sup> -NQR complex and its NqrF C378A, F406A and F406S variants .....	81
3.2.5.	Preparation of NqrA.....	82
3.2.6.	Analytical Methods .....	82
3.2.7.	Protein crystallization and X-ray analysis .....	83
3.2.8.	Structure determination and refinement.....	84
3.2.9.	Enzymatic activities.....	84
3.2.10.	Inhibition of growth of <i>Vibrio cholerae</i> by Ag <sup>+</sup> .....	85
3.2.11.	Fluorescence spectroscopy.....	86
3.2.12.	NMR spectroscopy.....	87

3.3. Results.....	88
3.3.1. Ag <sup>+</sup> -mediated killing of <i>Vibrio cholerae</i> originates in silver ion binding to cysteine 378 of subunit F of the Na <sup>+</sup> -NQR.....	88
3.3.2. Structure-function analysis of the NADH oxidizing domain of the Na <sup>+</sup> -NQR from <i>Vibrio cholerae</i> .....	96
3.3.3. The catalytic quinone binding site of the Na <sup>+</sup> -translocating NADH:quinone oxidoreductase from <i>Vibrio cholerae</i> accommodates two quinones .....	103
3.4. Discussion .....	115
3.4.1. Ag <sup>+</sup> -mediated killing of <i>Vibrio cholerae</i> originates in silver binding to Cys 378 of subunit F of the Na <sup>+</sup> -NQR .....	115
3.4.2. Structure-function analysis of the NADH oxidizing domain of the Na <sup>+</sup> -NQR from <i>Vibrio cholerae</i> .....	116
3.4.3. The catalytic quinone binding site of the Na <sup>+</sup> -translocating NADH:quinone oxidoreductase from <i>Vibrio cholerae</i> accommodates two quinones .....	119
Chapter 4	
Conclusion and outlook.....	123
Appendix.....	127
Contributions by collaborating authors .....	128
Abbreviations .....	129
References.....	130
Acknowledgements .....	146
Financial Disclosure .....	147
<i>Curriculum vitae</i> .....	148





## Summary

Electrogenic NADH:quinone oxidoreductases are large, membrane-embedded enzyme complexes found in the respiratory chain of prokaryotes and the mitochondria of eukaryotes. They represent the first module of the oxidative phosphorylation system which converts the energy from nutrients into an electrochemical gradient by coupling redox reactions to the translocation of cations across membranes. A long chain of events, such as the synthesis of ATP, ion homeostasis, reactive oxygen species production and bacterial motility depend on the activity of these complexes.

Complex I consists of up to 45 subunits and can be found in the inner mitochondrial membrane of eukaryotes and in prokaryotes, where it is called NDH I. We investigated the isolated, hydrophobic ND5 subunit, which shows homologies to cation/proton antiporters, from human or *Yarrowia lipolytica* complex I. *In vivo* and biochemical analyses provided data on the cation translocation function and the alteration of function by disease-associated mutations. Taken together with the recently published 3D structure of bacterial complex I, these data allowed us to demonstrate that the ND5 subunit could possibly act as an antiporter module of mitochondrial complex I.

Sodium ion translocating NADH:quinone oxidoreductase ( $\text{Na}^+$ -NQR) is an enzyme found in many pathogenic bacteria. It consists of six subunits (NqrA - NqrF) whose 3D structures and enzymatic mechanisms were not known in detail at the time this project was initiated. By using high-resolution X-ray structures and site-directed mutagenesis, combined with biochemical studies, we proposed a model for catalysis and substrate selectivity on the atomic level of the electron input module of the complex, the NADH oxidizing domain of subunit NqrF. Furthermore, we analyzed the binding of silver ions to a cysteine residue in the NADH binding pocket and found that it leads to the inhibition of the  $\text{Na}^+$ -NQR and to the killing of *Vibrio cholerae* in the nanomolar range. Subunit NqrA forms part of the quinone reductase module. By the use of physicochemical and biochemical methods we identified the herbicide 2,5-dibromo-3-methyl-6-isopropyl-p-benzoquinone (DBMIB) as a quinone antagonist and inhibitor of the  $\text{Na}^+$ -NQR complex and discovered two adjacent quinone binding sites on NqrA.

## Zusammenfassung

Elektrogene NADH:Chinon Oxidoreduktasen sind grosse, in die Membran eingebettete Enzym-Komplexe der Atmungskette von Prokaryoten und Eukaryoten. Sie repräsentieren das erste Modul der oxidativen Phosphorylierung, welche die Energie aus Nährstoffen in einen elektrochemischen Gradienten wandelt, indem Redox-Reaktionen an den Transport von Kationen über eine Membran gekoppelt werden. Eine lange Kette an Abläufen in der Zelle hängt von der Aktivität dieser Komplexe ab, so z.B. die Synthese von ATP, Ionen-Homöostase, Produktion von reaktiven Sauerstoffspezies und Motilität von Bakterien.

Komplex I besteht aus bis zu 45 Untereinheiten und findet sich in der inneren Mitochondrienmembran von Eukaryoten und in Prokaryoten, wo er als NDH I bekannt ist. Wir haben die isolierte, hydrophobe ND5 Untereinheit des Komplex I vom Menschen und der Hefe *Yarrowia lipolytica* untersucht, welche Homologien aufweist zu Kationen/Protonen Antiportern. *In vivo* und biochemische Analysen ermöglichten die funktionelle Untersuchung der Kationen-Translokation und der Veränderung der Funktion durch Krankheits-assoziierte Mutationen. Zusammen mit der kürzlich publizierten 3D Struktur des bakteriellen Komplex I haben es uns diese Daten erlaubt zu zeigen, dass die ND5 Untereinheit als Antiporter im mitochondriellen Komplex I fungieren könnte.

Die Na<sup>+</sup>-translozierende NADH:Chinon Oxidoreduktase (Na<sup>+</sup>-NQR) wird häufig in pathogenen Bakterien vorgefunden. Sie besteht aus sechs Untereinheiten (NqrA - NqrF), deren 3D Struktur und Funktion zu Beginn dieses Projekts nicht im Detail bekannt waren. Durch hochauflösende Röntgen-Kristallstrukturen und ortsgerichtete Mutagenese sowie mittels biochemischen Methoden ist es uns gelungen, auf der atomaren Ebene ein Modell für die Katalyse und die Substratselektivität des Elektroneninput-Moduls, der NADH oxidierenden Domäne der Untereinheit NqrF, zu generieren. Wir haben weiterhin die Bindung von Silberionen an ein Cystein der NADH-Bindestasche analysiert und festgestellt, dass nanomolare Konzentrationen von Ag<sup>+</sup> durch diese Bindung zur Hemmung der Na<sup>+</sup>-NQR und zum Abtöten von *Vibrio cholerae* führen. Die Untereinheit NqrA bildet einen Teil des Chinon-reduzierenden Moduls. Durch physikochemische und biochemische Untersuchungen konnten wir das Pflanzenschutzmittel 2,5-dibromo-3-methyl-6-isopropyl-p-benzoquinon (DBMIB) als Antagonisten zu Chinon und Inhibitor der Na<sup>+</sup>-NQR identifizieren, sowie zwei nebeneinanderliegende Chinon-Bindestellen auf NqrA charakterisieren.

## **Chapter 1**

### **General introduction**

### 1.1. *The electron transport chain: the electrochemical capacitor of nature*

The advent of complex life required the evolution of a system to efficiently harness and store the energy of nutrients in high-energy compounds such as ATP. ATP is generated during fermentation, for example in yeasts or under conditions of intense muscular exertion, where pyruvate is converted to lactic acid. However, these processes provide only a limited amount of ATP. For one, they use endogenous organic molecules as electron acceptors which have to be regenerated, and secondly, this electron transfer releases little free energy, e.g. glycolysis yielding 2 molecules of ATP per molecule of glucose (Voet and Voet 2004). The employment of an electron transport chain to deliver electrons to an exogenous acceptor with a highly positive redox potential - such as molecular oxygen, O<sub>2</sub> - is called oxidative phosphorylation (OXPHOS) and drastically increases the energetic yield to up to 36 molecules of ATP per molecule of glucose (Nicholls and Ferguson 1992). In the mitochondrial respiratory chain, OXPHOS is accomplished by a series of redox enzyme complexes located within the mitochondrial inner membrane. The electrons enter at either the NADH:ubiquinone oxidoreductase (complex I) or the succinate dehydrogenase (complex II) and are transferred by the help of quinones to ubiquinone:cytochrome c oxidoreductase (cytochrome-*bc*<sub>1</sub> or complex III), then to cytochrome c, on to cytochrome c oxidase (complex IV), and finally to O<sub>2</sub>, generating H<sub>2</sub>O (Alberts, Johnson et al. 2008). The electrons hereby follow a slope from negative to positive redox potential, formed by the various electron-accepting cofactors. Table 1 lists a selection of respiratory chain components and their midpoint redox potentials. The midpoint potential  $E_{m7.2}$  represents the voltage that needs to be applied at pH 7.2 to bring half of the molecules into the oxidized state. Chemical species with a tendency to donate electrons have a negative  $E_m$  and species that readily take up electrons have a positive  $E_m$ . The energy released by a redox reaction between two species with different  $E_m$  is described by the Gibbs function:

$$\Delta G'_0 = -nF\Delta E_m$$

where  $n$  is the number of electrons transferred and  $F$  is the Faraday constant.

**Table 1: Midpoint redox potentials of components of the mitochondrial respiratory chain.**

Respiratory chain fragment	Component	<i>n</i>	$E_{m7.2}$ [V]
Complex I	NAD <sup>+</sup> /NADH	2	- 0.315 <sup>a</sup>
	FMN	1	- 0.300 <sup>a</sup>
	(Fe-S) N-1a	1	- 0.380 ± 0.010
	(Fe-S) N-1b	1	- 0.250 ± 0.010
	(Fe-S) N-2	1	- 0.030 ± 0.015
	(Fe-S) N-3,4 *	1	- 0.245 ± 0.010
	(Fe-S) N-5,6 *	1	- 0.270 ± 0.010
Succinate dehydrogenase (complex II)	FAD/FADH <sub>2</sub>	2	- 0.040 ± 0.020
	fumarate/succinate	2	0.030 <sup>a</sup>
	(Fe-S) S-1	1	0.030 ± 0.010
	(Fe-S) S-2 <sup>b</sup>	1	- 0.245 ± 0.015
	(Fe-S) S-3	1	0.060 ± 0.015 <sup>c</sup>
Cytochrome- <i>bc</i> <sub>1</sub> (complex III)	ubiquinone-10	2	0.045
	Rieske Fe-S	1	0.280 ± 0.015
	cytochrome <i>c</i> <sub>1</sub> heme	1	0.215 ± 0.010
Cytochrome <i>c</i>	cytochrome <i>c</i>	1	0.235 ± 0.005
Cytochrome <i>c</i> oxidase (complex IV)	cytochrome <i>a</i> heme	1	0.210 ± 0.010
	copper A	1	0.245 ± 0.015
	cytochrome <i>a</i> <sub>3</sub> heme	1	0.385 ± 0.010
Molecular oxygen	O <sub>2</sub> /2 H <sub>2</sub> O	4	0.820 <sup>a</sup>

Adapted from (Wilson, Erecinska et al. 1974),  $E_m$  values of protein-bound components are derived from de-energized mitochondria.

\*: combined values

a:  $E_{m7.0}$ , from (Nicholls and Ferguson 1992).

b: remains oxidized, function unknown (Ohnishi and Salerno 1976)

c:  $E_{m7.4}$ , from (Ohnishi, Lim et al. 1976)

First observed by Peter Mitchell (Mitchell 1961; Mitchell and Moyle 1967), the energy that is released as the electrons travel along complexes I, III, and IV is coupled to the pumping of protons out of the mitochondrial matrix across the inner membrane, resulting in an electrochemical gradient  $\Delta\mu H^+$ .  $\Delta\mu H^+$  amounts to approximately 180 - 220 mV and consists of two components: the membrane potential  $\Delta\psi$ , accounting for 150 - 180 mV and of  $\Delta p H$ , contributing the remaining 30 - 70 mV (Mitchell and Moyle 1969; Nicholls 1974).

This gradient is the biological equivalent of a capacitor (Wallace 2008), an electric component used to store energy through the separation of charges.

The capacitance of a plate capacitor - the amount of energy it can store - is described as:

$$C = \varepsilon_0 \varepsilon_r \cdot \frac{A}{d}$$

where  $\varepsilon_0$  is the electric constant,  $\varepsilon_r$  the permittivity of the capacitors dielectric,  $A$  the electrode area and  $d$  the distance between electrodes.

The capacitance density of the inner mitochondrial membrane was determined to be in the range of 1.1 - 1.3  $\mu\text{F cm}^{-2}$  (Pauly and Packer 1960), which is a value comparable to conventional electrolytic capacitors (Yoshida, Imoto et al. 1992). This is an amazing number considering that this membrane does not act solely as a dielectric - a non-conducting layer separating charges - but simultaneously accommodates charge conducting elements such as ion channels and transporters. Combined with the high surface-to-volume ratio of the inner mitochondrion's cristae, the mitochondrial respiratory chain constantly provides enough potential energy to drive a multitude of cellular processes.  $F_1F_0$  type ATP synthase (complex V) for example directly converts the electrochemical gradient into the high-energy  $\gamma$ -phosphate bond of ATP, which is a chemical currency used when- and wherever work has to be done in a cell. In addition, the energy is used for the regulation of intracellular ion homeostasis, reactive oxygen species production and initiation of controlled cell death - apoptosis - in eukaryotic cells (Kumar, Abbas et al. 2004). It can also be simply dissipated as heat by the action of uncoupling proteins (Nedergaard, Ricquier et al. 2005).

## 1.2. **NADH:quinone oxidoreductases**

There are three known types of respiratory NADH:quinone oxidoreductases (Yagi 1991; Friedrich and Scheide 2000; Kerscher 2000; Yagi, Seo et al. 2001; Bogachev and Verkhovsky 2005; Zickermann, Kerscher et al. 2009): the proton- or sodium ion-translocating complex I (NDH I in bacteria) (Friedrich 1998), the non-electrogenic NADH:quinone oxidoreductases (NDH II) (Kerscher, Okun et al. 1999) and the sodium ion-translocating NADH:quinone oxidoreductases (Na<sup>+</sup>-NQR) (Barquera, Hellwig et al. 2002). These enzymes couple the oxidation of NADH, a reducing agent found in all living cells which is kept in its reduced state with the electrons that large organic nutrient molecules release during catabolism, to the reduction of ubiquinone (Q). The net reaction thus yields ubiquinol (QH<sub>2</sub>), the reducing substrate of enzyme complexes further along the respiratory chain, and NAD<sup>+</sup>, which is used as oxidizing agent in numerous cellular processes. NADH:quinone oxidoreductases of the NDH II type limit themselves to this reaction and do not participate in the generation of a transmembrane voltage, i.e. are non-electrogenic. Complex I and Na<sup>+</sup>-NQR in contrast tap into the exergonic energy released by the redox reaction by using it to pump H<sup>+</sup> or Na<sup>+</sup> from the mitochondrial matrix or the cytosol to the perimitochondrial space or the periplasm respectively. The accumulation of positively charged ions on the outside of the membrane leads to an electrical and chemical imbalance, summarized as  $\Delta\mu\text{H}^+$  (proton motive force, PMF) or  $\Delta\mu\text{Na}^+$  (sodium motive force, SMF).

Prokaryotes may contain all three types of NADH:quinone oxidoreductases but the expression of each is usually tightly regulated. The chromosome of *Escherichia coli* for example features genes for both NDH I and NDH II. Under aerobic conditions, the expression of NDH II is upregulated and more than 80 % of the electron flux is directed from NADH to Q by NDH II (Bongaerts, Zoske et al. 1995; Wackwitz, Bongaerts et al. 1999; Uden, Achenbach et al. 2002). During anaerobic fumarate respiration or at the onset of exponential growth, where high amounts of ATP are required, NDH I represents the dominant dehydrogenase, shuttling electrons from NADH to menaquinone, which serves as a substrate for the DMSO or fumarate reductases (Tran, Bongaerts et al. 1997) and translocating protons or sodium ions, driving H<sup>+</sup>- or Na<sup>+</sup>-ATP synthases. Many archaea and gram-positive bacteria only contain NDH II. *Chlamydia pneumoniae* only expresses the Na<sup>+</sup>-NQR. Bacteria of the genus *Vibrio* contain NDH II and Na<sup>+</sup>-NQR and a few bacteria such as *Klebsiella pneumoniae* and

*Yersinia pestis* harbor all three types of enzymes (Bertsova and Bogachev 2004; Melo, Bandejas et al. 2004).

In eukaryotic organisms, only enzymes of the NDH I and NDH II type have been found so far. The yeast *Yarrowia lipolytica* contains, in addition to mitochondrial complex I, a type two dehydrogenase, which is oriented towards the external lumen (perimitochondrial space). Mitochondria of plants and of the yeast *S. cerevisiae* exhibit expression of different subtypes of the NDH II. In the latter, NDH II is even the sole NADH:quinone oxidoreductase type (Kerscher 2000); its well-known preference of the fermentative lifestyle may explain why it lost the NDH I operon over the course of evolution. Mitochondria of mammals and higher eukaryotes almost exclusively contain an extended form of NDH I, the respiratory complex I. Table 2 summarizes and compares the characteristics of the three types of NADH:quinone oxidoreductases, taken from (Yagi 1987; Friedrich, Heek et al. 1994; Pfenninger-Li and Dimroth 1995; Yagi, Yano et al. 1998; Nakayama 1999; Ushakova, Grivennikova et al. 1999; Kerscher 2000; Steuber 2001; Steuber 2001; Yagi, Seo et al. 2001; Gemperli, Dimroth et al. 2002; Nakamaru-Ogiso, Seo et al. 2003; Melo, Bandejas et al. 2004; Eschemann, Galkin et al. 2005; Brandt 2006; Casutt, Huber et al. 2010).



**Table 2: The three different types of NADH:quinone oxidoreductases.**

	<b>NDH I (complex I)</b>	<b>NDH II</b>	<b>Na<sup>+</sup>-NQR</b>
Subunits	13 - 15, 40*, (45)	1	6
Molecular mass [kDa]	530, 947*, (980)	42 - 64	220
Cofactors	1 noncovalent FMN, 2 [2Fe-2S], 6 - 8 [4Fe-4S] clusters	1 noncovalent FAD or FMN	1 noncovalent FAD, 2 covalent FMN, 1 noncovalent riboflavin, 1 [2Fe-2S] cluster
Substrates	NADH, dNADH, ferricyanide, hexamine-ruthenium, menaquinone, Q <sub>1</sub> , Q <sub>6</sub> , Q <sub>8</sub> , Q <sub>9</sub> <sup>*</sup> , (Q <sub>10</sub> )	NADH, Q <sub>1</sub> , Q <sub>2</sub> , Q <sub>6</sub> , n-decyl-ubiquinone and other quinones	NADH, dNADH, ferricyanide, Q <sub>1</sub> , Q <sub>2</sub> , Q <sub>8</sub>
Coupling ion	H <sup>+</sup> or Na <sup>+</sup>	Not a pump	Na <sup>+</sup>
Inhibitors	Rotenone, rolliniastatin-1, annonin VI, pyridaben, fenpyroximate, piericidin A, Triton x-100, EIPA, DCCD, capsaicin	1-hydroxy-2-dodecyl-4(1H)-quinolone, platanetin	Ag <sup>+</sup> , korormicin, HQNO, DBMIB <sup>1</sup>

\* in eukaryotes only. Properties particular to mammalian complex I are in parentheses

<sup>1</sup> this study; see chapter 3.3.3.

### 1.2.1. Complex I (NDH I)

Electron microscopy revealed that complex I is L-shaped and consists of a hydrophilic peripheral domain which reaches into the mitochondrial matrix (or bacterial cytosol) and a membrane domain comprising numerous membrane-spanning segments (Leonard, Haiker et al. 1987; Hofhaus, Weiss et al. 1991; Guenebaut, Vincentelli et al. 1997; Grigorieff 1998; Guenebaut, Schlitt et al. 1998; Dudkina, Eubel et al. 2005; Radermacher, Ruiz et al. 2006; Clason, Ruiz et al.). Complex I from *E. coli* seems to exhibit an additional horseshoe conformation, where the peripheral arm folds onto the membrane domain. This conformation is proposed to be the active form of complex I (Böttcher, Scheide et al. 2002) but could so far not be reproduced in crystallographic studies (Efremov, Baradaran et al. 2010; Hunte, Zickermann et al. 2010). In 2006, the X-ray crystallographic structure of the peripheral arm of *Thermus thermophilus* complex I was determined (Sazanov and Hinchliffe

2006). This elucidated the spatial arrangement of the redox cofactors and established a model of the electron transfer chain (figure 1). In 2010, the 3D structure of the complete complex from *Thermus thermophilus* was solved (Efremov, Baradaran et al. 2010).

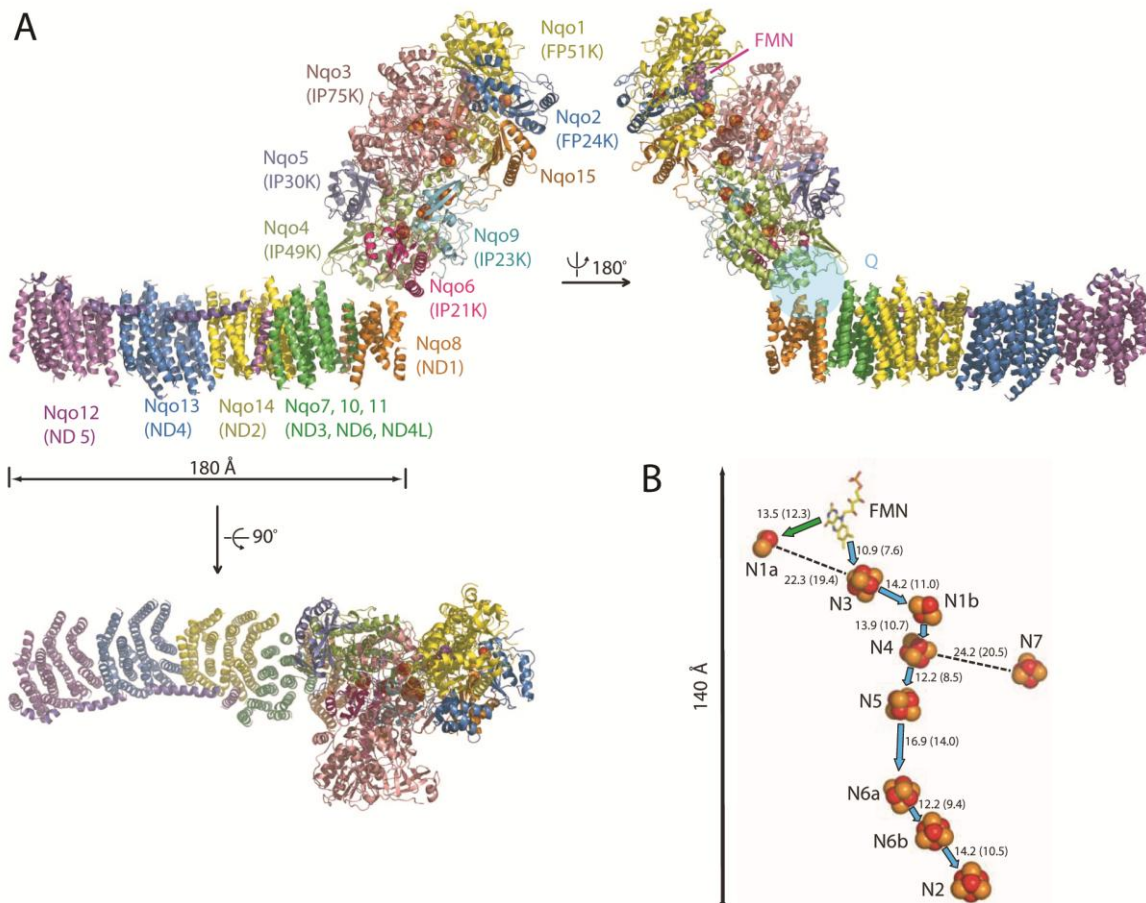


**Figure 1: The structure of complex I from *Thermus thermophilus*.** Adapted from (Sazanov and Hinchliffe 2006; Efremov, Baradaran et al. 2010) and edited. **A:** Side views from the membrane plane and top view from the cytoplasm into the membrane. The proposed NADH and quinone binding sites are indicated. Names of the analogous mitochondrial subunits are in parentheses. Fe-S clusters are shown as red and yellow spheres, and flavin mononucleotide (FMN) as magenta spheres. **B:** Arrangement of redox centers in the hydrophilic domain. The overall orientation is similar to that in **A**, right-hand side. Cluster N1a is in subunit Nqo2; N3 and FMN in Nqo1; N1b, N4, N5, and N7 in Nqo3; N6a/b in Nqo9; and N2 in Nqo6. The main pathway of electron transfer is indicated by blue arrows, and a diversion to cluster N1a by a green arrow. The distances between the centers given in angstroms were calculated both center-to-center and edge-to-edge (shown in parentheses).

The bacterial enzyme comprises 13 - 15 subunits encoded by the *nuoA - N* genes (or *nqo1 - 15*, the nomenclature differs, depending on the organism) and has a mass of about 530 kDa. The enzymes of certain Enterobacteria such as *Escherichia coli*, *Yersinia pestis*, *Aquifex aeolicus*, *Pseudomonas aeruginosa*, *Salmonella typhi*, *Buchnera* species and *Klebsiella pneumoniae* only contain 13 subunits, due to fusion of the *NuoC* and *NuoD* genes (Friedrich 1998). *Thermus thermophilus* contains, in addition to the 14 core subunits encoded by the *nqo* operon, *Nqo15*, a frataxin-like subunit (Sazanov and Hinchliffe 2006).

The eukaryotic enzyme comprises at least 40 subunits and has a mass in the range of 1 MDa. Bovine complex I is made of 45 (Carroll, Fearnley et al. 2006), complex I from the yeast *Yarrowia lipolytica* of 40 different polypeptides (Morgner, Zickermann et al. 2008). In addition to the 14 core subunits conserved from prokaryotes, which catalyze the central redox and electrogenic functions, eukaryotes exhibit accessory subunits which do not participate directly in energy conservation but play an important role in complex I assembly and activity (Yadava, Potluri et al. 2008). The core subunits can be divided into seven hydrophilic and seven hydrophobic proteins (Zickermann, Kerscher et al. 2009): The latter are mitochondrially encoded, and in fact their genes make up the bulk of the mitochondrial DNA, which only contains 13 protein-coding sequences. They are the ND1 - 6 and ND4L subunits, corresponding to the membrane-embedded *NuoA* (ND3), *NuoH* (ND1) and *NuoJ - N* (ND6, ND4L, ND5, ND4, ND2) of the bacterial enzyme. The hydrophilic core subunits can be attributed to a dehydrogenase fragment consisting of FP24K (*NuoE*), FP51K (*NuoF*) and IP75K (*NuoG*) and a connecting fragment containing IP21K (*NuoB*), IP30K (*NuoC*), IP49K (*NuoD*) and IP23K (*NuoI*).

As is the case with many multisubunit enzymes, complex I likely emerged from the fusion of preexisting modules for electron transfer and ion transport. The connecting fragment, together with hydrophobic subunits ND1 and ND5, is believed to have evolved from an ancestral enzyme which used hydrogen as an electron donor (Friedrich and Weiss 1996). Furthermore, subunits IP21K, IP30K and IP49K form an electron conducting module similar to membrane-bound [NiFe] hydrogenases (Friedrich and Scheide 2000). The dehydrogenase fragment is related to the flavin-containing diaphorase domain of NAD<sup>+</sup>-reducing hydrogenases. Subunits ND2, 4 and 5 very likely share a common ancestor (Kikuno and Miyata 1985) and exhibit sequence similarity to Na<sup>+</sup>/H<sup>+</sup> antiporters (Mathiesen and

Hägerhäll 2002; Mathiesen and Hägerhäll 2003). So far, no ancestors of the membrane-bound subunits ND3, ND4L and ND6 have been found.

### 1.2.2. NDH II

The so-called alternative or rotenone-insensitive NADH:quinone oxidoreductases, NDH II, are typically found in the inner mitochondrial membrane of plants and ascomycetous fungi, but also in many bacteria and archaea (Bandeiras, Salgueiro et al. 2002; Fang and Beattie 2002; Bandeiras, Salgueiro et al. 2003; Melo, Bandeiras et al. 2004). The first evidence of this non-electrogenic type of enzymes was found in 1961, when Bonner and Voss observed that plant mitochondria were capable of oxidizing externally added NAD(P)H, but mammalian mitochondria were not (Bonner and Voss 1961). The NDH II are monomeric enzymes with molecular masses between 42 (*Acidianus ambivalens*) and 64 kDa (*Neurospora crassa*) and a non-covalently attached flavin adenine dinucleotide (FAD) as only redox cofactor. As an exception for this rule, NDH II dimers, or NDH II enzymes containing non-covalently bound flavin mononucleotide (FMN) or, in thermophilic organisms, covalently bound FMN have been described (Kerscher 2000; Bandeiras, Salgueiro et al. 2002; Fang and Beattie 2002; Bandeiras, Salgueiro et al. 2003). The 3D structure of NDH II reveals two  $\beta\alpha\beta$  dinucleotide folds with conserved GxGxxG motifs which participate in the binding of the NAD(P)H and flavin cofactors. If the flavin is covalently attached, the respective dinucleotide fold does not contain the GxGxxG motif (Wierenga, Terpstra et al. 1986). Binding to the membrane is suggested to occur by amphipathic helices, and in some cases transmembrane helices are predicted (Bandeiras, Salgueiro et al. 2002). The binding mode of the hydrophobic substrate ubiquinone is unknown and no binding site has been identified yet, but evidence for a two-step, ping-pong type mechanism has been found, in which a hydride is transferred from NAD(P)H to the flavin, followed by two-electron transfer from the flavin to ubiquinone (Eschemann, Galkin et al. 2005; Yano, Li et al. 2006).

It is likely that the NDH II shares a common ancestor with bacterial lipoamide dehydrogenases which exhibits considerable sequence similarity. Moreover, the two enzymes catalyze similar redox reactions (Bjorklof, Zickermann et al. 2000). It has been proposed that the first alternative NADH:ubiquinone oxidoreductases were external enzymes, attached to the outside of the mitochondrial membrane and shuttling electrons

from NADH produced in the cytoplasm into the respiratory chain (Kerscher 2000). Support for this hypothesis comes from the yeast *Yarrowia lipolytica*, which contains only a single external but no internal NDH II. This prototypic enzyme may have evolved into the internal NDH II by gene duplication and acquisition of a mitochondrial targeting sequence (Kerscher, Okun et al. 1999).

### 1.2.3. Na<sup>+</sup>-NQR

The discovery of the Na<sup>+</sup>-NQR dates back to 1981 (Tokuda and Unemoto 1981), when cells of *Vibrio alginolyticus* were found to maintain a membrane potential ( $\Delta\Psi$ ) at alkaline pH through the extrusion of positive charges, despite the presence of a protonophore. Evidence for a NADH dehydrogenase activated by Na<sup>+</sup> was reported even before that (Unemoto, Hayashi et al. 1977).

Meanwhile numerous bacteria, many of them halophilic or halotolerant, have been found to exhibit similar Na<sup>+</sup>-dependent NADH:quinone oxidoreductases (Tokuda and Unemoto 1983; Khanna, Devoe et al. 1984; Tsuchiya and Shinoda 1985; Ken-Dror, Lanyi et al. 1986; Takada, Fukunaga et al. 1988; Tokuda and Kogure 1989; Semeykina and Skulachev 1990; Oh, Kogure et al. 1991; Unemoto, Akagawa et al. 1992; Hayashi, Nakayama et al. 1996; Kogure 1998; Barquera, Hellwig et al. 2002; Bogachev, Bertsova et al. 2002; Fujiwara-Nagata, Kogure et al. 2003). Interestingly, several of these organisms such as *Vibrio cholerae* and *Vibrio parahaemolyticus*, *Neisseria gonorrhoeae*, *Haemophilus influenzae*, *Yersinia pestis*, *Pseudomonas aeruginosa* and *Chlamydia trachomatis* are pathogenic (Häse 2000).

The Na<sup>+</sup>-NQR is a 220 kDa complex consisting of 6 subunits, NqrA - F, encoded by the *nqr* operon. It harbors at least five redox active cofactors: non-covalently bound FAD and [2Fe-2S] cluster in the NqrF subunit, two covalently bound FMNs in subunits NqrB und NqrC and one non-covalently bound riboflavin in subunit NqrB (Barquera, Ramirez-Silva et al. 2006; Tao, Casutt et al. 2008; Bogachev, Kulik et al. 2009; Casutt, Huber et al. 2010). Due to their homology to Na<sup>+</sup>-channeling proteins, NqrD and NqrE are thought to form the sodium-ion pore of the complex (Beattie, Tan et al. 1994). NqrA was shown to harbor at least one binding site for the terminal electron acceptor of the Na<sup>+</sup>-NQR, ubiquinone-8 (Casutt, Nedieltkov et al. 2011). In addition, mutagenesis experiments have revealed an interaction between NqrB and quinones or quinone-like inhibitors (Hayashi, Shibata et al. 2002; Juárez,

Neehaul et al. 2012). However, the exact mechanism of the coupling between the reduction of the substrate, quinone, and the sodium ion translocation is still largely unclear. The physicochemical properties of the subunits from *V. cholerae* Na<sup>+</sup>-NQR are listed in table 3. All subunits save NqrA have at least one predicted transmembrane helix (TMH), which later have been experimentally mapped (Duffy and Barquera 2006). NqrD and NqrE are very hydrophobic and comprise 6 TMH each, NqrB has 9 TMHs. Interestingly, the grand average of hydropathy (GRAVY) scores (Kyte and Doolittle 1982) are negative for NqrC and NqrF, despite containing 2 or 1 TMHs, respectively. In contrast, NqrA has only a slightly negative GRAVY score but contains no TMH. This allows the interpretation that NqrA may contain hydrophobic patches which allow the binding to a hydrophobic surface or cofactor. NqrC and NqrF on the other hand use TMHs as membrane anchor, but may otherwise consist of globular, very hydrophilic domains.

**Table 3: The physicochemical properties of the subunits from *V. cholerae* Na<sup>+</sup>-NQR.**

Subunit	NqrA	NqrB	NqrC	NqrD	NqrE	NqrF
Amino acid residues	446	415	256	209	198	408
M <sub>w</sub> [Da] <sup>1</sup>	48'623.9	45'357.1	27'488.1	22'706.1	21'497.8	45'094.6
App. M <sub>w</sub> [kDa] <sup>2</sup>	52	27	32	14	13	47
<i>pI</i>	6.05	7.16	6.40	8.56	6.55	4.98
GRAVY score	-0.087	0.556	-0.257	0.800	1.072	-0.141
TMHs	0	9	2	6	6	1
Cofactors		FMN, riboflavin	FMN			FAD, [2Fe-2S]

Adapted from (Casutt 2010) and edited.

GRAVY: grand average of hydropathy

<sup>1</sup> Covalently bound FMN of NqrB and NqrC increases their molecular weight (M<sub>w</sub>) by an additional 493.1 Da.

<sup>2</sup> Apparent molecular weight of subunits determined by their migration behavior on SDS-PAGE

Even though the overall reaction catalyzed by the Na<sup>+</sup>-NQR resembles that of complex I, its primary sequence shares almost no common motif with the H<sup>+</sup>- or Na<sup>+</sup>-translocating NDH I complexes, thus making a common ancestry unlikely (Beattie, Tan et al. 1994). One exception is the C-terminus of NqrA, which exhibits 21 amino acids that are conserved in the 9.8 kDa protein of *Neurospora crassa* complex I, corresponding to the MWFE subunit of mammalian complex I (Marques, Duarte et al. 2003). MWFE is an accessory subunit

important for the assembly of the holo-complex (Yagi and Matsuno-Yagi 2003). NqrB - NqrE have no homologs with known structure, but their genes show sequence similarity to the *Rhodobacter* nitrogen fixation genes *rnfD*, *rnfG*, *rnfE*, and *rnfA*, respectively (Müller, Imkamp et al. 2008). The sequences of subunits NqrD and NqrE are very similar. Furthermore, several transmembrane stretches of NqrB, NqrD and NqrE have counterparts in Na<sup>+</sup>-channel forming proteins and bear a slight resemblance to parts of the ND1, ND2, ND4 and ND5 subunits of complex I from different species (Beattie, Tan et al. 1994). NqrF can be divided into a C-terminal and an N-terminal domain (Türk, Puhar et al. 2004). The C-terminal domain contains the NADH and FAD binding site and is related to the family of ferredoxin:NADP<sup>+</sup> oxidoreductases (FNR) (Steuber 2001). This class of enzymes has been well-characterized and over 30 crystal structures have been solved (Karplus and Faber 2004). The N-terminal domain contains two iron atoms bound by two cysteine residues and is homologous to ferredoxins of the vertebrate type bearing a [2Fe-2S] cluster (Bogachev, Bertsova et al. 2001; Türk, Puhar et al. 2004).

### 1.3. Electron carriers of the NADH:quinone oxidoreductases

#### 1.3.1. NADH

Nicotinamide adenine dinucleotide consists of a nicotinamide-ribose and an adenosine diphosphate (ADP) moiety which are linked via a phosphate bond at the ribose-C5 of the nicotinamide-ribose. It exists in two redox states, the oxidized nicotinamide adenine dinucleotide ( $\text{NAD}^+$ ) and the reduced nicotinamide adenine dinucleotide hydride (NADH), as shown in figure 2. The nicotinamide can bind the C1 of the ribose in two different ways, forming two diastereomers,  $\alpha$  and  $\beta$ . Organisms only use the  $\beta$ -nicotinamide form of the compound, which they either synthesize *de novo* from tryptophan or aspartic acid or from niacin, known as vitamin B<sub>3</sub> (Tarr and Arditti 1982).

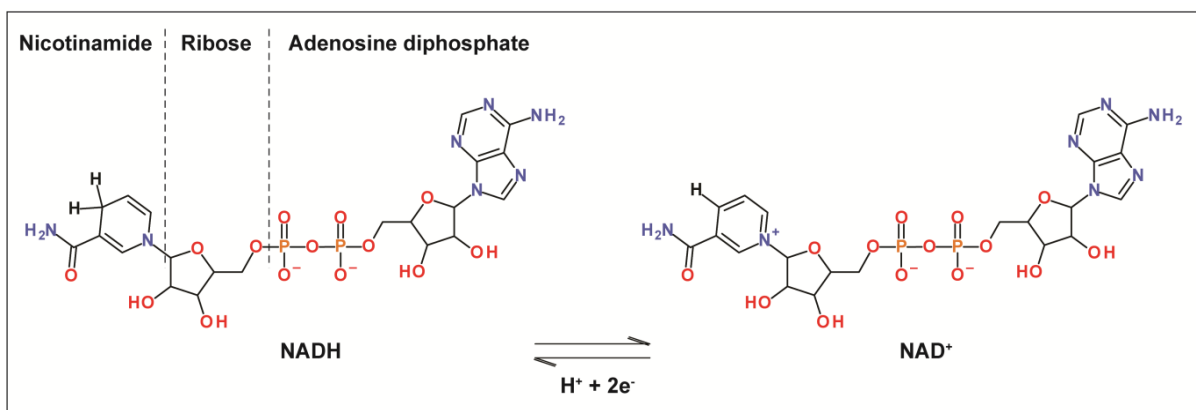


**Figure 2: The two redox states of nicotinamide adenine dinucleotide.**

Many vital redox reactions in a cell use or produce NADH: Glycolysis,  $\beta$ -oxidation and the citric acid cycle serve as pathways for the breakdown of nutrients. The energy released thereby is stored as NADH and further metabolized in the electron transport chain under generation of  $\Delta\psi$ . NADH also acts as a reducing agent and is used in anabolic reactions such as gluconeogenesis (Sistare and Haynes 1985). The total physiological concentration of  $\text{NAD}^+$  is estimated to be approximately 0.3 mM in animal cells (Yamada, Hara et al. 2006) and 1.0 to 2.0 mM in yeast (Belenky, Bogan et al. 2007). Mitochondrial and cytosolic  $\text{NAD}^+$  concentrations are balanced by the action of mitochondrial shuttles such as the malate-aspartate shuttle (Bakker, Overkamp et al. 2001). The total cellular amounts of  $\text{NAD}^+$  and of NADH are also comparable (Lin and Guarente 2003), but the ratio between free  $\text{NAD}^+$  and



NADH differs greatly (about 700:1, (Williamson, Lund et al. 1967)), due to the amount of protein-bound NADH.

In addition to its role as redox cofactor,  $\text{NAD}^+$  is used as substrate for ADP-ribosylation (Ziegler 2000), RNA modification (Chen, Kowtoniuk et al. 2009), second messenger synthesis (Guse 2004) and bacterial DNA ligases (Wilkinson, Day et al. 2001). Furthermore, it has been proposed that  $\text{NAD}^+$  acts as extracellular signaling molecule (Ziegler and Niere 2004) and as neurotransmitter in smooth muscle synapses (Mutafova-Yambolieva, Hwang et al. 2007).

$\text{NAD}^+$  which is phosphorylated at the ribose-C2 of the adenosine-ribose moiety is known as nicotinamide adenine dinucleotide phosphate  $\text{NADP}^+$ . Like  $\text{NAD}^+/\text{H}$ ,  $\text{NADP}^+/\text{H}$  is used as a redox pair in many cellular reactions, but is distinctly preferred in biosynthetic reactions such as lipid synthesis and is prominently featured in photosynthetic organisms. It is important to note that usually,  $\text{NAD}^+$  and  $\text{NADP}^+$  converting enzymes have a high specificity for their respective substrate: Ferredoxin- $\text{NADP}^+$  reductase (FNR), the terminal enzyme of the light reaction of photosynthesis, is highly specific for  $\text{NADP}^+$  over  $\text{NAD}^+$  (a 32'000-fold preference (Piubelli, Aliverti et al. 2000)), whereas the specificity of NADH:quinone oxidoreductases is vice-versa.

### 1.3.2. Flavins

Another class of nucleotide-based redox cofactors are the flavins. The name flavin is derived from the Latin word flavus, meaning yellow. The yellow color of flavins arises from the absorption of visible light in the range of 360 - 500 nm by the oxidized lumichrome moiety, which is a tricyclic isoalloxazine ring methylated at the C7 and C8 positions (figure 3). Lumichrome which has a linearized D-ribose bound to the N10 position is known as riboflavin, or vitamin B<sub>2</sub>. It is the most abundant flavin in nature and also serves as substrate for the biosynthesis of flavin mononucleotide (FMN) and flavin adenine dinucleotide (FAD). Riboflavin was first extracted from milk and natural sources are milk products, vegetables, egg, fish, meat and whole-grain bread. In FMN, riboflavin is phosphorylated at the 5'-hydroxyl of the ribose moiety. In FAD, a second nucleotide, ADP, is attached by a phosphate bond to the riboflavin (figure 3).

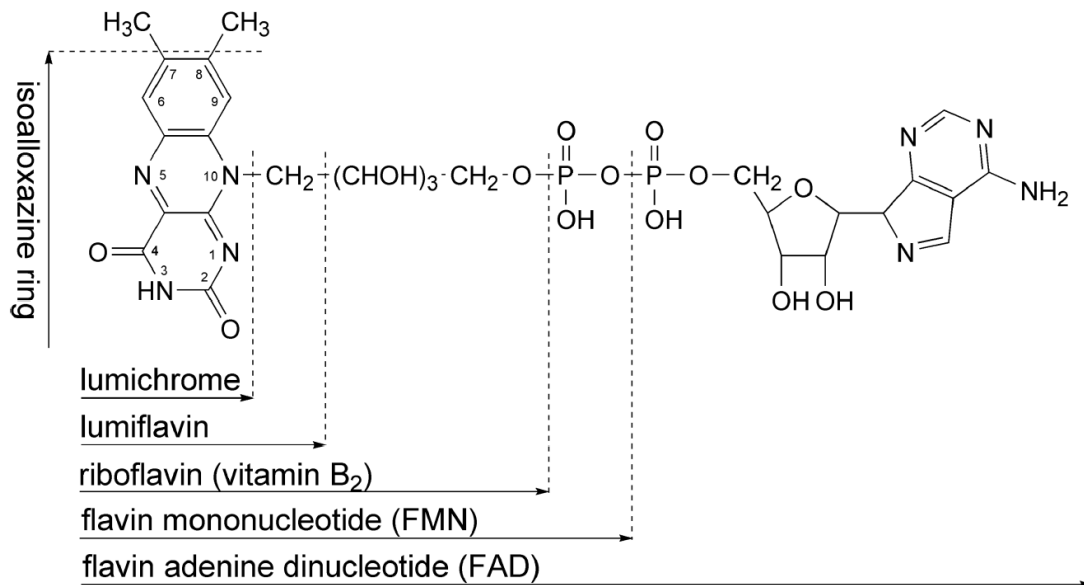


**Figure 3: The structure of flavin and flavin cofactors.** From: (Casutt 2010).

Flavins have three distinct redox states: the fully-oxidized flavoquinone, the one-electron reduced flavosemiquinone radical and the two-electron reduced flavohydroquinone. As the pH of the surrounding environment changes, each of these states could exist in a neutral, an anionic or a cationic form (Müller 1987). Depending on the redox and protonation state, flavins exhibit different optical properties: Oxidized flavoquinone appears yellow with characteristic maxima at 377 and 450 nm in the UV-visible spectrum. The neutral flavosemiquinone absorbs in the 550 - 650 nm range with a blue color. When deprotonated, the absorbance spectrum shifts to 370 - 490 nm, which appears red. Fully reduced flavohydroquinone shows a small but broad absorption maximum in the range of 350 nm and appears colorless (Massey and Palmer 1966).

Flavoproteins are extremely abundant: genome searches indicate that around 4 % of all microbial polypeptides are associated with FMN or FAD or both cofactors. This only represents confirmed flavoproteins and proteins with sequence similarity to known flavin-binding motifs. The actual number is likely to be even higher (Reid 2002).

Most flavoenzymes contain a FMN or FAD cofactor which is tightly, but non-covalently bound. Still, a large number of covalently bound flavin coenzymes exist (Kearney and Kenny 1974). Only a small subset of enzymes use riboflavin as a prosthetic group, most of which are involved in flavin synthesis, transport and storage (White and Merrill 1988). Examples of FAD-containing redox enzymes are monoamine-oxidase, ferredoxin-NADP<sup>+</sup> reductase,

nitrate reductase and glucose oxidase (Zhou, Lewis et al. 1995; Deng, Aliverti et al. 1999). FMN flavoenzymes include flavodoxin, flavodoxin, NADH-rubredoxin oxidoreductase, adenosine 5'-phosphosulfate reductase and FMN-binding protein (Kitamura, Kojima et al. 1994; Zhou and Swenson 1995).

### 1.3.3. Iron-sulfur clusters

Iron-sulfur (Fe-S) clusters are inorganic redox cofactors consisting of two or more iron atoms bridged by sulfide ions and tetrahedrally coordinated to cysteine or histidine residues of a protein (Beinert 2000). The most common forms are the [2Fe-2S], [4Fe-4S] and [3Fe-4S] clusters. Electrons are usually transferred by one or more irons switching between the Fe<sup>2+</sup> and Fe<sup>3+</sup> oxidation states.

Besides NADH:quinone oxidoreductases, there are many metalloproteins exhibiting iron-sulfur clusters, such as the ferredoxins, hydrogenases and nitrogenases (Lippard and Berg 1994). Since iron atoms have unpaired electrons, electron paramagnetic resonance (EPR) is known as the method of choice for the specific detection of iron-sulfur clusters and for the analysis of their properties.

### 1.3.4. Quinones

Quinones are a class of organic molecules containing a fully conjugated cyclic dione structure. The most abundant quinones in nature are aptly named ubiquinones, consisting of a 1,4-benzoquinone redox-active head group and a polyprenyl side chain of variable length. As depicted in figure 4, the quinone head groups may contain different substituents R1, R1' and R2, which determine their structural and optical properties, but do not affect the redox behavior. Ubiquinones (Q) have methoxy groups in the R1 and R1' positions and a methyl group at the R2 position. Menaquinones (known as vitamin K<sub>2</sub>) have their R1 and R1' positions joined by an aromatic ring, forming a naphthoquinone system. In *E. coli*, biosynthesis of menaquinone or ubiquinone involves methylation at the R2 position of the demethylmenaquinone or demethylubiquinone by a C-methyltransferase encoded by the *ubiE* gene. Mutation of this gene led to deficiencies in bacterial growth and respiration (Wissenbach, Ternes et al. 1992). Other common quinones are phyloquinone (vitamin K<sub>1</sub>)

and plastoquinone. The former is a menaquinone variant used in posttranslational modification reactions. It has a tail consisting of one isoprenoid and 3 isopentyl units. Plastoquinone comprises a 1,4-benzoquinone with methyl groups at the R1 and R1' positions and no substituent at the R2 position (Crane 1959; Collins and Jones 1981; Nishida, Nishijima et al. 2006). It is used by the photosystem II to shuttle electrons to the cytochrome *b<sub>6</sub>f* complex and simultaneously drive proton uptake into the thylakoid lumen. Ubiquinone exhibits an analogous function in the Q cycle between the mitochondrial complex I and cytochrome-*bc<sub>1</sub>* complex, where at least 1 mol ubiquinone/mol complex I is thought to act as an integral redox cofactor of the membrane, participating in the generation of  $\Delta\mu\text{H}^+$  (Yano, Magnitsky et al. 2000).

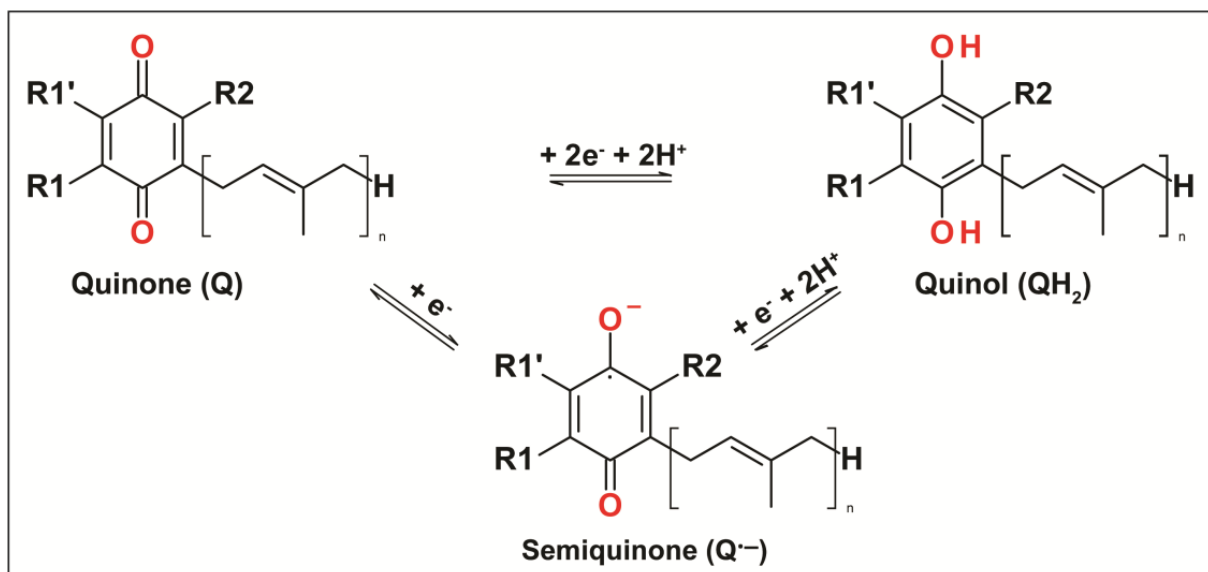


**Figure 4: The redox states and general structure of quinones.**

Quinone reductases either catalyze two one-electron transfer steps or a single two-electron transfer reaction. The one-step reaction has a midpoint redox potential at pH 7 ( $E_{m,7}$ ) of +60 mV (determined in aqueous solution), whereas the two-step reaction involves the formation of a semiquinone radical anion with a potential of -160 mV and the subsequent reduction to the quinol ( $\text{QH}_2$ ) with an  $E_{m,7}$  of +280 mV (determined in the *bc<sub>1</sub>* complex) and thus is the energetically favorable pathway (Nicholls and Ferguson 1992).

Quinones can be differentiated by optical spectroscopy: Ubiquinone exhibits a characteristic absorption maximum at 275 nm (Fato, Estornell et al. 1996), whereas plastoquinone absorbs at 254 nm (Crane 1959). Theoretically, it is also possible to distinguish the semiquinone

anion from quinone and quinol species optically, but this is often hindered by absorption of other molecules in this wavelength range, such as the NADH used in kinetic studies of NADH:quinone oxidoreductases or the absorption of aromatic amino acid residues. The semiquinone radical can be detected by EPR (Land and Swallow 1970). In the study presented here, the formation of QH<sub>2</sub> species by the Na<sup>+</sup>-NQR was followed using the difference in absorbance between 248 and 268 nm, as described by Tokuda and Unemoto (Tokuda and Unemoto 1984).

### 1.4. Inhibitors

Many of the specific NADH:quinone oxidoreductase inhibitors listed in table 2 exhibit a structural similarity to Q and are thought to compete with the substrate quinone or at least associate with the quinone binding site. They consist of a cyclic 'head' moiety with one or more conjugated ketone/enol groups and a long hydrophobic 'tail', facilitating interaction with the membrane (figure 5). Korormicin and 2-n-heptyl-4-hydroxyquinoline N-oxide (HQNO) are specific inhibitors of the  $\text{Na}^+$ -NQR in the nanomolar range, which show non-competitive inhibition in the presence of  $\text{Q}_1$  (Nakayama 1999). It is proposed that their tail groups interact with a hydrophobic pocket of NqrB (Hayashi, Shibata et al. 2002; Casutt, Nedielkov et al. 2011).

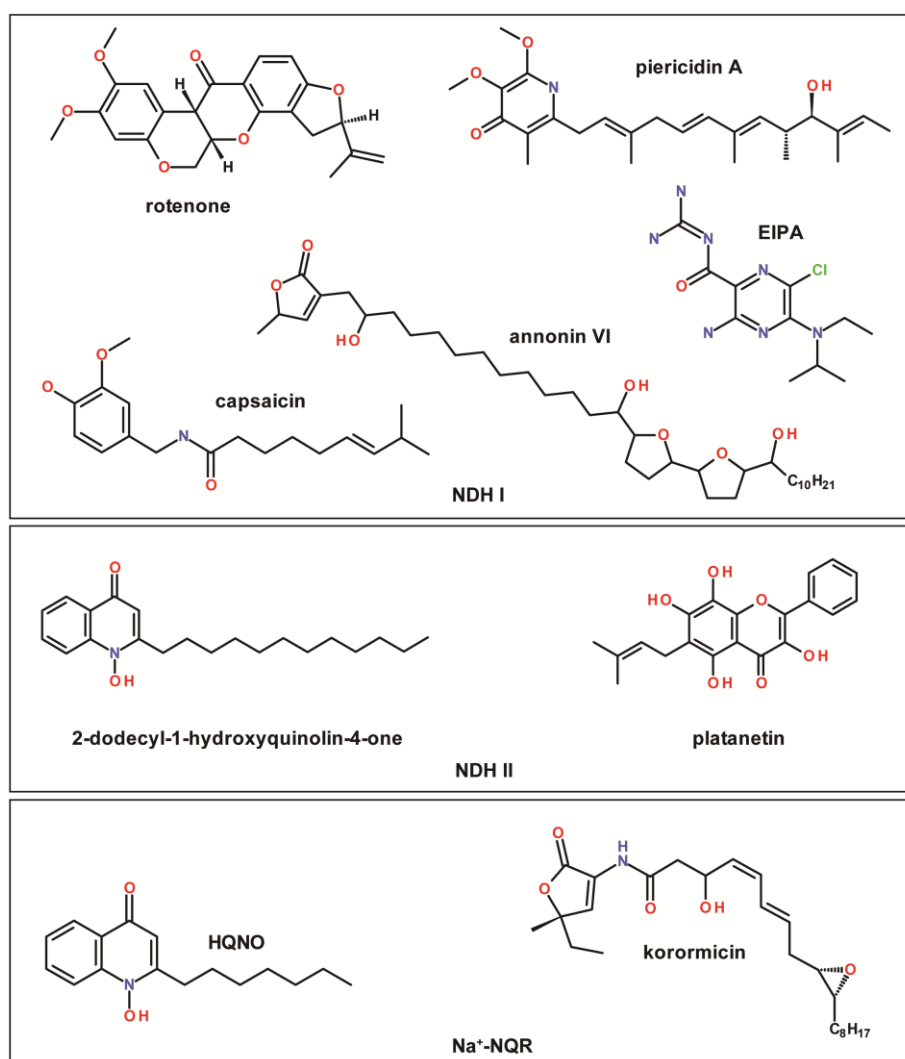


**Figure 5: Selected structures of NADH:quinone oxidoreductase inhibitors.** Inhibitors specific for complex I (NDH I), alternative NADH dehydrogenase (NDH II) or  $\text{Na}^+$ -NQR, as listed in table 2.

There are several known inhibitors which do not act as quinone analogs: rotenone and platanetin are flavonoids and are believed to interact with the flavoprotein regions of oxidoreductases. It is noteworthy that rotenone is a specific complex I inhibitor, whereas platanetin is specific for NDH II, hence why the NDH II is also called rotenone-insensitive NADH dehydrogenase. In addition, platanetin acts as uncoupler of the electron transport chain (Ravanel, Tissut et al. 1986). 5'-(N-ethyl-N-isopropyl)amiloride (EIPA) is a known inhibitor of cation/proton antiporters and has been shown to inhibit the Na<sup>+</sup> translocation of the isolated NuoL subunit of *E. coli* NDH I (Gemperli, Schaffitzel et al. 2007; Pedersen, King et al. 2007). Silver ions (Ag<sup>+</sup>) act as specific inhibitor on NADH dehydrogenase activity of the Na<sup>+</sup>-NQR (Nakayama 1999), and 2,5-Dibromo-3-methyl-6-isopropyl-p-benzoquinone (DBMIB) is a quinone analog and herbicide known to inhibit the mitochondrial cytochrome-*bc*<sub>1</sub> complex as well as *b*<sub>6</sub>*f* complex of photosynthetic organisms (Rich, Madgwick et al. 1991). The mechanisms of Na<sup>+</sup>-NQR inhibition by Ag<sup>+</sup> and DBMIB are investigated in chapters 3.3.1. and 3.3.3. of this thesis.

### **1.5. Scope of the study**

The aim of this work is to expand the current understanding of NADH:quinone oxidoreductases by investigating structural and functional properties of key catalytic subunits. The recently published X-ray structures of the membrane-embedded arm of bacterial complex I (Efremov, Baradaran et al. 2010; Efremov and Sazanov 2011) allow us to take a closer look at the sub-microscopic machinery that drives the generation of the electrochemical gradient which respiratory organisms depend on. Our experiments with the isolated ND5 subunit from human or *Yarrowia lipolytica* complex I, described in chapter 2, provide biochemical data on the ion translocation function and the alteration of function by disease-associated mutations.

The composition of Na<sup>+</sup>-NQR is completely different from that of complex I, although both enzymes catalyze the same redox reaction. We strive for the elucidation of this prime example of diversity in nature by focusing our investigations on the hinge points that both complexes have in common: the oxidation of NADH and the reduction of ubiquinone. Two electrons from NADH are transferred to a FAD cofactor by the NqrF subunit. Using site-directed mutagenesis and high-resolution X-ray structures combined with biochemical studies, it was possible to create a model for catalysis and substrate selectivity on the atomic level of this electron input module. In addition, Ag<sup>+</sup> was found to irreversibly bind to a cysteine residue in the NADH binding pocket, which leads to inhibition of the Na<sup>+</sup>-NQR and killing of *V. cholerae* in the nanomolar range. Looking at the electron acceptor part of the complex, we identified DBMIB as an inhibitor of the quinone reductase module supposedly formed by NqrA and NqrB. By the use of physicochemical and biochemical methods, we learn about the mode of substrate binding and inhibition and propose a redox mechanism of the Na<sup>+</sup>-NQR involving at least two quinones. The investigations relevant to the Na<sup>+</sup>-NQR are described in chapter 3 of this thesis.



## Chapter 2

### Production and functional characterization of the antiporter-like ND5 subunit of complex I from *Homo sapiens* and *Yarrowia lipolytica*

**Steffen, W.**, Gemperli, A.C., Cvetesic, N. and J. Steuber (2010)  
"Organelle-specific expression of subunit ND5 of human complex I (NADH dehydrogenase) alters cation homeostasis in *Saccharomyces cerevisiae*."  
FEMS Yeast Res 10(6): 648-59

**Steffen, W.** and Steuber, J. "Cation transport by the respiratory NADH:quinone oxidoreductase (complex I): facts and hypotheses."  
Manuscript submitted for publication

**Steffen, W.**, Grönheim, H., Karuppasamy, M., Schaffitzel, C. and J. Steuber  
"The individual subunit ND5 of complex I (NADH:quinone oxidoreductase) from *Yarrowia lipolytica* transports Na<sup>+</sup>."  
Manuscript in preparation

## 2.1. Introduction

### 2.1.1. The structure of respiratory complex I

Complex I is one of four energy-converting enzyme complexes of the respiratory chain in mitochondria, chloroplasts or bacteria. It represents the main site of entry for electrons into the respiratory chain and couples the transfer of two electrons from NADH to ubiquinone with the transport of four protons across the membrane, although the exact stoichiometry is still debated (Walker 1992; Yagi and Matsuno-Yagi 2003; Brandt 2006; Zickermann, Kerscher et al. 2009). The mitochondrial complex I consists of 45 subunits (Carroll, Fearnley et al. 2006). The comparison with the smaller, bacterial complex I (Friedrich, Abelmann et al. 1998; Gabaldon, Rainey et al. 2005) indicates that the core enzyme can be divided into two subcomplexes: seven hydrophilic subunits of the peripheral arm form the essential oxidoreductase module (FP51K, FP24K, IP75K, IP49K, IP30K, IP21K and IP23K), catalyzing all redox reactions between NADH and ubiquinone (Hirst 2005), whereas the seven ND subunits (ND1 - 6, ND4L), which are encoded by the mitochondrial genome (Fearnley and Walker 1992), represent the hydrophobic, membrane-spanning arm of the enzyme and catalyze its electrogenic activity.

In 2006, the X-ray crystallographic structure of the peripheral arm of *Thermus thermophilus* complex I was determined (Sazanov and Hinchliffe 2006). This structure elucidated the spatial arrangement of the redox cofactors, leading to a model of the electron transfer chain shown in figure 1. The peripheral domain contains a noncovalently bound FMN and 8 - 10 Fe-S clusters, of which 7 are thought to participate in the electron transfer reaction (figure 1B). In 2010, the structure of the complete complex from *Thermus thermophilus* was solved (Efremov, Baradaran et al. 2010) at a resolution of 4.5 Å, followed in 2011 by the structure of the membrane arm of *E. coli* NDH I at 3 Å (Efremov and Sazanov 2011). The knowledge of the complete structure gave insight into the coupling of the redox reaction to the electrogenic reaction: an indirect mechanism was proposed in which ubiquinone reduction leads to a change in the conformation of helices at the interface between the membrane arm and the peripheral arm. This conformational signal is relayed to the ion transporting modules ND2, ND4 and ND5 (and probably a fourth module at the interface between ND2, ND3, ND4L and ND6) by a 60 - 110 Å-long, amphipathic alpha-helix of subunit ND5, supposedly driving ion pumping in a manner reminiscent of a steam engine (Efremov and

Sazanov 2011). A similar mechanism was proposed in view of the 3D structure at 6.3 Å resolution of the complex I from *Y. lipolytica* (Hunte, Zickermann et al. 2010). Efremov and Sazanov propose that each ion transport module consists of two 5-helix repeats forming two half-channels which are connected by polar residues and thus constitute a continuous proton-translocation pore (Efremov and Sazanov 2011).

### 2.1.2. Homology to cation/proton antiporters

It has been first observed by Walker and colleagues (Fearnley and Walker 1992) that subunit ND5 from complex I exhibits significant sequence similarity to a subunit of multicomponent cation/proton antiporters belonging to the MrpA-type family of transporters. Members of this family are subunit MnhA of the cation/H<sup>+</sup> antiporter from *Staphylococcus aureus* and subunit EchA of the energy-converting hydrogenase from *Methanosarcina barkeri* (Hamamoto, Hashimoto et al. 1994; Mathiesen and Hägerhäll 2002; Mathiesen and Hägerhäll 2003). These antiporters couple the transport of cations like sodium, potassium or lithium with the antiport of H<sup>+</sup> and therefore play a role in the bacterial cation homeostasis (Hiramatsu, Kodama et al. 1998; Kosono, Morotomi et al. 1999; Blanco-Rivero, Leganes et al. 2005; Swartz, Ikewada et al. 2005). The central fragment of NuoL/ND5 constitutes the most conserved region, exhibiting the highest sequence similarity to cation/H<sup>+</sup> antiporters (Zhadanov, Grechanina et al. 2007). Experiments revealed that the ND5 homolog NuoL is even able to complement a Na<sup>+</sup>/H<sup>+</sup> antiporter deficient mutant from *Bacillus subtilis* (Moparthy, Kumar et al. 2011). The combined evidence of homology to cation/proton antiporters strongly suggests that ND5, as well as its relatives ND2 and ND4, are likely to provide cation transport channels through the hydrophobic part of complex I (Gemperli, Schaffitzel et al. 2007).

### 2.1.3. Mitochondrially encoded complex I subunits are hotspots for mutations causing muscular and neurodegenerative diseases

The absence of suitable genetic tools for manipulation of mitochondrial DNA has made it difficult to study mutations in genes encoding for respiratory chain components which are associated with neurodegenerative diseases. In particular, a functional analysis of the ND5 subunit of complex I is needed since it represents a hot spot for mutations (Liolitsa, Rahman

et al. 2003; Zhadanov, Grechanina et al. 2007). These mutations are frequently observed in mitochondrial and neurodegenerative diseases like Leber's hereditary optic neuropathy (LHON), MELAS syndrome (Mitochondrial encephalomyopathy, lactic acidosis, and stroke-like episodes), Leigh disease, Myoclonic epilepsy with ragged red fiber (MERRF) or Parkinson's disease (PD). Five of the most prevalent mutations are listed in table 4. All those diseases have in common that cells with a high energy demand are affected, which suggests a major disorder in the respiratory chain of these cells. A study aimed to elucidate the correlation between a dysfunction of complex I and neurodegenerative diseases. It showed that 1-methyl-4-phenylpyridinium and rotenone, inhibitors of complex I, cause drug-induced Parkinsonism in rodents (Caboni, Sherer et al. 2004).

**Table 4: Frequently observed mutations of human ND5 in neurodegenerative diseases and the corresponding amino acid exchanges introduced into ND5 from *Yarrowia lipolytica*.**

Human	<i>Y. lipolytica</i>	Disease	Reference
F124L	F123L	MELAS, PD, Leigh	(Taylor, Morris et al. 2002; Parker and Parks 2005; Zhadanov, Grechanina et al. 2007)
E145G	E144G	MELAS, PD	(Liolitsa, Rahman et al. 2003; Parker and Parks 2005)
A171V	A170V	LHON	(Mayorov, Biousse et al. 2005)
A236T	A239T	MELAS, MERRF	(Naini, Lu et al. 2005)
M237L	M240L	MELAS	(Liolitsa, Rahman et al. 2003)

MELAS: Mitochondrial encephalomyopathy, lactic acidosis and stroke-like episodes, LHON: Leber's hereditary optic neuropathy, MERRF: Myoclonic Epilepsy with Ragged Red Fibers, PD: Parkinson's disease.

#### 2.1.4. Cation transport of the ND5 subunit of mitochondrial complex I

The knowledge about complex I and its subunits was increased substantially in the last years. The crystallographic analysis of *Y. lipolytica* complex I (Hunte, Zickermann et al. 2010) and especially the recently published X-ray structure of the membrane bound subunits of NDH I from *E. coli* at 3.0 Å resolution (Efremov and Sazanov 2011) answers many open questions. However, a large number of unsolved questions remains. One of these questions is whether membrane bound subunits of complex I transport cations instead of, or in addition to, protons. Indications that the transport mechanism also includes a Na<sup>+</sup> translocation event become more frequent. Thus far it could be shown that NDH I from *E. coli* transports Na<sup>+</sup> in preference to H<sup>+</sup> in native inverted vesicles from the Na<sup>+</sup>/H<sup>+</sup> antiporter deficient *E. coli*

mutant EP432 (Steuber, Schmid et al. 2000). Sodium ion uptake could also be demonstrated with vesicles, containing a truncated version of the NDH I subunit NuoL (Steuber 2003). With other vesicles from *S. cerevisiae* cells expressing a protein A/NuoL fusion protein, Na<sup>+</sup> and also K<sup>+</sup> uptake was measurable (Gemperli, Schaffitzel et al. 2007). The ability to translocate sodium ions could also be shown for NDH I from other bacteria like *Klebsiella pneumoniae* (Gemperli, Dimroth et al. 2002; Gemperli, Dimroth et al. 2003; Vgenopoulou, Gemperli et al. 2006) and *Rhodothermus marinus* (Batista, Fernandes et al. 2010).

Recently, Roberts and Hirst presented evidence that the deactive form of mitochondrial complex I of *Bos taurus* (Roberts and Hirst 2012) catalyzes Na<sup>+</sup>/H<sup>+</sup> antiport. Prior to that Lin, Puhar and Steuber could already show that complex I from the yeast *Yarrowia lipolytica* has the capacity to catalyze NADH-driven Na<sup>+</sup> extrusion (Lin, Puhar et al. 2008) and that this function is thus not restricted to bacterial enzymes. This prompted us to investigate if the individual ND5 subunit of the *Y. lipolytica* complex also catalyzes Na<sup>+</sup> transport. In the present study, five of the most frequent mutations in human ND5 were transposed to *Y. lipolytica* ND5, with the aim to study their effect on the cation transport activity of ND5 (table 4). In addition, we hypothesized that cation transport by ND5 would interfere with alkali metal cation homeostasis in *S. cerevisiae* (Sychrova 2004). *S. cerevisiae* is an excellent model organism for the study of mitochondrial proteins (Schmidt, Hennig et al. 1983; Yaffe and Schatz 1984; Glick and Von Heijne 1996; Meisinger, Pfanner et al. 2006). The organism lacks complex I and relies on alternative NADH dehydrogenases for respiration (Foury, Roganti et al. 1998) which enabled us to study the function of a heterologously expressed ND5 subunit from human complex I.

## 2.2. Materials & Methods

### 2.2.1. Chemicals and enzymes

All chemicals were obtained from Sigma-Aldrich/Fluka, unless otherwise stated. Restriction enzymes and T4 DNA ligase were purchased from New England Biolabs. DNA polymerase and PCR buffers were obtained from Finnzymes.

### 2.2.2. Construction of plasmids

*Escherichia coli* K-12 strains DH5 $\alpha$  or BL21 (DE3) (Hanahan 1983) (MBI Fermentas) served as host for the amplification of plasmids which conferred ampicillin resistance. The synthetic *Homo sapiens* ND5 gene (Eurofins Medigenomix) was cloned into plasmid pNLt1 (Gemperli, Schaffitzel et al. 2007) at Sal I restriction sites. The *sfgfp* gene encoding for an engineered superfolding green fluorescent protein (GFP) (Pedelacq, Cabantous et al. 2006) was amplified using PCR primers 5'-AAAATAGCGGCCG**ACTAGTATGAGCAAAGGAG**-3' (forward) and 5'-TCAGCCG**AATTCTTGTAGAGTTCATCCATGCCATG**-3' (reverse) and inserted at NotI and EcoRI restriction sites of pNLt1 containing the ND5 insert to generate plasmid pG5N (table 5). Restriction sites are underlined, bases annealing to the *sfgfp* gene are shown in bold. Plasmid pG was generated by cloning the *sfgfp* gene into pNLt1 using NotI and XhoI restriction sites. Oligonucleotide primers were synthesized by Sigma Genosys. Sequences coding for the mitochondrial targeting sequence of ATPase delta subunit (UniProt accession No. Q12165, (Giraud and Velours 1994)) and the Flag peptide (Einhauer and Jungbauer 2001) were joined to the *Homo sapiens* ND5 gene using PCR primers 5'-TAGAGCGGCCG**ACTAGTATGTTACGTTCAATTATTGGAAAGAGTGCATCAAGATCATTGAATTCGT**CGCTAAGCGTTCATAT**ATGACAATGCACACCACG**-3' (forward) and 5'-GCAA**ACTCGAGTTATTTA**TCGTCATCATCTTTATAATCG**GTTATCAGTAAAAGAG**-3' (reverse). Religation into template plasmid at restriction sites NotI and Xho I yielded plasmid pM5NF (table 5). Restriction sites are underlined, bases annealing to the *Homo sapiens* ND5 sequence are shown in bold. Oligonucleotide primers were synthesized by Microsynth. The sequence of the synthetic *Homo sapiens* ND5 gene was codon-optimized for *E. coli* and *S. cerevisiae* expression under retention of the amino acid sequence of human ND5 (ND5<sub>Hs</sub>) as deposited on Swiss-Prot (UniProt accession No. P03915). Single nucleotide substitutions in plasmids pM5N1F,

pM5N2F, pG5N1 and pG5N2 (table 5) were introduced by the Quickchange mutagenesis kit (Stratagene) using primers 5'-ATAGGGTGGGTGGGAGTAGGC-3' (forward) and 5'-TAATCGAATTGGGGCTATCGGCTTATAC-3' (reverse) and their reverse complement counterparts. The calculated molecular masses of the fusion proteins are 94876.6 Da (GFPND5<sub>H5</sub>) and 70488.2 Da (MTS-ND5<sub>H5</sub>-Flag) respectively. Vector pETHP for production of protein A fused to six histidines at its N-terminus in *E. coli* was generated by cloning the *protA* gene from plasmid YEp (ProtA-TEV-002c) (Schenk, Rush et al. 2001) into pET2C (Stratagene).

The sequence of the *Yarrowia lipolytica* ND5 gene was codon-optimized for *E. coli* and *S. cerevisiae* expression under the retention of the amino acid sequence of *Yarrowia lipolytica* ND5 (ND5<sub>YI</sub>) as deposited on Swiss-Prot (UniProt accession no. Q9B6D3). The optimized gene was synthesized (DNA 2.0) and cloned into plasmid pG5N (Steffen, Gemperli et al. 2010) at EcoRI and XhoI restriction sites to generate plasmid pGYI5N which encodes for a GFP N-terminally fused to the ND5<sub>YI</sub> polypeptide. Using pGYI5N as template for site-directed mutagenesis (table 5), plasmid pGYI5N1 was created using primers 5'-ATGGAAACGGATCCGCACCAAGTTCGCTTCTTAGCCTGTTATCAATGCTCACCTTTTGG-3' and 5'-ATGTGGGGGGAGGGCGTGAATG-3'; pGYI5N2, pGYI5N3, pGYI5N4 and pGYI5N5 were created using primer pairs 5'-CGTCTTATTTGTGGGTTGGGGGTTTCATT-3' and 5'-CGCCAATGAACCCCAACCCACAAATAAGACG-3', 5'-CCGCACTGTCCGTTGTTCTGATGAATCGC-3' and 5'-CATCAGAACACGGACAGTGCGGATTTTCATGGC-3', 5'-GGTTAACGTTAACAAATGGAAGGCCCG-3' and 5'-GGAGTCGGGCCTTCCATTGTTAACGTTAAC-3', 5'-GTTAACGTTAGCACTGGAAGGCCCGAC-3' and 5'-GGAGTCGGGCCTTCCAGTGCTAACGTTAAC-3' as well as flanking primers 5'-ATGGAAACGGATCCGCACCAAGTTCGC-3' and 5'-ATGTGGGGGGAGGGCGTGAATG-3'. Mutated bases are shown in bold. BamHI and XhoI restriction sites were used for ligation into pGYI5N. Oligonucleotides were synthesized by Eurofins MWG Operon. PCR was performed on pGYI5N using primers 5'-AGAGGCGGCCGCACTAGTATGCATCAT**CATCACCATCACCATCACG**-3' (forward primer, Microsynth) and 5'-TCAGCCGAATTCTTGTAGAGTTCATCCATGCCATG-3' (reverse primer, Sigma Genosys) and inserted at NotI and EcoRI restriction sites of pGYI5N to generate plasmid pHGYI5N, which adds an N-terminal 8xHis tag to the fusion protein. Restriction sites are underlined; bases annealing to the *sfGfp* template are shown in bold. The calculated molecular mass of the fusion protein is 100'669.5 Da (GFPND5<sub>YI</sub>), the mass of

the histidine-tagged construct (His-GFPND5<sub>YI</sub>) is 102'402 Da. All constructs were confirmed by DNA Sequencing (Microsynth AG, Balgach, Switzerland).

**Table 5: Plasmids used in this study.**

Plasmid	Description and relevant characteristics	Origin or reference
pRS316	Yeast shuttle vector; pBluescript derivative; <i>URA3</i> ; <i>CEN6 ARS4</i> ; <i>Ap<sup>r</sup></i>	(Sikorski and Hieter 1989)
pNLt1	<i>E. coli nuoL<sub>N</sub></i> inserted into pGREG5006, a derivative of the pRS vector	(Gemperli, Schaffitzel et al. 2007)
pG	Codes for SFGFP; <i>URA3</i> ; <i>Ap<sup>r</sup></i> ; <i>KanMX</i>	(Steffen, Gemperli et al. 2010)
pG5N	Codes for ND5 <sub>Hs</sub> with N-terminal SFGFP tag; <i>URA3</i> ; <i>Ap<sup>r</sup></i> ; <i>KanMX</i>	(Steffen, Gemperli et al. 2010)
pG5N1	pG5N containing a mutation coding for E145V in ND5 <sub>Hs</sub>	(Steffen, Gemperli et al. 2010)
pG5N2	pG5N containing a mutation coding for D179A in ND5 <sub>Hs</sub>	(Steffen, Gemperli et al. 2010)
pM5NF	Codes for ND5 <sub>Hs</sub> with N-terminal MTS and C-terminal Flag tag; <i>URA3</i> ; <i>Ap<sup>r</sup></i> ; <i>KanMX</i>	(Steffen, Gemperli et al. 2010)
pM5N1F	pM5NF containing a mutation coding for E145V in ND5 <sub>Hs</sub>	(Steffen, Gemperli et al. 2010)
pM5N2F	pM5NF containing a mutation coding for D179A in ND5 <sub>Hs</sub>	(Steffen, Gemperli et al. 2010)
pETHP	Codes for His-tagged protein A; <i>Ap<sup>r</sup></i>	(Steffen, Gemperli et al. 2010)
pGYL5N	Derivative of pG5N, containing the <i>Y. lipolytica ND5</i> gene	This work
pHGYL5N	Codes for GFPND5 <sub>YI</sub> with N-terminal 8xHis-tag	This work
pGYL5N1	pGYL5N containing a mutation coding for F123L in ND5 <sub>YI</sub>	This work
pGYL5N2	pGYL5N containing a mutation coding for E144G in ND5 <sub>YI</sub>	This work
pGYL5N3	pGYL5N containing a mutation coding for A170V in ND5 <sub>YI</sub>	This work
pGYL5N4	pGYL5N containing a mutation coding for A239T in ND5 <sub>YI</sub>	This work
pGYL5N5	pGYL5N containing a mutation coding for M240T in ND5 <sub>YI</sub>	This work

*Ap<sup>r</sup>*: ampicillin resistance, *KanMX*: kanamycin resistance, *URA3*: uracil selection marker

### 2.2.3. Bioinformatic tools

The amino acid sequences of human ND5 (UniProt accession no. P03915) and the homolog from *Y. lipolytica* (Q9B6D3) were aligned to *Escherichia coli* NuoL (P33607), the H<sup>+</sup>/Na<sup>+</sup> antiporter MnhA from *Staphylococcus aureus* (Q9ZNG6) and to antiporter EchA from *Methanosarcina barkeri* (Q46G55) or complex I subunit Nqo12 from *Rhodothermus marinus* (Q4QSB1) respectively using the Clustal W (Thompson, Higgins et al. 1994) or the CLUSTAL Ω



(1.0.3) (Sievers, Wilm et al. 2011) multiple sequence alignment software on the EBI server (<http://www.ebi.ac.uk/Tools/msa/clustalo/>). The 3D structure of *E. coli* NuoL (PDB 3RKO) was analyzed for possible ion pathways and cavities using CAVER 2.1.2 (Petrek, Otyepka et al. 2006) and visualized with PyMOL (Schrödinger 2010).

A hydrophobicity-based model of the transmembrane arrangement of human ND5 was generated using ten different topology prediction methods: TMHMM (<http://www.cbs.dtu.dk/services/TMHMM-2.0/>) (Sonnhammer, von Heijne et al. 1998), Tmpred ([http://www.ch.embnet.org/software/TMPRED\\_form.html](http://www.ch.embnet.org/software/TMPRED_form.html)) (Hofmann and Stoffel 1993), SOSUI ([http://bp.nuap.nagoya-u.ac.jp/sosui/sosui\\_submit.html](http://bp.nuap.nagoya-u.ac.jp/sosui/sosui_submit.html)) (Hirokawa, Boon-Chieng et al. 1998), DAS (<http://www.sbc.su.se/~miklos/DAS/>) (Cserzo, Wallin et al. 1997), HMMTOP (<http://www.enzim.hu/hmmtop/>) (Tusnady and Simon 2001), TopPred (<http://mobyli.pasteur.fr/cgi-bin/portal.py?form=toppred>) (Claros and von Heijne 1994), MEMSAT (<http://bioinf.cs.ucl.ac.uk/psipred/>) (Jones, Taylor et al. 1994), Split 4.0 (<http://split.pmfst.hr/split/4/>) (Juretic, Zoranic et al. 2002), PHDhtm ([http://npsa-pbil.ibcp.fr/cgi-bin/npsa\\_automat.pl?page=/NPSA/npsa\\_htm.html](http://npsa-pbil.ibcp.fr/cgi-bin/npsa_automat.pl?page=/NPSA/npsa_htm.html)) (Rost, Casadio et al. 1995), PolyPhobius (<http://phobius.sbc.su.se/poly.html>) (Kall, Krogh et al. 2005). All methods were used with default settings and an eukaryotic dataset where available. In the consensus topology model, all residues predicted as certain transmembrane were assigned a value of 1.0. Residues predicted as 'putative transmembrane' or 'helical cap' were assigned a value of 0.5. The sum of the values from ten different prediction methods was calculated. Residues achieving a sum of 6.5 or higher were defined as 'transmembrane', residues achieving a sum of 5, 5.5 or 6 were defined as 'putative transmembrane'. In the consensus model, the N-terminus of ND5<sub>H5</sub> was predicted to be located in the intermembrane space (= 'out').

#### 2.2.4. Cell growth, protein expression and purification

Standard protocols were followed for yeast manipulation (Abelson, Guthrie et al. 2004) and transformation using lithium acetate (Gietz, St Jean et al. 1992). All ND5<sub>H5</sub> and ND5<sub>Y1</sub> constructs were expressed in *S. cerevisiae* strain BJ3505 ((Jones 1991), genotype *MAT $\alpha$  his3- $\Delta$ 200 pep4::HIS3 prb1- $\Delta$ 1.6R (gal3) ura3-52 lys2-801 trp1- $\Delta$ 101(gal2) can1*) which is *URA3* deficient and allows selecting for plasmids harboring the *URA3* gene required for uracil synthesis. This strain is furthermore deficient in endoproteinases A and B, which diminishes

proteolytic degradation (Jones 1991). Cells were grown as described previously (Gemperli, Schaffitzel et al. 2007). To grow cells expressing ND5 variants of *Y. lipolytica*, baffled flasks were used. *GAL1* controlled expression of the ND5 fusion proteins was induced by transfer to minimal YNB medium (0.67 % yeast nitrogen base with supplementary amino acids and adenine) containing 2 % galactose for 27 h (mid-log phase) prior to harvesting. Cells were counted using a hemocytometer (Fisher Scientific). Cells were harvested and disrupted by one passage through an Emulsiflex C3 (Avestin) cell disruptor at approx. 25 kPsi in 10 mM Tris-HCl, 10 mM KCl, pH 8.0 in the presence of protease inhibitor mix (complete EDTA-free, Roche). Cell debris and unbroken cells were removed by centrifugation for 5 min at 4'000 x g. Membranes from the endoplasmatic reticulum and the nuclear envelope were obtained as described in (Gemperli, Schaffitzel et al. 2007). Mitochondria were isolated as described in (Meisinger, Pfanner et al. 2006). Mitochondrial membranes were separated into outer membrane and inner membrane according to the protocol described in (Daum, Bohni et al. 1982). To obtain purified GFP as standard for the quantification of GFPND5<sub>HS</sub> fusion proteins, crude extracts from *S. cerevisiae* transformed with pG were centrifuged for 60 min at 35'000 rpm in a Beckman Type 70 Ti rotor. The supernatant containing the cytosolic fraction and GFP was concentrated by ultrafiltration and passed through a 0.2 µm filter. Proteins in 1.3 M NH<sub>4</sub>SO<sub>4</sub>, 10 mM Tris/HCl, 1 mM EDTA (pH 8.0) were applied to a HiTrap Phenyl HP column (GE Healthcare) and eluted with a linear gradient from 2 M to 0 M NH<sub>4</sub>SO<sub>4</sub> (Peckham, Bugos et al. 2006). Peak fractions were combined and loaded on a size exclusion chromatography column (Superdex 200 10/300, GE Healthcare), equilibrated with 200 mM NaCl in 10 mM Tris/HCl, 1 mM EDTA, pH 7.9. To purify His-GFPND5<sub>VI</sub> encoded by plasmid pHGYL5N, membranes were collected as described above and solubilized for 2 h at 4 °C in 20 mM Tris/HCl, 0.5 M NaCl, pH 8.0 containing 1 % Zwittergent 3-14. After centrifugation for 30 minutes at 126'000 x g, the supernatant was passed through a 0.2 µm filter and loaded onto a Ni Sepharose HP column (5 ml bed volume, GE Healthcare) equilibrated with 20 mM Tris/HCl, 0.5 M NaCl, pH 8.0 containing 0.02 % Zwittergent 3-14. A washing step was performed with 5 column volumes of buffer containing 30 mM imidazole. His-GFPND5<sub>VI</sub> was eluted with 400 mM imidazole. All steps were performed at 4 °C. His-tagged protein A used as standard for quantification of the protein A-NuoL fusion protein was produced in *E. coli* BL21 (DE3) transformed with pETHP (table 5). Following enrichment by Ni-NTA Agarose

(Qiagen), His-protein A was applied to a MonoQ anionic exchange column (GE Healthcare) and eluted with a linear gradient from 25 mM to 1 M NaCl in 20 mM Tris/HCl, pH 8.0.

### 2.2.5. Membrane solubilization and protease protection assay

Solubilization screening was performed in a volume of 200  $\mu$ l with a protein content of 1 mg and 0.8 % - 2 % detergent in TBS (Ausubel, Brent et al. 1995). Samples were gently shaken at 4 °C for 2 h and then centrifuged at 100'000 x g for 30 min. Pellets were resuspended in 200  $\mu$ l TBS and 20  $\mu$ l of each fraction analyzed by SDS-PAGE. For the protease protection assay, ER vesicles and 10 % Zwittergent 3-14 solution were mixed in TBS to a final concentration of 10 mg total protein/ml and 1 % or 0.8 % detergent. The membranes were gently agitated for 1 h at 4 °C. Centrifugation for 30 min at 100'000 x g yielded solubilized membranes in the supernatant. Solubilized and native membranes (400  $\mu$ g total protein) were incubated for 5 minutes at 37 °C with 20 U of Trypsin (1 x crystallized, Carl Roth GmbH). Aliquots were withdrawn after the indicated times and analyzed by SDS-PAGE.

### 2.2.6. Analytical methods

Protein was determined by the bicinchoninic acid method (Smith, Krohn et al. 1985) using the reagent from Pierce. ER membranes were analyzed by SDS-PAGE (Schägger and von Jagow 1987). Ten standard proteins in the range from 250 to 10 kDa were used (Precision Plus Protein Standards, Bio Rad). In some experiments the 25, 50, 75 kDa markers were fluorescently labeled (Western C Protein Standard, Bio Rad). The concentration of purified GFP and His-GFPND5<sub>YI</sub> was determined from the absorbance of GFP at 485 nm using an extinction coefficient of  $8.33 \times 10^4 \text{ M}^{-1} \times \text{cm}^{-1}$  (Pedelacq, Cabantous et al. 2006).

Rates of NADH oxidation by mitochondrial membranes with O<sub>2</sub> as electron acceptor were determined spectrophotometrically in quadruplicates as described in (Tao, Casutt et al. 2008). Antimycin was added at a concentration of 10 nM.

The localization of ND5<sub>H5</sub> and ND5<sub>YI</sub> variants was determined by immunostaining with antibodies against the Flag peptide (Sigma-Aldrich), subunit 2 of *Saccharomyces cerevisiae* cytochrome c oxidase (Cox2p, Invitrogen), porin (Invitrogen) and dolichol phosphate mannose synthase (Dpms, Invitrogen) followed by incubation with horseradish peroxidase

conjugated secondary antibody (Sigma-Aldrich). Aliquots of mitochondrial fractions in 10  $\mu$ l 10 mM Tris/HCl, pH 7.4, were spotted onto nitrocellulose membrane (Hybond-C Extra, Amersham Bioscience) and washed with 25 mM Tris, 192 mM glycine, 0.05 % SDS in 25 % (v/v) methanol. Detection was performed by chemiluminescence using the ECL kit (Amersham Bioscience) and a Bio-Rad ChemiDoc XRS+ CCD system with 5 min exposure time. The fluorescence of GFP-tagged ND5 variants (*Homo sapiens* and *Yarrowia lipolytica*) was detected on 10 % to 14 % acrylamide gels after size separation by SDS-PAGE according to protocols for GFP-tagged membrane protein expression (Drew, Lerch et al. 2006). Fluorescence imaging was performed using a Typhoon Trio system (GE Healthcare) with excitation at 488 nm and a 526 nm emission filter. GFP and protein A standards, and their respective fusion proteins, were separated by SDS-PAGE and quantified by in-gel fluorescence (GFP) or chemiluminescence after Western blotting (protein A) using the ImageQuant TL software (GE Healthcare).

LC-ESI-MS of purified His-GFPND5<sub>YL</sub> was performed with fragments obtained by tryptic in-gel digestion of the fluorescent band. The mass spectrometric analysis was performed by the Life Science Center service unit at the University of Hohenheim: The gel slices were first washed in 200  $\mu$ l ddH<sub>2</sub>O and subsequently in 150  $\mu$ l acetonitrile (ACN). The samples were incubated for 30 min at 56 °C in 150  $\mu$ l DTT solution (10 mM DTT in 100 mM ammonium bicarbonate). DTT was removed and the samples were washed with 150  $\mu$ l ACN, the liquid was discarded. 85  $\mu$ l iodacetamide solution (55 mM iodacetamide in 100 mM ammonium bicarbonate) was added and the reaction was incubated for 20 minutes. Afterwards the gel slices were washed with 150  $\mu$ l 100 mM ammonium bicarbonate and subsequently with 150  $\mu$ l ACN. Tryptic digest was done by addition of a trypsin solution (10 ng/ $\mu$ l in 40 mM ammonium bicarbonate) and performed at 37 °C over night. Samples were cooled to room temperature and 2  $\mu$ l 10 % trifluoroacetic acid were added. The supernatant was transferred to a fresh reaction vessel and extraction of proteins was achieved by addition of 100  $\mu$ l extraction buffer (5 % formic acid/ACN in a 1:2 concentration) at 37 °C. The tryptic peptides were dissolved in a volume of 10  $\mu$ l 0.1 % formic acid before they were applied on a nano-UPLC system (ultra performance liquid chromatography, Waters) connected to an FT-ESI-massspectrometer (Thermo Fischer Scientific). For detection both linear iontrap (LTQ) and an orbitrap analyzer were used in parallel.

### 2.2.7. Preparation and immunostaining of cells for microscopic analysis

A modified immunofluorescence protocol for yeast was used (Pringle 1991). Frozen *S. cerevisiae* BJ3505 cells were thawed and resuspended in PBS (Ausubel, Brent et al. 1995) containing 4 % paraformaldehyde, incubated for 1 h at room temperature and washed in PBS. Aliquots of  $2 \times 10^8$  cells were pelleted ( $4'000 \times g$ , 5 min) and resuspended in 1 ml PBS to which 150 U of lyticase and 2  $\mu$ l  $\beta$ -mercaptoethanol were added. Formation of spheroblasts was stopped after 2 min by centrifugation ( $1'000 \times g$ , 5 min) and washing twice in PBS. Coverslips (0.17 mm thickness) were coated with 100  $\mu$ l 0.01 % poly-L-lysine for 10 min at room temperature. The coverslips were rinsed in double distilled H<sub>2</sub>O and subsequently dried under air for 1 h. The coverslips were placed coating-side up into a 24 well microplate (Greiner) and covered with cell suspension which was allowed to dry for 1 h at room temperature. After rinsing with PBS, the coverslips were incubated in blocking buffer (1 % BSA in PBS) for 1 h. For the localization of cellular compartments, coverslips were applied cell side down onto 20  $\mu$ l drops of 5  $\mu$ g/ml of primary antibodies (mouse anti-Dpms, Invitrogen; rabbit anti-neurospora porin, gift from R. Lill, University of Marburg; mouse and rabbit anti-Flag, Sigma-Aldrich) and, if indicated, 10  $\mu$ g/ml of 4', 6-diamidino-2-phenylindol (DAPI) in blocking buffer. The coverslips were incubated in a humidified chamber at room temperature for 1 h. Excess antibody solution was removed with a fiber-free paper and the coverslips were washed five times with PBS. Incubation with secondary antibodies anti-rabbit IgG Alexa Fluor 488 (Invitrogen), anti-rabbit IgG Cy3 (Sigma-Aldrich) and anti-mouse IgG Alexa Fluor 555 (Invitrogen) was performed using the same procedure as described for the reaction with primary antibodies. To perform labeling of the entire cell (i.e. cytoplasm and nucleus) and provide a background for visualization of GFPND5<sub>HS</sub>, fixed and permeabilized *S. cerevisiae* BJ3505 cells were incubated in HCS CellMask Deep Red staining solution (Invitrogen) for 30 minutes at room temperature. Cells were washed three times in PBS. Coverslips were dried and subsequently inverted onto a clean microscopy slide containing a drop of fluorescent mounting medium (Dako).

### 2.2.8. Microscopic imaging

Confocal laser-scanning microscopy was performed on a CLSM SP5 system (Leica) in single image and z-stack sequential scan modes. Excitation wavelengths were 405 nm for DAPI, 488 nm for Alexa Fluor 488 and GFP, and 543 nm for Alexa Fluor 555 and Cy3.

Widefield microscopy was performed on a Zeiss AxioImager.M1 and AxioCam MRm, using a Plan-Apochromat 100x oil objective, HXP 120 lamp. For detection of GFPND5<sub>H<sub>5</sub>/Y1</sub> variants, a HE eGFP filter was used. For detection of the cellular background stained with HCS CellMask Deep Red, a CY5 filter was used. For computational image restoration, z-stacks were deconvoluted with the Huygens (SVI) or Axiovision (Zeiss) software and visualized as maximum intensity projection with the imaging software Imaris (Bitplane).

### 2.2.9. Influence of salt on growth of *S. cerevisiae*

*S. cerevisiae* BJ3505 cells transformed with plasmids encoding for ND5<sub>H<sub>5</sub></sub> variants (table 5) were grown for 24 h to saturation in liquid YNB-glucose, washed with water, and resuspended in YNB-galactose to induce ND5<sub>H<sub>5</sub></sub> expression. Ten-fold serial dilutions of cell suspension from OD<sub>600</sub> 10 to 0.001 were prepared and spotted in 5 µl aliquots onto YNB-galactose agar plates. YNB medium contains 28 mM Na<sup>+</sup>, 7 mM K<sup>+</sup> and no Li<sup>+</sup> (Wickerham, Flickinger et al. 1946; Wickerham and Burton 1948; Nolan and Nolan 1972). In some experiments 600 mM NaCl, 800 mM KCl or 100 mM LiCl were added as indicated. Growth was monitored for 10 days at 30 °C under air. For growth experiments in liquid media, cells grown in YNB-glucose were washed with 10 ml H<sub>2</sub>O and adjusted to an absorbance at 600 nm of 5. Aliquots of 1 ml were mixed with 4 ml YNB-galactose, and cells were grown aerobically under vigorous shaking (220 rpm) at 30 °C in the absence or presence of 100 mM LiCl.

### 2.2.10. Sodium ion transport into ER vesicles

Experiments were based on the protocol described in (Gemperli, Schaffitzel et al. 2007), with following modifications: Disposable 1 ml plastic syringes were equipped with a HDPE support screen (pore size 35 µm) and subsequently filled with 0.3 ml of a potassium ion loaded cation exchanger resin (DOWEX 50WX4-200). The resin was rinsed with ddH<sub>2</sub>O before use.

Vesicles were prepared in 50 mM MES, 50 mM KCl pH 6.0 and shock frozen in liquid nitrogen. 150  $\mu$ l of vesicle solution were thawed on ice, centrifuged for 30 minutes at 30'000 x g and resuspended in 312  $\mu$ l of 50 mM Tris/MES, 50 mM KCl, pH 8.0. Eight  $\mu$ l of a NaCl solution (400 mM) were added to establish a sodium ion gradient across the membrane of the vesicles. The final, external Na<sup>+</sup> concentration in the assay was 5 mM. To remove external Na<sup>+</sup> after 10, 30, 60 and 90 seconds, 70  $\mu$ l aliquots of the reaction mixture were withdrawn, immediately loaded on the Dowex column and eluted with 800  $\mu$ l of ddH<sub>2</sub>O instantaneously. As control, the reaction was performed with vesicles lacking GFPND5<sub>Y1</sub>. Internal Na<sup>+</sup> concentration of vesicles was determined by atomic absorption spectroscopy. The size and morphology of the ER vesicles containing GFPND5<sub>Y1</sub> variants used for transport measurements was studied by cryo electron microscopy as described previously (Gemperli, Schaffitzel et al. 2007).

## 2.3. Results

### 2.3.1. Organelle-specific expression of subunit ND5 of human complex I alters cation homeostasis in *Saccharomyces cerevisiae*

#### 2.3.1.1. Multiple sequence alignment of ND5 and related proteins

The amino acid sequences of the ND5 subunits from mitochondrial complex I, the ND5 homolog NuoL from bacterial complex I, the related subunit from multicomponent cation/H<sup>+</sup> antiporters, and the corresponding subunit from energy-conserving hydrogenases related to complex I were compared (figure 6). The regions from amino acid residues 83 to 179, and from 222 to 422 (human ND5 numbering) are highly conserved, but there is practically no conservation on the level of primary sequence in the C-terminal parts of the proteins (residues 432 to 603).

By summing the results of ten different methods and assigning an upper and lower probability threshold, topology prediction of the full length ND5<sub>Hs</sub> polypeptide (figure 7) resulted in a model consisting of 16 transmembrane segments with both N- and C-terminus pointing to the outside (intermembrane space), which is in accord with the experimentally determined topology model of NuoL of complex I from the bacterium *Rhodobacter capsulatus* (Mathiesen and Hägerhäll 2002). The topology is also in accordance with the 3D structure of the ND5 homolog (NuoL) from *E. coli* complex I, which was published during the course of this work (Efremov and Sazanov 2011). Several highly conserved residues cluster in the predicted transmembrane helices IV to VI, which may represent a functionally important region involved in cation translocation. The frequent occurrence of mutations in these residues in LHON, Leigh syndrome, MELAS and PD patients is noteworthy (Taylor, Morris et al. 2002; Liolitsa, Rahman et al. 2003; Mayorov, Biousse et al. 2005; Parker and Parks 2005; Zhadanov, Grechanina et al. 2007), for example at position E145 in the predicted transmembrane helix V studied here. We also investigated the possible effect on ND5<sub>Hs</sub> function of the D179A mutation in the predicted transmembrane helix VI, since negatively charged, conserved amino acid residues in transmembrane segments were frequently reported to directly participate in cation translocation (Dimroth 1997).



```

human      MTHMTMTTLTTLTSLIPPILTTLVNPKNKNSYPHYVKS-IVASTFIIS----- 47
Yl         --MYNAISLIIILPCISWLFPLFFGRQLGYVVFVTRMTSTLIIITTLIT----- 46
Ec         ---MNLALTIILPLIGFVLLAFSRGRWSENVSAIVGVGVSGLAALVT----- 45
Sa         -----MSLLHIAVILPLIFALIIPILYRFFKRIHLGWFLVSPVIVIF----- 42
Mb         MIENTVMLLIIVPLLFSLFVALPKSLYRYLAWAFFIIGVALSVSLVLGGTGVVPEGPN 60
           :   :   :   :   :   :   :   :   :   :   :   :   :   :
human      -----LFPTTMFMCL-DQEVIIISNWHWATTQTTLQLSLS-----FKLD 83
Yl         -----YFFYQLLGN-NNPINLELFNYLNIDYLDINYN-----FEID 82
Ec         -----AFIGVDFFANGEQTYSQLWTWMSVGFENIGFN-----LVLD 82
Sa         -----IYMLTLIKTTMSGNTVMKTLNWP--HFGMNF-----LYLD 77
Mb         FAMYENIVLLLEVLVILYILAVSAKYKNWPTLGLGIIISALFAYTYANVPGAEGASFNID 120
           :   :   :   :   :   :   :   :   :   :   :   :   :   :
human      YFSMMFIPVALFVTSIMEFSLWYMNSDPN-----INQFFKYLLIFLITMLLIVTANNL 137
Yl         ALTITMLLAITTISSMVHIYSIGYMETDPH-----QVRFFSLLSMFTFWMIIIVTGSNY 136
Ec         GLSLTMLSVVTVGVGLIHMYSWYMRGEEG-----YSRFFAYTNLFIASMVVLVADNL 136
Sa         GLGLLFSLLISGIGSLVLYSIGYLSKSEQ-----LGNFYCYLLLFMGAMLVVSDNV 131
Mb         PLAQLMILIVNIVGTAILFATGYMDQYEEHRHLNRQKIFYFTMSFFLAAMNGLVMSDTL 180
           :   :   :   :   :   :   :   :   :   :   :   :   :   :
human      FQLFIGWEGVIGMSFLLISWWYARADANTAAIQAILYNRIGDIGFILALAWFILHSNSWD 197
Yl         FVLFVWGEFIGVTSYLLISFWVTRLQAMKSALSAVLMNRFGDFAFFVLGLCVIAYVFTLN 196
Ec         LLMYLGWEGVGLCSYLLIGFYTDPKNGAAAMKAFVVTRVGDVFLAFALFILYNELGTLN 196
Sa         IILYLFWELTSFSSFLLISFWRERQASIIYGAQKSLIITVFGGLSLLGGIILLAIPTQSFS 191
Mb         GWLYLFWELTTLCSFVLSYNMDE-EGINNGFRALSLLNLVGGVAMSIGIILLATNYNISS 239
           :   :   *   .   *   :   :   :   :   .   .   .   .   *   :   :   :   .
human      P----QQMALLNAN---PSLTPLLGLLLAAAGKSAQLGLHPWLPSAMEGPTPVSAALLHSS 250
Yl         YSTIFATAYLINTD---LLVLIMLALFIAAMAKSAQFGLHNWTLAMEGPTPVSSLLHAA 253
Ec         FREMVELAPAHFADGNNMLMWATLMLLGGAVGKSAQLPLQTLWADAMAGPTPVSAIHHAA 256
Sa         IQYMIQHASEIQNS--PFFIFAMILIMIGAFTKSAQFPFYIWLDPAMEAPTIVSAYLHSA 249
Mb         LTGIATYAGTDAVA-LAALALPVALLCIGGFAKSAQMPFHSWLLGAMVAPTIVSALLHSS 298
           :   .   .   *   *   :   :   *   *   *   *   *   *   :   :   :
human      TMVVAGIFLLIRFHPLAENSPLIQTTLTCLGAIITTLFAAVCALTONDIKKIVAFSTSSQL 310
Yl         TLVTAGIYLLLRSANILEYTPVLEFIILWIGALTTLTSLAGLIAICSNLDKRIIALSTMSQL 313
Ec         TMVTAGVYLIARTHGLFLMTPEVLHLVGVIVGAVTLLLAGFAALVQTDIKRVLAYSTMSQI 316
Sa         TMVKAGLYLIARMTPIFAASQGWVWVTLVGLITLFWASLNATKQQDLKGLIFSTVSQL 309
Mb         TMVNAGVFLVVKLVPAYAN-TSLGTAAIVYGSFTFVICSALALSQRNAKRVLAYSTIANL 357
           *   :   *   *   :   :   :   :   *   .   *   .   .   *   .   :   *   :   *   *   :   :
human      GLMMVTIGI-----NQPHLAFHLCIETHAFKAMLFMCSGSIHNLNNE- 353
Yl         GMMTIAIGL-----SAYNLALFHLLGHAFKALLFMSAGSIIHSLNES 357
Ec         GYMFLALGV-----QAWDAAI FHLMT HAFKALLFLASGSVILACHHE- 359
Sa         GMIMAMLGIGAI SYHYQGDDSKIYAAFTA AIFHLINHATFKGALFMITGAVDHS TGTR- 368
Mb         GLIIASAGIG-----TPLAVAASMMLILFHAI SKGLLFLCTGEIEHTIGSR- 403
           *   :   *   :   :   :   :   :   :   :   :   :   :   :   :

```

**Figure 6: Alignment of human ND5 with related proteins from yeast and bacteria.** Human ND5 (UniProt accession No. P03915), *Yarrowia lipolytica* ND5 (Yl ND5; accession no. Q9B6D3), *Escherichia coli* NuoL (Ec NuoL; accession no. P33607), *Staphylococcus aureus* MnhA (Sa MnhA; accession no. Q9ZNG6), *Methanosarcina barkeri* EchA (Mb EchA; accession no. Q46G55). Predicted transmembrane segments are underlined. Conserved residues are marked with stars (\*), similar residues with colons (:). E145 represents a hot spot for mutations that were found in patients suffering from PD or MELAS. D179 is an amino acid residue strictly conserved in ND5 homologs but not in cation/H<sup>+</sup> antiporters.

```

human      QDIRKMGGLLKTMPLTSTSLTIGSLALAGMPFLTG-FYSKDHIETAN--MSYTNA---- 406
Yl         QDIRTYGGLLSYLPYTYICITIASLSLMAMPGLTG-YYTKDIIESTYGSYSISNY---- 412
Ec         QNIFKMGGLRKSIPLVYLCFLVGAALSALPLVTAGFFSKDEILAGAMANGHIN----- 413
Sa         -DVKKLGGLLTIMPISFTITVITALS MAGVPPFNG-FLSKESFLETTFTASQANLFSVDT 426
Mb         -DIEDMSGLIKAPLLTSIAALGMVSMMLPP--FGVLLTKWVSMEAAASNNP----- 451
          :: .** . * : :: * . :* : :

human      ---WALSITLIATSLTSAYSTRMILLTLTGQPRFPTLT--NINENNPTLLNPIKR---LA 458
Yl         ---VVYWIAYLSAVLTCVYSMKILYLTFYSNPNNTITYYNAHESNIYITLPMFI---LA 466
Ec         ----LMVAGLVGAFMTSFLYTFRMI FIVFHGKEQIHAAHAVKGVTHS-----LPLIV---LL 461
Sa         LGYLFPIIGIVGVSFTFVYSIKFIMHIFFGQYKPEQLPKKAHEVSIILMLLSPAILATLVI 486
Mb         ---VVIIFIVLGSALTTVYYSKWLG TILSTSM DKNVPHKKLETYFPLSVLGLSIIGTSI 508
          :. : * * : : : . .

human      AGSLFAGFLIT-----NNISPASPFQTTIPLYLKLALAVTFLGLLTA 501
Yl         IFAMFAGWILKDIYLVGVTDFVGTHTILPNNFSYFDTEFSITQFYKLLPLISAILVSI LIV 526
Ec         ILSTFVGALIVP-----PLQGVLPQTTEL AHGSMLTLEITSGVVA 501
Sa         VFGFLPFGILTNS-----IIEPATSSINHTVIDDVEFHMFHGLTPAFLSTLVIY 534
Mb         FIFSIYDYFIRP-----QVEILLKVAVPAVTGQAGQFTS 541
          : . :

human      LDNLNLTNKLKMKSPLECTFYFSNMLG--FYPSITHRTI PYLGLLTSQNLP-----LLL 552
Yl         VLNEFFAIVENLNNKYINTVYSIFNQKLVSDQILNHFIIFKGLVTSGNIAHHVDKGSILYR 586
Ec         VVGILLAAWLWL GKRTLVTSIANSAPGRLLGTWYNAWGF DWLYDKVFVKPFLG--IAWL 559
Sa         ILGILLIVTFSYWVKLLQRQPGKLT FNYWYNRSANVIPNYSEKMTNSYVTDYSRNNLVII 594
Mb         EIGAFAYAAI FAVLALAILIYLATKNMFT PRTAGYYMCGENNLEKD-----RLMFR 592
          :

human      LDLTWLEKLLPKTISQHQISTSIITSTQKGMIKLYFLSFFFPLILTL LLLIT----- 603
Yl         LGPVGINRLLNKAS-YNVINLSSNTRSSLSMNSMLLITIVSLLLLLVLMNVNFIIVIPV 645
Ec         LKRDPLNSMMNIPAVLSRFAGKLLLS ENGYLRWYVASMSIGAVVVLALLMVLR----- 613
Sa         FGALILLTFVTIFSVPFNINFKDVSP IRIFEVCIVILLLSAAFLILFAKSRFLFSIIMLSA 654
Mb         NGLCSYEKCSVSNIIYLQNI FGESKLTTFGYAISIIILIVIALAGGVGL----- 639
          : . . : .

human      -----
Yl         LISILYILFS----- 655
Ec         -----
Sa         VGYAVSVLFIFFKAPDLALTQFV VESISTALFLLCFYHLPNLNRYNEKRSFQLTNALIAG 714
Mb         -----

human      -----
Yl         -----
Ec         -----
Sa         GVGLSV 720
Mb         -----

```

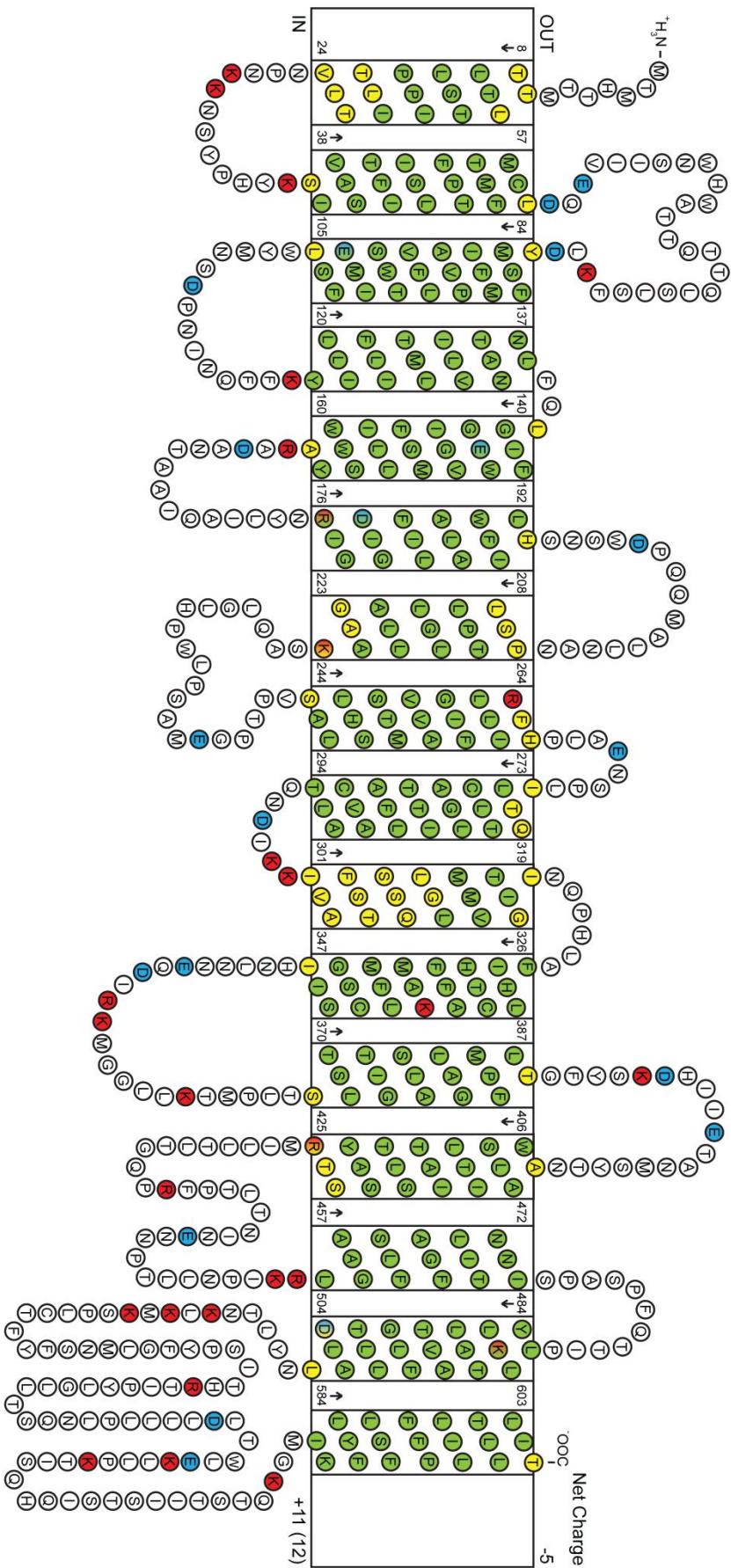


**Figure 7: Predicted membrane topology of human ND5.** Amino acid residues are colored as follows: Green: transmembrane residue, yellow: putative transmembrane residue, blue: negatively charged residue, red: positively charged residue. The net charge of the domains exposed to the mitochondrial matrix ('IN') or the intermembrane space ('OUT') was calculated by assigning acidic residues (D, E) a value of -1 and basic residues (K, R) a value of 1.

### 2.3.1.2. Expression strategy

We previously cloned the 3'-truncated *nuoL* gene encoding for the N-terminal part of the ND5 homolog from *E. coli* complex I and heterologously expressed the protein in *S. cerevisiae* (Gemperli, Schaffitzel et al. 2007). No signal sequences were fused to this hydrophobic protein which was localized to membranes of the endoplasmatic reticulum in the default sorting pathway. The same strategy was applied for the *ND5* gene encoding for the ND5 subunit from human complex I (ND5<sub>Hs</sub>) attached to a GFP at its N-terminus. To target ND5<sub>Hs</sub> to mitochondria, a fusion protein comprising a mitochondrial targeting sequence at the N-terminus and a Flag tag at the C-terminus was expressed (figure 8). The mutations E145V and D179A were introduced into the GFP- and Flag-tagged ND5<sub>Hs</sub> fusion proteins, respectively (figure 8). An N-terminal GFP tag was chosen for reasons of convenient detection and presumed beneficial effect on folding and stability of the very large, hydrophobic ND5<sub>Hs</sub> subunit. Fusion of a Flag peptide to the C-terminus of ND5<sub>Hs</sub> in case of ND5<sub>Hs</sub> directed to the mitochondrion by the N-terminal targeting sequence allowed for immunological detection of the full-length protein after insertion into the mitochondrial membrane.

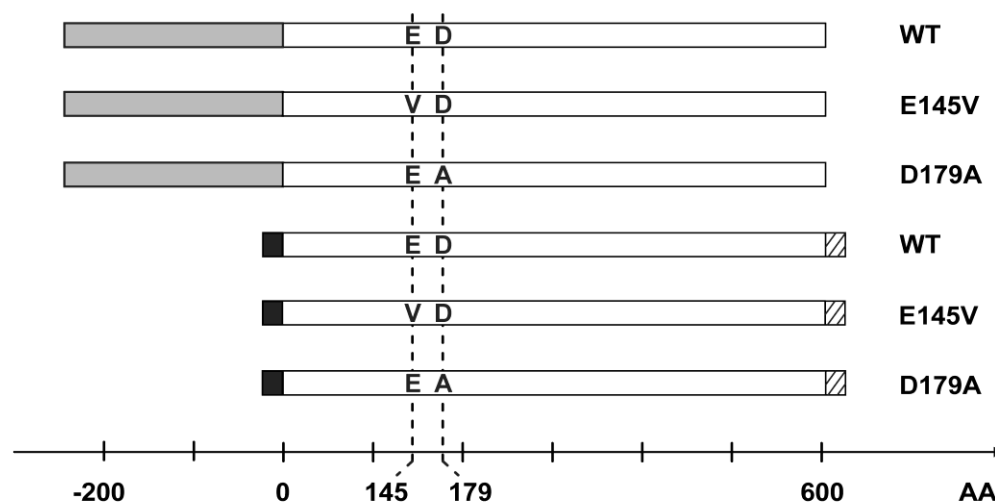


**Figure 8: Fusion proteins and mutated variants of ND5<sub>Hs</sub> for insertion in the endoplasmatic reticulum or inner mitochondrial membrane.** Wild type ND5<sub>Hs</sub> (vector pG5N), ND5<sub>Hs</sub>-E145V (vector pG5N1) and ND5<sub>Hs</sub>-D179A (vector pG5N2) were produced as N-terminal GFP (gray) fusion proteins. Adding the 22 residue signal sequence of *S. cerevisiae* ATP-synthase delta subunit at the N-terminus (black), and the Flag peptide to the C-terminus (hatched) yielded wild type ND5<sub>Hs</sub> (vector pM5NF), ND5<sub>Hs</sub>-E145V (vector pM5N1F) and ND5<sub>Hs</sub>-D179A (vector pM5N2F) targeted to mitochondria. AA: amino acid residue (ND5<sub>Hs</sub> numbering).

### 2.3.1.3. ND5<sub>H5</sub> devoid of a targeting signal is inserted in membranes from the endoplasmic reticulum

ND5<sub>H5</sub> variants were visualized in fixed and permeabilized cells, allowing the *in-situ* co-localization of organelle-resident proteins by immunofluorescence. To detect ER membranes, *S. cerevisiae* BJ3505 cells were immunostained with anti-Dpms. Dolichol phosphate mannose synthase is required for glycosyl phosphatidyl-inositol anchoring, N-glycosylation and O-mannosylation of protein in the rough endoplasmic reticulum (Orlean 1990). Mitochondria were visualized with antibody against porin which is localized in the outer mitochondrial membrane (Freitag, Benz et al. 1983). GFPND5<sub>H5</sub> almost completely co-localized with Dpms whereas no overlap was detected with porin (figure 9A). SDS-PAGE, followed by in-gel fluorescence of GFP and immunostaining against Dpms confirmed that in the absence of a signal sequence, GFPND5<sub>H5</sub> was predominantly localized in intracellular membranes of the ER obtained by fractionated centrifugation (figure 9B). Identical results were obtained with the E145V and D179A variants of GFPND5<sub>H5</sub> (data not shown). We did not detect GFPND5<sub>H5</sub> in the plasma membrane of *S. cerevisiae*, suggesting that this large, hydrophobic protein was retained in the ER (figure 10).

The amount of ND5<sub>H5</sub> and its variants in ER membranes was quantified (figure 11). GFPND5<sub>H5</sub> wild type and its E145V variant were present in similar amounts ( $95 \pm 3$  ng versus  $42 \pm 6$  ng per mg total protein,  $n = 3$ ). Quantification of the D197A variant of ND5<sub>H5</sub> was not possible, since the intensity of its fluorescence signal was less than 10 % of the intensity observed with the lowest GFP standard. Much higher yields were observed with the C-terminally truncated NuoL homolog of ND5 fused to the Protein A epitope expressed in *S. cerevisiae*. ER vesicles contained 1 - 1.6  $\mu$ g ProtA-NuoL per mg total ER protein, which allowed studying its cation transport activities. Our attempts to measure cation transport by GFPND5<sub>H5</sub> in ER vesicles were not successful, the likely reason being its low content.

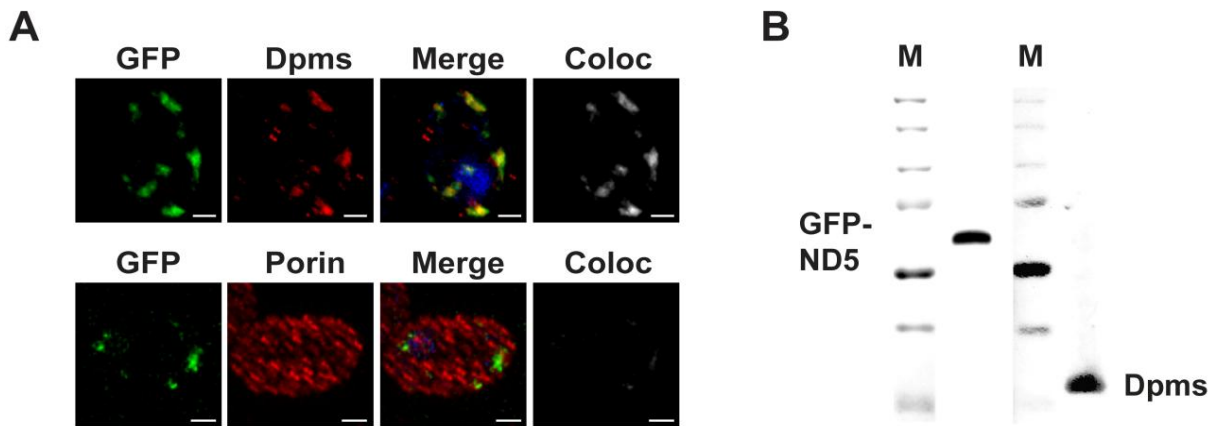


**Figure 9: GFPND5<sub>Hs</sub> chimerical protein is targeted exclusively to ER in *S. cerevisiae*.** **A:** *In vivo* localization of recombinant GFPND5<sub>Hs</sub>. Fixed and permeabilized *S. cerevisiae* cells stained with DAPI and anti-Dpms or anti-porin antibodies followed by staining with Alexa 555 or Cy3 coupled secondary antibodies. The cells were visualized by confocal laser scanning microscopy (excitation wavelengths: 405 nm for DAPI, 488 nm for GFP and 543 nm for Alexa 555) and are shown as top-down view of z-stacks. Upper panels: green; GFP, red; Dpms (ER-anchored protein), blue; DAPI (nucleus, only shown in merge). Lower panels: green; GFP, red; porin (mitochondrial outer membrane), blue; DAPI. The images were merged (Merge) and the overlap between GFP and Dpms was analyzed (Coloc). Scale bar represents 1  $\mu$ m. **B,** Left: in-gel fluorescence of *S. cerevisiae* ER membranes containing GFPND5<sub>Hs</sub> (0.2 mg protein) separated on 10 % SDS-PAGE. Right: Western blot of the SDS-PAGE shown left and immunodetection of the ER enzyme dolichol phosphate mannose synthase (Dpms). M: molecular weight marker proteins (from top to bottom: 250 kDa, 150 kDa, 100 kDa, 75 kDa, 50 kDa, 37 kDa, 25 kDa). Due to its hydrophobic nature, GFPND5<sub>Hs</sub> exhibited an apparent molecular mass on SDS-PAGE which was approximately 30 - 35 % lower than its calculated mass of 95 kDa.

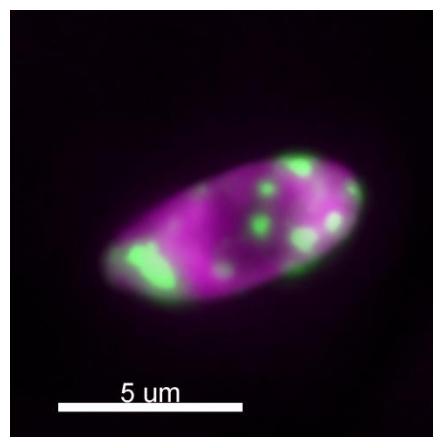


**Figure 10: Cortical and perinuclear ER localization of GFPND5<sub>Hs</sub> chimerical protein in *S. cerevisiae*.** HCS CellMask stain (red) labels the entire cell (i.e. cytoplasm and nucleus) and provides a background for visualization of GFPND5<sub>Hs</sub> (green).

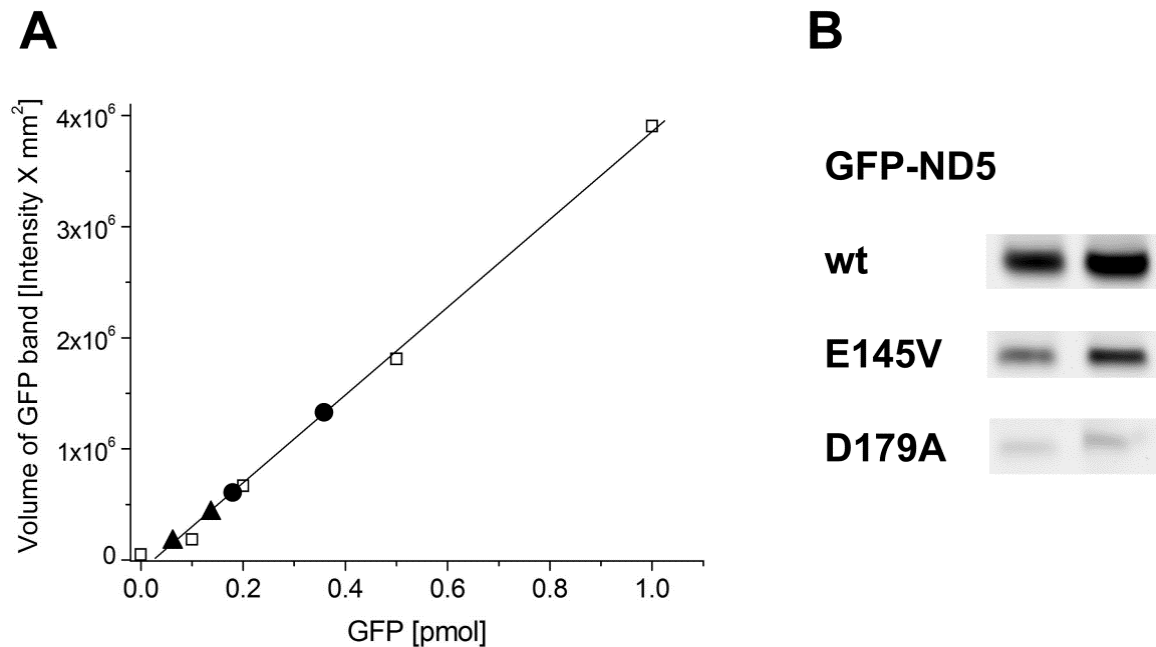


**Figure 11: Expression levels of GFPND5<sub>Hs</sub> and its E145V and D179A variants in membranes from the ER.** **A:** Purified GFP was separated on SDS-PAGE, and its fluorescence signal intensity was determined (0 - 1 pmol GFP). Within the applied GFP concentration range, the signal intensity increased linearly with the amount of protein loaded. **B:** ER vesicles containing GFPND5<sub>Hs</sub> or its E145V or D179A variants were separated on SDS-PAGE. Left lane, 0.2 mg total ER protein; right lane, 0.4 mg total ER protein. In **A**, the fluorescence signal intensities of GFPND5<sub>Hs</sub> (circles) and GFPND5<sub>Hs</sub>-E145V (triangles) of the ER membranes (0.2 or 0.4 mg protein) shown in **B** are indicated. The intensities observed with the GFPND5<sub>Hs</sub>-D179A variant (panel B) were less than 10 % of the intensity observed with the lowest GFP standard (panel A) and were therefore excluded from the quantitative analysis.

#### 2.3.1.4. ND5<sub>Hs</sub> comprising a matrix signal sequence is integrated in the mitochondrial inner membrane

We tried to change the sorting mode of GFPND5<sub>Hs</sub> to mitochondria by adding N-terminally the signal sequence of ATPase delta subunit (MTS). This resulted in aggregation of the fusion protein outside the mitochondria (data not shown), from which we concluded that the bulky, superfolding GFP might hinder membrane translocation or correct processing of the signal sequence. To circumvent this problem, the short Flag peptide was fused to the C-terminus of ND5<sub>Hs</sub>. Using this fusion protein (MTS-ND5<sub>Hs</sub>-Flag), ND5<sub>Hs</sub> wild type and mutant proteins were successfully targeted into mitochondria as shown by co-localization with mitochondrial porin (figure 12A). The same results were obtained with the E145V and D179A variants of MTS-ND5<sub>Hs</sub>-Flag. Cells incubated with anti-Dpms displayed only residual amounts of MTS-ND5<sub>Hs</sub>-Flag in the ER (figure 12B).

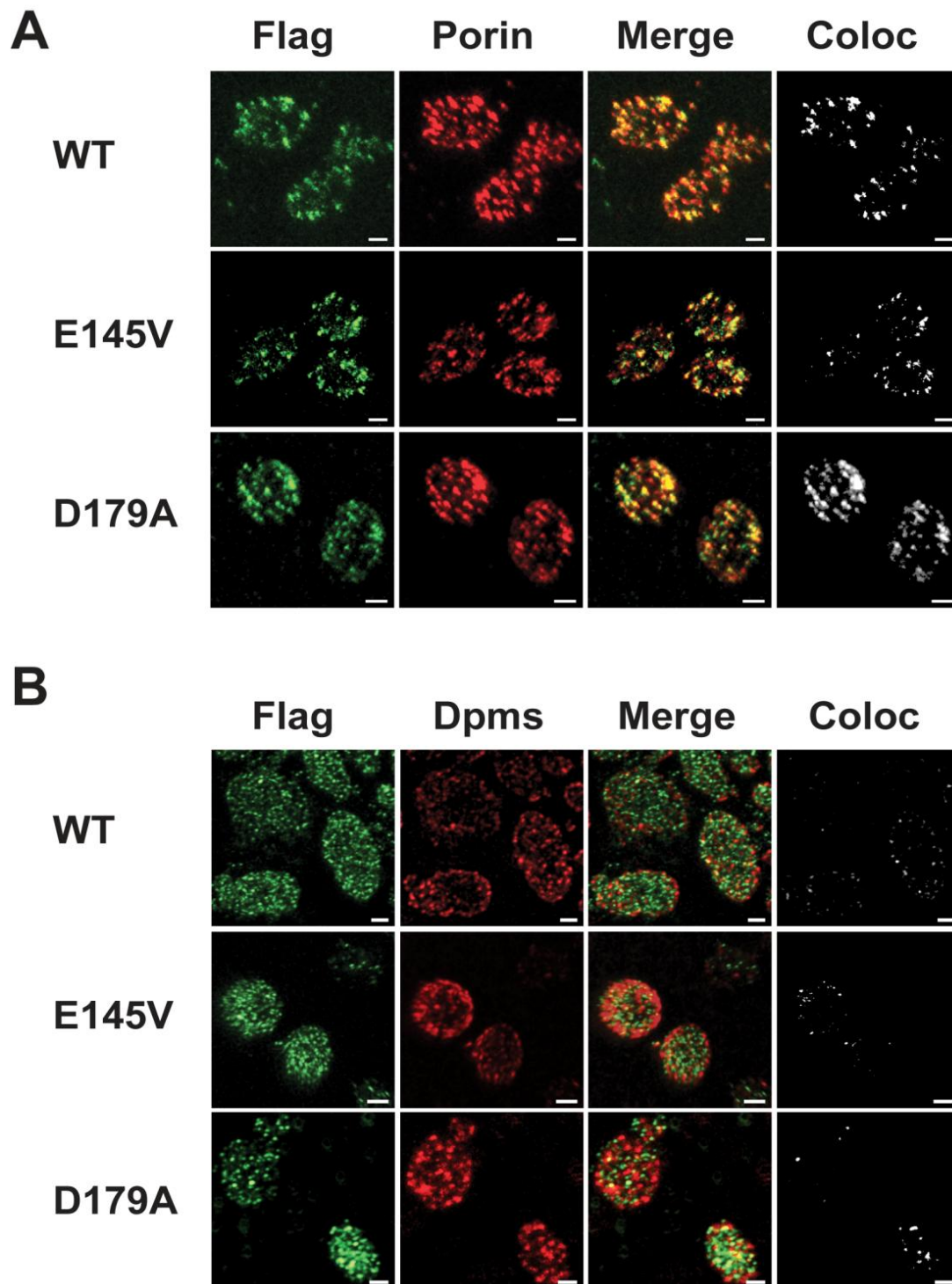


**Figure 12: Targeting of ND5<sub>H5</sub> to the inner mitochondrial membrane.** C-terminally Flag-tagged human ND5 protein variants containing the signal sequence of *S. cerevisiae* ATP-synthase delta subunit were expressed in *S. cerevisiae*. **A:** Cells were immunostained with anti-Flag followed by incubation with Alexa 488 coupled secondary antibodies (Flag), or anti-mitochondrial porin followed by incubation with Cy3 coupled secondary antibodies (Porin). **B:** Cells were immunostained with anti-Flag followed by incubation with Alexa 488 coupled secondary antibodies (Flag), or Dpms antibodies followed by incubation with Alexa 555 coupled secondary antibodies (Dpms). The images were merged (Merge) and the overlap analyzed (Coloc). The scale bar is 1  $\mu$ m.



Fractionation of mitochondria into inner and outer membrane resulted in co-purification of ND5<sub>H5</sub> with cytochrome c oxidase, a respiratory complex of the inner mitochondrial membrane (figure 13). This demonstrated that ND5<sub>H5</sub> was inserted into the inner membrane of mitochondria. Note that the hydrophobicity of the MTS-ND5<sub>H5</sub>-Flag fusion protein impeded its mobilization from SDS gels, which prompted us to use native MTS-ND5<sub>H5</sub>-Flag for immunostaining of mitochondrial fractions (figure 13). The presence of ND5<sub>H5</sub> in the inner mitochondrial membrane had no significant influence on the respiratory activity of *S. cerevisiae*. Rates of antimycin-sensitive NADH oxidation of mitochondrial membranes were  $0.16 \pm 0.02 \mu\text{mol min}^{-1} \text{mg}^{-1}$  in the absence of ND5<sub>H5</sub> (control vector),  $0.16 \pm 0.01 \mu\text{mol min}^{-1} \text{mg}^{-1}$  in the presence of wild type ND5<sub>H5</sub> (vector pM5NF), and  $0.19 \pm 0.01 \mu\text{mol min}^{-1} \text{mg}^{-1}$  with the ND5<sub>H5</sub>-D179A variant (vector pM5NF2). In the presence of ND5<sub>H5</sub>-E145V, NADH was oxidized at a rate of  $0.27 \pm 0.02 \mu\text{mol min}^{-1} \text{mg}^{-1}$ .

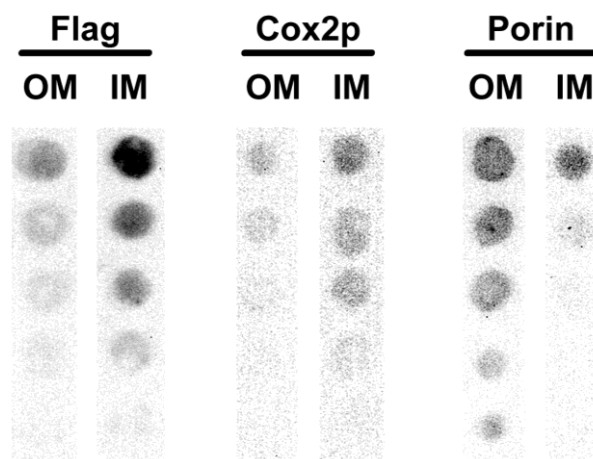


**Figure 13: Submitochondrial localization of MTS-ND5<sub>H5</sub>-Flag.** Detection was performed by immunostaining using anti-Flag antibodies. Outer membrane, OM; inner membrane, IM. Marker for inner mitochondrial membranes was the cytochrome c oxidase detected with anti-Cox2p antibodies. Marker for outer mitochondrial membranes was porin detected with anti-porin antibodies. Dilutions of each fraction were analyzed, containing, from top to bottom: 2.5  $\mu\text{g}$ , 1  $\mu\text{g}$ , 0.5  $\mu\text{g}$ , 0.25  $\mu\text{g}$ , 0.1  $\mu\text{g}$  protein.

#### 2.3.1.5. Salt-dependent growth phenotypes of *S. cerevisiae* producing ND5<sub>H5</sub>

Without salt added, *S. cerevisiae* cells producing ND5<sub>H5</sub> fusion proteins inserted in the ER or inner mitochondrial membrane exhibited the same growth behavior as cells transformed with the control vector pRS316 devoid of the *ND5* gene. It is concluded that the large, hydrophobic ND5<sub>H5</sub> protein was not toxic for *S. cerevisiae* (figure 14).

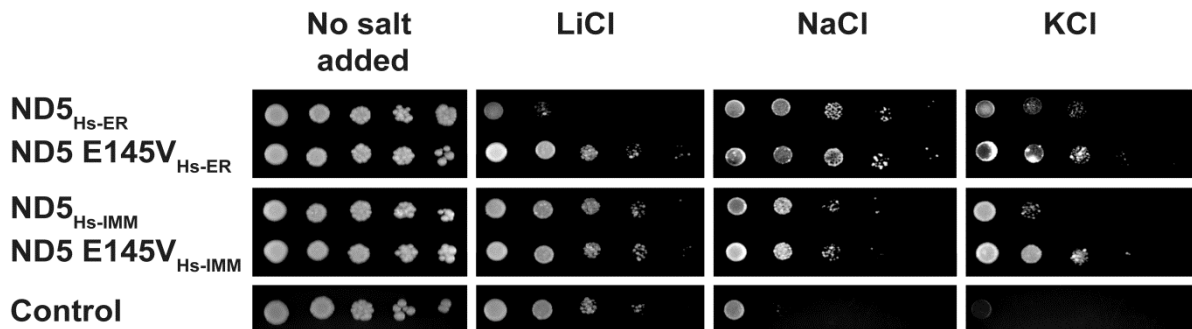


**Figure 14: Salt-dependent growth phenotypes of *S. cerevisiae* producing ND5<sub>Hs</sub> and ND5<sub>Hs</sub> mutant variants.** *S. cerevisiae* cell cultures, grown to saturation for 24 h in YNB-glucose and washed in water and YNB-galactose, were pipetted as 1:10 dilution series onto YNB-galactose agar plates containing either no added salt, 100 mM LiCl, 600 mM NaCl or 800 mM KCl. Growth was recorded after 10 days. ND5<sub>Hs</sub>, ND5 E145V<sub>Hs</sub>: Cells expressing the wild type or E145V variant of ND5<sub>Hs</sub> respectively; ER: ND5 protein localized in the ER, IMM: ND5 protein localized in the inner mitochondrial membrane. Control: Cells transformed with vector pRS316 devoid of the *ND5* gene.

We next studied the influence of alkali cations on growth. In the absence of ND5<sub>Hs</sub> fusion proteins, growth of cells transformed with the control vector was prevented at high external concentrations of Na<sup>+</sup> or K<sup>+</sup>. Expression of the ND5<sub>Hs</sub> fusion proteins rescued the cells, suggesting that ND5<sub>Hs</sub> located in the ER or the inner mitochondrial membrane participated in detoxification under conditions of elevated [Na<sup>+</sup>] and [K<sup>+</sup>]. The observation that ND5<sub>Hs</sub> and its E145V variant were expressed at similar levels (figure 11) allowed us to compare their impact on growth of *S. cerevisiae*. No significant difference in growth behavior was observed at high K<sup>+</sup> for the wild type and E145V variant of ND5<sub>Hs</sub> inserted into the ER. In contrast, growth in the presence of wild type ND5<sub>Hs</sub> was impaired compared to the E145V variant when present in the inner mitochondrial membrane under these conditions (figure 14). At elevated Na<sup>+</sup> concentrations, highest salt resistance was observed with ND5<sub>Hs</sub> present in the ER. Introducing a mutation at position 145 in ND5<sub>Hs</sub> had no effect compared to wild type ND5<sub>Hs</sub> under these conditions. Next, the effect of Li<sup>+</sup> on growth of *S. cerevisiae* in the presence or absence of ND5<sub>Hs</sub> was investigated. Li<sup>+</sup> is toxic at elevated concentrations but is exported from the cells by the Na<sup>+</sup>-dependent ATPase or Na<sup>+</sup> exchangers which transport Li<sup>+</sup> in addition to Na<sup>+</sup> (Kinclova-Zimmermannova, Flegelova et al. 2004; Kinclova-Zimmermannova and Sychrova 2006). Growth of *S. cerevisiae* transformed with the control vector was not impaired at an external Li<sup>+</sup> concentration of 100 mM (figure 14). Under these conditions, a very similar phenotype was observed with cells containing ND5<sub>Hs</sub> wild type and

the E145V variant in the inner mitochondrial membrane or with the E145V variant located in the ER. In contrast, the presence of wild type ND5<sub>H5</sub> in the ER membrane strongly inhibited growth at 100 mM Li<sup>+</sup>, indicating that the protein interfered with the systems for detoxification of Li<sup>+</sup> in *S. cerevisiae*. The qualitative findings shown in figure 14 were confirmed in a quantitative analysis (table 6).

**Table 6: Survival of *S. cerevisiae* producing ND5<sub>H5</sub> variants at elevated salt concentrations.**

ND5 <sub>H5</sub> variant	No salt added	100 mM LiCl	800 mM KCl
Located in the ER			
ND5 wild type	> 4 %	0.009 %	0.1 %
ND5 E145V	> 4 %	3 %	0.4 %
Located in mitochondria			
ND5 wild type	> 4 %	0.4 %	0.01 %
ND5 E145V	> 4 %	2 %	0.08 %
No ND5 present	> 4 %	0.4 %	< 0.001 %

Number of cells which formed colonies is given as percentage of total number of cells in the inoculum. Growth was monitored after 10 days. A representative set of data from three independent growth experiments is shown.

The number of colony-forming units of *S. cerevisiae* with or without ND5<sub>H5</sub> fusion proteins observed in the presence of 100 mM LiCl or 800 mM KCl was monitored after 10 days and compared with the number of cells initially present in the inoculum. Again, growth without added salt was not affected in control cells, or in cells expressing the ND5<sub>H5</sub> wild type or E145V variant. In the presence of Li<sup>+</sup>, growth of *S. cerevisiae* was heavily impaired when wild type ND5<sub>H5</sub> was present in the ER, while the E145V variant of ND5<sub>H5</sub> was less toxic for the cells. When ND5<sub>H5</sub> was targeted to mitochondria, the viability of cells producing the ND5<sub>H5</sub> E145V variant in the presence of Li<sup>+</sup> was slightly improved compared to cells containing ND5<sub>H5</sub> wild type (table 6). In the presence of K<sup>+</sup>, the viability of *S. cerevisiae* producing ND5<sub>H5</sub> fusion proteins was generally higher than in the absence of ND5<sub>H5</sub>. Again, better growth was observed when cells produced the E145V variant. We also followed the growth of *S. cerevisiae* containing GFPND5<sub>H5</sub> fusion proteins in the ER in liquid culture under aerated conditions. Without added salt, the doubling time of *S. cerevisiae* was not significantly influenced by the presence of GFPND5<sub>H5</sub> (6 ± 1 hours in the absence or presence of ND5<sub>H5</sub> fusion proteins; data not shown). Adding LiCl (100 mM) to the growth medium drastically inhibited growth of *S. cerevisiae* producing wild type ND5<sub>H5</sub>, whereas cells containing the

E145V variant reached final cell densities comparable to *S. cerevisiae* cells transformed with the control vector lacking the ND5<sub>HS</sub> fusion proteins (figure 15). These results further support the notion that ND5<sub>HS</sub> affects cation homeostasis in *S. cerevisiae* in a sequence-dependent and organelle-specific manner.

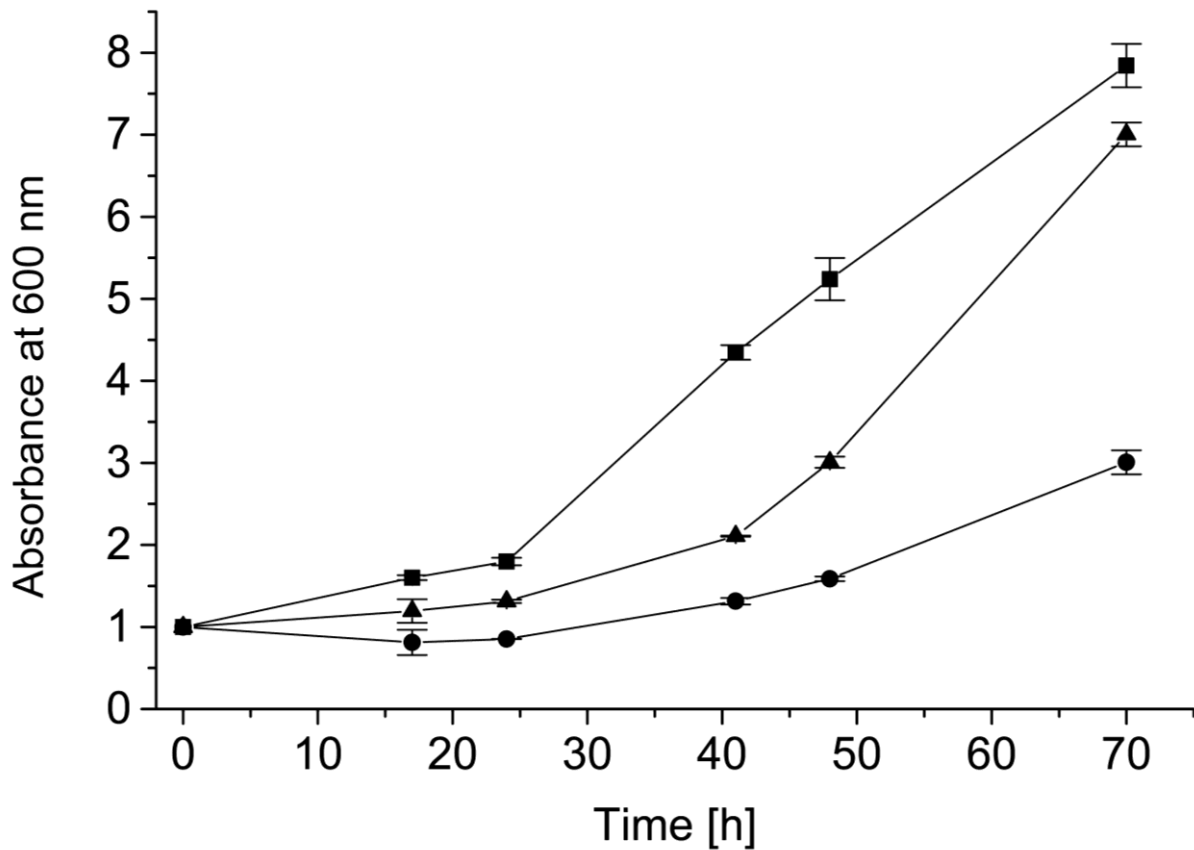


**Figure 15: Increased Li<sup>+</sup> sensitivity of *S. cerevisiae* containing ND5<sub>HS</sub> in ER membranes.** Growth was followed in the presence of 100 mM LiCl. Squares, no ND5<sub>HS</sub> present; triangles, with ND5<sub>HS</sub>-E145V; circles, with wild type ND5<sub>HS</sub>. Mean values from duplicates are presented.

### 2.3.2. Expression, purification and functional characterization of subunit ND5 of complex I from the yeast *Yarrowia lipolytica*

In chapter 2.3.1., we found strong indications for cation transport activity of the isolated ND5 subunit of human complex I in growing cells. However, the expression yield of GFPND5<sub>HS</sub> variants in *S. cerevisiae* was too low to successfully perform *in vitro* cation transport experiments in native membrane vesicles or proteoliposomes (50 - 100 ng/mg membrane protein). Sufficiently strong expression is an absolute requirement for the solubilization, purification and reconstitution of the enzyme into liposomes. Preliminary tests showed that the expression level of GFP-tagged ND5 from complex I of the yeast *Yarrowia lipolytica* (GFPND5<sub>YI</sub>) was one to two orders of magnitude higher than the expression level of the human analog (1 - 5 µg GFPND5<sub>YI</sub> variant/mg membrane protein). The following chapter now describes the characterization of ND5<sub>YI</sub> after expression in *S. cerevisiae*.

#### 2.3.2.1. Sequence alignment of ND5<sub>YI</sub> and related proteins

It is proposed that at least two energy coupling sites exist in the NADH:ubiquinone oxidoreductase of *E. coli* (Steuber 2003; Stolpe and Friedrich 2004); a primary electrogenic proton pump and a secondary Na<sup>+</sup>/H<sup>+</sup> antiporter-like site. The same is proposed for *R. marinus* complex I (Batista, Fernandes et al. 2010). The sequence alignment of *E. coli* NuoL, ND5 from human and *Y. lipolytica*, Nqo12 from *R. marinus* with the Na<sup>+</sup>/H<sup>+</sup> antiporter MnhA from *S. aureus* indicates a high degree of identity, especially within the areas which form the two ion half-channels proposed by (Efremov and Sazanov 2011) (figure 16).

Human ND5	FSLWYMNSDPNINQFFKYLLIFLITMLILVTANNLFQLFIGWEGVGVGIMSFLLLISWYYARA	162
<i>E. coli</i> NuoL	YASWYMRGEEGYSRFFAYTNLFIASMVVLVLADNLLLMYLGWEGVGLCSYLLIGFYTDP	161
<i>Y. lipolytica</i> ND5	YSIGYMETDPHQVRFSSLLSM <b>F</b> TFWMIILVTGSNYFVLFVGV <b>E</b> FIGVTSYLLISFWVTRL	161
<i>R. marinus</i> Nqo12	YSIGYMYEDRGYWKYFSYLNLFIFMMLNLVLADNLTLLFLGWEGVGLCSYLLIGFWYEDF	166
<i>S. aureus</i> MnhA	YSIGYLSKSEQLGNFYCYLLLFMGAMLGVLSDNVIILYLFWELTSFSSFLLLISFWRERQ	156
	:: * : . : : * * : * * . . . : : * * . . * : * * : : :	
Human ND5	DANTAAIQAILYNRIGDIGFILALAWFILHSNS--WDP--QQ--MALLNANPSLTPLLG	215
<i>E. coli</i> NuoL	KNGAAMKAFVVTRVGDVFLAFALFILYNELGTLNFREMVELAPAHFADGNNMLMWATLM	221
<i>Y. lipolytica</i> ND5	QAMKSALS <b>S</b> AVLMNRFGDFAFFVLGLCVIAYVFGTLNYSITIFAT--AYLINTDLLVLIMLA	218
<i>R. marinus</i> Nqo12	KNSEAANKAFIVNRVGDAAFLLAMFLLFREVGSLNFGALLA--DPAALPSGVVAAAVLL	223
<i>S. aureus</i> MnhA	ASIYGAQKSLIITVFGGLSLLGGIILLAIPTQSFYQYMIQH--ASEIQNSPFFIFAMIL	214
	. * . : : . . * : . : : : : : : :	
Human ND5	LLLAAAGKSAQLGLHPWLPSAMEGPTPVSAALLHSSTMVVAGIFLLIRFHPLAENSPLIQT	275
<i>E. coli</i> NuoL	LLGGAVGKSAQLPLQTLWADAMAGPTPVSALHAATMVTAGVYLIARTHGLFLMTPEVLH	281
<i>Y. lipolytica</i> ND5	LFIAAMAKSAQFGLHNWLT <b>L</b> AMEGPTPVSSLLHAATLVTAGIYLLRSANILEYTPTVLF	278
<i>R. marinus</i> Nqo12	LFIGATGKSAQIPLFVWLPDAMAGPTPVSALHAATMVTSGLYLFARISPLALAAPGVLV	283
<i>S. aureus</i> MnhA	IMIGAFTKSAQFPFYIWLDPAMEAPTVSAYLHSATMVKAGLYLIARMTPIFAASQGWVW	274
	:: . * * * * : : * * * * . * * * * : : * * * * : * * * * : * * * * : :	
Human ND5	LTLC LGAITTLFAAVCALTONDIKKIVAFSTSSQLGLMMVTIGINQ-----	321
<i>E. coli</i> NuoL	LVGIVGAVTLLLAGFAALVQTDIKRVLAYSTMSQIGYMFALGVQA-----	327
<i>Y. lipolytica</i> ND5	IILWIGALTTL SAGLIAICSNLKRRI IALSTMSQLGMMTIAIGLSA-----	324
<i>R. marinus</i> Nqo12	VVALVGALTAFMAATI AVTQYDIKKVLA YSTVSQLGYMFMAAGVGA-----	329
<i>S. aureus</i> MnhA	TVT LVGLITLFWASLNATKQDLKGI LAFSTVSQLGMIMAMLGIG AISYHQGDDSKIYA	334
	: * : * . . * . * : * * : * * * * * : * * :	
Human ND5	--PHLAF LHICTHAFKAMLFMCSGSI IHNL-N-----NEQDIRKMGGLLK	364
<i>E. coli</i> NuoL	--WDAAIFHLMTHAFFKALLFLASGSVILACH-----HEQNI FKMGGLRK	370
<i>Y. lipolytica</i> ND5	--YNLALFHL LGHAFKALLFMSAGSI IHSILN-----ESQDIRTYGGLLS	368
<i>R. marinus</i> Nqo12	--FFVSI FHVLT HAFKACFLGSGSVI HAMHHVEHTLHERGHGHGLDPQDMRNMGG LGR	387
<i>S. aureus</i> MnhA	AAFTA AIFHLINHATFKGALFMI TGAVDHST-----GTRDVKKLGGLLT	378
	: : * : * * * * . * * : * * :	
Human ND5	TMPLTSTSLTIGSLALAGMPF-LTG FYSKDHI IETANM--SYTN----AW--ALSI-TLI	414
<i>E. coli</i> NuoL	SIPLVYLCFLVGGAAALSALPLV TAGFFSKDEILAGAMANGHIN-----LMVAGLV	420
<i>Y. lipolytica</i> ND5	YLPYTYICITIASLSLMAMPG-LTGYYTKDII ESTYG--SYSI----SNYVVYWI-AYL	420
<i>R. marinus</i> Nqo12	FMPATR TTYLIATLAIAGFPL-TAGFFSKDEILFKAF EYGYNGH----AYAWIAWILGVV	442
<i>S. aureus</i> MnhA	IMPISFTITVITALSMAGVPP-FNGFLSKESFLETTFTASQANLFSVDTLGYLFPFIIGIV	437
	: * : : : : . * * : * * :	
Human ND5	ATSLTSAYSTRMILLTLTGQPRFPPTLTNINENNT---LLNPIKRLAAG----SLFAGFL	467
<i>E. coli</i> NuoL	GAFM TSLYTFRMI FIVFHGKEQIH-----AHAVKGVTHSLPLIVLLIL----STFVGAL	470
<i>Y. lipolytica</i> ND5	SAVLT CVYSMKILYLFYSNPNNTITYYNAHESN-IYITLPMFILAI F----AMFAGWI	475
<i>R. marinus</i> Nqo12	TALLTAFYMMRSYVLT FEGTPRPW PADQVHPHESP-ATMTLPLWVLAAL----SLVGGFV	497
<i>S. aureus</i> MnhA	GSVFTFVYSIKFIMHIFFGQYKPEQLP-KKAHEVS-I LMLLSPAILATLVIVLGLFP GIL	495
	: : * * : : : . . . . * . . * :	

**Figure 16: Partial sequence alignment of human ND5 and its homologues from *Escherichia coli*, *Yarrowia lipolytica*, *Rhodothermus marinus* and related prokaryotic  $\text{Na}^+/\text{H}^+$  antiporter subunit MnhA of *Staphylococcus aureus*. The areas which may build the first ion half-channel are accentuated in light gray, the areas forming the second potential half-channel are highlighted in dark gray. The investigated mutations are marked in bold. UniProt accession numbers: human ND5 (P03915), *E. coli* NuoL (P33607), *Y. lipolytica* ND5 (Q9B6D3), *R. marinus* Nqo12 (Q4QSB1), *S. aureus* MnhA (Q9ZNG6).**

### 2.3.2.2. The position of disease-associated mutations in ND5

Five of the most frequently observed mutations of ND5 associated with diseases (table 4) were investigated concerning their impact on the transport properties of ND5. It is apparent that they are all clustered inside the membranous layer, and moreover, they are all found in the area of the first of two ion half-channels which were proposed by Efremov and Sazanov (Efremov and Sazanov 2011) and elaborated in this work (figures 17 and 26). Mutations F123L (TM 4), A170V (TM 6), A239T and M240T (TM7) point into the inner lumen of the putative channel, while mutation E144G (TM 5) is situated on the outside of the channel but in immediate vicinity to the neighboring ND4 subunit.

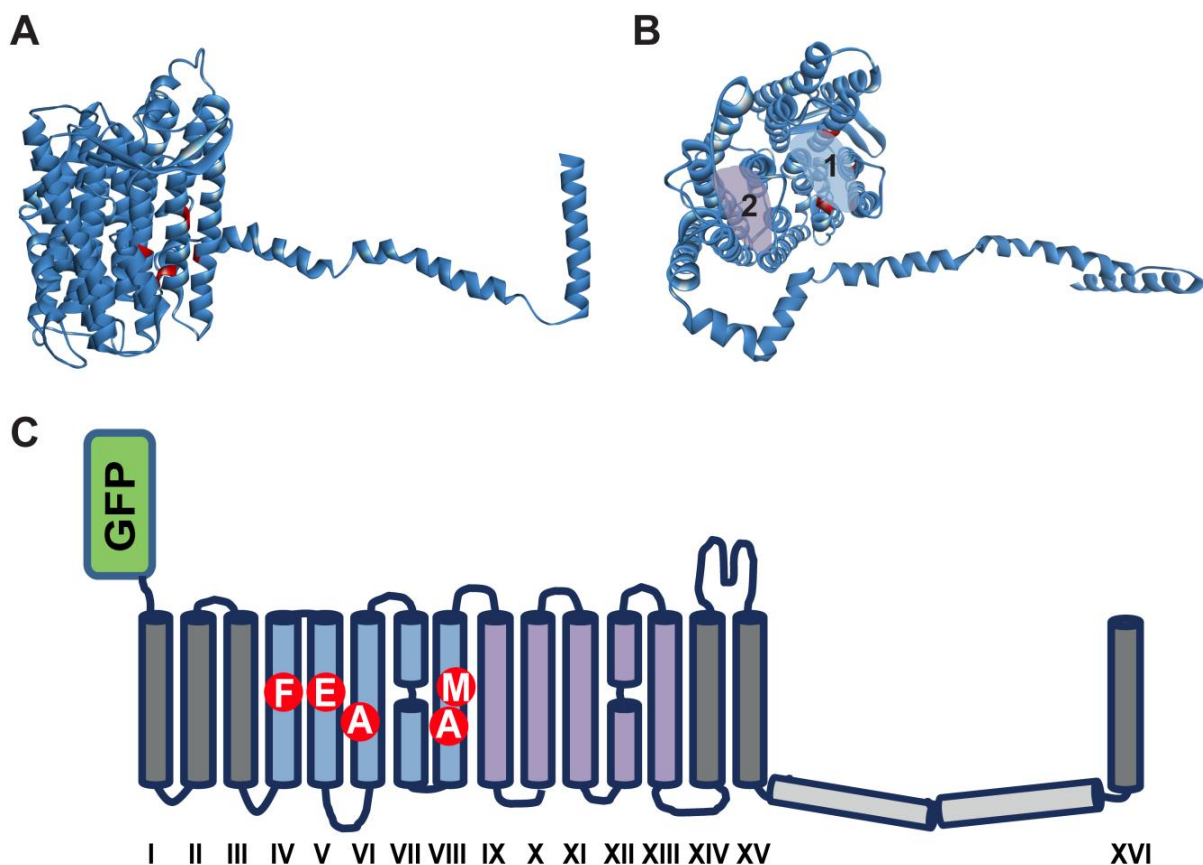


**Figure 17: Position of ND5<sub>YI</sub> in the inner mitochondrial membrane.** **A:** Side view of NuO<sub>L</sub> from *E. coli* complex I (PDB ID: 3RKO). **B:** Top view from the cytoplasm onto NuO<sub>L</sub> (PDB ID: 3RKO), the putative ion half-channels are highlighted in blue and lavender. **C:** Structure-based topology model of GFPND5<sub>YI</sub>. The positions of the investigated mutations in ND5<sub>YI</sub> within the membrane layer are shown in red (F123L, E144G, A170V, A239T, M240T, *Y. lipolytica* numbering).

### 2.3.2.3. Localization of GFPND5<sub>YI</sub> in the ER of *S. cerevisiae*

In accordance with previous results obtained with human ND5 (chapter 2.3.1.3.), *Y. lipolytica* ND5 was found to insert into membranes of the endoplasmatic reticulum of *S. cerevisiae*. The GFP fluorescence displayed almost complete co-localization with the ER membrane protein dpms. A co-localization of immunostained mitochondria and GFPND5<sub>YI</sub> could not be observed (figure 18). Also, expression of the F123L, A170V, A239T, M240T and E144G variants of GFPND5<sub>YI</sub> did not lead to a change in the expression or co-localization pattern (Data not shown).

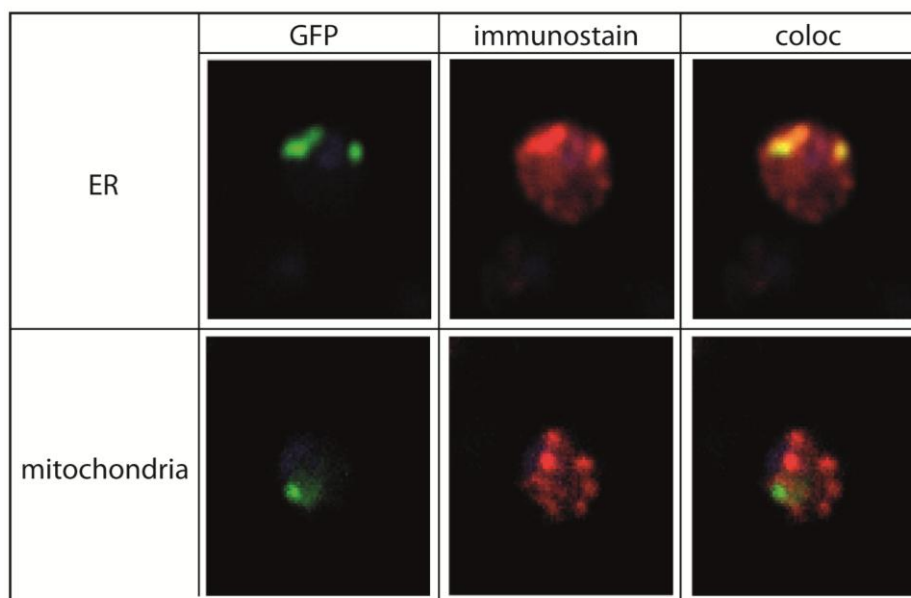


**Figure 18: Localization of GFPND5<sub>YI</sub> in *S. cerevisiae*.** ND5<sub>YI</sub> is detected by the fluorescence of GFP. ER or mitochondria were immunostained (ER: anti-dpms, mitochondria: anti-porin, both in red). The co-localization of both signals (yellow) shows the expression of ND5 in the ER. No visible co-localization of GFPND5<sub>YI</sub> and mitochondria is observed.

### 2.3.2.4. Orientation of GFPND5<sub>YI</sub> within the membrane of native vesicles

The preparation of membrane vesicles with uniformly oriented ND5 was a prerequisite for ion transport measurements. The intactness and sphericity of the vesicles containing GFPND5<sub>YI</sub> was confirmed by cryo-electron microscopy (figure 19). We next investigated the orientation of GFPND5<sub>YI</sub> using a protease protection assay. This method is based on the assumption that lumen-oriented protease cleavage sites in the protein are protected against proteases added to the external medium. In our particular case, cleavage by trypsin after



R24 (numbering ND5 *Y. lipolytica*), an amino acid in the loop after the first transmembrane helix, would yield a fragment of a calculated mass of 29.79 kDa if the loop was exposed to the outside, but no fragment if R24 was oriented towards the inside of the membrane vesicles. By disrupting the membranes with detergent, previously protected sites become accessible and a statement about the uniformity of the orientation of GFPND5<sub>YI</sub> is possible. After 5 minutes of incubation with trypsin, a fragment with an apparent mass of about 26 kDa was found when solubilized vesicles were digested (figure 20A, labeled as GFPND5t). The fragment was not detected in non-solubilized vesicles. Since the fragment did not migrate as far as GFP alone on a 14 % acrylamide gel, we assume it represents GFPND5<sub>YI</sub> cleaved after R24. These results indicate that GFPND5<sub>YI</sub> is uniformly orientated in the membrane, with the N-terminally linked GFP being exposed to the external lumen of the vesicles (figure 20B). In our previous study we used the C-terminally truncated NuoL homolog of ND5 fused to Protein A at its N-terminus, and also observed the 'N-terminus out' orientation of ProtA-NuoL<sub>truncated</sub> in native ER vesicles from *S. cerevisiae* (Gemperli, Schaffitzel et al. 2007).

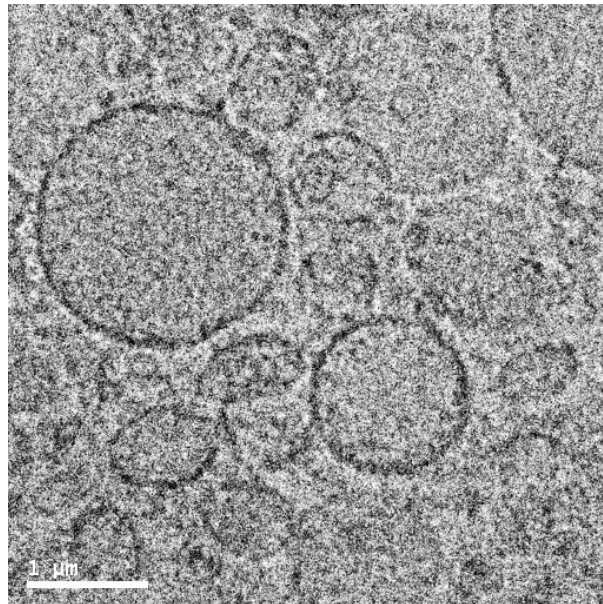


**Figure 19: Cryo electron microscopy of vesicles from *S. cerevisiae* containing GFPND5<sub>YI</sub>.** Micrographs were recorded at a magnification of x 53'000.

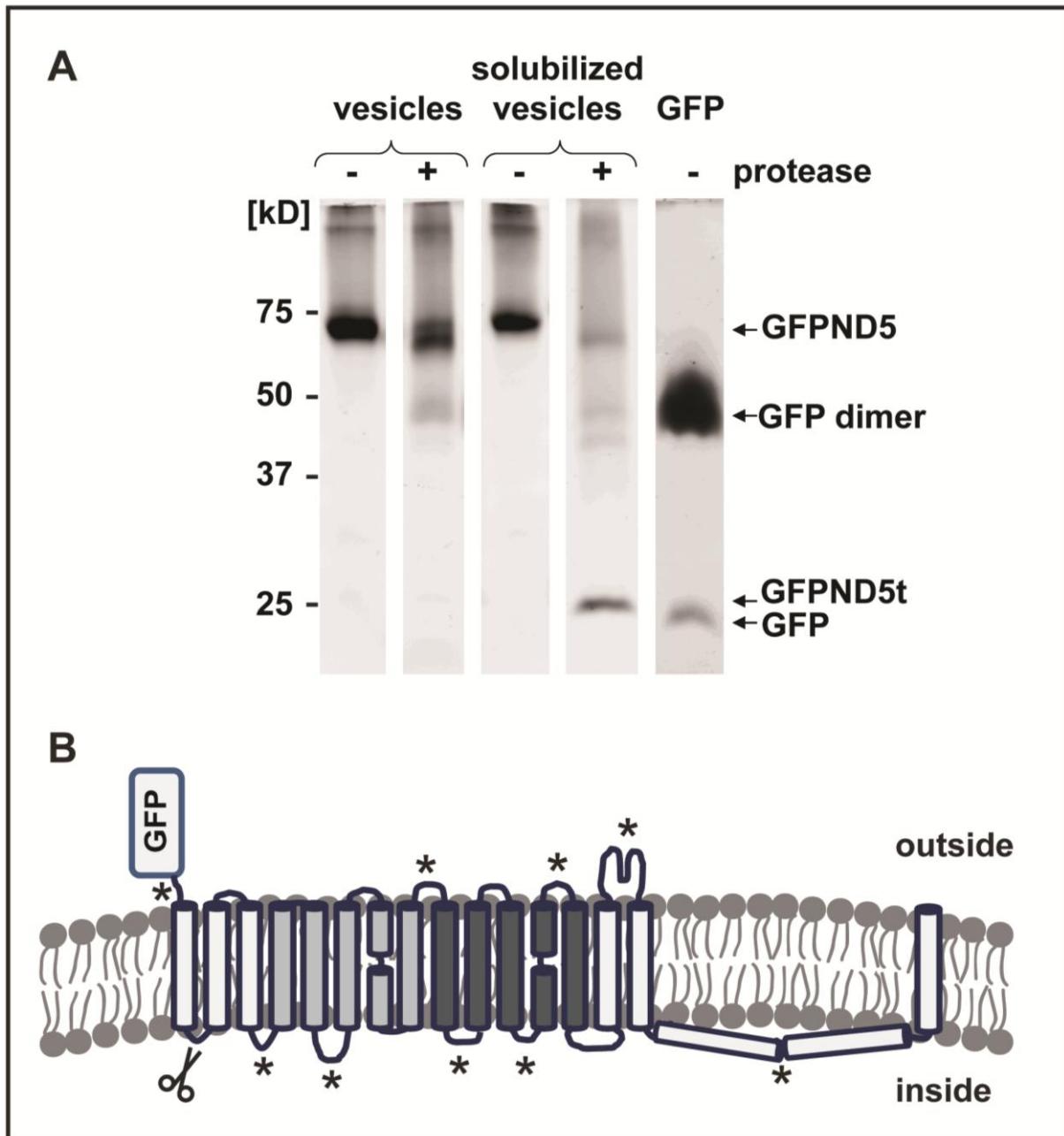


**Figure 20: Fluorescent SDS-PAGE of fragments from a protease protection assay, using trypsin on native and solubilized vesicles from *S. cerevisiae*, containing GFPND5<sub>YI</sub>.** **A:** To analyze the orientation of GFPND5<sub>YI</sub> within the membrane the accessibility of predicted trypsin sites in native (Lane 1 + 2) and solubilized (Lane 3 + 4) membrane vesicles was examined. 150 µg total protein were loaded per lane. **B:** Schematic view of the GFPND5<sub>YI</sub> orientation in the vesicles. Scissors mark the likely cleavage site R24 in the loop after TM1 of ND5<sub>YI</sub>. Asterisks mark other potential trypsin cleavage sites.

### 2.3.2.5. Na<sup>+</sup> transport by GFPND5<sub>YI</sub>

The sodium ion transport properties of the ND5 subunit were investigated using native ER vesicles from GFPND5<sub>YI</sub> expressing *S. cerevisiae* cells. Note that we prepared vesicles at slightly acidic conditions (pH 6.0), while applying a basic pH 8.0 during the assays, since this gave the most stable results of the conditions tested. If ND5<sub>YI</sub> possesses Na<sup>+</sup>/H<sup>+</sup> antiporter activity as proposed for bacterial complex I from *E. coli* (Stolpe and Friedrich 2004), *R. marinus* (Batista, Fernandes et al. 2010) and bovine complex I (Roberts and Hirst 2012), an increased inside [H<sup>+</sup>] may induce Na<sup>+</sup> uptake. The assay was started by adding 5 mM sodium chloride to the external lumen, applying a  $\Delta\mu\text{Na}^+$ . As a control, vesicles from *S. cerevisiae* which did not express GFPND5<sub>YI</sub> were used. Measuring the internal Na<sup>+</sup> content of vesicles by atomic absorption spectroscopy revealed a measurable sodium ion uptake into vesicles containing GFPND5<sub>YI</sub> and into vesicles lacking GFPND5<sub>YI</sub>, but a significantly higher uptake rate was observed with the GFPND5<sub>YI</sub> vesicles between 30 and 90 seconds after the addition of Na<sup>+</sup> (figure 21). During the first 30 seconds, there was an expulsion of Na<sup>+</sup> from the vesicles, with no significant difference between vesicles containing GFPND5<sub>YI</sub> and control vesicles. We do not have an explanation for this observed flux of Na<sup>+</sup> yet. The transport properties of the pathologically relevant ND5<sub>YI</sub> E144G, F123L, A170V, A239T and M240T variants were also investigated. The E144G variant of ND5<sub>YI</sub> showed a significantly lowered uptake of Na<sup>+</sup> compared to wild type ND5<sub>YI</sub> between 60 and 90 seconds (figure 21). The F123L, A170V, A239T and M240T variants of ND5<sub>YI</sub> exhibited Na<sup>+</sup> uptake which was not significantly different from the Na<sup>+</sup> uptake of wild type ND5<sub>YI</sub> (data not shown).

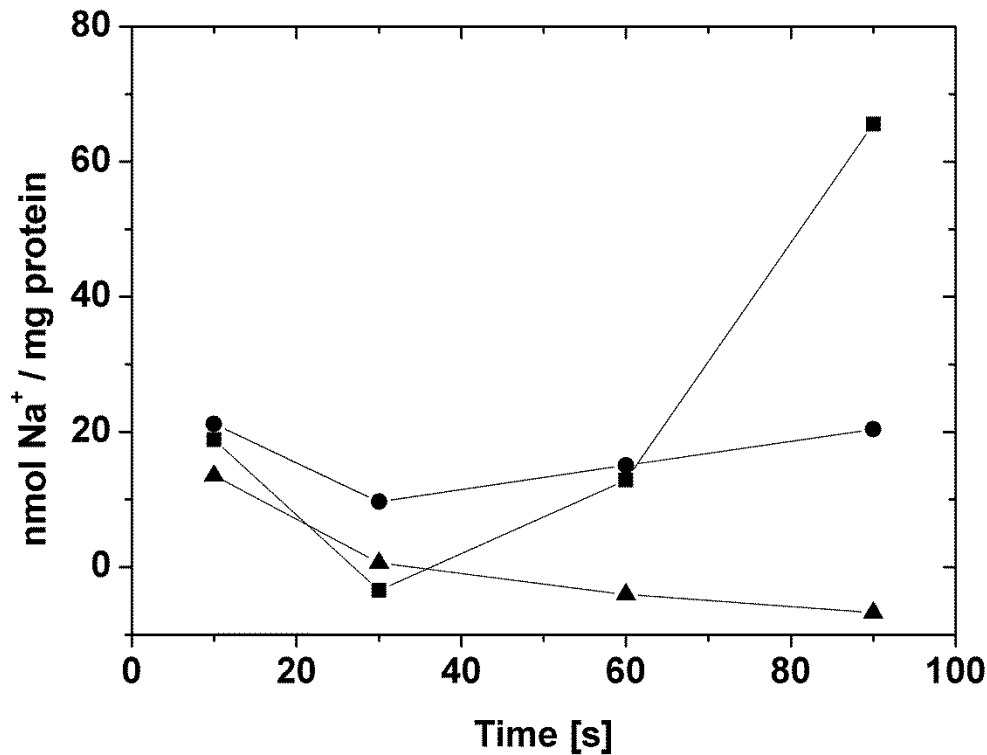


**Figure 21: Na<sup>+</sup> uptake by vesicles containing ND5<sub>VI</sub>, its E144G variant or no ND5.** Net Na<sup>+</sup> uptake by native vesicles containing wild type ND5<sub>VI</sub> (squares), the E144G variant (circles) or control vesicles (triangles) in the presence of a pH gradient (inside acidic). To start the reaction at  $t = 0$  s, 5 mM Na<sup>+</sup> were added to the reaction mixture, and aliquots were withdrawn after 10, 30, 60 and 90 seconds. The internal Na<sup>+</sup> content of the vesicles was determined by atomic absorption spectroscopy. Na<sup>+</sup> content at  $t = 0$  s corresponds to the Na<sup>+</sup> content of the buffer. In the control reactions, vesicles from *S. cerevisiae* transformed with plasmid pRS316 were used. Each uptake experiment was done in triplicate, shown are representative single experiments.

### 2.3.2.6. Solubilization trials

Solubilization screens encompassing 13 different detergents revealed the preference of GFPND5<sub>VI</sub> for zwitterionic detergents. The highest yield of solubilized GFPND5<sub>VI</sub> was achieved with 1 % lauryl dimethylamine oxide (LDAO) (figure 22). LDAO is a detergent with favorable properties for crystallization studies but will denature many membrane proteins (Prive 2007). We thus performed subsequent solubilizations with *n*-Hexadecyl-N,N-dimethyl-3-ammonio-1-propanesulfonate (Zwittergent 3-16) or Tetradecyl-N,N-dimethyl-3-ammonio-1-propanesulfonate (Zwittergent 3-14), which also yielded satisfactory results. The unusually long alkyl chain of these Zwittergents may stabilize the transmembrane domains of the protein by mimicking the lipid bilayer which promotes co-purification of proteins with lipids (Infed, Hanekop et al. 2011).

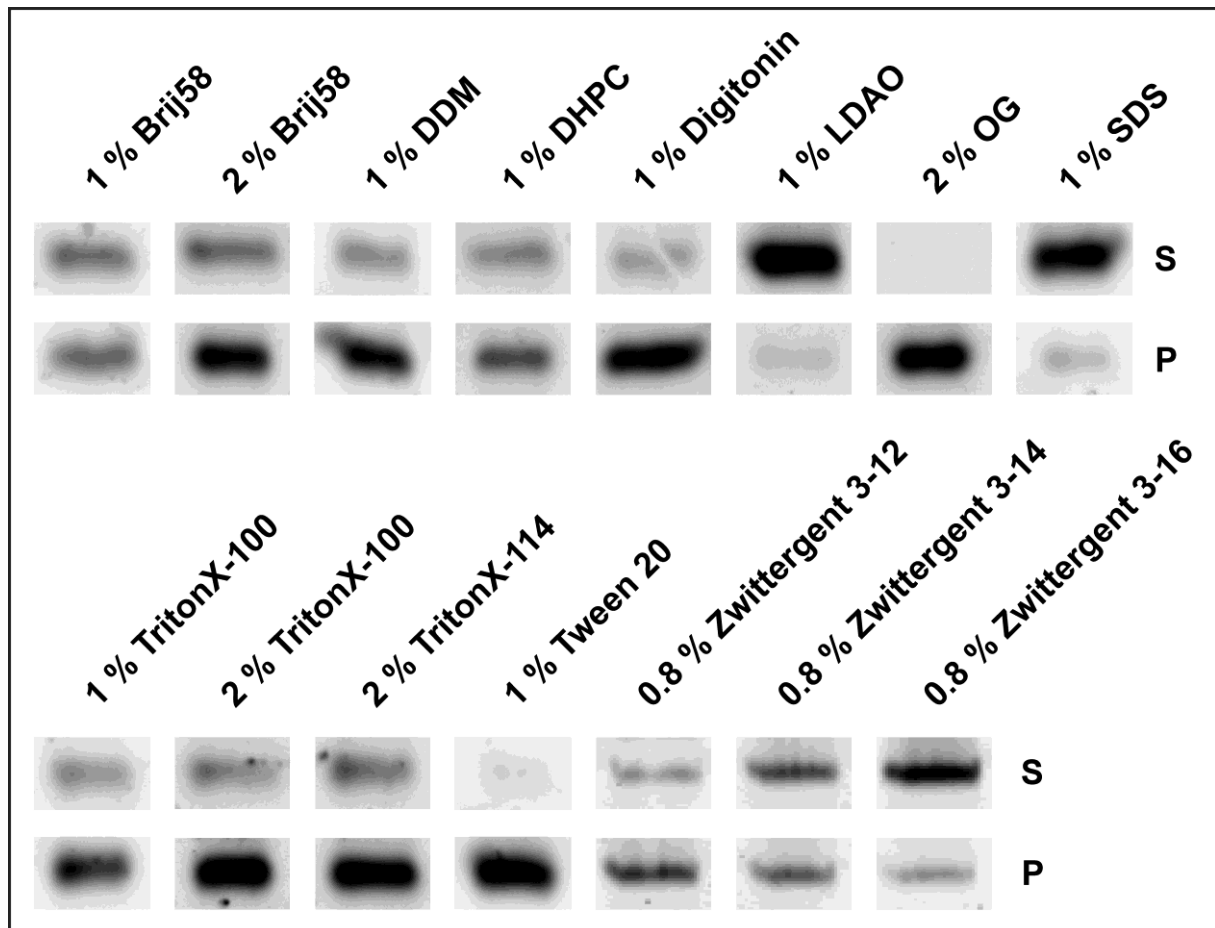


**Figure 22: Solubilization of GFPND5<sub>YI</sub> with different ionic, non-ionic and zwitterionic detergents.** Membranes containing 1 mg protein and indicated amounts of detergent in 200  $\mu$ l TBS were gently agitated at 4 °C for 2 h and then centrifuged at 100'000 x g for 30 min. The pellet was resuspended in the same volume. The supernatants S and pellets P containing non-solubilized membrane proteins were analyzed with SDS-PAGE. GFPND5<sub>YI</sub> was detected by its fluorescence.

### 2.3.2.7. Purification

The enrichment of functional GFPND5<sub>YI</sub> in detergent micelles is a prerequisite for its reconstitution into proteoliposomes. We chose Zwittergent 3-14 to purify His-tagged GFPND5<sub>YI</sub> from *S. cerevisiae* membranes by Ni affinity chromatography (figure 23). The yield of enriched GFPND5<sub>YI</sub> from 60 g of cells (wet weight) was approximately 0.5 mg. The concentration of GFPND5<sub>YI</sub> was determined by absorption spectroscopy of GFP and compared with the total protein concentration determined by the bicinchoninic acid method. A ratio of 0.052 mg ND5<sub>YI</sub>/mg total protein was achieved. When the imidazole concentration in the eluate from the Ni affinity column was decreased by dilution with buffer, GFPND5<sub>YI</sub> precipitated from the solution. Possible reasons are instability of the protein in diluted

solutions, or drop of detergent concentration below the critical micelle concentration. Nevertheless, we used denatured GFPND5<sub>YI</sub> which was solubilized with sodium dodecyl sulfate as standard for the detection and quantification of GFPND5<sub>YI</sub> variants in ER vesicles (see below).

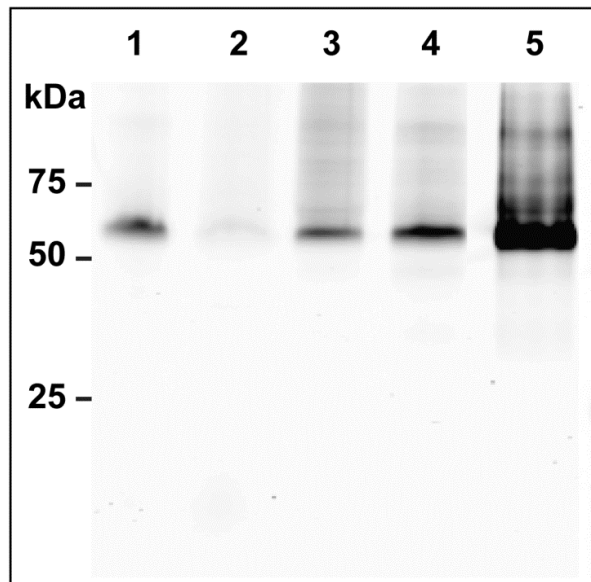


**Figure 23: Purification of GFPND5<sub>YI</sub>.** The fluorescent SDS-PAGE is depicting the enrichment of GFPND5<sub>YI</sub> from ER membranes, after solubilization and immobilized metal ion affinity chromatography. Lane 1: cellular debris, lane 2: supernatant after 50'000 x g centrifugation step, lane 3: ER membrane fraction, lane 4: supernatant after solubilization, lane 5: eluate from Ni-Sepharose HP. In lane 1 - 4, 100 µg total protein were loaded per lane, in lane 5, 25 µg were loaded.

### 2.3.2.8. Quantification and mass spectrometric analysis

GFPND5<sub>YI</sub> and mutant variants from *S. cerevisiae* membranes were quantified by SDS-PAGE as described in chapters 2.2.6. and 2.3.1.3. The membranes contained between 1 - 5 µg GFPND5<sub>YI</sub> variant/mg membrane protein. The expression of all the analyzed ND5<sub>YI</sub> variants was thus comparable. This is shown in figure 24, which depicts the fluorescent SDS-PAGE of the wild type and E144G variant of GFPND5<sub>YI</sub>. Purified His-GFPND5<sub>YI</sub> was used as a standard for quantification. The purified protein as well as the protein from membrane fractions display a lower apparent mass on the gel than expected. This effect can be attributed to the hydrophobicity of the protein, since LC-ESI-MS analysis of tryptic digests confirmed full length expression (figure 25). Since transmembrane stretches contain only few or no cutting sites for trypsin, the fragments that were found mainly originate from GFP and from

hydrophilic loops of the membrane protein, thus a complete sequence coverage could not be obtained. Nevertheless, the simultaneous finding of fragments from the N-terminus and the C-terminus in a single specimen indicate that no proteolytic degradation has taken place (figure 25).

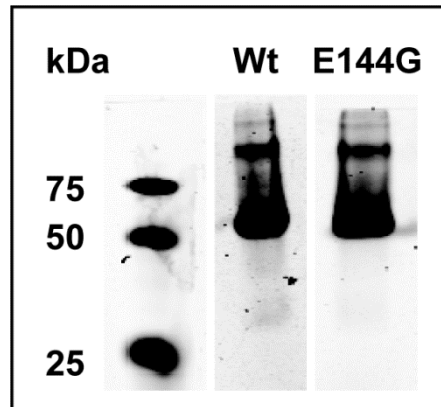


**Figure 24: GFPND5<sub>YI</sub> and its E144G variant are expressed in comparable amounts.** Wt: Lane loaded with membranes containing wild type GFPND5<sub>YI</sub>, 124 µg total protein, E144G: membranes containing the E144G variant of GFP-tagged ND5<sub>YI</sub>, 191 µg total protein. Shown is the in-gel fluorescence of each lane.

MHHHHHHHHGGGGSTSM**SGEELFTGVVPILVELDGDVNGHKFSVRGEGEGDATNGKLT**LKFICTTGK****  
*LPVPWPTLVTTLT***YGVQCFSRYPDHMKRHDFFKSAMPEGYVQERTISFKDDGYKTRAEVK**FEGDTLVN****  
**RIELKGIDFKEDGNILGHKLEYNFN***SHNVYITADKQKNGIKANFKIRHNVEDGSVQLADHYQQNTPIGDGP*  
*VLLPDNHYLSTQSVLSKDPNEKRDHMLLEFVTAAGITHGMDELYKNSMYNAISLIILPCISWLFPLFFGR*  
**QLGYV**FVTR**MTSTLIITTLITYYYFYQLLGNNNPINLELFNYLNIDYLDINYNFEIDALTITM**L**LAITTISSMVH**  
*IYSIGYMETDPHQVRRFFSLLSMFTFWMIILVTGSNYFVLFVGVWFEFIGVTSYLLISFWVTRLQAMK**SALSAVL***  
**MNRFGDAFFVLGLCVIAYVFGTLNYSTIFATAYLINTDLLVIMLALFIAAMAKSAQFGLHNWLT**L**AMEGP**  
*TPVSSLLHAATLVTAGIYLLRSANILEYTPVLFIIILWIGALTTLSAGLIAICSNDLKRIIALSTMSQLGMMTIA*  
*IGLSAYNLALFHLLGHAFKALLFMSAGSIIHSILNESQDIRTYGGLLSYLPYTYICITIASLSLMAMPGLTGY*  
*TKDIIIESTYGSYSISNYVVYWIAYLSAVLTCVYSMKILYLT**FYS**NPNNNTITYYNAHESNIYITLPMFILAI**FAM***  
*FAGWILKDIYLGVGTDVFGTHILPNNFSYFDTEFSITQFYKLLPLISAILVSVILIVVLNEFFAIVFNLN**KYINTV***  
**YSIFNQKL**VSDQILNHFIIFKGLV**TSGNIAHHV**DKG**SLYRLGPVGINRLLNKASYNVINLSSNTRSSLSMN**  
*SMLILITIVSLLLLVLMNVNFIIVIPVLISILYILFS*

**Figure 25: LC-ESI-MS analysis of purified His-GFPND5<sub>YI</sub>.** The fragments of ND5<sub>YI</sub> which were found in the mass spectrometric analysis are highlighted in bold. The sequence of SFGFP has an italic font.

## 2.4. Discussion

### 2.4.1. Sequence alignment of ND5 and related proteins

The structure of NuoL reported by Efremov and Sazanov strengthens the notion that this subunit - and its eukaryotic homolog ND5 - are involved in ion channeling and the generation of a proton motive force (PMF) and also provide a structural means to couple the energy from the electron transport chain to the opening and closing of ion channels (Efremov and Sazanov 2011; Efremov and Sazanov 2011). The mechanism of channeling and the nature and stoichiometry of the charged moieties involved is still unclear. Studies investigating the holo-complex from *E. coli* and from the related enterobacterium *K. pneumoniae*, supplied indications that the complex works as a primary Na<sup>+</sup> pump which is not driven by the PMF (Steuber, Schmid et al. 2000; Steuber 2003). For the ND5 homolog from *E. coli*, a Na<sup>+</sup> transport function without any evidence for stimulation by the PMF was proposed (Gemperli, Schaffitzel et al. 2007). Other studies revealed a secondary Na<sup>+</sup> transport function, stimulated by the PMF, but with differing evidence concerning the direction of Na<sup>+</sup> and H<sup>+</sup> translocation (Stolpe and Friedrich 2004; Roberts and Hirst 2012). Investigations of different *E. coli* complex I subunits (NuoL, M, and N) showed that the ND5 homolog NuoL was able to complement a Na<sup>+</sup>/H<sup>+</sup> antiporter deficient mutant of *B. subtilis* (Mathiesen and Hägerhäll 2002; Mathiesen and Hägerhäll 2003). This suggests that the mitochondrial homolog of NuoL, the ND5 subunit of complex I, also exhibits antiporter activity. A PMF-dependent antiporter function is also proposed for complex I from *R. marinus* (Batista, Fernandes et al. 2010). These hypotheses prompted us to include the corresponding ND5 homologs from *E. coli* and *R. marinus* complex I, as well as the sequence of a Na<sup>+</sup>/proton antiporter, the MnhA subunit from *S. aureus* in the alignment. It is noteworthy that the areas which show the highest sequence conservation are the ones proposed to build the ion channels (Efremov and Sazanov 2011). Particularly, these regions comprise TM4 - TM8, forming the predicted channel 1, and TM9 - TM13, forming the predicted channel 2 (figures 17 and 26). The identity of ND5 homologs and bacterial Na<sup>+</sup>/proton antiporters in key areas strongly suggests that ND5 and its homologs are also able to transport sodium ions, which we went on to demonstrate in this study.



### 2.4.2. Expression and localization of ND5

Allotopic expression and mitochondrial targeting of the mitochondrially encoded, hydrophobic ND4 subunit of complex I has been demonstrated in mammalian cells (Guy, Qi et al. 2002) but could not be reproduced in a later study (Oca-Cossio, Kenyon et al. 2003). Here we describe the targeted production of the mitochondrially encoded ND5 subunit from man and from the yeast *Y. lipolytica* in *Saccharomyces cerevisiae*, paving the way for the functional and structural analysis of a whole family of these very hydrophobic, mitochondrial proteins which are frequently altered in neurodegenerative diseases (Wallace 1999; Leonard and Schapira 2000). In the absence of a signal sequence, ND5<sub>H5</sub> and ND5<sub>YI</sub> were localized to the ER membrane. The sorting mode of ND5<sub>H5</sub> was altered by adding a mitochondrial targeting sequence, with the majority of ND5<sub>H5</sub> co-localizing with mitochondrial marker protein. We chose a signal sequence of a matrix-resident ATPase subunit, previously used to engineer a matrix-targeted GFP (Arimura and Tsutsumi 2002), and could confirm the integration of the 67 kDa, hydrophobic ND5<sub>H5</sub> polypeptide in the inner mitochondrial membrane. The insertion of ND5<sub>H5</sub> probably required the TOM and TIM complexes (Pfanner and Meijer 1997). Transfer of ND5<sub>H5</sub> into the matrix space and subsequent reinsertion into the inner mitochondrial membrane could depend on the action of TIM23, mtHsp70 and OXA1, or could be catalyzed via the TIM22 complex (Stuart and Neupert 1996; Stojanovski, Johnston et al. 2003).

### 2.4.3. Orientation of GFPND5<sub>YI</sub> in native ER vesicles

Knowledge of the orientation of the GFPND5<sub>YI</sub> fusion protein within the vesicle or liposome membrane was a requirement for the subsequent transport studies aimed at elucidating the function of the ND5<sub>YI</sub> subunit from complex I. More important than to know the effective orientation was to assure that the protein is uniformly orientated. The analysis with a protease protection assay using trypsin indicates that a uniform orientation is given. The lack of a similar cleavage pattern in non-solubilized vesicles indicates that a majority of the vesicles adopt the same orientation and that most trypsin sites are oriented to the internal side of the vesicles and thus only become accessible after solubilization. In addition, we can say with high confidence from these and previous (Gemperli, Schaffitzel et al. 2007) experiments that the vesicles are formed in the 'right side out' orientation, with the N-

terminally fused GFP on the outside (figure 20B). This is best seen with the fragment appearing at about 25 kDa when using solubilized vesicles; it lies above the band of GFP alone, but is too small to be the fragment cleaved after TM 8 at R265, which is the closest potential trypsin site that lies on the 'outside'. Instead it is most likely a fragment cleaved on the 'inside', directly after TM 1 at R24 of *Y. lipolytica* ND5. There is the possibility that the appearance of additional fragments after solubilization does not stem from the 'opening' of uniformly oriented vesicles but is an effect of denaturation of the protein by the detergent, as a denatured and partially unfolded protein would also result in more accessible trypsin sites. Although zwitterionic detergents, such as Zwittergent 3-16 used in this work, are usually reported as being less denaturing than ionic detergents and able to stabilize membrane proteins (Infed, Hanekop et al. 2011), this possibility has to be taken into account. By mass spectrometric analysis, we could show that ND5<sub>YI</sub> was isolated in its full length. However, after proteolysis with trypsin we were not able to detect fragments from the more hydrophobic stretches of ND5<sub>YI</sub>. Better results may be achieved by proteolysis with chymotrypsin or other endopeptidases that preferably cleave at hydrophobic residues. Once the Na<sup>+</sup> transport activity of solubilized and reconstituted ND5 (in proteoliposomes) has been confirmed, this would unequivocally demonstrate that no denaturation and unfolding have occurred during solubilization.

#### **2.4.4. ND5 imbalances the cation homeostasis of intracellular organelles**

We previously showed that the ND5 homolog from a bacterial complex I, the NuoL subunit, functions as transporter for Na<sup>+</sup> and K<sup>+</sup> when inserted in ER membranes from *S. cerevisiae* (Gemperli, Schaffitzel et al. 2007). The ND5/NuoL proteins are evolutionary related to subunits of multicomponent cation/H<sup>+</sup> antiporters (Mathiesen and Hägerhäll 2003). Understanding the catalytic function of mitochondrially encoded complex I subunits like ND5 which are frequently altered in neurodegenerative disorders is of utmost importance when it comes to understanding the causative link between mutations in mitochondrial DNA and diminished complex I activity in patients (Thorburn, Sugiana et al. 2004). We found that the isolated ND5 subunit of human complex I increased the resistance to elevated Na<sup>+</sup> and K<sup>+</sup> concentrations if present in mitochondria and ER from *S. cerevisiae*. This is in marked contrast to the situation observed in the presence of Li<sup>+</sup>, where ND5<sub>HS</sub> in the ER increased

the sensitivity of cells towards this alkali cation. Interestingly, the toxic effect of  $\text{Li}^+$  was diminished when the E145V variant of ND5<sub>H5</sub> was present in the ER, supporting the notion of  $\text{Li}^+$  flux catalyzed by ND5<sub>H5</sub> which is diminished in case of the E145V variant of the protein. *S. cerevisiae* possesses several transport systems for the detoxification of alkali metal cations. Surplus  $\text{Li}^+$  and  $\text{Na}^+$  are sequestered by  $\text{Na}^+$ -ATPase Ena1/Pmr2 and  $\text{Na}^+/\text{H}^+$  antiporter Nha1 or internalized by endosomal  $\text{Na}^+/\text{H}^+$  exchanger Nhx1p (Kinclova-Zimmermannova, Flegelova et al. 2004; Kinclova-Zimmermannova and Sychrova 2006) Intracellular  $\text{K}^+$  levels are held at an optimal steady state of 200 - 300 mM by active import (Trk1p and Trk2p) and  $\text{K}^+$  channels (Tok1p and Nsc1p) (Rodriguez-Navarro 2000; Sychrova 2004). Yeast mitochondria are lacking the specific  $\text{Na}^+/\text{H}^+$  antiporter, but contain a homolog of the mammalian  $\text{K}^+/\text{H}^+$  antiporter which is unspecific as it will extrude all alkali cations out of the mitochondrial matrix (Welihinda, Trumbly et al. 1993). It is proposed that the altered salt tolerance of *S. cerevisiae* expressing ND5<sub>H5</sub> reflects a change of intracellular cation gradients caused by ND5<sub>H5</sub>. The effect of ND5<sub>H5</sub> could be due to a general stress response of *S. cerevisiae*, induced by expression of this hydrophobic membrane protein. However, we favor a direct role for ND5<sub>H5</sub> linked to its putative cation transport activity: Introducing a single point mutation (E145V) altered  $\text{Li}^+$ - and  $\text{K}^+$ -dependent growth behavior, yet the expression levels of wild type ND5<sub>H5</sub> and its E145V variant did not differ significantly. The E145V mutation of ND5<sub>H5</sub> is observed in PD patients (Parker and Parks 2005), but an impact of this mutation on the function of ND5<sub>H5</sub> has not yet been reported. Our study illustrates how *S. cerevisiae* is suited to study the effect of mutations on the function of mitochondrially encoded complex I subunits by an *in vivo* test based on the cation-dependent growth behavior of the cells, and paves the way for the *in vitro* analysis of the catalytic properties of ND5.

#### **2.4.5. A putative role of E144 of the ND5<sub>Y1</sub> subunit of complex I in cation transport**

The results of the transport studies clearly show that the presence of wild type GFPND5<sub>Y1</sub> in native vesicles raises the  $\text{Na}^+$  uptake rate in comparison to the control vesicles without ND5<sub>Y1</sub>. The quantification of the uptake rate is difficult: The observation of the effective sodium ion content within the vesicles is always discontinuous, and GFPND5<sub>Y1</sub> only represents a percentage of the total protein content within the membranes (1 - 5  $\mu\text{g}/\text{mg}$  total protein). Still, it is possible to differentiate the  $\text{Na}^+$  content of vesicles containing wild type, mutant, or

no GFPND5<sub>Yl</sub>. The most drastic effect on Na<sup>+</sup> uptake was observed with the E144G variant of ND5<sub>Yl</sub>. The detected Na<sup>+</sup> uptake was significantly lower than with wild type GFPND5<sub>Yl</sub>, which strongly suggests that the glutamic acid residue on position 144 in the *Y. lipolytica* ND5 participates in cation translocation. We have shown here that a mutation of E144 reverts the negative impact of human ND5 on cation homeostasis in *S. cerevisiae*, and an involvement of E144 in proton translocation was also already demonstrated for the ND5 homolog from *E. coli* (Nakamaru-Ogiso, Kao et al. 2010).

#### 2.4.6. Correlation between structure and function of ND5

The results described herein allow speculating about the structure-function relationship of ND5 with respect to the structure of the related NuoL subunit of complex I from *E. coli* (Efremov and Sazanov 2011). Efremov and Sazanov propose two opposing half-channels connected by a series of polar or charged residues in the middle of the membrane. They argue that the first putative channel is closed to the periplasm and the second channel is closed to the cytoplasm by hydrophobic residues and thus a single, proton translocating pathway is most likely. Indeed residues such as Leu 130, Trp 143, Ala 261 and Leu 265 on one side and Leu 308, Phe 341, Leu 345 and Phe 346 on the other side create hydrophobic 'choking points' that seem to block off further progress of the respective pathways. Interestingly, these residues are strongly conserved in complex I and H<sup>+</sup>/Na<sup>+</sup> antiporter subunits, which raises the question what role they might play in an antiporter environment. Further analysis of the structure of NuoL concerning cavities and additional pathways revealed that the areas behind the choking points contain cavities linking to the surface that can accommodate protons or sodium ions. These cavities are lined with hydrophilic residues, most of which are conserved (figure 26). One can thus propose that instead of two half-channels, two continuous channels exist, the passage through which is controlled by essential hydrophobic residues, acting as gates opened and closed by conformational change. The first such channel is accessible on the cytoplasmic side as described in (Efremov and Sazanov 2011), but with Phe 123 has to pass a first choking point on this side already. Phe 123 is highly conserved and mutations in its human homolog F124 are linked to MELAS, PD and Leigh disease (Taylor, Morris et al. 2002; Parker and Parks 2005; Zhadanov, Grechanina et al. 2007). The channel continues on past Trp 143 to the periplasm, supported

by the sulphurs of Met 127 and Met 139 and the side chains of Tyr 264, Arg 268, Ser 85, Asp 134 and Asp 82. Mutations in Asp 134 and Asp 82 were shown to decrease proton pumping activity (Nakamaru-Ogiso, Kao et al. 2010). The second channel comprises the periplasmic half-channel as described in (Efremov and Sazanov 2011), continues on by Lys 342, His 338, Thr 312 and His 254 and further to the cytoplasm by Met 234, Ser 250, Lys 305, Thr 247, Asp 303, Gln 360, Ser 349, Tyr 106 and Glu 359. Mutation of Asp 303 has been shown to decrease proton pumping activity (Nakamaru-Ogiso, Kao et al. 2010) and the human Met 234 homolog was mutated in patients suffering from MELAS syndrome (Liolitsa, Rahman et al. 2003).

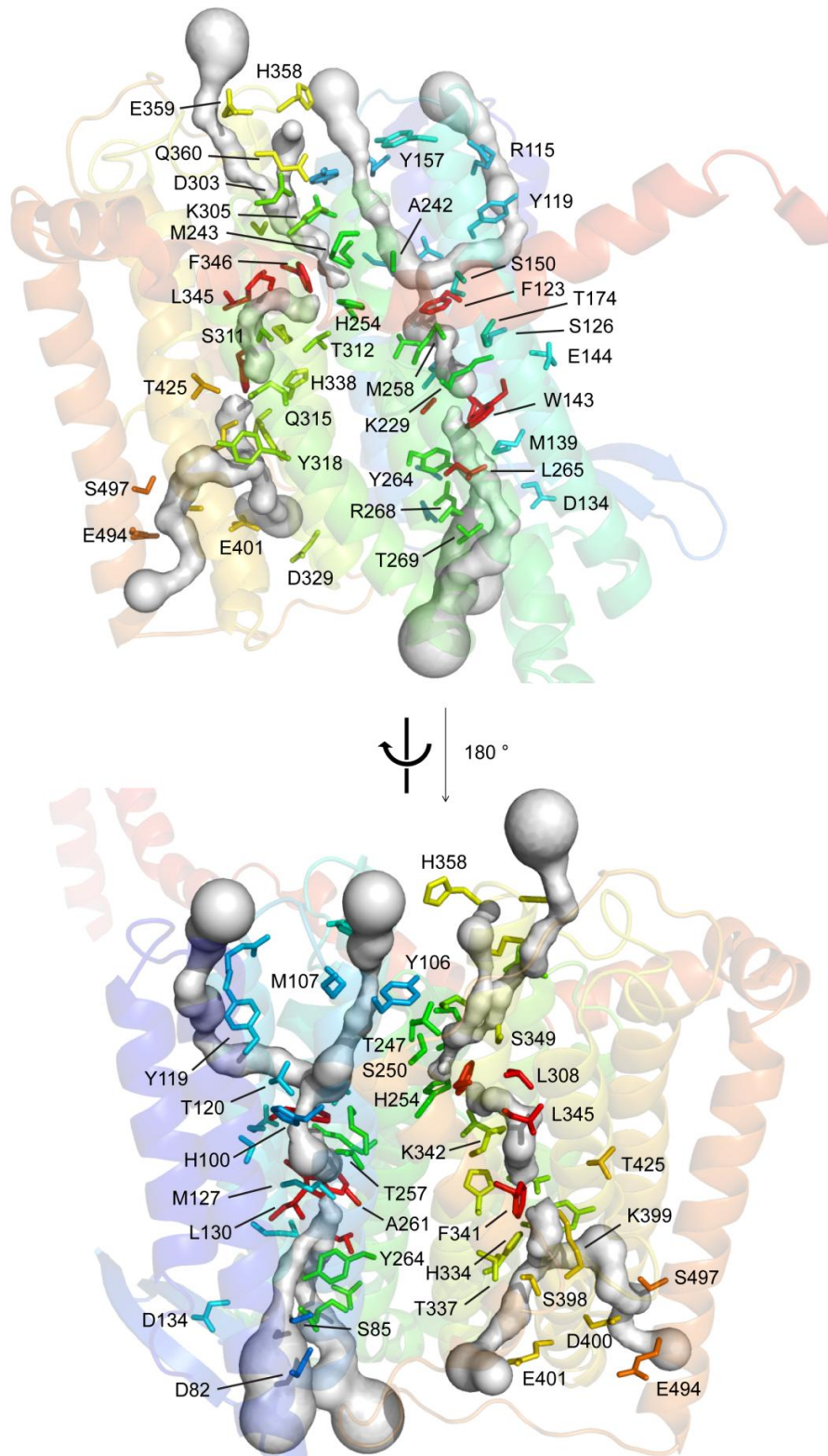


**Figure 26: Cavity search suggests the existence of two membrane-spanning ion transport pathways in ND5 homolog NuoL.** Subunit NuoL of the membrane arm of *E. coli* complex I (PDB 3RKO) was analyzed for cavities with a 1.4 Å radius probe using the program CAVER. Tunnels that could support ion translocation and supporting polar side chains were visualized with PyMOL. Two putative ion transport pathways to the cytosolic or periplasmic surface respectively are shown for each channel. Hydrophobic side chains forming chocking points in the channels are drawn in red.

### 2.4.7. Model of H<sup>+</sup>/Na<sup>+</sup> Antiport in NuoL (ND5)

The homology of NuoL/M/N to antiporter subunits prompted us to ask if antiporter function is retained in complex I. Secondary Na<sup>+</sup> transport coupled to proton translocation would be in accord with findings that the ND5 homolog from *E. coli* translocates protons in the opposite direction as Na<sup>+</sup> (Mathiesen and Hägerhäll 2003) and that Na<sup>+</sup> was not necessary for the proton transport but only stimulated proton transport by the holo-complex I from *R. marinus* (Batista, Fernandes et al. 2010). The Na<sup>+</sup> uptake experiments presented in this study indicate an important role of the E144 in the transport process (figure 21). With the elucidation of the crystal structure of the membrane domain of complex I, the functional understanding of this complex machine has increased. A continuously rising number of mutation and transport studies will eventually narrow down the pathways and precise transport mechanism. Using the data available, we present three different models of H<sup>+</sup>/Na<sup>+</sup> antiport:

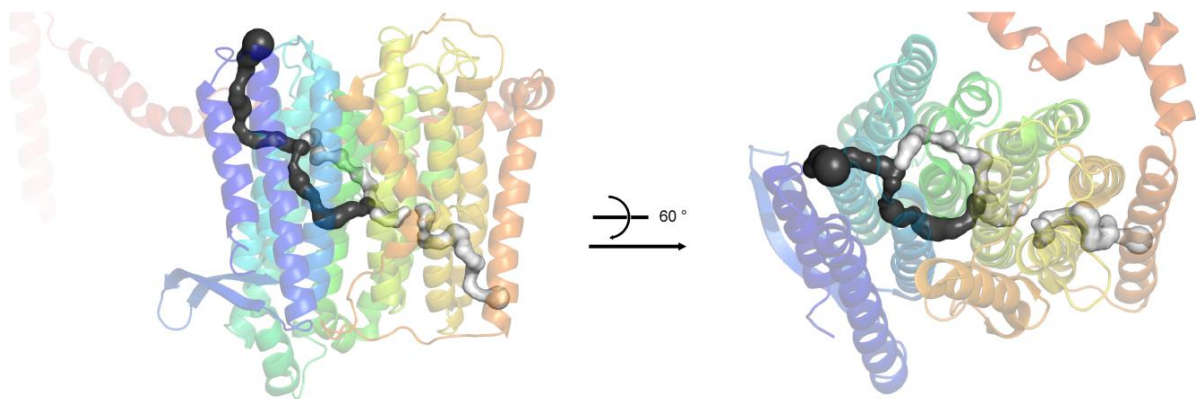


**Figure 27: Two half-channels.**

Assuming there is only a single continuous channel through the membrane, antiport function is still thinkable: A proton entering from the cytoplasmic side and a sodium ion coming from the periplasm coordinate to polar residues Thr 257 and His 254 respectively on central TM8. A conformational signal, transmitted by the long, amphipathic helix of NuoL on to discontinuous transmembrane helix 7, allows the two ions to exchange simultaneously (figure 27). The cavities on either side of TM8 are large enough to accommodate two ions at once. This model requires a gating mechanism that keeps the half-channels closed from the outside until an antiport cycle is fully completed. Phe 123 and Phe 341 seem ideally placed

to assume a conformation which interrupts incoming ion flow from the cytoplasm or the periplasm respectively (figure 26).

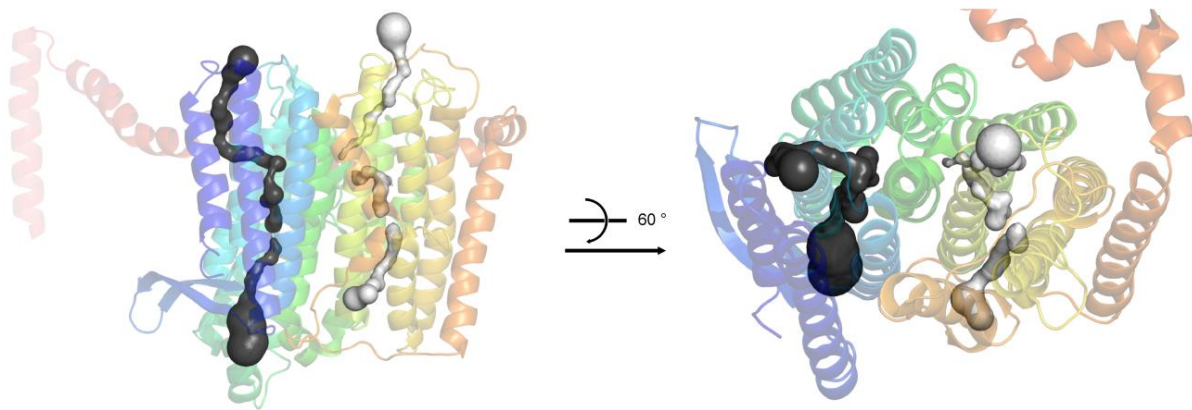


**Figure 28: Two discrete channels.**

As ionizable residues in the proposed connection between ion half-channels 1 and 2 are quite far apart, it can be argued that no ion transport occurs across this cavity, but rather that the space is necessary for the conformational flexibility of TM8 (figure 28). As central helix of NuoL, TM8 'communicates' between the two channels, coordinating the gating system which is invariably necessary in any directed ion transport. One such gating mechanism may be formed by the electrostatic interactions of Lys 229, Glu 144 and or Asp 178; a salt bridge between the glutamate and lysine residues may induce a rotation in TM5, closing off channel 1 from the periplasm with the bulky Trp 143.

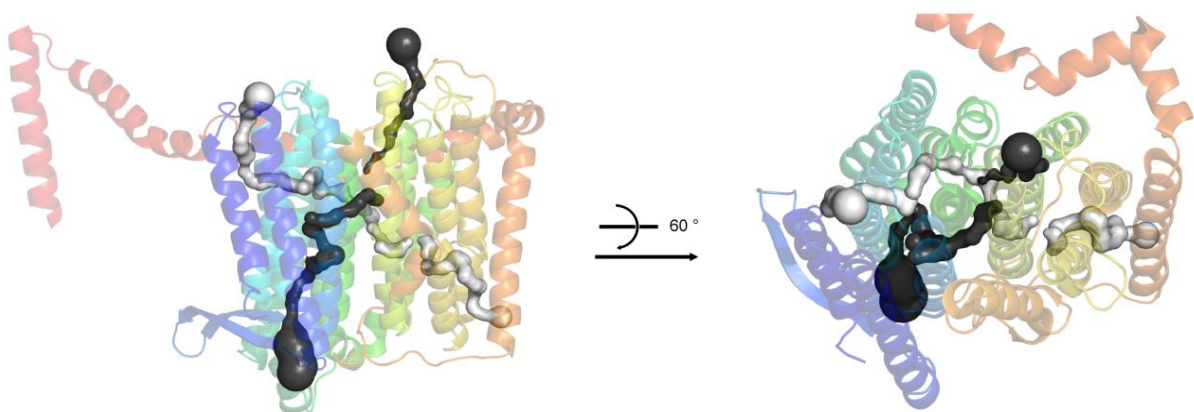


**Figure 29: Two crossing channels.**



Figure 29 depicts a combination of the first two models. Ions enter from the cytoplasmic and the periplasmic half-channel and are exchanged by a simultaneous or alternating-access mechanism at TM8, which therefore controls most of the gating. In the light that most mutation studies in NuoL/ND5 up to date have focused on charged conserved residues of the first putative ion channel, it would be promising to investigate mutations which are localized in putative channel two and in conserved hydrophobic residues to further investigate the sodium ion transport and gating properties of the ND5 subunit.

## Chapter 3

### Structure-function analysis of catalytic subunits of the Na<sup>+</sup>-translocating NADH:ubiquinone reductase from *Vibrio cholerae*

**Steffen, W.**, Muras, V., Tao, M., Steuber, J. and G. Fritz  
"Structural basis for silver inhibition of *Vibrio cholerae*."  
Manuscript in preparation

**Steffen, W.**, Casutt, M.S., Steuber, J. and G. Fritz  
"Structure-function analysis of the NADH-oxidizing domain of the Na<sup>+</sup>-translocating NADH:quinone oxidoreductase from *Vibrio cholerae*."  
Manuscript in preparation

**Steffen, W.\***, Nedielkov, R.\*, Steuber, J. and Möller, H. M. "NMR reveals double occupancy of quinone-type ligands in the catalytic quinone binding site of the Na<sup>+</sup>-translocating NADH:quinone oxidoreductase from *Vibrio cholerae*."  
\*Authors contributed equally.  
Manuscript in revision

### 3.1. Introduction

#### 3.1.1. Silver, a potent bactericide and inhibitor of the Na<sup>+</sup>-NQR

Safe drinking water is the *sine qua non* of public health (Aldhous 2003). Since antiquity, silver is used for disease control without reports on toxic side effects, and nowadays, many effective water purification systems for public and individual applications rely on the bacteriotoxic effect of silver (Davies and Etris 1997; Silver 2003). The mode of action of Ag<sup>+</sup> against bacteria is not understood, but the microcidal activity of silver was proposed to result from the inhibition of bacterial respiration (Silver 2003). However, the target molecule, and the mechanism of its modification by Ag<sup>+</sup>, remained unknown. Pathogenic strains of the water-borne bacterium *Vibrio cholerae* cause the diarrheal disease cholera (Sack, Sack et al. 2004) and are efficiently killed by Ag<sup>+</sup> (Aguilar, Jimenez et al. 2006). By the help of a respiratory Na<sup>+</sup> pump, *V. cholerae* maintains an electrochemical Na<sup>+</sup> gradient across the inner membrane to drive central processes like flagellar rotation, nutrient uptake, and detoxification (Häse and Barquera 2001). The respiratory Na<sup>+</sup> pump, also called Na<sup>+</sup>-translocating NADH:quinone oxidoreductase (Na<sup>+</sup>-NQR), is a membrane-bound enzyme complex composed of six subunits (NqrABCDEF) which contains four flavins, one [2Fe-2S] cluster and ubiquinone-8 as cofactors (Barquera, Ramirez-Silva et al. 2006; Tao, Casutt et al. 2008; Casutt, Nediellkov et al. 2011) (table 2). Ag<sup>+</sup> inhibited O<sub>2</sub>-dependent NADH oxidation by subcellular membrane fractions from *V. cholerae* (Lin, Türk et al. 2007), and the Na<sup>+</sup>-NQR from the related *Vibrio alginolyticus* was inhibited by Ag<sup>+</sup> *in vitro* (Unemoto, Ogura et al. 1993; Steuber, Krebs et al. 1997). We speculated that the reported sensitivity of *V. cholerae* cells towards Ag<sup>+</sup> (Aguilar, Jimenez et al. 2006) resulted from the inactivation of the Na<sup>+</sup>-NQR, leading to diminished respiratory activity and energy production, and eventually, to the killing of this human pathogen. Here, the characterization of an Ag<sup>+</sup>-insensitive C378A variant of the NADH-oxidizing FAD domain of the Na<sup>+</sup>-NQR is presented, and the 3D structure of the FAD domain in complex with Ag<sup>+</sup> is shown. Furthermore, we demonstrate that the insertion of this cysteine mutation into *V. cholerae* expressing the Na<sup>+</sup>-NQR causes the bacteria to exhibit an increased tolerance against Ag<sup>+</sup>. The results are the basis for the development of silver-based drugs targeting the Na<sup>+</sup>-translocating NADH dehydrogenase, a central enzyme of bacterial catabolism which is not found in higher eukaryotes.

### 3.1.2. Structure and function of the NADH oxidizing domain of the Na<sup>+</sup>-NQR, a flavoprotein

Flavoproteins belong to the most-studied and versatile classes of enzymes, catalyzing redox reactions ranging from apoptotic signaling to DNA repair, photosynthesis, bioluminescence and cellular respiration (Massey 2000). The Na<sup>+</sup>-translocating NADH:quinone oxidoreductase (Na<sup>+</sup>-NQR) from the pathogenic bacterium *Vibrio cholerae* is a membrane-spanning respiratory complex consisting of six subunits NqrA - F. It contains three distinct flavin species: two covalently bound flavin mononucleotides (FMN), a non-covalently bound flavin adenine dinucleotide (FAD) and a riboflavin (Casutt, Huber et al. 2010). The NqrF subunit comprises a ferredoxin-like N-terminal domain that harbors a [2Fe-2S] cluster and a C-terminal part with binding motifs for NADH and FAD. Its role in the catalysis of the initial electron transfer from NADH to FAD, and from there to the [2Fe-2S] cluster has been discussed (Türk, Puhar et al. 2004) but not yet structurally elucidated. Local regions of strong homology place NqrF into the family of ferredoxin-NADP<sup>+</sup> reductases (FNR) (Rich, Meunier et al. 1995). Several crystal structures of different FNRs have been reported (Karplus and Faber 2004). Among these, the structure showing a productive NADP<sup>+</sup>/H binding mode of pea FNR has been particularly helpful in understanding the mechanism of hydride transfer in this widespread enzyme family (Deng, Aliverti et al. 1999). It revealed that the nicotinamide moiety lies at an angle of 30 ° against the plane of the flavin isoalloxazine ring and that four active site residues fulfill important roles in the catalysis: Ser 90, Cys 266, Glu 306 and Tyr 308 (pea FNR numbering). Ser 90 and Glu 306 and their conserved equivalents seem to be primarily involved in nicotinamide binding (Aliverti, Bruns et al. 1995; Aliverti, Deng et al. 1998; Deng, Aliverti et al. 1999). The sulfhydryl group of Cys 266 has been found in close proximity to the C4 atom of the nicotinamide ring and is substantially involved in catalytic turnover, but less so in nicotinamide binding (Aliverti, Piubelli et al. 1993; Deng, Aliverti et al. 1999). These findings were confirmed with the Na<sup>+</sup>-NQR in chapter 3.3.1. of this thesis. It was proposed that the cysteine forces the nicotinamide to adopt boat conformations that pucker towards the flavin and thus facilitate hydride transfer. Productive puckering conformations, induced by the binding of the nicotinamide to the protein, are suggested for lactate dehydrogenase and other enzymes (Young and Post 1996). The stacking of the aromatic ring of Tyr 308 with the isoalloxazine ring of the flavin in the nicotinamide binding pocket appears to be a thermodynamically favored conformation. Tyr 308 does not seem to

be directly involved in the catalysis of hydride transfer, but rather in product release and stabilization of the flavin (Orellano, Calcaterra et al. 1993; Deng, Aliverti et al. 1999; Piubelli, Aliverti et al. 2000; Nogues, Tejero et al. 2004).

Here, a structure-function study of the C-terminal domain of the NqrF subunit of the respiratory Na<sup>+</sup>-NQR is presented. By site-directed mutagenesis of the Phe 406 residue, a 3D crystal structure of NAD<sup>+</sup>/H in complex with the enzyme was obtained. We observed a productive binding mode in which the nicotinamide is angled towards the flavin. In addition, kinetic data of F406A and F406S variants are presented which show that the phenyl ring acts as intrinsic competitor to the nicotinamide and that it also exercises a stabilizing effect on the flavin.

In contrast to FNRs, which mainly catalyze the two-electron transfer from flavohydroquinone to oxidized nicotinamide, the Na<sup>+</sup>-NQR catalyzes the transfer of a hydride from the reduced nicotinamide of NADH to the fully oxidized flavoquinone. It can thus be postulated that despite the high structural identity to FNRs, a unique selectivity mechanism must exist in the NADH-binding domain of Na<sup>+</sup>-NQR, which allows the enzyme to discriminate between the oxidized and the reduced form of the cofactor. We present structural evidence of such a mechanism which involves a conformational change in the nicotinamide and the formation or loss of hydrogen bonds with serine 213 and aspartate 404 of NqrF.

### 3.1.3. The catalytic quinone binding site of Na<sup>+</sup>-NQR

*Vibrio cholerae* is a marine-born pathogen causing in 3 - 5 million disease cases estimated 100'000 - 130'000 deaths per year (World Health Organization, 2010). This pathogen, like many other bacteria, harbors a unique respiratory enzyme complex, the Na<sup>+</sup>-translocating NADH:quinone oxidoreductase (Na<sup>+</sup>-NQR), that is unrelated to the eukaryotic complex I on the level of primary structure, but serves a similar purpose in that it generates an electrochemical gradient across the cytoplasmic membrane which in turn drives many other cellular processes like H<sup>+</sup>/Na<sup>+</sup>-antiporters, solutes uptake and rotation of the flagellum (Häse and Barquera 2001).

Na<sup>+</sup>-NQR is composed of six subunits NqrA - F and harbors at least five redox active cofactors: non-covalently bound FAD and [2Fe-2S] cluster in the NqrF subunit, two covalently bound FMNs in subunits NqrB und NqrC and one non-covalently bound riboflavin in subunit NqrB

(Barquera, Ramirez-Silva et al. 2006; Tao, Casutt et al. 2008; Bogachev, Bloch et al. 2009; Bogachev, Kulik et al. 2009; Casutt, Huber et al. 2010). Upon oxidation of NADH, electrons are transferred from NADH via FAD and [2Fe-2S] cluster on NqrF to FMN on NqrC, FMN on NqrB, and finally, to riboflavin on NqrB (Juárez, Morgan et al. 2009). However, the final step of the reaction cycle - the reduction of the quinone substrate - as well as the coupling of redox chemistry to sodium ion translocation are still largely unclear.

Already in 1992 it was recognized that the resistance of *V. alginolyticus* towards korormicin, a putative quinone analogue, is brought about by two mutations in the NqrB subunit of its Na<sup>+</sup>-NQR (Hayashi, Shibata et al. 2002). It was therefore expected that the NqrB subunit would carry the active site for quinone binding and reduction. Instead, we have recently identified the NqrA subunit to bind ubiquinone-8 and to interact with short chain quinones - in the context of the membrane-embedded/detergent-solubilized holo-Na<sup>+</sup>-NQR enzyme complex as well as with the isolated, soluble NqrA subunit (Casutt, Nediakov et al. 2011). On the other hand, Juárez et al. have shown that the point mutations at glycine 140 and glycine 141 of the NqrB subunit affect Na<sup>+</sup>-NQR reduction activity (Juárez, Neehaul et al. 2012), which led them to conclude that NqrB would harbor the binding site for Q<sub>1</sub>.

The quinone analogue 2,5-dibromo-3-methyl-6-isopropylbenzoquinone (DBMIB, figure 30) is a potent inhibitor of the mitochondrial *bc*<sub>1</sub> complex and the cytochrome *b*<sub>6</sub>*f* complex of chloroplasts (Draber, Trebst et al. 1970; Loschen and Azzi 1974; Chain and Malkin 1979; Degli Esposti, Rugolo et al. 1983; Rich 1984), but can also serve as an electron acceptor with a favorable potential of E<sub>0</sub> = +180 mV (Simkovic and Frerman 2004). The binding of two equivalents of DBMIB into the quinol oxidase (Q<sub>o</sub>) pocket of the *b*<sub>6</sub>*f* complex has been proposed. One equivalent binds with high affinity to a proximal niche, whereas the binding of a second equivalent with low affinity to a distal niche induces a rotation of the Rieske iron-sulfur protein domain of the complex (Roberts, Bowman et al. 2004). By EPR it was shown that DBMIB attaches to and modifies the iron-sulfur center in the *bc*<sub>1</sub> complex with inhibition in the nanomolar range and also interacts with cytochrome b. A mechanism was proposed where DBMIB does not just act as a simple competitor or redox mediator at the quinol oxidase site, but as antagonist to ubiquinone, inducing a redox bypass of the respiratory chain (Degli Esposti, Rotilio et al. 1984).

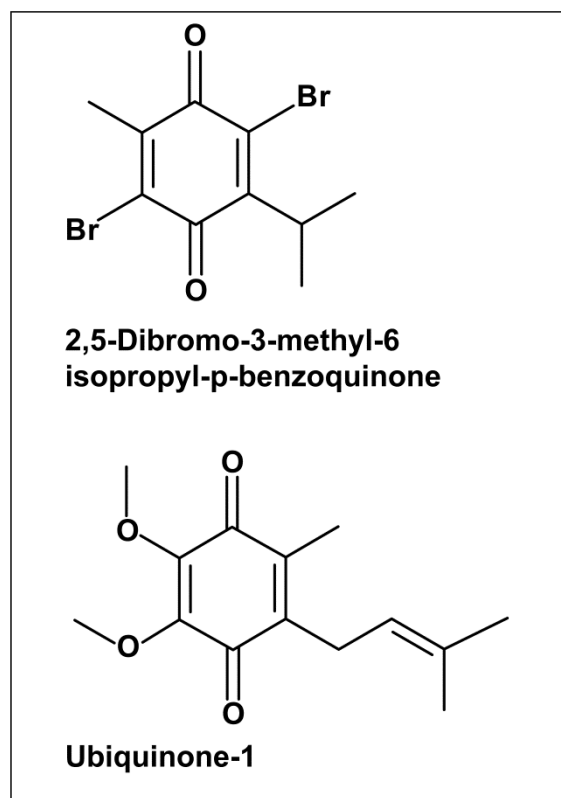


**Figure 30: Structures of 2,5-Dibromo-3-methyl-6 isopropyl-p-benzoquinone (DBMIB) and ubiquinone-1 (Q<sub>1</sub>).**

Here, we show that DBMIB both acts as an inhibitor and as alternative substrate of the Na<sup>+</sup>-NQR of *V. cholerae* by a specific interaction with the NqrA subunit of the complex.

Furthermore, NMR experiments indicate that the NqrA subunit possesses an extended binding site for quinone-type ligands that can simultaneously accommodate two quinones involving a high-affinity and a low-affinity binding mode. Similar dual occupancy models have been proposed for other quinone-converting enzymes based on indirect experimental evidence (Ding, Moser et al. 1995; Bartoschek, Johansson et al. 2001; Efremov, Baradaran et al. 2010). Our findings provide important insight into mechanistic aspects of the final redox step catalyzed by the Na<sup>+</sup>-NQR.

## 3.2. Materials and Methods

### 3.2.1. Chemicals and enzymes

Unless otherwise noted, all chemicals and reagents were purchased from Sigma-Aldrich. Restriction enzymes and T4 DNA ligase were purchased from New England Biolabs. DNA polymerase and PCR buffers were obtained from Finnzymes.

### 3.2.2. Construction of plasmids

The gene coding for the N-terminally hexa-histidine-tagged polypeptide consisting of amino acids 129 - 408 of NqrF, in the following termed FAD domain, from the Na<sup>+</sup>-translocating NQR of *Vibrio cholerae* (Tao, Fritz et al. 2008) was synthesized taking into account optimal codon usage of *E. coli* (Mr. Gene, Regensburg). The synthetic gene was cloned into pET15b to generate plasmid pFNF53. Likewise, plasmids pFNF378A, pFNF406A and pFNF406S encoding for Cys 378 Ala, Phe 406 Ala and Phe 406 Ser substituted variants of the FAD domain were constructed (Trenzyme, Konstanz). The plasmids include a rhinovirus 3C protease cleavage site which allows removal of the histidine-tag from the FAD domain and its variants. To introduce the mutations C378A, F406A and F406S into the subunit NqrF of the NQR complex, PCR on plasmid pNQR1 (Tao, Casutt et al. 2008) was performed using primers 5'-GACAGGCTACACCGGTTTCATCCATAACG-3' (forward), 5'-CATCGGAGGTCCCGC CATGTAGTATTCAC-3' (reverse) and 5'-GTGAATACTACATGG**CGGG**ACCTCCGATG-3' (forward), 5'-CGTCTTCAAGAATTCTTAACCACCGAAGTC-3' (reverse), 5'-GACAGGCTACACCGGTTTCATCCAT AACG-3' (forward), 5'-TCAAGAATTCTTAACCAC**CCGCG**TCATCCAG-3' (reverse) and 5'-GACAGGCTACACCGGTTTCAT CCATAACG-3' (forward), 5'-TCAAGAATTCTTAACCAC**AGAG**TCA TCCAG-3' (reverse). Mutation sites are marked in bold font. PCR products were inserted in pNQR1 using restriction sites EcoRI and AgeI to obtain plasmids pNQR378A, pNQR406A and pNQR406S respectively. All constructs were confirmed by DNA sequencing (GATC Biotech AG, Konstanz).

### 3.2.3. Preparation of FAD domain and its variants

*E. coli* Tuner<sup>TM</sup> (DE3) strain was transformed with plasmid pFNF53, pFNF378A, pFNF406A or pFNF406S. Cells were grown in DYT medium containing 100 µg ml<sup>-1</sup> ampicillin at 37 °C.



Expression of the FAD domain was induced with 1 mM isopropylthio- $\beta$ -D-galactoside (IPTG) at an OD<sub>600</sub> of 0.9. Cells were harvested after 5 h at 30 °C and washed in 10 mM Tris-HCl, 0.3 M NaCl, 5 mM MgCl<sub>2</sub>, pH 7.4. Cells were broken by one passage through an Emulsiflex C3 cell disruptor (Avestin) at approx. 20 kPsi in the presence of 1 mM DTT and protease inhibitors (complete EDTA-free, Roche Diagnostics). Cell debris was removed by centrifugation at 20'000 x g for 20 minutes. After ultracentrifugation of the cellular extract at 150'000 x g (Beckman Type 70Ti), the supernatant was filtrated and loaded onto a Ni Sepharose HP column (5 ml bed volume, GE Healthcare) equilibrated with buffer A (20 mM Tris-HCl, 0.5 M NaCl, pH 8.0). The column was washed with 5 volumes of buffer A containing 30 mM imidazole and histidine-tagged protein was eluted with 400 mM imidazole in buffer A. Peak fractions were combined and diluted at least 1:10 in 50 mM HEPES-NaOH, pH 7.0. The histidine tag was cleaved off by incubation for 15 h at 4 °C with PreScission protease (GE Healthcare). Per 1 mg of protein, 6.7  $\mu$ g of protease was added. By loading the digest onto the Ni<sup>+</sup> column and washing with 50 mM HEPES-NaOH, pH 7.0, FAD domain devoid of the histidine tag was obtained. The target protein was further enriched by loading it onto a SourceQ column (10 ml bed volume, GE Healthcare) equilibrated with 50 mM HEPES-NaOH, pH 7.0 and eluting with a linear gradient from 0 to 0.4 M NaCl. Protein for crystallization and enzymatic assays was frozen in liquid nitrogen in the presence of 5 % glycerol. The yield from 15 g of cells (wet weight) was 45 mg, 23 mg, 36 mg and 30 mg of the wild type FAD domain, the C378A variant, its F406A and F406S variants, respectively. All chromatographic steps were performed at 4 °C using an Äkta Prime chromatography system (GE Healthcare).

#### **3.2.4. Preparation of Na<sup>+</sup>-NQR complex and its NqrF C378A, F406A and F406S variants**

The Na<sup>+</sup>-NQR complex linked to an N-terminal hexa-histidine tag on subunit NqrA and its variants with single amino-acid substitutions C378A, F406A or F406S in subunit F were purified from *Vibrio cholerae* strain O395 N1  $\Delta$ nqr transformed with the corresponding plasmids, using methods described previously (Casutt, Wendelspiess et al. 2010). The yield from 12 g of cells (wet weight) was 15, 14, 15 and 16 mg of the Na<sup>+</sup>-NQR, Na<sup>+</sup>-NQR C378A, Na<sup>+</sup>-NQR F406A and the Na<sup>+</sup>-NQR F406S variant respectively.

### 3.2.5. Preparation of NqrA

Subunit NqrA encoded on plasmid pBR322 (Casutt, Nediakov et al. 2011) was produced in *E. coli* BL21 (DE3). Perdeuterated NqrA was produced in labeled M9 media according to (Marley, Lu et al. 2001). The cells were grown in unlabelled lysogeny broth (LB) medium at 37 °C, shaken at 150 rpm. At an optical cell density at 600 nm (OD<sub>600</sub>) of approximately 0.7, the cells were pelleted by centrifugation for 15 minutes at 5'000 x g at room temperature. The cells were then washed once with M9 medium in D<sub>2</sub>O and pelleted again. Cells were resuspended in deuterated M9 medium supplemented with perdeuterated glucose and incubated for one hour at 37 °C and 150 rpm. Subsequently, protein expression was started by addition of IPTG to a concentration of 1 mM. After 4 hours of incubation the cells were harvested. To purify His<sub>6</sub>-NqrA, washed cells (25 g) were suspended in 50 mM sodium phosphate, pH 8.0, 300 mM NaCl, 5 % (v/v) glycerol. One spatula tip of MgCl<sub>2</sub>, DNase I (Roche) and one tablet of protease inhibitor cocktail (Roche) were added to the cell suspension which was passed twice through a French pressure cell at 7.58 MPa. Cell lysate was centrifuged at 100'000 x g for 60 min. The supernatant was filtrated through a syringe filter with 0.2 µm SFCA membrane (Corning) and loaded onto a His-Trap 2 ml (GE Healthcare) column equilibrated with running buffer (50 mM sodium phosphate, pH 8.0, 300 mM NaCl, 5 % (v/v) glycerol, 4 mM NaN<sub>3</sub>) containing 20 mM imidazole. NqrA was eluted with running buffer containing 130 mM imidazole. All experiments were performed with monomeric NqrA which was separated from NqrA aggregates on a Superdex 200 16/60 (GE Healthcare) column in 50 mM phosphate buffer, pH 8.0, 300 mM NaCl, 5 % (v/v) glycerol, and 4 mM NaN<sub>3</sub> (Casutt, Nediakov et al. 2011).

### 3.2.6. Analytical Methods

The concentration of catalytically active FAD domain variants was calculated from the concentration of FAD in the supernatant of the trichloroacetic acid precipitated purified protein. FAD, NADH and ubiquinone-1 (in ethanol) were determined photometrically using extinction coefficients  $\epsilon_{450}$  (11.3 mM<sup>-1</sup> cm<sup>-1</sup>),  $\epsilon_{340}$  (6.22 mM<sup>-1</sup> cm<sup>-1</sup>) and  $\epsilon_{275}$  (13.7 mM<sup>-1</sup> cm<sup>-1</sup>), respectively (Türk, Puhar et al. 2004). Photometric measurements were performed on a Cary 50 spectrophotometer (Agilent) at 25 °C if not stated otherwise. Purity of protein-associated FAD was verified with a C18 column (Grom) on a Sykam HPLC system using a gradient from 1

to 50 % methanol in 50 mM sodium acetate pH 5.0 and comparing the elution profile measured at 450 nm to the profile of a 1 to 1 mix of commercial flavin adenine dinucleotide and flavin mononucleotide standards. Protein was determined by the bicinchoninic acid method (Smith, Krohn et al. 1985) using the reagent from Pierce. Molecular weight and purity of protein was estimated by SDS-PAGE (Schägger and von Jagow 1987) by comparison with a prestained molecular weight marker (Carl Roth GmbH). 20 µg of protein was loaded per lane. Gels were stained with Coomassie Blue Silver (Candiano, Bruschi et al. 2004).

### 3.2.7. Protein crystallization and X-ray analysis

FAD domain crystals for X-ray analysis were grown using the hanging-drop vapor-diffusion method by mixing 2 µl FAD domain (7 mg ml<sup>-1</sup>, in 5 mM Tris/HCl, pH 7.5) with 2 µl of crystallization solution (0.1 M citric acid, pH 5.0, 35 % (by weight) monomethyl polyethylene glycol 5'000 (PEG 5'000 MME), 0.2 M MgOAc) equilibrated against 500 µl crystallization solution at 293 K. The yellow crystals with a size of 40 x 80 x 80 µm were flash-frozen in the cryo-nitrogen stream.

Crystals of the C378A variant of the FAD domain were grown by mixing 2 µl of 5 mg ml<sup>-1</sup> FAD domain C378A in 5 mM Tris-HCl, pH 7.5 with 2 µl reservoir solution containing 28 % PEG 5'000 MME, 0.1 M sodium acetate, pH 5.0, 0.2 M magnesium acetate, and equilibrating the drops against 500 µl reservoir solution at 19 °C.

Crystals of the F406A and the F406S variants of the FAD domain were grown using the hanging-drop vapor diffusion method by mixing 2 µl 6 mg ml<sup>-1</sup> protein solution in 5 mM Tris-HCl, pH 7.5 with 2 µl reservoir solution (22 - 27 % PEG 5'000 MME, 0.2 M magnesium acetate, 0.1 M sodium citrate, pH 5.0 or 5.2). This was followed by streak-seeding of the drops (using a cat whisker) with seeding crystals from the FAD domain C378A variant (see below). The seeded drops were equilibrated against 0.5 ml reservoir solution at 292 K. To obtain seeds, crystals of the FAD domain C378A variant were transferred to 50 µl stabilization solution (24 % PEG 5'000 MME, 0.1 M sodium acetate, pH 5.2, 0.2 M magnesium citrate) and grinded using the Seed Bead kit (Hampton Research). The concentrated seed stock was diluted 1:10 with stabilizing solution to obtain the final seed solution. Crystals of all FAD domain variants were soaked for 15 to 20 min in the crystallization solution containing 0.1 M NAD<sup>+</sup>, 0.2 M NADH (disodium salt, Carl Roth GmbH) or 0.2 M NADH with some grains of dithionite, respectively.

Crystals were passed through crystallization solution containing 35 % PEG 5'000 MME as cryo-protectant and were immediately flash-frozen in liquid nitrogen. X-ray data were collected at 100 K using monochromatic synchrotron radiation ( $\lambda = 0.9 \text{ \AA}$ ) at the beamlines X06SA and X10SA, Swiss Light Source, Paul Scherrer Institut, Villigen, Switzerland. The diffraction data were processed with the program package *XDS* (Kabsch 2010).

### 3.2.8. Structure determination and refinement

Optimization of the initial crystallization conditions of the FAD domain (Tao, Türk et al. 2006) yielded yellow crystals with a size of 40 x 80 x 80  $\mu\text{m}$ . Crystals diffracted to 1.8  $\text{\AA}$  and belonged to space group  $P2_12_12_1$ . Phases were determined by MAD of a crystal soaked with  $\text{K}_2\text{Pt}(\text{NO}_2)_4$  for 3 days. Selected crystals were soaked with mother liquor containing 40 mM NADH for 10 - 60 min, or 0.1 mM  $\text{AgNO}_3$  for 2 - 48 h, prior to flash-freezing. Phases of FAD domain C378A, F406A and F406S variants were determined by molecular replacement, carried out with the molrep program (Vagin and Teplyakov 2010) from the CCP4 suite (Winn, Ballard et al. 2011) and using the structure of the NqrF FAD domain wild type (unpublished data, provided by Günter Fritz) as a search model. Refinement was performed with the refmac5 program (<http://www2.mrc-lmb.cam.ac.uk/groups/murshudov/>, access date 28.9.2011) from the CCP4 suite. Structural alignment and images were generated with Coot (Emsley, Lohkamp et al. 2010), PyMOL (Schrödinger 2010) and Discovery Studio (Accelrys).

### 3.2.9. Enzymatic activities

NADH dehydrogenase activities of Na<sup>+</sup>-NQR and FAD domain variants were determined with NADH (0.002 - 0.1 mM) and 0.1 mM ubiquinone-1 ( $\text{Q}_1$ ; MCAT GmbH) at pH 7.5 in the absence of chloride (Tao, Fritz et al. 2008). Quinone reductase activities were determined with  $\text{Q}_1$  (0.005 - 0.05 mM) as electron acceptor at a fixed NADH concentration of 50  $\mu\text{M}$ . Rates of NADH oxidation were followed at 340 nm and quinol formation was determined from the difference in absorption at 248 nm - 268 nm. Kinetic measurements were performed under aerobic or anaerobic conditions under magnetic stirring on a Cary 50 spectrophotometer (Agilent) or a HP 8452A diode array spectrophotometer (Agilent) in a temperature-controlled quartz cuvette at 25 °C and 37 °C. Specific enzyme activities were

determined in the presence of 50 μM NADH in buffer tempered to 25 °C if not indicated otherwise. For the calculation of  $K_M$ , apparent  $K_M$  and  $V_{max}$ , the Michaelis-Menten or the Hill equations were used. The turnover number  $k_{cat}$  was calculated using a molecular weight of 32 kDa for the FAD domain and a molecular weight of 220 kDa for the Na<sup>+</sup>-NQR complex. Ag<sup>+</sup> inhibition was assayed by incubating the enzymes for 24 h at 4 °C in the absence or presence of AgNO<sub>3</sub> and starting the reaction by the addition of NADH. For demonstrative purposes, kinetic data are depicted in the double-reciprocal Lineweaver-Burk projection. The inhibition constant for Ag<sup>+</sup> was calculated assuming an irreversible inactivation (resembling mixed inhibition) of the enzyme by silver binding. DBMIB inhibition of the Na<sup>+</sup>-NQR was assayed by incubating the enzyme for 17 h at 4 °C in reaction buffer containing DBMIB and Q<sub>1</sub> in 0.1 % or 0.25 % ethanol and starting the reaction by addition of NADH.  $K_i$  for inhibition of NADH dehydrogenase activity by DBMIB was calculated assuming an uncompetitive mode of inhibition (Voet and Voet 2004). The inhibition of specific quinone reductase activity was analyzed assuming a mixed mode of inhibition (Voet and Voet 2004). The correlation coefficients and kinetic constants are listed in table 11. The rates were background-corrected by the changes in absorbance arising from DBMIB reduction by the Na<sup>+</sup>-NQR to enable kinetic analysis of ubiquinol-1 formation only. The reductase activity of Na<sup>+</sup>-NQR using only DBMIB as electron acceptor (Simkovic and Frerman 2004) was assayed under identical conditions as Q<sub>1</sub> reductase activity with DBMIB concentrations between 0 - 100 μM and using the same extinction coefficient as for Q<sub>1</sub>. Kinetic constants are given in table 12.

### 3.2.10. Inhibition of growth of *Vibrio cholerae* by Ag<sup>+</sup>

The effect of Ag<sup>+</sup> on the viability of *Vibrio cholerae* O395 N1 Δnqr expressing Na<sup>+</sup>-NQR wild type and the NqrF C378A Na<sup>+</sup>-NQR variant was investigated by growth assays: *Vibrio cholerae* cells were grown in Erlenmeyer flasks under agitation in chloride free minimal medium with succinate as energy and carbon source. Single colonies of both strains were used to inoculate 2 ml minimal medium and were grown at 37 °C overnight. These cultures were used to inoculate 20 ml expression cultures. At an OD<sub>600 nm</sub> = 0.4, expression of Na<sup>+</sup>-NQR wild type and C378A variant was induced by the addition of 5 mM arabinose. Cultures were grown for another 16 h to allow expression of Na<sup>+</sup>-NQR. Cells were harvested by centrifugation at 4'000 x g and resuspended in phosphate-free minimal medium. The cell

density was adjusted to OD<sub>600 nm</sub> = 0.1. Different concentrations (0 - 20 μM) of AgCl were added and cells were incubated for 26 h at 37 °C under agitation. To address final cell mass and growth, the OD<sub>600 nm</sub> of the cultures with AgCl was determined.

### 3.2.11. Fluorescence spectroscopy

To measure the thermal stability during heat denaturation, FAD domain variants were diluted in 20 mM Tris-H<sub>2</sub>SO<sub>4</sub>, pH 7.5, 50 mM NaSO<sub>4</sub> to a concentration of 0.02 mg ml<sup>-1</sup>. Starting at 10 °C, temperature was increased in steps of 5 °C to a final temperature of 60 °C. The intensity of tryptophan fluorescence emission was determined at indicated temperatures at 348 nm ( $\lambda_{\text{excitation}}$  295 nm). Alternatively, the fluorescence emission of dissociated FAD was measured at 522 nm ( $\lambda_{\text{excitation}}$  450 nm) in steps of 2.5 or 5 °C. Melting points were defined as the midpoint temperature of a sigmoidal fit of fluorescence intensity plotted against temperature. The correlation coefficient  $R^2$  was  $\geq 0.995$ . The dissociation of FAD by Ag<sup>+</sup> was measured over time at 527 nm. The experiment was started by the addition of 5 μM AgCl to 0.63 μM of FAD domain variant in a fluorescence cuvette at 25 °C. Binding of DBMIB to NqrA was determined as follows: NqrA was diluted in 50 mM Tris-HCl, 300 mM NaCl, pH 8.0 and 5 % (v/v) glycerol to a concentration of 0.25 μM. DBMIB was added from an ethanol stock solution to final concentrations between 0 and 200 μM (final ethanol concentration  $\leq 2$  %). Measurements were performed in triplicate at 25 °C. The intensity of tryptophan fluorescence emission was determined at 338 nm ( $\lambda_{\text{excitation}}$  = 295 nm). The increase in quenching ( $\Delta F$ ) of the tryptophan emission was normalized to values between 0 and 1 and plotted against the concentration of DBMIB. Non-linear regression analyses using the Hill equation and the Michaelis-Menten equation were performed. In addition, the data were transformed into a linear form using the methods of Rosenthal and Scatchard (Scatchard 1949; Rosenthal 1967) and fitted with a second degree polynomial. All fluorescence measurements were performed with a Fluorolog 3 spectrofluorometer (Horiba Scientific) using a temperature-controlled fluorescence cuvette.

### 3.2.12. NMR spectroscopy

NqrA was transferred to D<sub>2</sub>O containing 10 mM potassium phosphate, pH 8.0, 150 mM NaCl, 4 mM NaN<sub>3</sub> by repeated ultrafiltration with Ultrafree 4 membranes (Millipore; molecular weight cut-off, 10 kDa). To 10 μM NqrA, Q<sub>1</sub> was added from 20 mM stock solutions in DMSO-d<sub>6</sub> to a final concentration of 100 μM. DBMIB was added from stock solutions in DMSO-d<sub>6</sub> to obtain NqrA samples containing 0 - 150 μM DBMIB as indicated. Additional DMSO-d<sub>6</sub> was added to keep its concentration constant within the series (1.5 % v/v). The STD NMR experiment with DBMIB alone was performed with 2.5 μM NqrA in PBS buffer. DBMIB was added to a concentration of 100 μM. Controls were prepared in the same way without NqrA. All NMR experiments were acquired at 300 K on a Bruker AVANCE III 600 MHz spectrometer equipped with a cryogenic 5 mm TCI-H/C/N triple resonance probe with actively shielded z-gradient. The samples were transferred to 5 mm NMR tubes and STD NMR experiments (Mayer and Meyer 1999) were performed as described (Casutt, Nediakov et al. 2011). The resonances of Q<sub>1</sub> were assigned as described in (Casutt, Nediakov et al. 2011). Water suppression was achieved by excitation sculpting (Hwang and Shaka 1995). Resonances of NqrA were saturated by applying a train of low-power Gaussian-shaped pulses at 0.2 ppm with a total saturation time of 2 s. Off-resonance irradiation was set to 33 ppm. On- and off-resonance spectra were acquired in an interleaved manner and subtracted after processing. Up to 4096 transients were collected at a spectral width of 12 ppm. STD effects were determined within the multiple display mode by scaling the off-resonance spectrum down to superimpose with the signal of interest in the difference (off - on) spectrum. The influence of DBMIB on Q<sub>1</sub> STD effects was plotted in Origin 8.1G and fitted to a one-site binding model. One value for k was obtained from globally fitting all Q<sub>1</sub> signals. Experiments for interligand Overhauser effects (ILOEs) were performed in the same buffer as STD NMR experiments. To 25 μM NqrA or perdeuterated NqrA, 200 μM Q<sub>1</sub> or 400 μM DBMIB from 20 mM stock solutions in DMSO-d<sub>6</sub> were added. DMSO-d<sub>6</sub> was added as required to achieve a constant concentration of 5 % in the sample. Two samples for the control experiments were prepared in the same manner excluding NqrA or quinones respectively. Water suppression was achieved by low-power presaturation of water signal during relaxation delay and mixing time (Hoult 1976; Hore 1989). The mixing time was set to 600 ms. Up to 960 increments with 48 scans in each increment were collected at a spectral width of 10 ppm. Spectra were processed and analyzed with the software TopSpin (Bruker; v3.1).

### 3.3. Results

#### 3.3.1. Ag<sup>+</sup>-mediated killing of *Vibrio cholerae* originates in silver ion binding to cysteine 378 of subunit F of the Na<sup>+</sup>-NQR

The Na<sup>+</sup>-NQR is a six-subunit membrane-bound complex with a molecular mass of 220 kDa (Tao, Casutt et al. 2008). In the Na<sup>+</sup>-NQR, NADH is oxidized by the subunit NqrF which is composed of the FAD domain accepting the hydride from NADH, and the ferredoxin domain catalyzing electron transfer to other redox centers present in the complex (Türk, Puhar et al. 2004; Tao, Casutt et al. 2008). The FAD domain of NqrF was previously overproduced in *V. cholerae*, crystallized and biochemically characterized (Türk, Puhar et al. 2004; Tao, Türk et al. 2006). It comprises amino acids 129 - 408 and represents the C-terminal part of the NqrF subunit. The following chapters describe the production of the FAD domain of the Na<sup>+</sup>-NQR from *V. cholerae* in *E. coli*. The protein was purified and the 3D crystal structure was determined. By introducing mutations in conserved residues of the active site of NADH oxidation, we were able to identify Cys 378 of the NqrF subunit as a strong binder of silver ions and as a key player in conferring Ag<sup>+</sup> sensitivity to *Vibrio cholerae*. Furthermore, the mutagenesis of the Phe 406 residue of NqrF served to analyze the mechanism of NADH oxidation in-depth, as described in chapter 3.3.2.

##### 3.3.1.1. Production and purification of the FAD domain of Na<sup>+</sup>-NQR

The FAD domain and its variants were purified based on established protocols (Türk, Puhar et al. 2004). Figure 31 depicts the enrichment of the wild type FAD domain by immobilized metal affinity and anion exchange chromatography. The purified protein exhibited migration behavior on SDS-PAGE corresponding to the calculated molecular masses of 34'272 Da (with His-tag) and 31'981 Da (His-tag cleaved) respectively. The non-covalently bound FAD adds another 786 Da to the molecular mass.



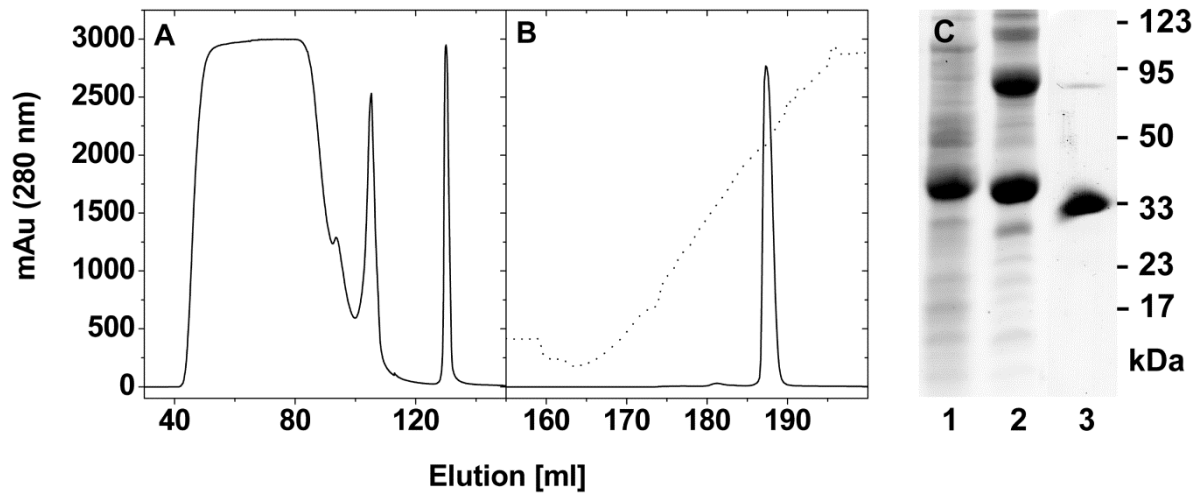


**Figure 31: Purification of the FAD Domain of the Na<sup>+</sup>-NQR from *Vibrio cholerae*.** Au: Absorption units. **A:** Enrichment by nickel affinity chromatography. The broad peak represents the flow-through fraction. Protein eluting at 110 ml represents the fraction collected after washing with 30 mM imidazole. The final maximum at 130 ml contains His-tagged FAD domain. **B:** Polishing step by ion exchange chromatography. Dotted line represents conductivity of the elution buffer (linear gradient from 0 to 0.4 M NaCl). **C:** SDS-PAGE depicting the enrichment of the FAD domain. Lane 1: cellular extract of *E. coli* expressing FAD domain, the amount of cells contained in 200  $\mu$ l of a culture with  $OD_{600\text{ nm}} = 1$  was loaded. Lane 2: Elution fraction from **A**. Lane 3: Elution fraction from **B**, representing purified FAD domain without His-tag. The gel was stained with Coomassie blue.

It was unknown if the *E. coli* cells used as expression host for the *V. cholerae* enzyme would be able to supply enough FAD to complement the polypeptide or if the *E. coli* host would resort to incorporate other flavin species. HPLC analysis confirmed that only the flavin adenine dinucleotide was inserted into the holo-enzyme (figure 32). Only residual amounts of FMN and riboflavin were detected. The FAD domain wild type contained 0.81 mol FAD/mol, the C378A variant contained 0.93 mol FAD/mol.

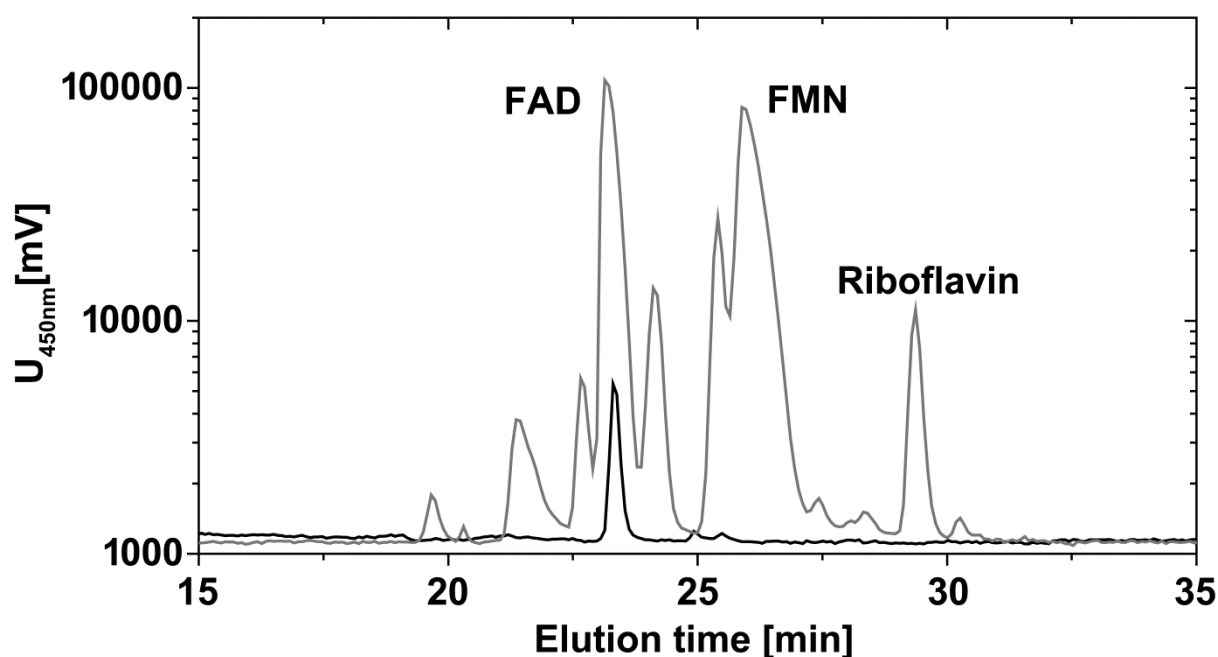


**Figure 32: FAD domain produced in *E. coli* contains flavin adenine dinucleotide as sole cofactor.** HPLC elution profile of a mixture of flavin standards (grey) is superimposed with the profile of the supernatant from trichloroacetic acid precipitation of the purified FAD domain (black).

### 3.3.1.2. Binding of Ag<sup>+</sup> to the FAD Domain of Na<sup>+</sup>-NQR

The FAD domain catalyzed NADH oxidation with Q<sub>1</sub> as electron acceptor. A  $V_{\max}$  of  $225.2 \pm 6.5 \mu\text{mol min}^{-1} \text{mg}^{-1}$  and a  $K_M$  of  $7.4 \pm 0.8 \mu\text{M}$  was observed (figure 33). This is in accord with the activity of the Na<sup>+</sup>-NQR complex which was overproduced in *V. cholerae*. The kinetic constants are summarized in table 7. The activities of the isolated FAD domain and the Na<sup>+</sup>-NQR were further assayed in the presence of Ag<sup>+</sup> (figure 33; dashed lines). In both cases, a significant decrease in  $V_{\max}$  and almost no change in  $K_M$  was observed, which is best interpreted as the inhibition mode of an irreversible inactivator (Voet and Voet 2004), effectively lowering the total concentration of catalytically active enzyme. The derived inhibition constants  $K_i = K_i'$  were 36 nM for the Na<sup>+</sup>-NQR and 20 nM for the FAD domain (table 7). This inactivation by low nanomolar concentrations of Ag<sup>+</sup> most likely resulted from the binding of the heavy metal cation to a cysteine residue close to the NAD(H) binding pocket, which in turn prevented hydride transfer from the nicotine amide moiety of NADH to the isoalloxazine moiety of the FAD cofactor. To confirm this notion, and to describe the interaction of the substrate with the electron input domain of the Na<sup>+</sup>-NQR at atomic resolution, we determined the 3D structure of the FAD domain in complex with Ag<sup>+</sup> or NADH.

Indeed, the binding of silver ions to a cysteine residue corresponding to position 378 of NqrF, in close vicinity to the NADH binding site could be observed (figure 34). Hereupon, a mutation of the Cys 378 residue of the FAD domain was introduced which was expected to cause a significant loss in the ability of  $\text{Ag}^+$  to bind to and inhibit the NADH oxidation activity.

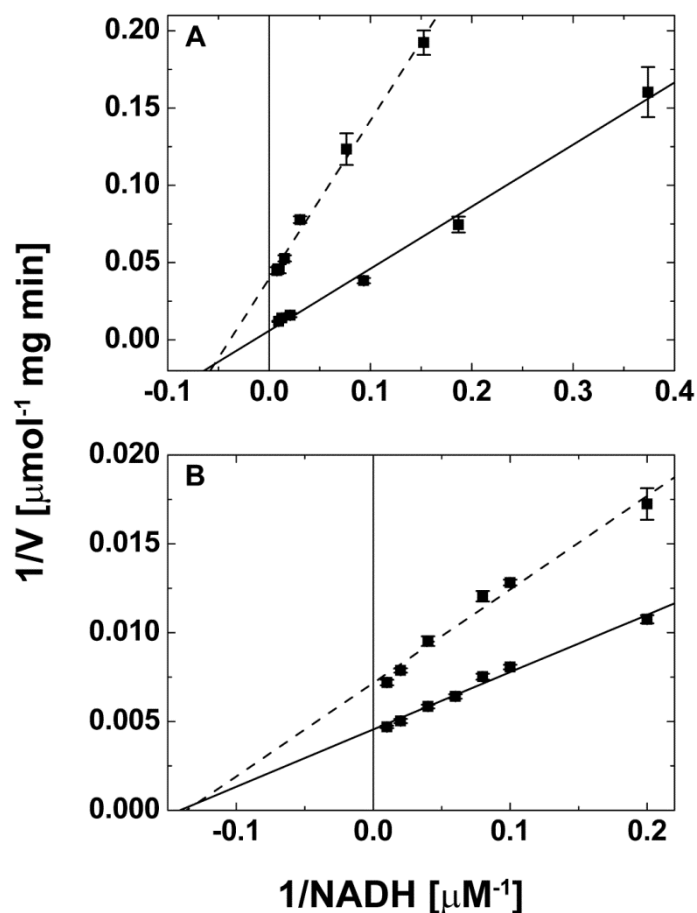


**Figure 33: Inhibition of the  $\text{Na}^+$ -NQR and its NADH-oxidizing FAD domain by  $\text{Ag}^+$ .** Rates of NADH oxidation with ubiquinone-1 as electron acceptor were determined in the presence or absence of  $\text{AgCl}$ . Mean values from three experiments are presented. Data are shown as a Lineweaver-Burk plot and were fitted by linear regression to illustrate the mode of irreversible inhibition. **A:**  $\text{Na}^+$ -NQR complex in the presence (dashed line) or absence (solid line) of 100 nM  $\text{Ag}^+$ . **B:** isolated FAD domain from subunit NqrF in the presence (dashed line) or absence (solid line) of 10 nM  $\text{Ag}^+$ .

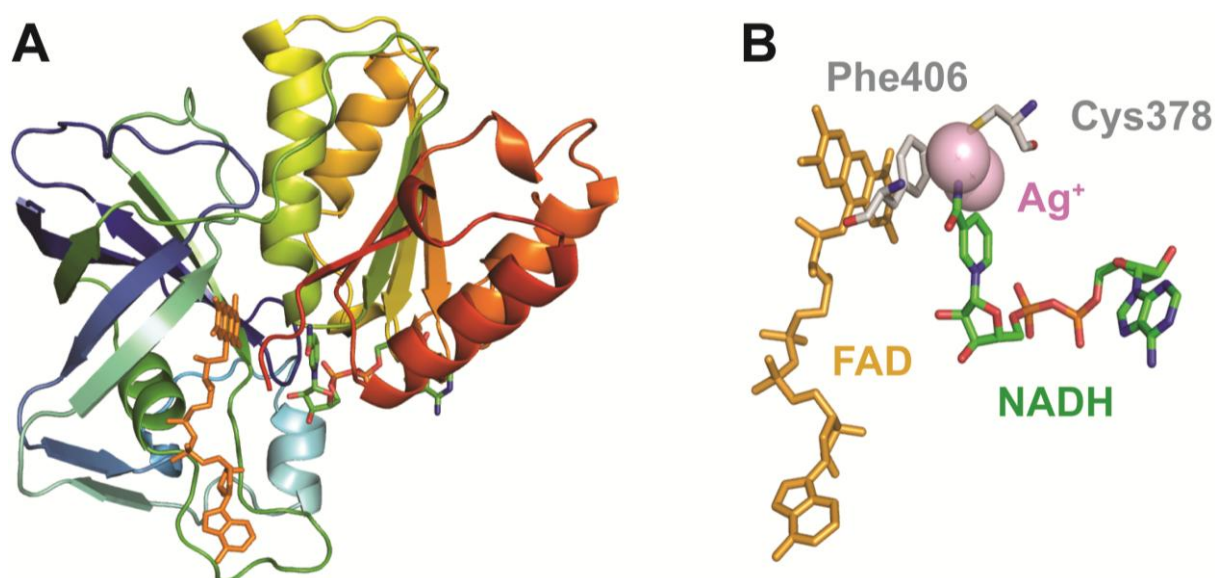


**Figure 34: Structure of the NADH-oxidizing FAD domain in complex with Ag<sup>+</sup> and/or NADH.** **A:** Cartoon view of the FAD domain in complex with NADH. **B:** Binding of silver atoms to Cys 378 in the active site of the FAD domain of subunit NqrF from the Na<sup>+</sup>-NQR. The FAD cofactor (orange) as well as NADH (green) and the conserved amino acids Cys 378 and Phe 406 (grey) are shown. The pink orbs represent two silver ions close to Cys 378, which spatially overlap with the nicotinamide in its binding pocket. The position of NADH was determined from a different crystal of the FAD domain, soaked with NADH.

### 3.3.1.3. Ag<sup>+</sup> inhibition is lost in the C378A variant

Substitution of cysteine 378 by an alanine resulted in the lowering of  $V_{\max}$  to  $60.1 \pm 1.0 \mu\text{mol min}^{-1} \text{mg}^{-1}$  and the lowering of the  $K_M$  to  $1.2 \pm 0.2 \mu\text{M}$  in the isolated FAD domain and a lowering of  $V_{\max}$  to  $58.3 \pm 3.4 \mu\text{mol min}^{-1} \text{mg}^{-1}$  and of  $K_M$  to  $12.0 \pm 2.8 \mu\text{M}$  in the Na<sup>+</sup>-NQR complex (table 7). These results indicate that the mutation induced a conformational change in the active site, to a point where NADH is bound more efficiently by the enzyme, but is processed more slowly. It was found that the NADH oxidation activity of the C378A variant was completely unaffected at Ag<sup>+</sup> concentrations at which the wild type was inhibited (figure 35), confirming our notion that cysteine 378 of the NqrF is responsible for the irreversible binding and inhibition by Ag<sup>+</sup>. The inhibition constants were increased by one order of magnitude in the C378A variant of the Na<sup>+</sup>-NQR complex and even by three orders of magnitude in the C378A variant of the isolated FAD domain (table 7).

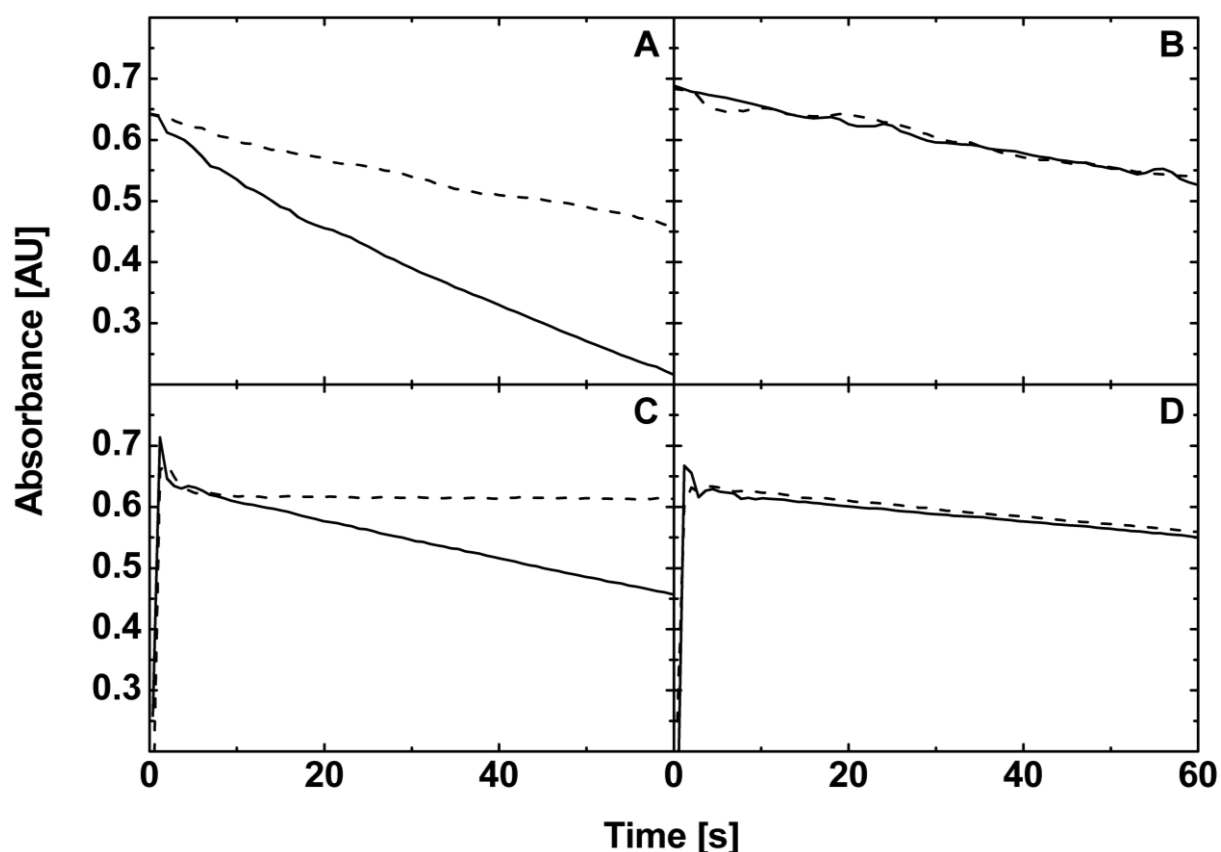


**Figure 36: Ag<sup>+</sup> Inhibition of the Na<sup>+</sup>-NQR and its NADH-oxidizing FAD domain is reverted in the C378A variant.** Absorbance of reduced NADH, plotted against time. Reactions were started by the addition of 0.1 mM NADH to enzyme pre-incubated in chloride-free buffer containing 0.1 mM ubiquinone-1 and either no Ag<sup>+</sup> (solid lines), 150 nM (A + B, dotted lines) or 1 μM Ag<sup>+</sup> (C + D, dotted lines). A: Na<sup>+</sup>-NQR wild type, B: Na<sup>+</sup>-NQR C378A, C: FAD domain wild type, D: FAD domain C378A. Experiments were done in triplicates, of which one trace each is shown.

**Table 7: Kinetic constants and Ag<sup>+</sup> inhibition of the NADH dehydrogenase activity in the wild type and C378A variants of the Na<sup>+</sup>-NQR complex and its FAD domain.**

	V <sub>max</sub> [μmol mg <sup>-1</sup> min <sup>-1</sup> ]	k <sub>cat</sub> [s <sup>-1</sup> ]	K <sub>m</sub> [μM]	K <sub>i</sub> [nM]
NQR wt	108.5 ± 5.6	397.8	36.3 ± 5.2	3.6 × 10 <sup>1</sup>
NQR C378A	58.3 ± 3.4	213.8	12.0 ± 2.8	2.8 × 10 <sup>2</sup>
FAD Domain wt	225.0 ± 7.0	119.9	7.4 ± 0.8	2.0 × 10 <sup>1</sup>
FAD Domain C378A	60.0 ± 1.0	31.9	1.2 ± 0.2	3.0 × 10 <sup>4</sup>

The mode of Ag<sup>+</sup> inhibition was further analyzed by assessing the increase in fluorescence of FAD after addition of 5 μM Ag<sup>+</sup> to the FAD domain variants. Enhanced flavin fluorescence indicates the dissociation of the cofactor from the enzyme. It was found that the C378A variant of the FAD domain exhibits a strongly decelerated release of FAD compared to the

wild type (figure 36). Additionally, the FAD dissociation over time was best fitted with a sigmoidal curve for the wild type FAD domain (Hill coefficient  $n = 1.3$ ), whereas the dissociation of FAD from the C378A variant resembled a hyperbolic curve (sigmoidal and hyperbolic fitting data not shown). This indicates that FAD is released from the wild type FAD domain in a cooperative manner, involving the specific Ag<sup>+</sup> binding site at C378 and one or more unspecific binding sites. In the C378A variant only the unspecific Ag<sup>+</sup> binding site(s) remain, resulting in an uncooperative FAD dissociation mechanism.

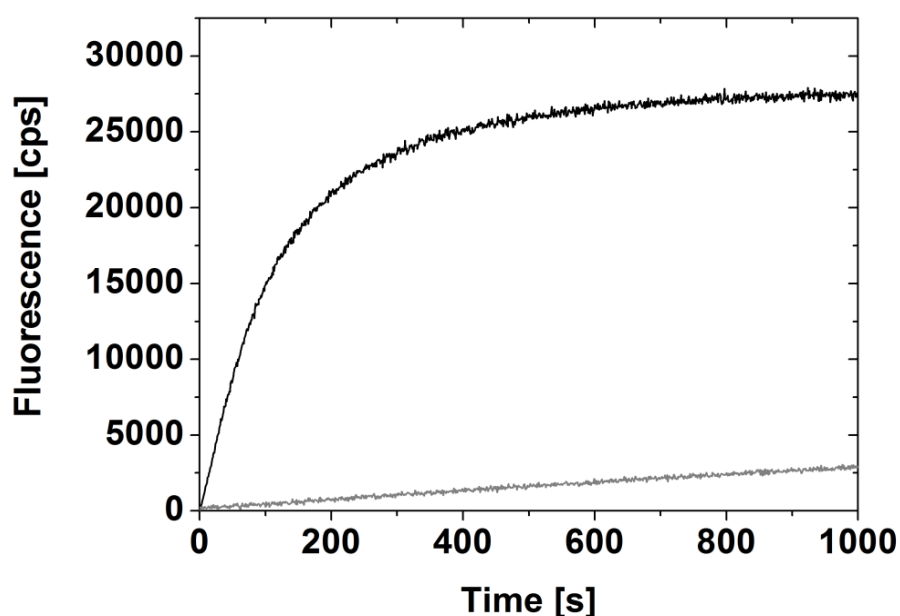


**Figure 36: Dissociation of FAD from the FAD domain and its C378A variant in the presence of 5  $\mu\text{M}$  AgCl<sub>2</sub>.** Ag<sup>+</sup> was added at  $t = 0$  s. Black: FAD domain wild type. Grey: FAD domain C378A variant.

The sensitivity of *Vibrio cholerae* to Ag<sup>+</sup> was analyzed by growth experiments in which the expression medium was supplemented with Ag<sup>+</sup> concentrations in the nanomolar to micromolar range. After 26 h of exposure to silver ions, *V. cholerae* cells expressing the wild type Na<sup>+</sup>-NQR were either killed or did not replicate at Ag<sup>+</sup> concentrations higher than 1  $\mu\text{M}$  (figure 37). Concentrations up to 0.5  $\mu\text{M}$  had no effect on cell density or growth. At concentrations between 0.5  $\mu\text{M}$  and 1  $\mu\text{M}$  Ag<sup>+</sup> the cells grew to significantly higher densities. In contrast, cells expressing the C378A variant of the Na<sup>+</sup>-NQR could sustain Ag<sup>+</sup> concentrations up to 1.5  $\mu\text{M}$  and showed only a slight increase in final cell mass at concentrations between 0.5  $\mu\text{M}$  and 1.1  $\mu\text{M}$  Ag<sup>+</sup>.

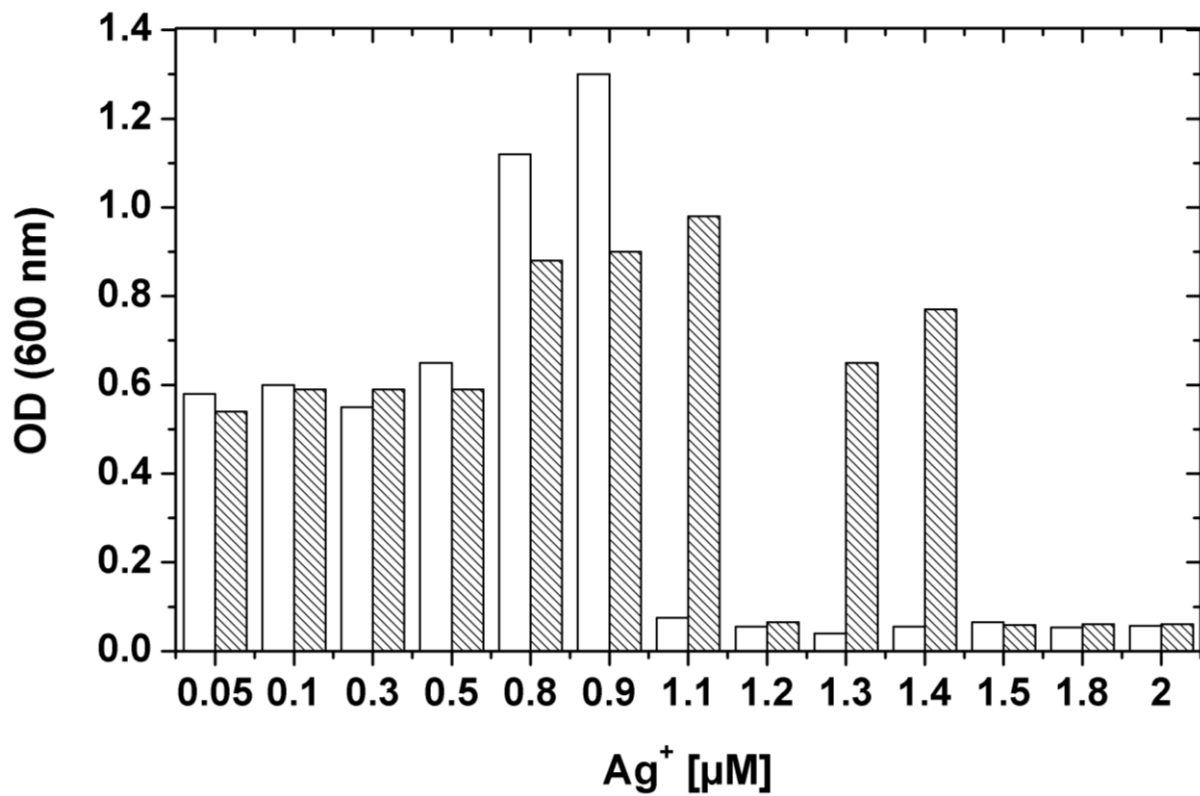


**Figure 37: Ag<sup>+</sup> mediated killing of *Vibrio cholerae* and rescue in the mutant expressing the C378A variant of the Na<sup>+</sup>-NQR.** Effect of Ag<sup>+</sup> on cell density, recorded after 26 h of incubation in chloride free minimal medium containing indicated amounts of Ag<sup>+</sup>. White: cells expressing the wild type Na<sup>+</sup>-NQR. Hatched: cells expressing the C378A variant of the Na<sup>+</sup>-NQR.

### 3.3.2. Structure-function analysis of the NADH oxidizing domain of the Na<sup>+</sup>-NQR from *Vibrio cholerae*

#### 3.3.2.1. Crystal structure of the FAD domain in complex with NADH

Elucidation of the X-ray structure of the FAD domain in complex with NADH revealed an unproductive binding mode as reported before for plant-like FNR and related flavoproteins (Deng, Aliverti et al. 1999) (figure 38). Phenylalanine 406 is stacked with the isoalloxazine ring of FAD and hinders hydride transfer from nicotinamide.

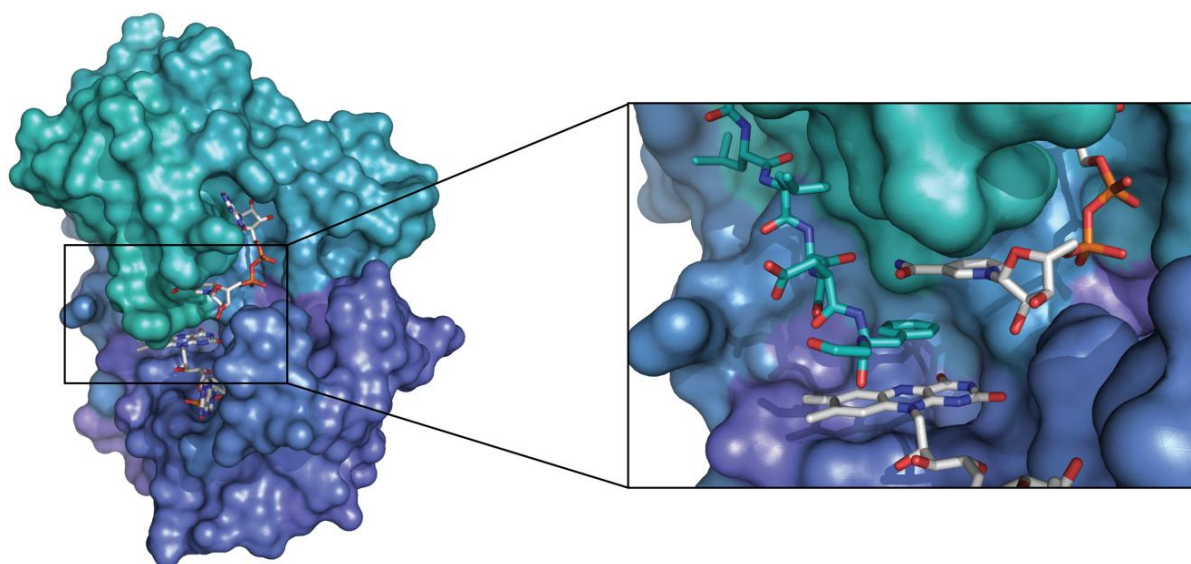


**Figure 38: Crystal Structure of the FAD Domain in complex with NADH.** The structure of the holo-enzyme is represented as a space-filling model. The FAD and NADH cofactors (white) and the magnified C-terminus (cyan) are shown in a stick representation.

#### 3.3.2.2. Phe 406 variants display enhanced nicotinamide binding and catalytic efficiency but loss of stability and FAD binding

The visible spectra of the F406A and F406S variants of the FAD domain displayed a significant blue-shift and increased extinction of the 400 nm flavin peak compared to the wild type, indicating the loss of stacking interaction from the phenyl ring with the isoalloxazine ring (figure 39). A further difference was observed in the absorbance shoulder of the second flavin peak at about 480 nm, corresponding to the adenine part of FAD, which was reduced in the F406A and F406S variants. The F406S and F406A variants of the FAD domain notably exhibit almost identical spectra.



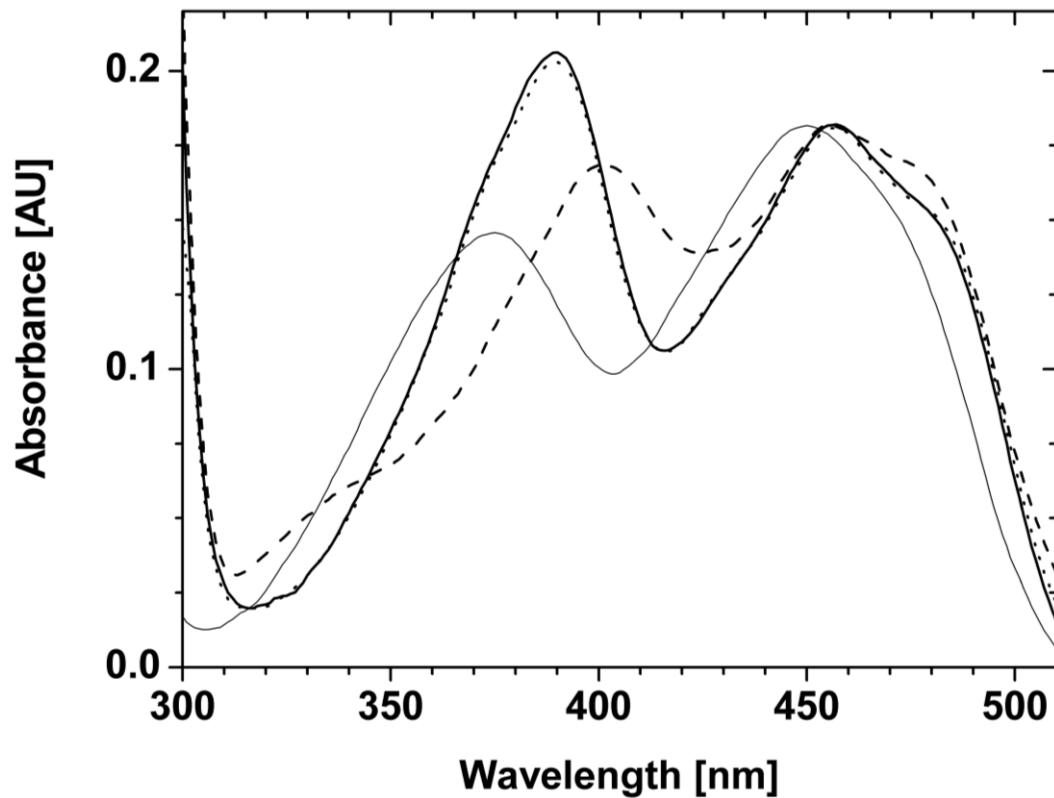


**Figure 39: UV-visible spectra of free FAD and the wild type, F406A and F406S variants of the FAD domain of the Na<sup>+</sup>-NQR.** Spectra were scaled to the measured absorbance of free FAD at 451 nm. Solid gray line; FAD, dashed line; FAD domain wild type, solid black line; FAD domain F406A, dotted line; FAD domain F406S.

The mutagenesis of the phenylalanine 406 residue led to an increase in catalytic efficiency of the NADH oxidase reaction at 25 °C (figure 40). The Michaelis constant  $K_M$  was significantly decreased compared to the wild type (wt  $7.4 \pm 0.8$ , F406A  $2.1 \pm 0.2$ , F406S  $3.5 \pm 0.4$   $\mu\text{M}$ ) and the maximal reaction rates were determined to be about twice as high (wt  $225 \pm 7$ , F406A  $410 \pm 7$ , F406S  $509 \pm 11$   $\mu\text{mol mg}^{-1} \text{min}^{-1}$ ). By increasing the reaction temperature to 37 °C, reaction rates of the F406 variants decreased to 3 and 5 % of their respective activity at 25 °C, whereas wild type activity almost doubled (table 8).

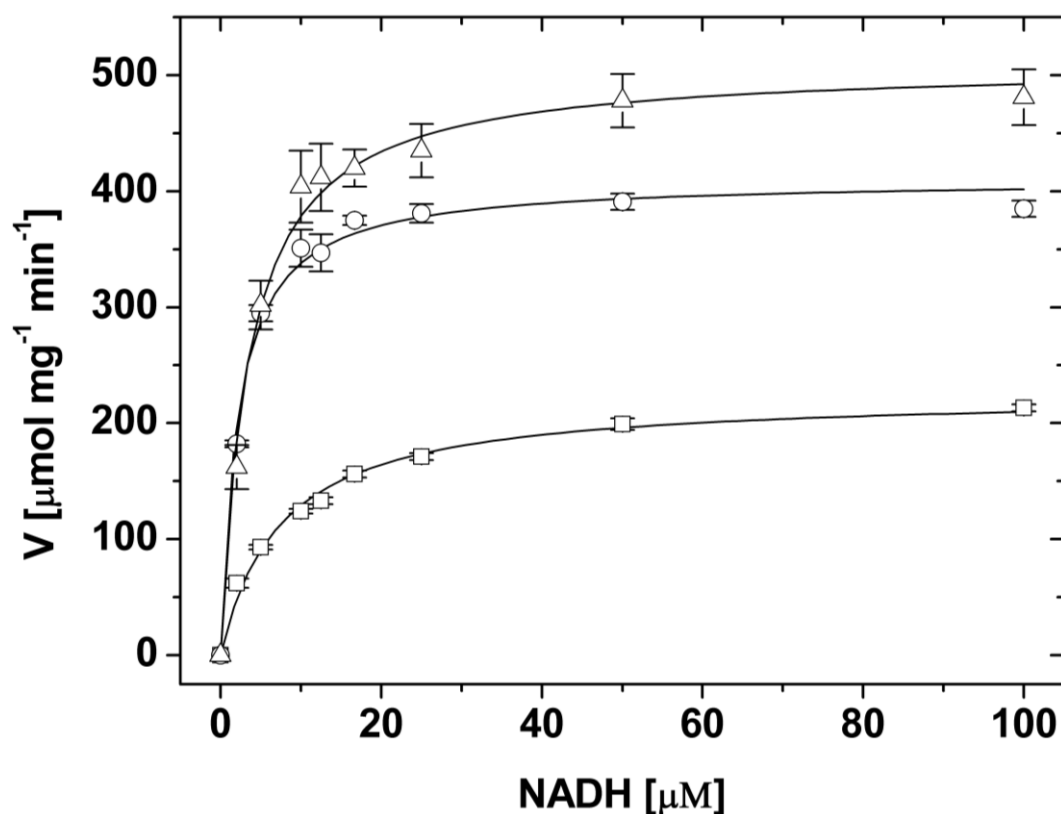


**Figure 40: Kinetics of NADH oxidation of FAD Domain variants at 25 °C.** Initial NADH oxidation rates were determined in triplicate for each substrate concentration and  $V_{\text{max}}/K_M$  pairs were calculated by non-linear curve fit. Squares; FAD domain wild type, circles; F406A variant, triangles; F406S variant.

Thermal stability of the FAD domain variants was analyzed by plotting fluorescence emission of tryptophan or free FAD cofactor against temperature (figure 41). The mean fluorescence intensity of these molecules in general increases when a protein unfolds and can be described by a sigmoidal curve. Melting points were defined as slope maxima temperatures of the curve fits. The melting point of the wild type enzyme was observed at 49 - 50 °C, whereas the F406A and F406S variants exhibited lower melting points (39 - 43 °C, table 8).

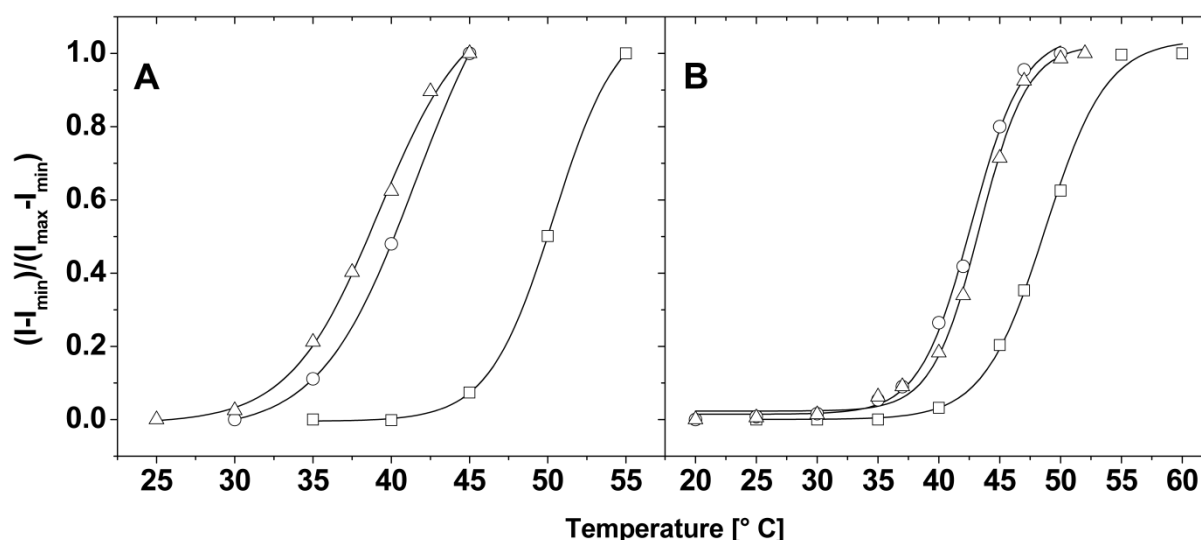


**Figure 41: Thermal stability of FAD domain variants.** Increase in Fluorescence emission intensities of intrinsic **A:** tryptophan or **B:** FAD. Melting points were determined by sigmoidal curve fit. Squares; FAD domain wild type, circles; F406A variant, triangles; F406S variant. Experiments were done in triplicate, of which one each is presented.

**Table 8: Kinetic constants and thermal stability of FAD domain and Na<sup>+</sup>-NQR variants, n = 3.**

	FAD d. wild type	FAD d. F406A	FAD d. F406S	Na <sup>+</sup> -NQR wild type	Na <sup>+</sup> -NQR F406A	Na <sup>+</sup> -NQR F406S
$V_{max}$ [ $\mu\text{mol mg}^{-1} \text{min}^{-1}$ ]	$225.0 \pm 7.0$	$410.2 \pm 7.2$	$509.2 \pm 11.3$	$108.5 \pm 5.6$	n.d.	n.d.
$K_M$ [ $\mu\text{M}$ ]	$7.4 \pm 0.8$	$2.1 \pm 0.2$	$3.5 \pm 0.4$	$36.3 \pm 5.2$	n.d.	n.d.
$k_{cat}$ [ $\text{s}^{-1}$ ]	119.9	218.0	270.8	397.8	n.d.	n.d.
Tryptophan melting point [ $^{\circ}\text{C}$ ]	$50.4 \pm 0.1$	41.6	$39.2 \pm 0.4$	n.d.	n.d.	n.d.
Flavin melting point [ $^{\circ}\text{C}$ ]	$48.7 \pm 0.2$	$42.7 \pm 0.2$	$43.4 \pm 0.2$	n.d.	n.d.	n.d.
Sp. activity 25 $^{\circ}\text{C}$ [ $\mu\text{mol mg}^{-1} \text{min}^{-1}$ ]	$199 \pm 5$	$391 \pm 7$	$478 \pm 23$	$37.8 \pm 2.1$	$14.9 \pm 0.8$	$10.5 \pm 0.7$
Sp. activity 37 $^{\circ}\text{C}$ [ $\mu\text{mol mg}^{-1} \text{min}^{-1}$ ]	$389 \pm 21$	$20 \pm 3$	$15 \pm 2$	$20.8 \pm 2.9$	$2.1 \pm 0.5$	$2.5 \pm 0.3$
$\frac{\text{Sp. activity } 25^{\circ}\text{C}}{\text{Sp. activity } 37^{\circ}\text{C}}$ Ratio in [%]	195	5	3	54	14	24

Sp. activity: Specific enzymatic activity. Melting points are defined as midpoints of the sigmoidal fit of the fluorescence of flavin dissociation or tryptophan unfolding.

Additionally, analysis of NADH oxidase activity of the F406 variants displayed their increased product inhibition. The presence of 1 mM NAD<sup>+</sup> had only minor impact on the specific activity of the wild type, but reaction velocities of F406A and F406S decreased by 55 % and 73 %, respectively (table 9).

**Table 9: Product inhibition data of FAD domain variants.**

Specific NADH oxidation rates [ $\mu\text{mol mg}^{-1} \text{min}^{-1}$ ]	FAD Domain wild type	FAD Domain F406A	FAD Domain F406S
No NAD <sup>+</sup> added	190 ± 15	457 ± 22	489 ± 10
1 mM NAD <sup>+</sup> added	184 ± 8	206 ± 19	130 ± 15
% inhibition in the presence of 1 mM NAD <sup>+</sup>	3	55	73

### 3.3.2.3. Productive binding with NAD<sup>+</sup> and NADH

Soaking of crystals obtained from the purified F406A and F406S variants of the FAD domain with 0.1 M NAD<sup>+</sup> or 0.2 M NADH yielded electron density maps with the nicotinamide ring in a productive binding mode for hydride transfer. A superposition of F406S structures with either form of the cofactor is shown in figure 42. Both NAD<sup>+</sup> and NADH nicotinamide are tilted relative to the plane of the isoalloxazine ring. C4 of nicotinamide is about equidistant from Cys 378 S<sub>y</sub> and isoalloxazine N5 (3 - 3.6 Å) in both the oxidized and reduced forms. NAD<sup>+</sup> nicotinamide is slightly shifted, increasing the distance from carboxamide to Ser 213 O<sub>y</sub> by 2 - 2.5 Å. The C-terminal residues are flexible (high B-factors) and could not completely be modeled in all cases. Positions of the FAD cofactors are comparable, but the isoalloxazine is tilted by 16 ° counterclockwise in the NAD<sup>+</sup> structure.

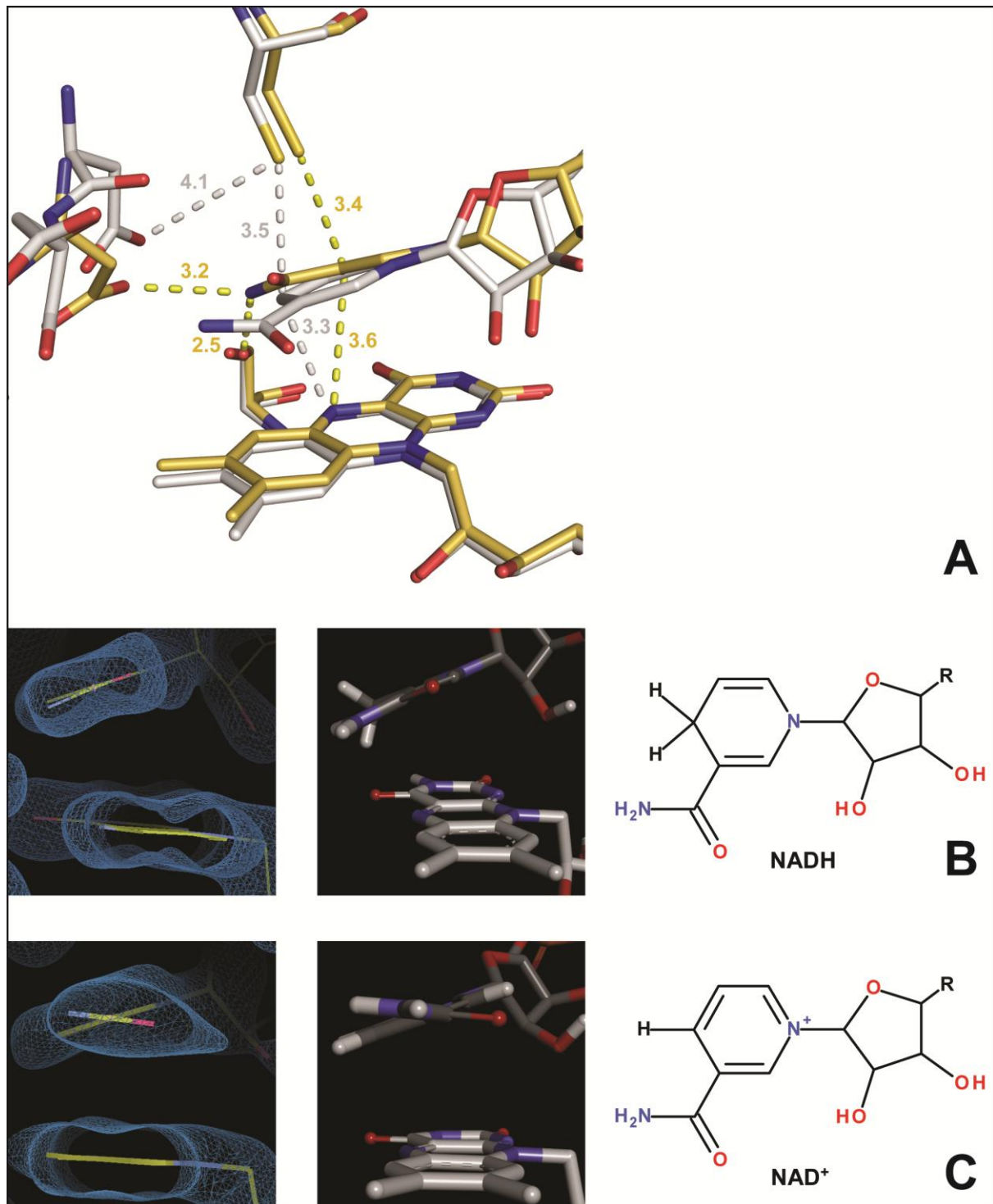


**Figure 42: Nicotinamide binding mode in the F406S variant of the FAD domain bound to NAD<sup>+</sup> or NADH.** **A:** Superposition of the active site. Yellow: FAD domain F406S-NADH complex. White: FAD domain F406S-NAD<sup>+</sup> complex. Dotted lines show stabilizing interactions between the nicotinamide and the surrounding isoalloxazine, serine, cysteine and aspartate moieties. **B + C:** Side views of the NADH and NAD<sup>+</sup> complexes, respectively with 2F<sub>o</sub>-F<sub>c</sub> electron density maps contoured at 1 σ (left panels). Hydrogen atoms are highlighted in the middle panels. For clarity, the right panels show the formulas of the ribosyl-nicotinamide of NADH and NAD<sup>+</sup>.

### 3.3.2.4. Structural superposition of ferredoxin:NADP<sup>+</sup> reductase Y308S and FAD Domain F406S variants in complex with NAD<sup>+</sup>

The F406S-NAD<sup>+</sup> complex was also compared with the structure of the FNR Y308S-NADP<sup>+</sup> complex (PDB 1QFY). The Rossmann fold forming the nicotinamide dinucleotide binding pocket and the anti-parallel beta-sheet structure which forms part of the flavin adenine dinucleotide pocket are highly conserved (figure 43). Residues Cys 378, Ser 213 and Asp 404 are closely positioned to their respective counterparts. Similar to the situation in F406S-NAD<sup>+</sup>/NADH superposition, the carboxamide group of the F406S NAD<sup>+</sup> is slightly shifted and rotated around the C7 - C3 bond. The isoalloxazine moiety in the FNR structure is shifted by about 1 Å and also rotated clockwise by 22°, leading to a shorter distance between nicotinamide C4 and isoalloxazine N5. The adenine groups of FAD are arranged differently by rotation of about 180° around the 4'C - 5'C bond of the ribose.

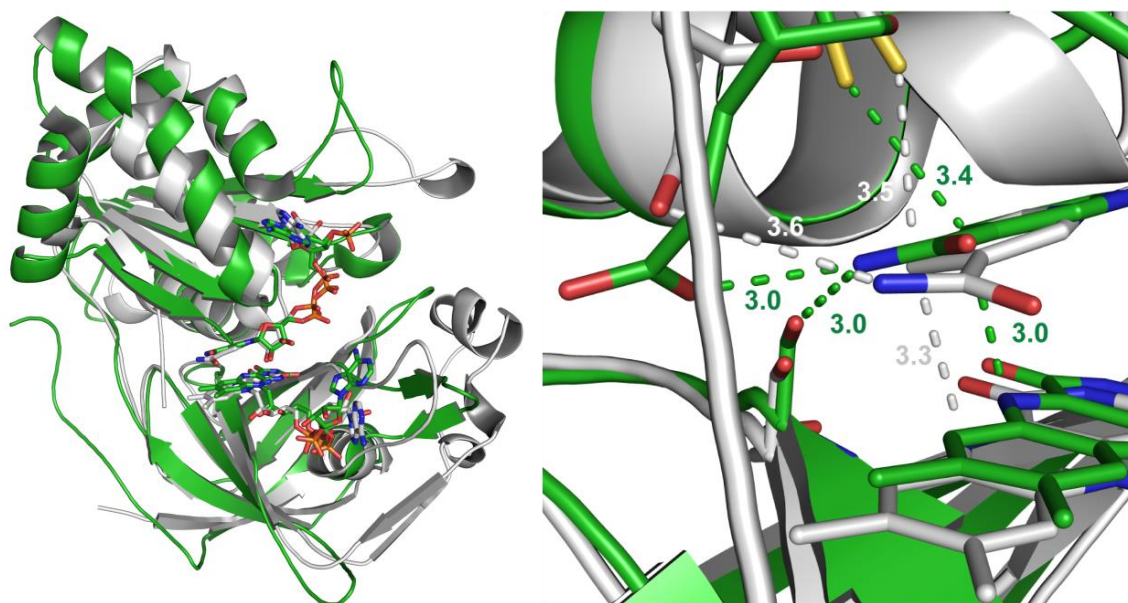


**Figure 43: Structural alignment of the Na<sup>+</sup>-NQR FAD domain F406S-NAD<sup>+</sup> complex (white) and the FNR Y308S-NADP<sup>+</sup> complex (green).** Right panel: Magnification of the nicotinamide binding site. Dotted lines show stabilizing interactions between the nicotinamide and the surrounding isoalloxazine, serine, cysteine and aspartate/glutamate moieties.

### 3.3.3. The catalytic quinone binding site of the Na<sup>+</sup>-translocating NADH:quinone oxidoreductase from *Vibrio cholerae* accommodates two quinones

#### 3.3.3.1. Interaction of Na<sup>+</sup>-NQR with Q<sub>1</sub> and DBMIB monitored by the electron transfer activities

As DBMIB is an analogue and antagonist of ubiquinone, it was used in this work to obtain information on quinone binding by the Na<sup>+</sup>-NQR. First, we asked whether DBMIB has an influence on NADH oxidation by the Na<sup>+</sup>-NQR. The effect of DBMIB on NADH oxidase activity was assayed by maintaining a constant concentration of the artificial electron acceptor Q<sub>1</sub> while varying the concentration of the substrate NADH. Both NADH oxidation and quinol formation were recorded. Determined  $V_{\max}$  and  $K_m$  values were  $147.5 \pm 1.7 \mu\text{mol min}^{-1} \text{mg}^{-1}$  and  $29.6 \pm 0.6 \mu\text{M}$ , respectively, for NADH oxidation and  $38.9 \pm 1.2 \mu\text{mol min}^{-1} \text{mg}^{-1}$  and  $24.5 \pm 1.5 \mu\text{M}$ , respectively, for quinol formation (table 10). Pre-incubation of the enzyme with  $10 \mu\text{M}$  DBMIB led to a decrease in the NADH oxidation rate  $V_{\max}$  as well as in the Michaelis constant  $K_M$  with similar manifestations on the NADH oxidation and the quinol formation rates (figure 44, table 10).

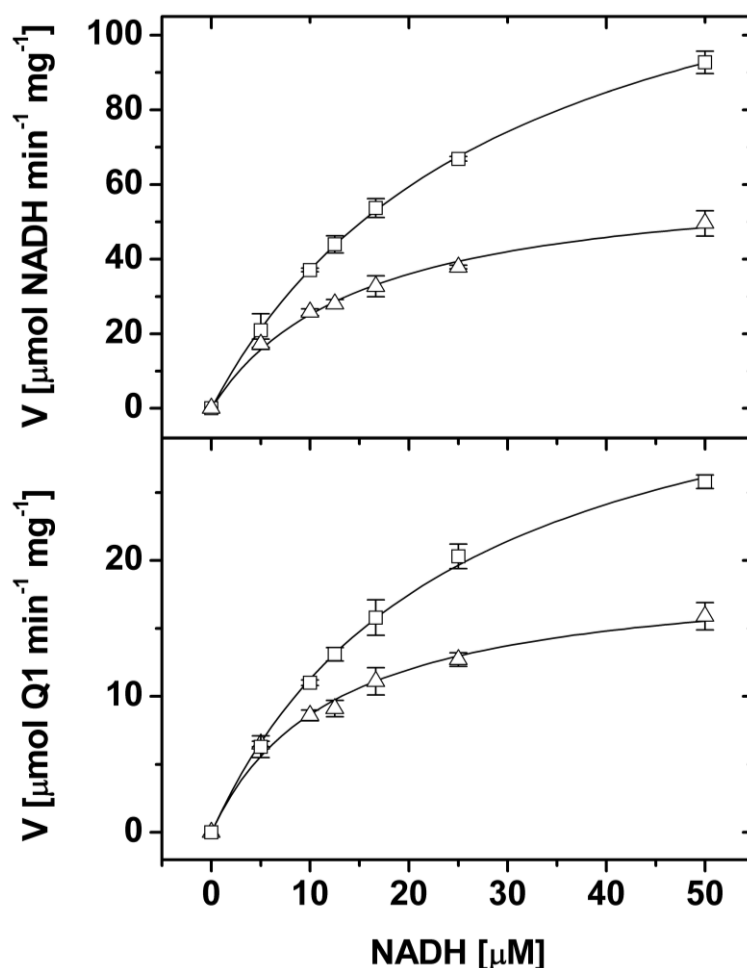


**Figure 44: Inhibition of Na<sup>+</sup>-NQR by DBMIB determined at varying concentrations of NADH.** Assays were performed in the presence of 0.1 mM Q<sub>1</sub>. Specific activities (V) are expressed as μmol NADH used or μmol QH<sub>2</sub> formed per mg of enzyme per minute in the absence (squares) or presence of 10 μM DBMIB (triangles). Kinetic constants are summarized in table 10. Upper panel: NADH oxidation. Lower panel: Quinol formation.

**Table 10: Inhibition of Na<sup>+</sup>-NQR by DBMIB at varying NADH concentrations described by the Michaelis-Menten formalism.**

Activity recorded as	Kinetic constants	0 μM DBMIB	10 μM DBMIB
NADH oxidation	R <sup>2</sup>	0.9998	0.9956
	V <sub>max</sub> [μmol min <sup>-1</sup> mg <sup>-1</sup> ]	147.5 ± 1.7	63.1 ± 2.5
	K <sub>M</sub> [μM]	29.6 ± 0.6	15.1 ± 1.4
	K <sub>M</sub> /V <sub>max</sub>	0.2	0.24
	K <sub>i</sub> <sup>1</sup> [μM]	-	7.5
Quinol formation	R <sup>2</sup>	0.9985	0.9904
	V <sub>max</sub> [μmol min <sup>-1</sup> mg <sup>-1</sup> ]	38.9 ± 1.2	19.4 ± 1.0
	K <sub>M</sub> [μM]	24.5 ± 1.5	12.4 ± 1.7
	K <sub>M</sub> /V <sub>max</sub>	0.63	0.64
	K <sub>i</sub> <sup>1</sup> [μM]	-	9.9



The concentration of Q<sub>1</sub> in the assays was 0.1 mM. Corresponding rates are presented in figure 44. For calculation of K<sub>i</sub>' , the equation for uncompetitive inhibition was applied:

$$v_0 = \frac{V_{max} [S]}{K_M + \alpha' [S]}$$

where  $\alpha' = 1 + [I] / K_i'$  (Voet and Voet 2004).

Varying the ubiquinone-1 concentration of the buffer while starting the assay always by the addition of 50 μM NADH allowed the kinetic description of the quinone reductase activity of the Na<sup>+</sup>-NQR. Assays in the absence of DBMIB displayed a clearly defined Michaelis-Menten-like behavior of the enzyme (figure 45, upper panel) with a V<sub>max</sub> value of 25.8 ± 0.6 μmol min<sup>-1</sup> mg<sup>-1</sup> and a K<sub>M</sub> value of 14.0 ± 0.9 μM for quinol formation (table 11). No cooperativity in substrate binding was detectable (Hill coefficient n = 1.1 ± 0.1, table 11), indicative of only one catalytically active quinone site. If quinone reductase activity was measured in the presence of 10 μM or 25 μM DBMIB (figure 45, middle and lower panel respectively), decrease of V<sub>max</sub> and increase of K<sub>m</sub> values was observed, however, when assuming pure Michaelis-Menten behavior the quality of the fit was significantly decreased compared to the situation without DBMIB, manifested in lower correlation coefficients (table 11). Fits using the Hill equation yielded better results with respect to the squared correlation coefficient R<sup>2</sup>, with cooperativities of n = 1.3 ± 0.2 in the presence of 25 μM DBMIB and n = 1.5 ± 0.2 in the presence of 10 μM DBMIB (table 11).

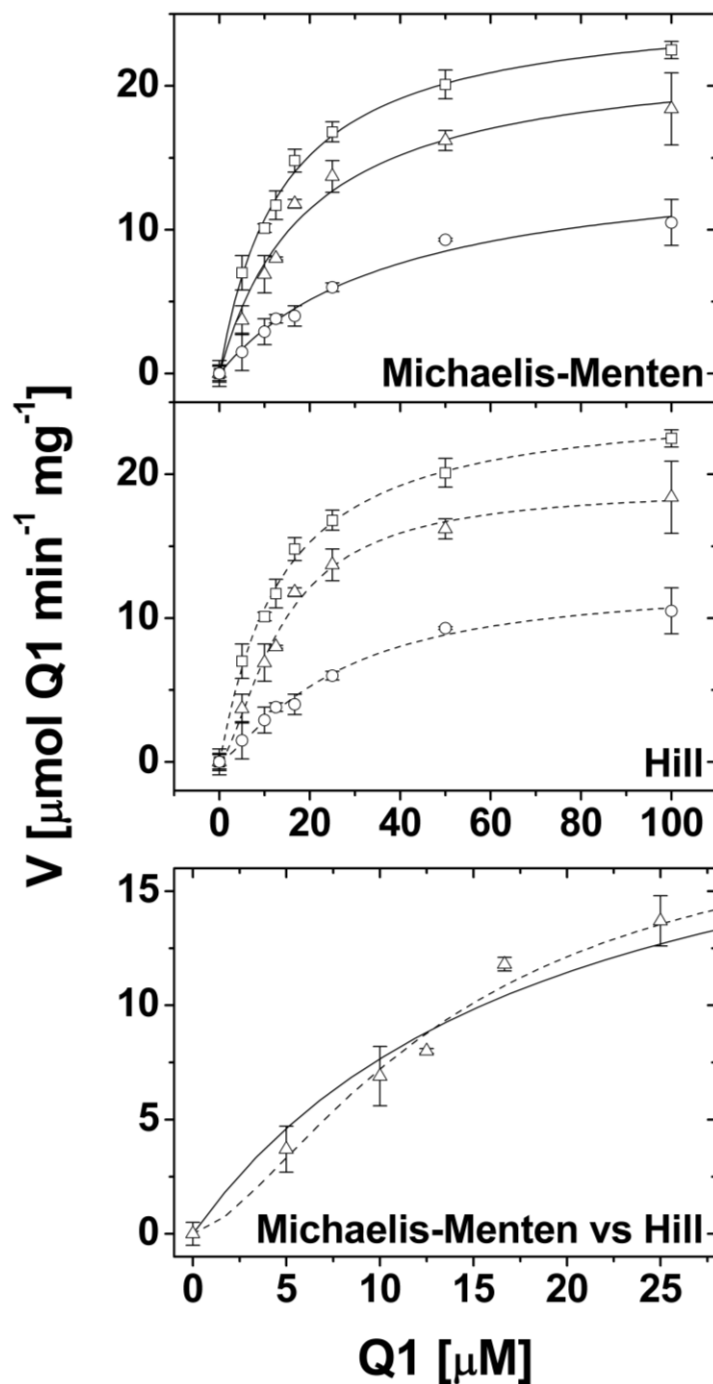


**Figure 45: Quinone reductase activities of Na<sup>+</sup>-NQR in presence or absence of DBMIB.** Specific activity ( $V$ ) is expressed as  $\mu\text{mol Q}_1$  reduced per mg of enzyme per minute. Rates were measured without addition of DBMIB (squares) and in the presence of 10  $\mu\text{M}$  (triangles) or 25  $\mu\text{M}$  (circles) DBMIB. The upper panel depicts Michaelis-Menten fits, the middle panel shows the same data with sigmoidal Hill fits. The lower panel shows a close-up of the data from the inhibition with 10  $\mu\text{M}$  DBMIB where the difference between fitting models is the most distinctive.

**Table 11: Analysis of the rates of quinol formation by Na<sup>+</sup>-NQR at varying Q<sub>1</sub> concentrations in the absence or presence of DBMIB by the Michaelis-Menten or the Hill formalism.**

<b>Michaelis-Menten</b> $v_0 = (V_{max} * [S]) / (K_M + [S])$	<b>No DBMIB</b>	<b>10 μM DBMIB</b>	<b>25 μM DBMIB</b>
R <sup>2</sup>	0.9963	0.9811	0.9874
V <sub>max</sub> [μmol min <sup>-1</sup> mg <sup>-1</sup> ]	25.8 ± 0.6	22.6 ± 1.4	15.2 ± 1.1
K <sub>M</sub> [μM]	14.0 ± 0.9	19.4 ± 3.1	39.5 ± 6.0
K <sub>i</sub> [μM]	-	35.9	38.7
K <sub>i</sub> ' [μM]	-	70.6	35.8

<b>Hill</b> $v_0 = (V_{max} * [S]^n) / (K^n + [S]^n)$	<b>No DBMIB</b>	<b>10 μM DBMIB</b>	<b>25 μM DBMIB</b>
R <sup>2</sup>	0.993	0.9878	0.9896
V <sub>max</sub> [μmol min <sup>-1</sup> mg <sup>-1</sup> ]	25.1 ± 1.2	19.1 ± 0.9	12.5 ± 1.1
K [μM]	13.3 ± 1.5	13.9 ± 1.2	25.7 ± 4.7
n	1.1 ± 0.1	1.5 ± 0.2	1.3 ± 0.2

The NADH concentration in the assays was 50 μM. Corresponding rates are presented in figure 45. For calculation of K<sub>i</sub> and K<sub>i</sub>', the equation for mixed inhibition was applied:

$$v_0 = \frac{V_{max} [S]}{\alpha K_M + \alpha' [S]}$$

where  $\alpha = 1 + [I] / K_i$  and  $\alpha' = 1 + [I] / K_i'$  (Voet and Voet 2004).

As DBMIB can also serve as electron acceptor in quinone reducing enzymes (Simkovic and Frerman 2004), reductase activity of the Na<sup>+</sup>-NQR using DBMIB as substrate was determined separately (table 12). DBMIB inhibition data were corrected for this effect.

**Table 12: Kinetic constants of the Na<sup>+</sup>-NQR quinone reductase activity using DBMIB as substrate.**

<b>Michaelis-Menten</b> $v_0 = (V_{max} * [S]) / (K_M + [S])$		
NADH oxidation	R <sup>2</sup>	0.9956
	V <sub>max</sub> NADHox [μmol min <sup>-1</sup> mg <sup>-1</sup> ]	14.39 ± 0.65
	K <sub>M</sub> NADHox [μM]	39.97 ± 3.77
DBMIB reduction	R <sup>2</sup>	0.9944
	V <sub>max</sub> [μmol min <sup>-1</sup> mg <sup>-1</sup> ]	5.62 ± 0.34
	K <sub>M</sub> [μM]	53.67 ± 6.29

### 3.3.3.2. Binding of DBMIB to the NqrA subunit

It was recently shown that subunit NqrA of the Na<sup>+</sup>-NQR harbors a Q binding site (Casutt, Nedielkov et al. 2011). We now asked if NqrA also interacts with DBMIB. NqrA contains three tryptophan residues. Measurement of tryptophan fluorescence during DBMIB titration enabled us to detect changes in the microenvironment of the binding site. Incubation of NqrA with DBMIB lead to quenching of the fluorescence. Saturation of the quenching was observed at concentrations > 100 μM DBMIB, with 15 % of the original fluorescence remaining, indicating that at least two of the three tryptophan residues of the protein are closely affected by DBMIB binding. The data were fitted to a one-site binding and a Hill model (figure 46). The goodness of fit was significantly higher with the sigmoidal Hill model yielding an apparent  $K_D$  of  $5.05 \pm 0.25 \mu\text{M}$  and Hill coefficient of  $n = 1.95 \pm 0.20$  (table 13). The Scatchard plot of the data revealed a parabola which is open at the bottom, confirming the findings of a positive cooperativity (figure 46, lower panel).

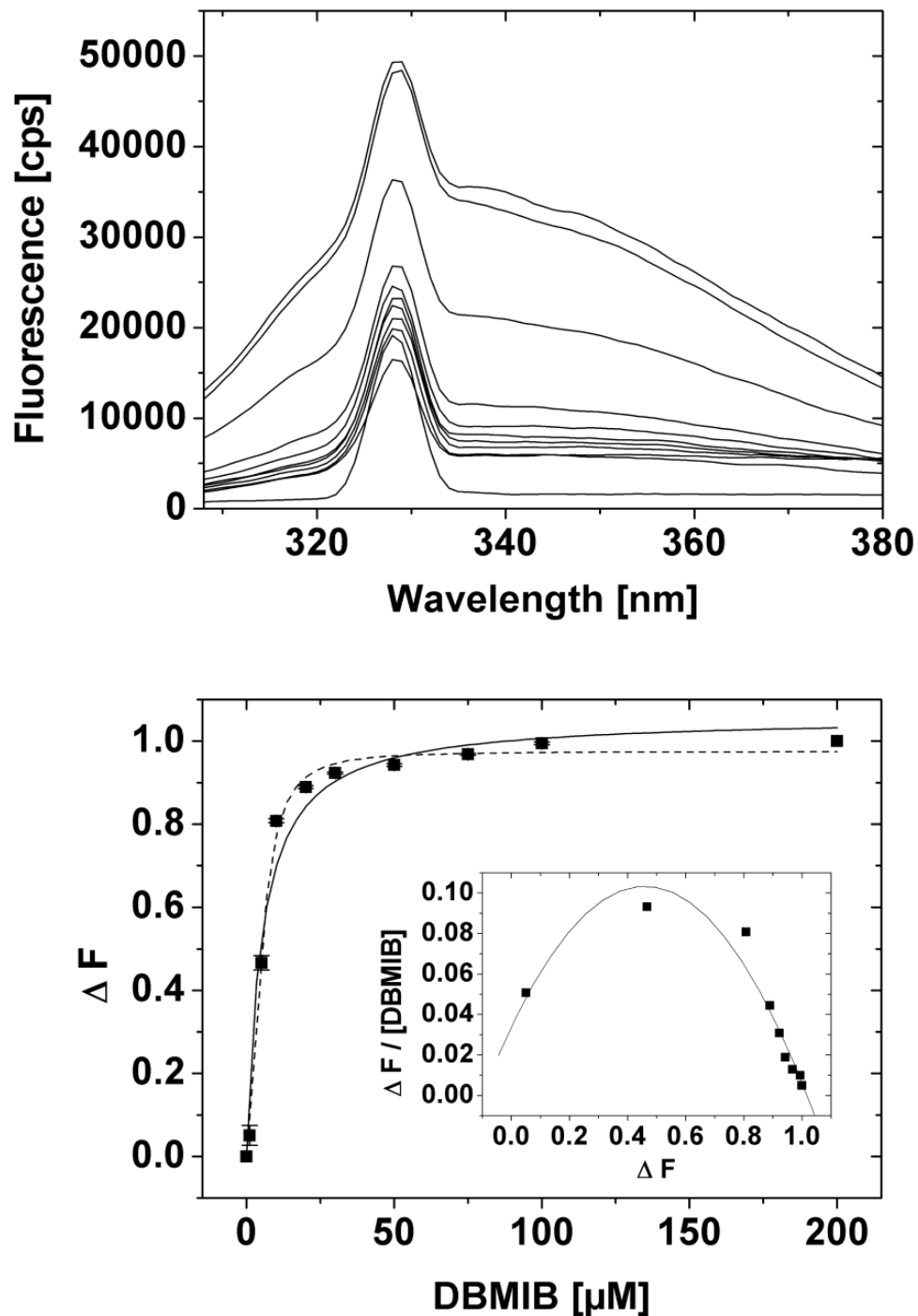


**Figure 46: Binding of DBMIB to NqrA monitored by quenching of tryptophan fluorescence.**

Upper panel: Fluorescence emission spectra, from top to bottom (using 338 nm as reference): 0.25  $\mu\text{M}$  NqrA titrated with 0, 1, 5, 10, 20, 30, 50, 75, 100 and 200  $\mu\text{M}$  DBMIB. Bottom-most spectrum is buffer only (50 mM Tris-HCl, 300 mM NaCl, pH 8, 5 % glycerol). Excitation wavelength was 295 nm. Samples were measured in triplicates, one spectrum is shown of each condition. DBMIB exhibits no fluorescence in the analyzed wavelength range. Lower panel: The increase in quenching ( $\Delta F$ ) of the tryptophan emission at 338 nm depicted in the upper panel was normalized to values between 0 and 1 and plotted against the concentration of DBMIB. Non-linear regression analysis using the Hill equation (dashed line) and a one-site binding model (solid line) was performed. Inset: Scatchard plot with polynomial fit, visualizing the cooperative binding of two equivalents of DBMIB to NqrA.

**Table 13: Binding of DBMIB to the NqrA subunit according to tryptophan fluorescence quenching.**

<b>One-site binding model:</b> $y = (P_1 * x) / (P_2 + x)$	
R <sup>2</sup>	0.97495
P <sub>1</sub>	1.06 ± 0.04
P <sub>2</sub>	5.14 ± 1.05 μM
<b>Hill equation:</b> $y = (P_1 * x^n) / (P_2^n + x^n)$	
R <sup>2</sup>	0.99464
P <sub>1</sub>	0.98 ± 0.01
P <sub>2</sub>	5.05 ± 0.25 μM
n	1.95 ± 0.20
<b>Polynomial, 2nd degree:</b> $y = A + B * x + C * x^2$	
R <sup>2</sup>	0.93672
A	0.03 ± 0.01
B	0.30 ± 0.05
C	-0.33 ± 0.04

Fluorescence data were fitted to a one site binding model and to the Hill equation (cooperative binding of more than one ligand). In addition, the data, plotted according to Scatchard, were fitted to a 2<sup>nd</sup> degree polynomial.

STD NMR confirmed DBMIB binding to NqrA with, at a given ligand-to-protein-ratio, STD effects that were even stronger (max. 25 %) than with Q<sub>1</sub> (max. 8.5 %) (figure 47). Furthermore, signals in the proton NMR spectrum of DBMIB became broad and shifted upon binding to NqrA which is indicative for a binding kinetic at the intermediate NMR time scale. In order to circumvent problems caused by exchange broadening, STD effects were quantified at a higher excess of DBMIB (40:1) as compared to experiments with Q<sub>1</sub>. The strongest STD signals originated from the isopropyl group of DBMIB (methyl groups: 25.0 %, CH group: 24 - 25 %). The methyl group bound directly to the quinone ring showed an STD effect of 16.1 %. This suggests that the isopropyl group of DBMIB is in closest contact to NqrA.

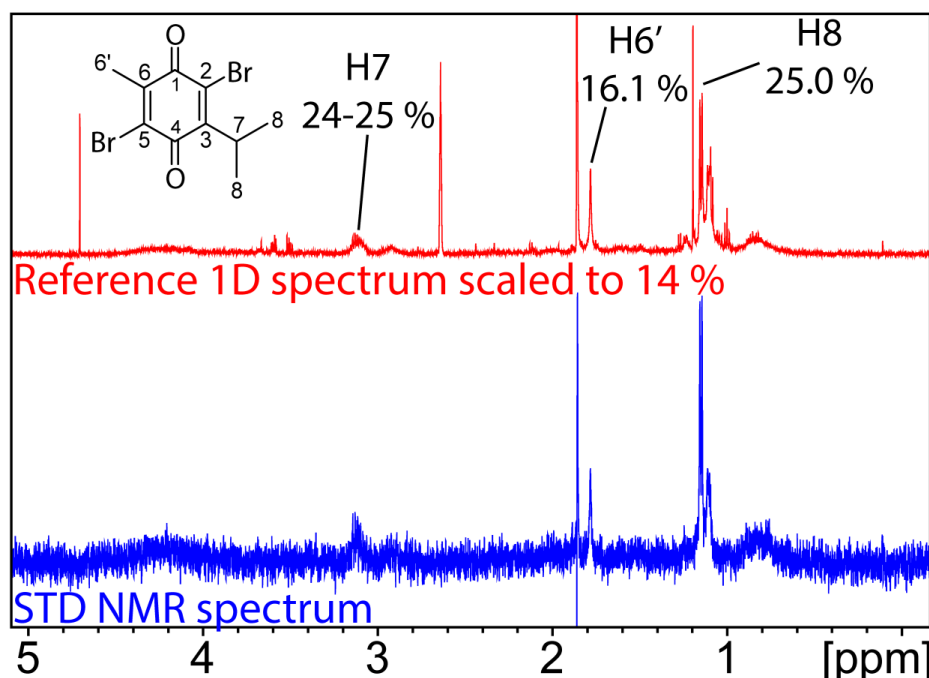


**Figure 47: Saturation transfer difference NMR of DBMIB interacting with NqrA.** Reference (upper panel) and STD NMR (lower panel) spectra of DBMIB in the presence of NqrA (molar ratio = 40:1). The reference spectrum was scaled to 14 % of its original intensity. Signals of the same intensity in the STD spectrum correspond to an STD effect of 14 %.

### 3.3.3.3. DBMIB and ubiquinone Q<sub>1</sub> bind simultaneously to the NqrA subunit

In order to investigate how DBMIB affects the binding of Q<sub>1</sub> to the NqrA subunit we studied the influence of DBMIB on the STD effects of Q<sub>1</sub> at a constant concentration of Q<sub>1</sub> (figure 48A). The changes of STD effects of all Q<sub>1</sub> signals were quantified and are presented in figure 48B. To this end, STD effects in the absence of DBMIB were set as a reference and subtracted from all other effects measured in the presence of the inhibitor. Importantly, STD effects increased with increasing concentrations of DBMIB. STD effects of Q<sub>1</sub> were affected by DBMIB in a concentration dependent fashion. This effect leveled off at DBMIB concentrations above 80 - 100 μM. STD changes of all five signals of Q<sub>1</sub> were fitted globally to a one-site binding model, leading to an EC<sub>50</sub> value of  $k = 26.1 \pm 2.5 \mu\text{M}$ .

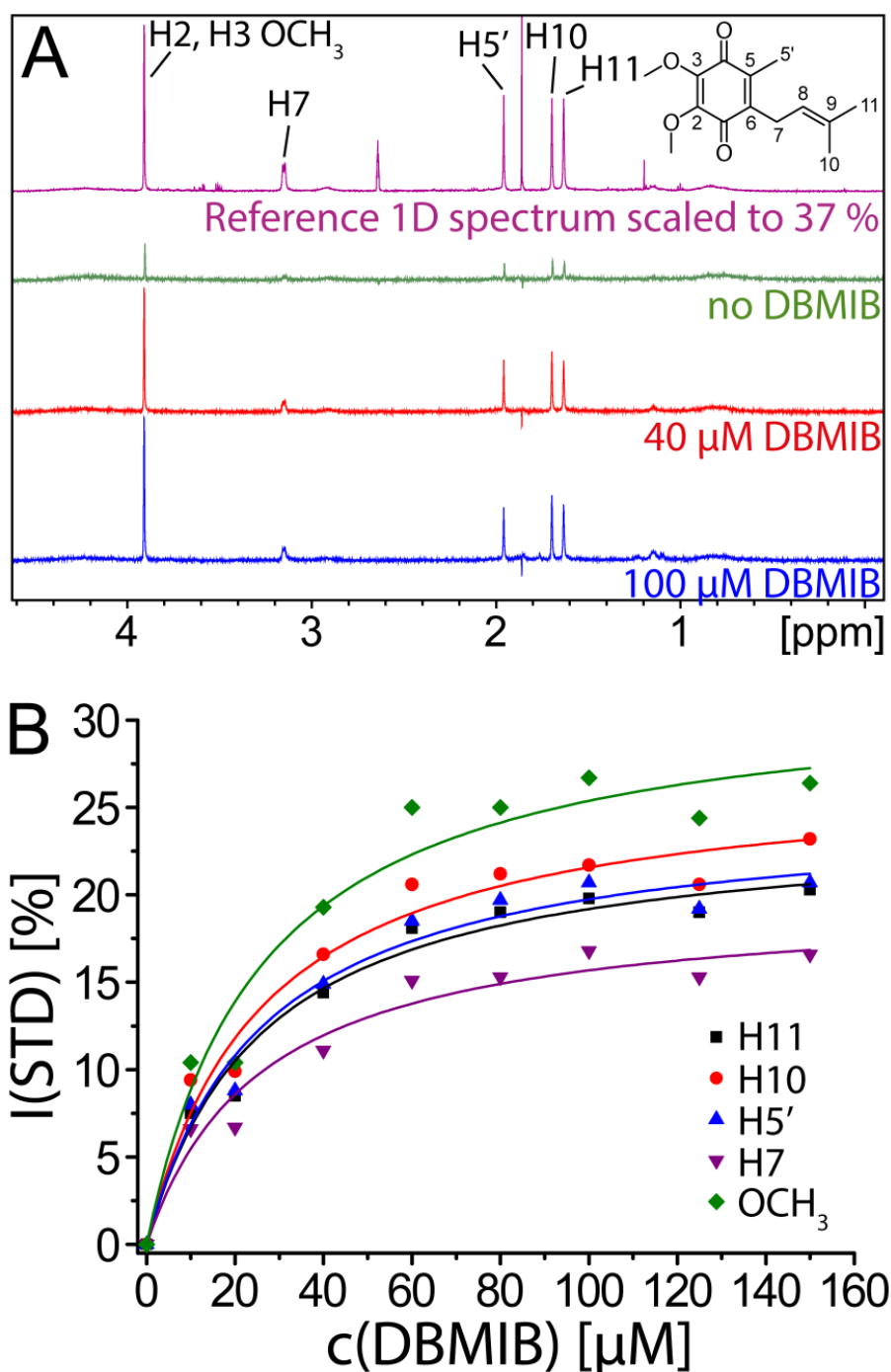


**Figure 48: Saturation transfer difference NMR spectroscopy of Q<sub>1</sub> and DBMIB in the presence of NqrA.** **A:** Reference (upper panel) and three STD NMR (three lower panels) spectra of Q<sub>1</sub> with increasing DBMIB concentration in the presence of NqrA. The reference spectrum was scaled to 37 % of its original intensity. Signals of the same intensity in the STD spectrum correspond to an STD effect of 37 %. The picture shows growing STD effects of Q<sub>1</sub> signals with increasing DBMIB concentration. **B:** Changes of saturation transfer difference NMR effects of Q<sub>1</sub> depending on the concentration of DBMIB. Experimental data points are fitted to a one-site binding model ( $y = B_{\max} * x / (k + x)$ , solid lines), the constant  $k$  was fitted globally for all curves.



The influence of DBMIB on STD effects of Q<sub>1</sub> was also analyzed with regard to the binding mode of Q<sub>1</sub> (table 14). For this purpose a ratio between STD effect of Q<sub>1</sub> at maximal concentration of DBMIB and in the absence of DBMIB was calculated. These ratios were then normalized to the minimal ratio (for H10) that was set to 1. Rather than increasing or decreasing all STD effects of Q<sub>1</sub> homogeneously, the quinone analogue DBMIB affected the STD intensities of H-5' and H-7 more strongly than the remaining signals of Q<sub>1</sub>. Our analysis shows that STD effects of H-5' and H-7 increase disproportionately upon addition of DBMIB.

**Table 14: Relative changes of the STD effects of Q<sub>1</sub> induced by the presence of DBMIB.**

Signal	STD effects of Q <sub>1</sub> , %		Ratio 150 μM / 0 μM DBMIB	Relative ratio, ratio(H10) = 1
	no DBMIB	DBMIB 150 μM		
H11	6.0	26.3	4.38	1.07
H10	7.5	30.7	4.09	1.00
H5'	5.1	25.8	5.06	1.24
H7	3.4	20.0	5.88	1.44
OCH <sub>3</sub>	8.5	34.9	4.11	1.00

#### 3.3.3.4. DBMIB and ubiquinone Q<sub>1</sub> occupy an extended quinone binding site

The fact that, according to STD NMR, DBMIB does not displace Q<sub>1</sub> from the binding site but alters the binding mode of the native substrate led us to ask whether both quinones interact with NqrA in direct vicinity to each other. To test this we recorded NOESY spectra of both ligands in the presence of NqrA (figure 49). Indeed, we observed interligand NOE correlations (ILOEs) between Q<sub>1</sub> and DBMIB (London 1999). These correlations are only observed in the presence of NqrA. A mixture of both ligands in the absence of NqrA does not show ILOEs (figure 49) nor does NqrA show crosspeaks at these positions in the absence of Q<sub>1</sub> and DBMIB. It is important to note that the observation of ILOEs critically depends on the presence of NqrA but proved independent on whether protonated or perdeuterated NqrA was used during NOESY experiments. That means that the correlations observed originate from direct transfers between the ligands and not from protein-mediated effects.

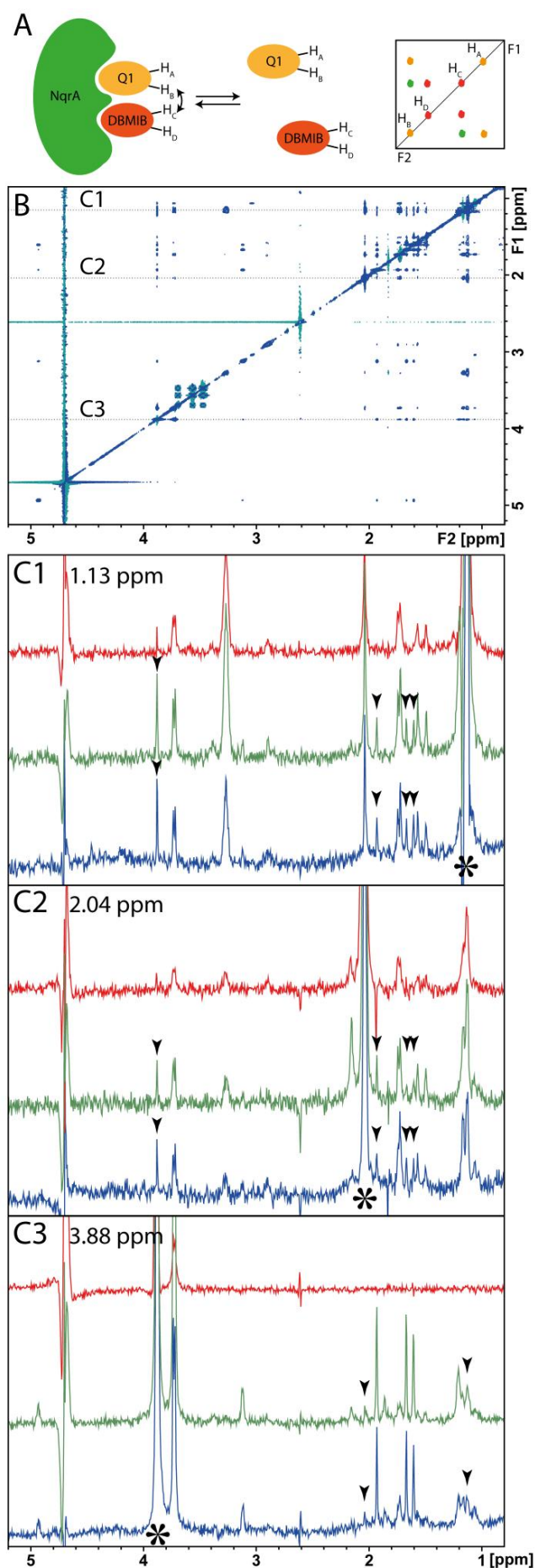


**Figure 49: Interligand Overhauser effects between Q<sub>1</sub> and DBMIB in the presence of NqrA.** **A:** Scheme illustrating the build-up of an intermolecular NOE due to simultaneous binding of both ligands in direct vicinity to each other. **B:** Expansion of the NOESY spectrum of 200  $\mu$ M Q<sub>1</sub> and 400  $\mu$ M DBMIB in the presence of 25  $\mu$ M NqrA in deuterated PBS buffer (150 mM NaCl, 10 mM NaP<sub>i</sub>, 4 mM NaN<sub>3</sub> in D<sub>2</sub>O). The mixing time was 600 ms. Chemical shifts at which traces were extracted for panel C are indicated by dashed lines. **C:** Three panels **C1**, **C2**, and **C3**, showing traces extracted from the NOESY spectrum of Q<sub>1</sub> and DBMIB. In each panel, the blue trace originates from the NOESY spectrum measured in the presence of protonated NqrA; the green trace was measured in the presence of perdeuterated NqrA; the red trace was measured in the absence of NqrA. ILOEs are indicated by arrowheads. The position of the diagonal signal is marked with an asterisk.

### 3.4. Discussion

#### 3.4.1. Ag<sup>+</sup>-mediated killing of *Vibrio cholerae* originates in silver binding to Cys 378 of subunit F of the Na<sup>+</sup>-NQR

We determined the high-resolution 3D structures of the FAD domain in complex with NADH or Ag<sup>+</sup>. An overlay of the two structures (figure 34) revealed the presence of the heavy metal cation in a site occupied by the nicotine amide moiety of the enzyme during catalysis. Ag<sup>+</sup> was ligated to the thiolate sulfur of C378 protruding into the active site. In parallel, kinetic studies determined that the Na<sup>+</sup>-NQR and the isolated FAD domain are irreversibly inactivated by nanomolar concentrations of Ag<sup>+</sup> (figure 33). The C378A variants of these enzymes did not exhibit this inactivation, or only in a very diminished form (figure 35, table 7).

A study on the Na<sup>+</sup>-translocating NADH-quinone reductase from *Vibrio alginolyticus* found Ag<sup>+</sup> to act as a competitive inhibitor in respect to quinones (Unemoto, Ogura et al. 1993). However, effects on NADH oxidation were not investigated. Furthermore, the inhibition experiments were performed in the presence of 200 mM Cl<sup>-</sup>. Due to the low solubility of AgCl (solubility product constant [AgCl] =  $1.7 \times 10^{-10} \text{ mol}^{-2} \text{ l}^{-2}$ ; (Weast 1981)), it can be assumed that the free Ag<sup>+</sup> concentration in these experiments was much lower than specified. A subsequent study concluded that the mode of inhibition by nanomolar concentrations of Ag<sup>+</sup> on Na<sup>+</sup>-NQR must be one of irreversible inactivation, most likely involving the displacement of FAD from the NADH dehydrogenase site by Ag<sup>+</sup> (Steuber, Krebs et al. 1997). Our findings confirm this mode of inhibition and reinforce the conclusion that the cysteine 378 of subunit NqrF is the primary attack point for silver ions in the Na<sup>+</sup>-NQR.

Our *in vivo* experiments show that *V. cholerae* exhibits increased viability if expressing the Na<sup>+</sup>-NQR C378A variant versus the Na<sup>+</sup>-NQR wild type when 1 - 1.5 μM Ag<sup>+</sup> are present in the medium. This implies that the Na<sup>+</sup>-NQR represents one of the most sensitive and essential components in the cell. Ag<sup>+</sup> concentrations lower than 1 μM did not have a measurable effect in spite of the Na<sup>+</sup>-NQR having a K<sub>i</sub> in the low nanomolar range (table 7). There might be several reasons accounting for this fact: Ag<sup>+</sup> most likely cannot easily pass the cell membrane. Since Cys 378 of NqrF is located on the cytoplasmic side of the membrane, there might be limited access of the free Ag<sup>+</sup> to this residue. Also, succinate present in the medium may chelate Ag<sup>+</sup> and lower the free Ag<sup>+</sup> concentration. Other components of the cell may

bind Ag<sup>+</sup> as well, diminishing the drastic toxic effect on the bacterial cell. Such a component is e.g. glutathione. At Ag<sup>+</sup> concentrations above 1.5 μM, there is no visible protective effect of the C378A mutation. Since we a look at whole cell viability, there may be many factors which influence the survival of the bacterial cell. Energy metabolism is just one aspect. Higher concentrations of Ag<sup>+</sup> very likely target other essential systems, as well leading to bacterial death.

Central processes like synthesis of proteins and respiration are essential for the survival of microorganisms. Respiratory enzymes like the Na<sup>+</sup>-NQR are putative targets for antibacterial drugs, as shown for the complex V (ATP synthase) from *Mycobacterium tuberculosis* (Andries, Verhasselt et al. 2005). The Na<sup>+</sup>-NQR does not exhibit sequence homology to the mitochondrial complex I from eukaryotes, an enzyme which is not inhibited by Ag<sup>+</sup> (Lin, Puhar et al. 2008) and whose NADH binding site does not contain a cysteine residue which could act as a ligand for Ag<sup>+</sup> (Sazanov and Hinchliffe 2006). In accord with that finding, the toxicity of Ag<sup>+</sup> in humans is very low (Silver 2003), and it seems as if the full potential of silver, especially as constituent of different chemical entities, is not yet tapped. Our study represents the basis for the development of novel, silver-based strategies to combat bacterial infections in the future.

#### **3.4.2. Structure-function analysis of the NADH oxidizing domain of the Na<sup>+</sup>-NQR from *Vibrio cholerae***

Cysteine residues in active sites of enzymes are often stabilized in their thiolate state as they are readily deprotonated by the microenvironment of the surrounding protein (Klomsiri, Karplus et al. 2011). It is observed in numerous NADH dehydrogenases that cysteines are involved in critical catalytic steps. In liver alcohol dehydrogenase, two deprotonated cysteines help coordinate the catalytic Zn<sup>2+</sup> ion. In addition, one of these cysteines, Cys 174, was found in close distance to the C4 of the NAD<sup>+</sup> nicotinamide, so that sulfhydryl-nicotinamide adducts have been proposed (Hackett, Novoa et al. 1986). Such adducts were also implicated with the first catalytic step of glyceraldehyde-3-phosphate dehydrogenase (Moras, Olsen et al. 1975) and in cytochrome *b*<sub>5</sub> reductase (Hackett, Novoa et al. 1986). In the flavoprotein family of ferredoxin:NADP<sup>+</sup> reductases, to which the FAD domain of NQR belongs, a cysteine is structurally conserved directly in the binding pocket of the nicotine

amide moiety, as shown in figure 34. It has been proposed that this cysteine helps forcing the nicotinamide against the flavin and restricting its conformational freedom to facilitate hydride transfer (Deng, Aliverti et al. 1999). Based on our functional and structural findings, we suggest a more active role of this residue and propose that the thiolate group of cysteine 378 catalyses hydride transfer by directly stabilizing the  $\delta^+$  on C4 of the nicotine amide ring during the transition state of the reaction, either as a charge-transfer complex or in a S<sub>N</sub>2-like substitution. Supporting this hypothesis are data presented in chapter 3.3.1., in which the C378A variant of the FAD domain showed improved NADH binding but significantly decreased catalytic turnover (27 % of wild type).

The role of the phenylalanine 406 residue in the NADH-oxidizing FAD domain seems in many ways comparable to the role of the C-terminal tyrosine in ferredoxin:NADP<sup>+</sup> reductase which has been described, among others, in (Orellano, Calcaterra et al. 1993; Piubelli, Aliverti et al. 2000) and (Nogues, Tejero et al. 2004). The authors of latter publication described the function of the C-terminal tyrosine as "[...] lowering the affinity for NADP<sup>+</sup>/H to levels compatible with steady-state turnover [...]". In this work, phenylalanine mutants F406A and F406S were analyzed, resulting in enhanced nicotinamide binding of the respective FAD domain variant. In addition, both FAD domain variants were not impaired in their catalytic activity, but surprisingly displayed even higher turnover rates than the wild type at 25 °C. This effect, not observed in the respective FNR analogs, comes at the cost of losing enzyme stability, the FAD cofactor, and is accompanied with a loss of function at increasing temperatures. It cannot completely be ruled out that the presence of the ferredoxin-like N-terminal domain, which harbors the [2Fe-2S] cluster of NqrF and which was not part of this study, would diminish this effect and lead to tighter FAD binding, but kinetic data of the phenylalanine variants of the holo-NQR complex (table 8) also suggest a destabilizing effect of the mutation. We thus conclude that phenylalanine acts as an internal competitor for the nicotinamide and that it enhances stability by keeping the FAD in place. Stabilization by stacking interaction with the isoalloxazine ring seems plausible and has been proposed before (Orellano, Calcaterra et al. 1993). When phenylalanine lowers the affinity for NAD<sup>+</sup>/H, it does so without much discrimination. The K<sub>M</sub> for NADH of the Na<sup>+</sup>-NQR was determined at 36 μM in this work. The K<sub>I</sub> for competitive inhibition of Na<sup>+</sup>-NQR by NAD<sup>+</sup> is reported as 11 mM (Bogachev, Belevich et al. 2009). The reason for the at least 100-fold higher affinity of

the enzyme for the reduced over the oxidized nicotinamide is still unclear, but possibly best explained by conformational differences between the oxidized/reduced nicotinamide moiety. In the structure of pea FNR where productive NADP<sup>+</sup>/H binding was observed, Ser 90 and Glu 306 have been identified as active site residues forming hydrogen bonds with the amide group and thus are pivotal in the binding of nicotinamide (Deng, Aliverti et al. 1999). In the FAD domain of Na<sup>+</sup>-NQR, Ser 213 and Asp 404 take analogous roles, positioned very similarly in the nicotinamide binding pocket. With the structural elucidation of the productive binding mode, a direct involvement of the serine residue in hydride transfer could be excluded. That this residue is nevertheless critical for catalysis has been shown in (Aliverti, Bruns et al. 1995), where a serine 96 to valine mutation of the spinach FNR led to an almost complete loss of activity. Similar conclusions were made regarding the function of the Glu 312 residue of FNR from the same species (Aliverti, Deng et al. 1998).

While the alignment between the FNR-Y308S-NADP<sup>+</sup> and NADPH structures revealed no significant differences in the coordinates of the nicotinamide group (Deng, Aliverti et al. 1999), we found that the nicotinamide ring was shifted by about 2 Å between the NADH and NAD<sup>+</sup> soaked structures (figure 42) of FAD domain F406S as well as F406A. This shift causes the distances between the amide nitrogen to Ser 213 O<sub>γ</sub> to increase from 2.5 Å to 5.2 Å and the distance from the amide nitrogen to the Asp 404 O<sub>ε2</sub> to increase from 3.2 Å to 3.6 Å in the oxidized form, effectively losing its hydrogen bonding. This difference, especially the serine/amide shift, was found consistently in both monomers of the asymmetric unit and in all measured crystals with small variations in the overall position of the nicotinamide-ribose and the C-terminus (n NAD<sup>+</sup>-soaks = 14, n NADH soaks = 20). Model bias can be excluded, since the coordinates of a crystal soaked with NADH were used for molecular replacement to solve the structure of the FAD domain soaked with NAD<sup>+</sup>.

In addition, we found that the carboxamide group of NAD<sup>+</sup> is best fitted into the 2F<sub>o</sub>-F<sub>c</sub> density map with a torsion angle of 20 ° to 25 ° relative to the plane of the nicotinamide ring, whereas the carbonyl amide group of NADH stays mostly planar with the ring (figure 42B + 42C). This turn of the carboxamide group has been observed in various protein structures with NAD<sup>+</sup> cofactors (Eklund, Samama et al. 1984) and in the X-ray structure of the NAD<sup>+</sup> molecule (Wright and King 1954) and represents an energetic minimum with respect to the relative orientation of the C7 - C3 bond (Coubeils, Pullman et al. 1971). In this orientation,

the amide hydrogens are arranged in a synclinal manner with respect to the hydrogen on the sp<sup>2</sup>-hybridized C4 atom.

It may well be that this internal change in nicotinamide conformation can tip the scales towards formation or loss of hydrogen bonding, the productive binding of nicotinamide and thus represents the determinant of the selectivity mechanism of the Na<sup>+</sup>-NQR.

### **3.4.3. The catalytic quinone binding site of the Na<sup>+</sup>-translocating NADH:quinone oxidoreductase from *Vibrio cholerae* accommodates two quinones**

The kinetic characterization of the Na<sup>+</sup>-NQR complex suggests that quinone reduction is best described by pure Michaelis-Menten formalism, indicating a single quinone binding site.

However, our recent surface plasmon resonance study of ubiquinone-1 (Q<sub>1</sub>) binding to the isolated NqrA subunit provided hints for the presence of a second quinone binding site with lower affinity (Casutt, Nediolkov et al. 2011). Furthermore, numerous studies report uncompetitive inhibition of the Na<sup>+</sup>-NQR by inhibitor molecules that are supposed to interact with the quinone binding site (Nakayama 1999; Yoshikawa, Nakayama et al. 1999; Hayashi, Shibata et al. 2002). It is also noteworthy that enzyme complexes catalyzing related chemical reactions (*bc*<sub>1</sub> complex, *b<sub>6</sub>f* complex, complex I) were indirectly shown to have quinone binding sites that can accommodate more than one quinone equivalent at a time - at least according inhibitor studies by HR-MAS NMR spectroscopy (Bartoschek, Johansson et al. 2001), according to EPR experiments (Ding, Moser et al. 1995) and when taking into account the locations of different inhibitors in various crystal structures (Efremov, Baradaran et al. 2010).

Here we show that the NqrA subunit of the Na<sup>+</sup>-NQR binds two quinone-type ligands adjacent to each other in an extended binding site.

We employed the quinone analogue and antagonist DBMIB, a well-known inhibitor of electron transfer complexes, to serve as a second quinone-type ligand that can easily be distinguished from Q<sub>1</sub> by NMR spectroscopy.

In the current study we provide - to our knowledge for the first time in the case of quinone binding enzymes - direct experimental evidence that two quinone-type molecules are situated in immediate vicinity to each other in the binding pocket of NqrA. This result was obtained by measuring interligand NOEs (ILOEs) between ubiquinone-1 and DBMIB. NOEs

between both molecules could, in principle, derive from several situations. If Q<sub>1</sub> and DBMIB formed stable complexes in solution one would expect intermolecular NOEs, however, in the absence of NqrA we do not detect intermolecular NOEs. Alternatively, NOEs between Q<sub>1</sub> and DBMIB could have been mediated by protons of the binding site of NqrA. Such intermolecular NOEs called INPHARMA effects could build-up even in a purely competitive binding situation (Sanchez-Pedregal, Reese et al. 2005). However, for INPHARMA effects to develop, the magnetization has to be 'stored' on the receptor during the ligand exchange process. This transfer is not possible if the experiment is carried out with a perdeuterated receptor and, thus, INPHARMA effect should be absent or at least strongly reduced under these conditions. We have performed the same experiment with protonated as well as perdeuterated NqrA and see no significant reduction in the intensity of the ILOE crosspeaks (figure 49). The only plausible interpretation is simultaneous binding of both ligands directly adjacent to each other within an extended quinone binding site of NqrA.

The precise relative arrangement of both ligands in the binding site cannot be determined to great accuracy from the ILOEs because of the in general low signal intensity and because essentially all protons of Q<sub>1</sub> show ILOEs to all protons of DBMIB with slightly varying intensity. According to this the most likely arrangement is a stacking interaction of both quinone moieties in the binding site.

That DBMIB does not displace Q<sub>1</sub> from the binding site in a competitive manner is furthermore supported by an STD NMR titration. In a competitive binding situation the STD effects of Q<sub>1</sub> should decrease upon titrating in DBMIB because DBMIB would displace Q<sub>1</sub> from the binding site lowering the fraction bound of Q<sub>1</sub> and, thus, lowering the amount of saturation transferred from NqrA to Q<sub>1</sub>. However, we observe exactly the opposite. Increasing the concentration of DBMIB leads to markedly increasing STD effect of Q<sub>1</sub>. In addition, in presence of DBMIB the ratio of STD effects of individual protons differs from the situation without inhibitor. This suggests that DBMIB alters the binding mode of Q<sub>1</sub> which in turn leads to a more efficient saturation transfer and therefore stronger STD effects. The EC<sub>50</sub> of this interaction is 26 μM.

The presence of two binding sites for quinone-type ligands is furthermore supported by tryptophan fluorescence quenching experiments. The fluorescence of NqrA depending on the concentration of added DBMIB can be fitted by a Hill-model consistent with positively cooperative binding of two equivalents of this inhibitor.



Can these results obtained with the isolated NqrA subunit be transferred to the holo-NQR complex? To gain insight into the physiological relevance we have performed enzyme inhibition experiments with the entire enzyme complex. In presence of DBMIB the rate of NADH oxidation ( $V_{\max}$ ) is decreased and  $K_M$  is lowered. This is characteristic of an uncompetitive mode of inhibition typical for multi-substrate enzymes (Voet and Voet 2004). That the catalytic site of NADH oxidation is not perturbed by DBMIB is indicated by the fact that the ratios of  $V_{\max}$  to  $K_M$  in presence or absence of DBMIB remain constant (table 10). First, this confirms the notion that DBMIB disrupts the electron pathway further downstream, most likely at the quinone reductase site due to the structural resemblance with ubiquinone (figure 30). Second, this ascertains that NADH oxidase and quinone reductase sites of the Na<sup>+</sup>-NQR are coupled in our experimental setup and no electrons short-circuit to quinone at the level of the NADH oxidase. This needs to be considered since Q<sub>1</sub> can serve as an artificial electron acceptor when assaying the isolated NADH dehydrogenase domain (Türk, Puhar et al. 2004).

For quinone reduction we observe a mixed mode of inhibition in the presence of DBMIB as documented by the rates of quinol formation.

Evaluating our experiments according to a Michaelis-Menten model yields an average inhibition constant of  $K_I = 53.2 \mu\text{M}$ , and also in a Hill model  $V_{\max}$  drops to 50 % at a DBMIB concentration of 25  $\mu\text{M}$ . These IC<sub>50</sub> values are strikingly similar to the EC<sub>50</sub> ( $26.1 \pm 2.5 \mu\text{M}$ ) determined in the STD NMR experiment with the NqrA subunit. Taken together, this strongly indicates that the interaction of the inhibitor DBMIB with the extended binding site of the NqrA subunit is causing the inhibition of enzymatic turnover measured with the holo-enzyme complex.

Recently, Juarez et al. investigated two mutations in the Na<sup>+</sup>-NQR of *V. cholerae* (Juárez, Neehaul et al. 2012) that had been discovered earlier in the Na<sup>+</sup>-NQR of *V. alginolyticus*. These mutations in subunit NqrB conferred resistance towards the antibiotic korormicin to *V. alginolyticus* (Hayashi, Shibata et al. 2002). Mutation of glycine residues G140 and G141 located in the NqrB subunit to alanines were found to have a profound effect on enzymatic activity of Na<sup>+</sup>-NQR leading the authors to propose that the NqrB subunit would carry the site of quinone reduction (Juárez, Neehaul et al. 2012). Our current study supports our earlier results indicating that the NqrA subunit carries the catalytically relevant quinone binding site of the Na<sup>+</sup>-NQR. One should consider that long range structural perturbations

induced by mutations on subunit NqrB might affect the quinone binding properties of subunit NqrA.

Our results suggest that holo-Na<sup>+</sup>-NQR binds two equivalents of the natural substrate ubiquinone Q<sub>8</sub> with their hydrophilic head groups. We propose that these two quinones are central to the last electron transfer steps. In this model, two subsequent one-electron transfers - probably from a flavosemiquinone located on the NqrB subunit - would reduce ubiquinone to the ubisemiquinone and subsequently to ubiquinol which is then released by the enzyme.

The presence of two quinones in the binding site could enhance the efficiency of catalysis in at least two ways: One quinone ligand could serve essentially as a cofactor that remains tightly bound to the enzyme and switches between the quinone and the semiquinone state while the other quinone ligand is much less tightly bound, reduced in two steps to the quinol, and then released from the enzyme. Alternatively, the second, low-affinity binding site could constitute a waiting position for the next ubiquinone substrate to enter the site of reduction leading to faster supply of fresh substrate and, thus, accelerated enzymatic turnover. Which of these mechanisms is finally operational in the Na<sup>+</sup>-NQR will be addressed in future studies.

## **Chapter 4**

### **Conclusion and outlook**

The results presented in this work characterize structural and functional properties of key catalytic subunits of NADH:quinone oxidoreductases. Due to the elaborate nature of these enzyme complexes, we seek to reduce complexity to its necessary minimum, as someone who seeks to deduce the function of a sophisticated machine would disassemble it to its basic components and analyze each one of them separately and in detail. We were able to draw conclusions about the ion transport capabilities of subunit ND5 of complex I, about the structure, mechanism and silver ion inhibition of the NADH-oxidizing electron input component of the Na<sup>+</sup>-NQR and about its quinone-reducing electron output module, the subunit NqrA. Together with many excellent previous studies by various investigators, these findings enhance the understanding of large electrogenic, redox-type enzymes. However, the 'holy grail' of this type of membrane-embedded complexes, the molecular mechanism underlying the energetic coupling between electron transfer and ion transport, remains enigmatic.

Concerning complex I, earlier theories assumed direct redox coupling where proton shuttling is accomplished by 2 or even 3 quinone sites (Brandt 1997; Ohnishi and Salerno 2005) or where the two-electron reduction of quinone is connected to the simultaneous unidirectional translocation of two protons and two sodium ions (Steuber 2001). In contrast, some studies proposed an indirect mechanism of conformational coupling involving a hydrophobic ramp or other means of long-range transmission elements (Brandt, Kerscher et al. 2003; Zickermann, Bostina et al. 2003; Hunte, Zickermann et al. 2010). The elucidation of the high-resolution structure (Efremov, Baradaran et al. 2010; Efremov and Sazanov 2011) has led to a plethora of new suggestions on how the coupling mechanism might work: In the current opinion, a mixed model is preferred, where at least two protons per two electrons are pumped through indirect coupling by the antiporter-like subunits and one or two protons are directly transferred by ubiquinone at the ND1/ND3/ND6/ND4L interface (Ohnishi, Salerno et al. 2010; Ohnishi, Nakamaru-Ogiso et al. 2010; Efremov and Sazanov 2011; Treberg and Brand 2011). Based on mechanical coupling by the long, rod-like amphipathic helix of ND5, the operating mode of complex I has been compared to a steam engine (Efremov and Sazanov 2011) or even to a semi-automatic shotgun (Gonzalez-Halphen, Ghelli et al. 2011). The stoichiometry of the proton/electron ratio and the vectors of ion translocation remain controversial (Wikstrom 1984; Bogachev, Murtazina et al. 1996; Brandt 1997; Mathiesen and Hägerhäll 2003; Efremov and Sazanov 2011; Roberts and Hirst 2012).

In particular, different models for cation/ $H^+$  transport need to be established and empirically scrutinized. Our study with the isolated ND5 subunit of complex I paves the way for such experiments, e.g. the *in vitro* analysis of antiporter-like subunits reconstituted into liposomes.

As of now, the  $Na^+$ -NQR holo-complex has been successfully crystallized (Casutt, Wendelspiess et al. 2010), but no high-resolution structures are yet available. Nevertheless, advances in recent years have determined the subunit and cofactor composition of the enzyme and have drawn a rough roadmap of the electron transfer pathway (Hayashi, Nakayama et al. 2001; Barquera, Zhou et al. 2002; Türk, Puhar et al. 2004; Juárez, Morgan et al. 2009; Casutt, Huber et al. 2010; Casutt, Nedielkov et al. 2011; Casutt, Schlosser et al. 2012). Also, residues from subunits NqrB, D and E which are potentially involved in  $Na^+$  translocation have been identified (Juárez, Athearn et al. 2009). Figure 50 depicts a current working model of the complex, which integrates the findings of two adjacent quinone binding sites on NqrA, as investigated in the present thesis.

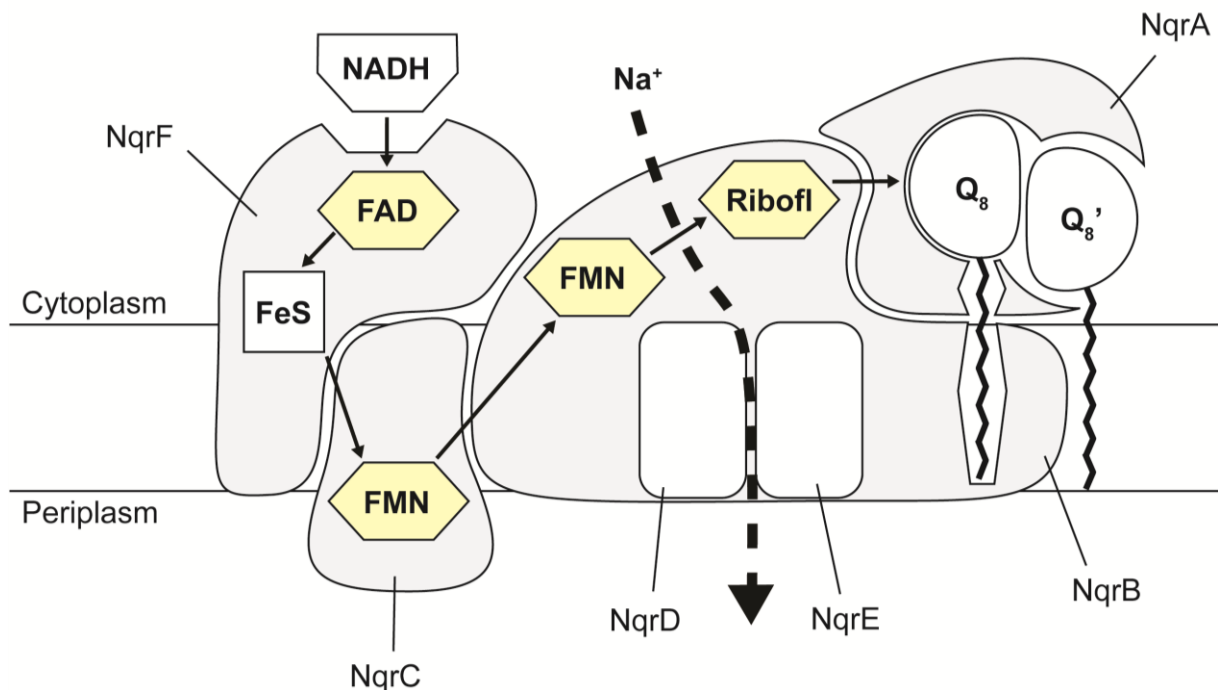


**Figure 50: Current working model of the  $Na^+$ -NQR from *Vibrio cholerae*.** The likely flow of electrons between cofactors is indicated by arrows. Flavin cofactors are colored yellow.

The energetic coupling between redox reaction and  $\text{Na}^+$  translocation in the  $\text{Na}^+$ -NQR is still a black box. In analogy to complex I, direct (Rich, Meunier et al. 1995) and indirect (Bogachev and Verkhovsky 2005) coupling mechanisms are proposed. However, direct redox coupling would require an additional one-electron cofactor, since none of the known cofactors exhibits a midpoint potential  $E_{m,7.5}$  corresponding to the redox dependency of  $\text{Na}^+$  binding (Bogachev, Bertsova et al. 2007). Such a cofactor could not be found to date (Bogachev, Kulik et al. 2009) but cannot be excluded. Evidence exists for long-range indirect coupling effects, such as correlation of  $\text{Na}^+$  translocation with the [2Fe-2S] cluster (Bogachev, Bloch et al. 2009), with the FMNs on NqrB and NqrC and with riboflavin (Juárez, Morgan et al. 2009). A mechanism operating by conformational changes at multiple sites in the complex is proposed (Juárez and Barquera 2012). These results are derived from de-energized and detergent-solubilized  $\text{Na}^+$ -NQR, which may be misleading. A more native and promising approach might be to analyze energetic coupling in phospholipid bilayers such as nanodiscs (Ritchie, Grinkova et al. 2009), which allow the direct application of a  $\Delta\mu\text{Na}^+$ . In addition, structure-function analysis of the hydrophobic subunits NqrB, C, D and E as well as high-resolution structures of the holo-complex could provide evidence for solving the coupling mechanism or could at the very least shed some light on this black box of energy conversion machinery.

## Appendix

## Contributions by collaborating authors

### Chapter 1:

Figure 3 and the data depicted in table 3 were generated by Marco Casutt.

### Chapter 2:

Figures 16 - 18 were generated in collaboration with Hanna Grönheim.

Analyses with electron microscopy as depicted in figure 19 were performed by Manikandan Karuppasamy and Christiane Schaffitzel.

The data depicted in figure 21 was generated by Hanna Grönheim.

### Chapter 3:

The construction of plasmids pNQR378A, pNQR406A and pNQR406S used throughout chapter 3 was performed in collaboration with Valentin Muras.

The protein crystals used to generate the results in chapter 3.3.2. were produced by and X-ray data collected by Marco Casutt and Günter Fritz.

The data depicted in figures 34, 37 and 38 were provided by Günter Fritz.

Data depicted in figure 36 and table 7 were generated in collaboration with Valentin Muras.

Analyses by NMR spectroscopy as depicted in figures 47 - 49 and table 14 were performed by Ruslan Nediolkov and Heiko Möller.



## Abbreviations

ACN	Acetonitrile
DAPI	4', 6-Diamidino-2-phenylindol
DBMIB	2,5-Dibromo-3-methyl-6-isopropyl-p-benzoquinone
Dpms	Dolichol phosphate mannose synthase
EIPA	5'-(N-ethyl-N-isopropyl)amiloride
ER	Endoplasmatic reticulum
GFP	Green fluorescent protein
FAD	Flavin adenine dinucleotide
Fe-S	Iron-sulfur
FMN	Flavin mononucleotide
FNR	Ferredoxin:NADP <sup>+</sup> oxidoreductase
HQNO	2-n-heptyl-4-hydroxyquinoline N-oxide
ILOE	Interligand Overhauser effects
IPTG	Isopropylthio- $\beta$ -D-galactoside
LDAO	Lauryl dimethylamine oxide
LHON	Leber's hereditary optic neuropathy
MELAS	Mitochondrial myopathy, encephalopathy, lactic acidosis and stroke
MERRF	Myoclonic epilepsy with ragged red fiber
MTS	Mitochondrial targeting sequence
Na <sup>+</sup> -NQR	Sodium ion translocating NADH:quinone oxidoreductase
OXPHOS	Oxidative phosphorylation
PD	Parkinson's disease
PEG MME	Polyethylene glycol monomethyl ether
PMF	Proton motive force
Q	Ubiquinone
QH <sub>2</sub>	Ubiquinol
STD	Saturation transfer difference
TMH	Transmembrane helix
YNB	Yeast nitrogen base

## References

- Abelson, J. N., C. Guthrie, et al., Eds. (2004). Guide to Yeast Genetics and Molecular Biology, Part a. Methods Enzymol., Academic Press Inc., U.S.
- Aguilar, P., B. Jimenez, et al. (2006). "Disinfection of sludge with high pathogenic content using silver and other compounds." Water Sci Technol **54**(5): 179-87.
- Alberts, B., A. Johnson, et al. (2008). Molecular Biology of The Cell 5th Edition. New York, Garland Science.
- Aldhous, P. (2003). "The world's forgotten crisis." Nature **422**(6929): 251.
- Aliverti, A., C. M. Bruns, et al. (1995). "Involvement of serine 96 in the catalytic mechanism of ferredoxin-NADP<sup>+</sup> reductase: structure--function relationship as studied by site-directed mutagenesis and X-ray crystallography." Biochemistry **34**(26): 8371-9.
- Aliverti, A., Z. Deng, et al. (1998). "Probing the function of the invariant glutamyl residue 312 in spinach ferredoxin-NADP<sup>+</sup> reductase." J Biol Chem **273**(51): 34008-15.
- Aliverti, A., L. Piubelli, et al. (1993). "The role of cysteine residues of spinach ferredoxin-NADP<sup>+</sup> reductase As assessed by site-directed mutagenesis." Biochemistry **32**(25): 6374-80.
- Andries, K., P. Verhasselt, et al. (2005). "A diarylquinoline drug active on the ATP synthase of Mycobacterium tuberculosis." Science **307**(5707): 223-7.
- Arimura, S. and N. Tsutsumi (2002). "A dynamin-like protein (ADL2b), rather than FtsZ, is involved in Arabidopsis mitochondrial division." Proc Natl Acad Sci U S A **99**(8): 5727-31.
- Ausubel, F., R. Brent, et al., Eds. (1995). Short Protocols in Molecular Biology. Current Protocols in Molecular Biology, Wiley.
- Bakker, B. M., K. M. Overkamp, et al. (2001). "Stoichiometry and compartmentation of NADH metabolism in *Saccharomyces cerevisiae*." FEMS Microbiol Rev **25**(1): 15-37.
- Bandeiras, T. M., C. Salgueiro, et al. (2002). "Acidianus ambivalens type-II NADH dehydrogenase: genetic characterisation and identification of the flavin moiety as FMN." FEBS Lett **531**(2): 273-7.
- Bandeiras, T. M., C. A. Salgueiro, et al. (2003). "The respiratory chain of the thermophilic archaeon *Sulfolobus metallicus*: studies on the type-II NADH dehydrogenase." Biochim. Biophys. Acta **1557**: 13-19.
- Barquera, B., P. Hellwig, et al. (2002). "Purification and characterization of the recombinant Na<sup>+</sup>-translocating NADH:quinone oxidoreductase from *Vibrio cholerae*." Biochemistry **41**: 3781-3789.
- Barquera, B., L. Ramirez-Silva, et al. (2006). "A new flavin radical signal in the Na<sup>+</sup>-pumping NADH: quinone oxidoreductase from *Vibrio cholerae*. An EPR/ENDOR investigation of the role of the covalently bound flavins in subunits B and C." J. Biol. Chem. **281**: 36482-36491.
- Barquera, B., W. Zhou, et al. (2002). "Riboflavin is a component of the Na<sup>+</sup>-pumping NADH-quinone oxidoreductase from *Vibrio cholerae*." Proc. Natl. Acad. Sci. USA **99**(16): 10322-10324.
- Bartoschek, S., M. Johansson, et al. (2001). "Three molecules of ubiquinone bind specifically to mitochondrial cytochrome bc1 complex." J Biol Chem **276**(38): 35231-4.
- Batista, A. P., A. S. Fernandes, et al. (2010). "Energy conservation by *Rhodothermus marinus* respiratory complex I." Biochim Biophys Acta **1797**(4): 509-15.

- Beattie, P., K. Tan, et al. (1994). "Cloning and sequencing of four structural genes for the Na<sup>+</sup>-translocating NADH-ubiquinone oxidoreductase of *Vibrio alginolyticus*." FEBS Lett. **356**: 333-338.
- Beinert, H. (2000). "Iron-sulfur proteins: ancient structures, still full of surprises." J Biol Inorg Chem **5**(1): 2-15.
- Belenky, P., K. L. Bogan, et al. (2007). "NAD<sup>+</sup> metabolism in health and disease." Trends Biochem Sci **32**(1): 12-9.
- Bertsova, Y. V. and A. V. Bogachev (2004). "The origin of the sodium-dependent NADH oxidation by the respiratory chain of *Klebsiella pneumoniae*." FEBS Lett. **563**(1-3): 207-212.
- Bjorklof, K., V. Zickermann, et al. (2000). "Purification of the 45 kDa, membrane bound NADH dehydrogenase of *Escherichia coli* (NDH-2) and analysis of its interaction with ubiquinone analogues." FEBS Lett **467**(1): 105-10.
- Blanco-Rivero, A., F. Leganes, et al. (2005). "*mnpA*, a gene with roles in resistance to Na<sup>+</sup> and adaptation to alkaline pH in the cyanobacterium *Anabaena* sp. PCC7120." Microbiology **151**(Pt 5): 1671-82.
- Bogachev, A. V., N. P. Belevich, et al. (2009). "Primary steps of the Na<sup>+</sup>-translocating NADH:ubiquinone oxidoreductase catalytic cycle resolved by the ultrafast freeze-quench approach." J Biol Chem **284**(9): 5533-8.
- Bogachev, A. V., Y. V. Bertsova, et al. (2007). "Redox-dependent sodium binding by the Na<sup>+</sup>-translocating NADH:quinone oxidoreductase from *Vibrio harveyi*." Biochemistry **46**(35): 10186-91.
- Bogachev, A. V., Y. V. Bertsova, et al. (2001). "Sodium-dependent steps in the redox reactions of the Na<sup>+</sup>-motive NADH:quinone oxidoreductase from *Vibrio harveyi*." Biochemistry **40**(24): 7318-7323.
- Bogachev, A. V., Y. V. Bertsova, et al. (2002). "Kinetics of the spectral changes during reduction of the Na<sup>+</sup>-motive NADH:quinone oxidoreductase from *Vibrio harveyi*." Biochim. Biophys. Acta **1556**: 113-120.
- Bogachev, A. V., D. A. Bloch, et al. (2009). "Redox properties of the prosthetic groups of Na<sup>+</sup>-translocating NADH:quinone oxidoreductase. 2. Study of the enzyme by optical spectroscopy." Biochemistry **48**(27): 6299-304.
- Bogachev, A. V., L. V. Kulik, et al. (2009). "Redox properties of the prosthetic groups of Na<sup>+</sup>-translocating NADH:quinone oxidoreductase. 1. electron paramagnetic resonance study of the enzyme." Biochemistry **48**(27): 6291-8.
- Bogachev, A. V., R. A. Murtazina, et al. (1996). "H<sup>+</sup>/e<sup>-</sup> stoichiometry for NADH dehydrogenase I and dimethyl sulfoxide reductase in anaerobically grown *E. coli* cells." FEBS Lett. **178**: 6233-6237.
- Bogachev, A. V. and M. I. Verkhovskiy (2005). "Na<sup>+</sup>-translocating NADH:quinone oxidoreductase: progress achieved and prospects of investigations." Biochemistry (Mosc.) **70**(2): 143-149.
- Bongaerts, J., S. Zoske, et al. (1995). "Transcriptional regulation of the proton translocating NADH dehydrogenase genes (*nuoA-N*) of *Escherichia coli* by electron acceptors, electron donors and gene regulators." Mol. Microbiol. **16**: 521-534.
- Bonner, W. D. and D. O. Voss (1961). "Some Characteristics of Mitochondria Extracted from Higher Plants." Nature **191**(4789): 682-684.
- Böttcher, B., D. Scheide, et al. (2002). "A novel, enzymatically active conformation of the *Escherichia coli* NADH:ubiquinone oxidoreductase (complex I)." J. Biol. Chem. **277**: 17970-17977.

- Brandt, U. (1997). "Proton-translocation by membrane-bound NADH:ubiquinone-oxidoreductase (complex I) through redox-gated ligand conduction." Biochim Biophys Acta **1318**(1-2): 79-91.
- Brandt, U. (2006). "Energy converting NADH:quinone oxidoreductase (complex I)." Annu Rev Biochem **75**: 69-92.
- Brandt, U., S. Kerscher, et al. (2003). "Proton pumping by NADH:ubiquinone oxidoreductase. A redox driven conformational change mechanism?" FEBS Lett **545**(1): 9-17.
- Caboni, P., T. B. Sherer, et al. (2004). "Rotenone, deguelin, their metabolites, and the rat model of Parkinson's disease." Chem Res Toxicol **17**(11): 1540-8.
- Candiano, G., M. Bruschi, et al. (2004). "Blue silver: a very sensitive colloidal Coomassie G-250 staining for proteome analysis." Electrophoresis **25**(9): 1327-33.
- Carroll, J., I. M. Fearnley, et al. (2006). "Bovine complex I is a complex of 45 different subunits." J Biol Chem **281**(43): 32724-7.
- Casutt, M. S. (2010). Functional and Structural Investigations of a Multisubunit Redox Pump, the Na<sup>+</sup>-translocating NADH:Quinone Oxidoreductase from *Vibrio cholerae*. Mathematisch-naturwissenschaftliche Fakultät, Universität Zürich. **Dissertation for the degree of Doctor of Natural Sciences**.
- Casutt, M. S., T. Huber, et al. (2010). "Localization and function of the membrane-bound riboflavin in the Na<sup>+</sup>-translocating NADH:quinone oxidoreductase (Na<sup>+</sup>-NQR) from *Vibrio cholerae*." J Biol Chem **285**(35): 27088-99.
- Casutt, M. S., R. Nediakov, et al. (2011). "Localization of ubiquinone-8 in the Na<sup>+</sup>-pumping NADH:quinone oxidoreductase from *Vibrio cholerae*." J Biol Chem **286**(46): 40075-82.
- Casutt, M. S., A. Schlosser, et al. (2012). "The single NqrB and NqrC subunits in the Na(+)-translocating NADH: Quinone oxidoreductase (Na(+)-NQR) from *Vibrio cholerae* each carry one covalently attached FMN." Biochim Biophys Acta.
- Casutt, M. S., S. Wendelspiess, et al. (2010). "Crystallization of the Na<sup>+</sup>-translocating NADH:quinone oxidoreductase from *Vibrio cholerae*." Acta Crystallogr Sect F Struct Biol Cryst Commun **66**(Pt 12): 1677-9.
- Chain, R. K. and R. Malkin (1979). "On the interaction of 2,5-dibromo-3-methyl-6-isopropylbenzoquinone (DBMIB) with bound electron carriers in spinach chloroplasts." Arch Biochem Biophys **197**(1): 52-6.
- Chen, Y. G., W. E. Kowtoniuk, et al. (2009). "LC/MS analysis of cellular RNA reveals NAD-linked RNA." Nat Chem Biol **5**(12): 879-81.
- Claros, M. G. and G. von Heijne (1994). "TopPred II: an improved software for membrane protein structure predictions." Comput Appl Biosci **10**(6): 685-6.
- Clason, T., T. Ruiz, et al. (2010). "The structure of eukaryotic and prokaryotic complex I." J Struct Biol **169**(1): 81-8.
- Collins, M. D. and D. Jones (1981). "Distribution of isoprenoid quinone structural types in bacteria and their taxonomic implications." Microbiol. Rev. **45**(2): 316-354.
- Coubeils, J. L., B. Pullman, et al. (1971). "A molecular orbital study of the conformational properties of nicotinamides." Biochem Biophys Res Commun **44**(5): 1131-4.
- Crane, F. L. (1959). "Isolation of Two Quinones with Coenzyme Q Activity from Alfalfa." Plant Physiol **34**(5): 546-51.
- Cserzo, M., E. Wallin, et al. (1997). "Prediction of transmembrane alpha-helices in prokaryotic membrane proteins: the dense alignment surface method." Protein Eng **10**(6): 673-6.

- Daum, G., P. C. Bohni, et al. (1982). "Import of proteins into mitochondria. Cytochrome b2 and cytochrome c peroxidase are located in the intermembrane space of yeast mitochondria." J Biol Chem **257**(21): 13028-33.
- Davies, R. L. and S. F. Etris (1997). "The development and functions of silver in water purification and disease control." Catalysis Today. **36**(1): 107-114.
- Degli Esposti, M., G. Rotilio, et al. (1984). "Effects of dibromothymoquinone on the structure and function of the mitochondrial bc1 complex." Biochim Biophys Acta **767**(1): 10-20.
- Degli Esposti, M., M. Rugolo, et al. (1983). "Inhibition of the mitochondrial bc1 complex by dibromothymoquinone." FEBS Lett **156**(1): 15-9.
- Deng, Z., A. Aliverti, et al. (1999). "A productive NADP<sup>+</sup> binding mode of ferredoxin-NADP<sup>+</sup> reductase revealed by protein engineering and crystallographic studies." Nat Struct Biol **6**(9): 847-53.
- Dimroth, P. (1997). "Primary sodium ion translocating enzymes." Biochim Biophys Acta **1318**(1-2): 11-51.
- Ding, H., C. C. Moser, et al. (1995). "Ubiquinone pair in the Qo site central to the primary energy conversion reactions of cytochrome bc1 complex." Biochemistry **34**(49): 15979-96.
- Draber, W., A. Trebst, et al. (1970). "On a new inhibitor of photosynthetic electron-transport in isolated chloroplasts." Z Naturforsch B **25**(10): 1157-9.
- Drew, D., M. Lerch, et al. (2006). "Optimization of membrane protein overexpression and purification using GFP fusions." Nat Methods **3**(4): 303-13.
- Dudkina, N. V., H. Eubel, et al. (2005). "Structure of a mitochondrial supercomplex formed by respiratory-chain complexes I and III." Proc Natl Acad Sci U S A **102**(9): 3225-9.
- Duffy, E. B. and B. Barquera (2006). "Membrane topology mapping of the Na<sup>+</sup>-pumping NADH:quinone oxidoreductase from *Vibrio cholerae* by PhoA/GFP fusion analysis." J. Bacteriol. **188**(24): 8343-8351.
- Efremov, R. G., R. Baradaran, et al. (2010). "The architecture of respiratory complex I." Nature **465**(7297): 441-5.
- Efremov, R. G. and L. A. Sazanov (2011). "Respiratory complex I: 'steam engine' of the cell?" Curr Opin Struct Biol **21**(4): 532-40.
- Efremov, R. G. and L. A. Sazanov (2011). "Structure of the membrane domain of respiratory complex I." Nature **476**(7361): 414-20.
- Einhauer, A. and A. Jungbauer (2001). "The FLAG peptide, a versatile fusion tag for the purification of recombinant proteins." J Biochem Biophys Methods **49**(1-3): 455-65.
- Eklund, H., J. P. Samama, et al. (1984). "Crystallographic investigations of nicotinamide adenine dinucleotide binding to horse liver alcohol dehydrogenase." Biochemistry **23**(25): 5982-96.
- Emsley, P., B. Lohkamp, et al. (2010). "Features and development of Coot." Acta Crystallogr D Biol Crystallogr **66**(Pt 4): 486-501.
- Eschemann, A., A. Galkin, et al. (2005). "HDQ (1-hydroxy-2-dodecyl-4(1H)quinolone), a high affinity inhibitor for mitochondrial alternative NADH dehydrogenase: evidence for a ping-pong mechanism." J. Biol. Chem. **280**(5): 3138-42.
- Fang, J. and D. S. Beattie (2002). "Novel FMN-containing rotenone-insensitive NADH dehydrogenase from *Trypanosoma brucei* mitochondria: isolation and characterization." Biochemistry **41**(9): 3065-3072.
- Fato, R., E. Estornell, et al. (1996). "Steady-state kinetics of the reduction of coenzyme Q analogs by complex I (NADH:ubiquinone oxidoreductase) in bovine heart mitochondria and submitochondrial particles." Biochemistry **35**: 2705-2716.

- Fearnley, I. M. and J. E. Walker (1992). "Conservation of sequences of subunits of mitochondrial complex I and their relationships with other proteins." Biochim Biophys Acta **1140**(2): 105-34.
- Foury, F., T. Roganti, et al. (1998). "The complete sequence of the mitochondrial genome of *Saccharomyces cerevisiae*." FEBS Lett **440**(3): 325-31.
- Freitag, H., R. Benz, et al. (1983). "Isolation and properties of the porin of the outer mitochondrial membrane from *Neurospora crassa*." Methods Enzymol **97**: 286-94.
- Friedrich, T. (1998). "The NADH:ubiquinone oxidoreductase (complex I) from *Escherichia coli*." Biochim. Biophys. Acta **1364**: 134-146.
- Friedrich, T., A. Abelmann, et al. (1998). "Redox components and structure of the respiratory NADH:ubiquinone oxidoreductase (complex I)." Biochim Biophys Acta **1365**(1-2): 215-9.
- Friedrich, T., P. v. Heek, et al. (1994). "Two binding sites of inhibitors in NADH:ubiquinone oxidoreductase (complex I): relationship of one site with the ubiquinone-binding site of bacterial glucose:ubiquinone oxidoreductase." Eur. J. Biochem. **219**: 691-698.
- Friedrich, T. and D. Scheide (2000). "The respiratory complex I of bacteria, archaea and eukarya and its module common with membrane-bound multisubunit hydrogenases." FEBS Lett. **479**: 1-5.
- Friedrich, T. and H. Weiss (1996). Origin and evolution of the proton-pumping NADH:ubiquinone oxidoreductase (complex I). Origin and evolution of bacterial energy conservation. H. Baltscheffsky. New York, VCH Publishers: 205-220.
- Fujiwara-Nagata, E., K. Kogure, et al. (2003). "Characteristics of Na<sup>+</sup>-dependent respiratory chain in *Vibrio anguillarum*, a fish pathogen, in comparison with other marine *Vibrios*." FeMS Microbiol. Ecol. **44**: 225-230.
- Gabaldon, T., D. Rainey, et al. (2005). "Tracing the evolution of a large protein complex in the eukaryotes, NADH:ubiquinone oxidoreductase (Complex I)." J Mol Biol **348**(4): 857-70.
- Gemperli, A. C., P. Dimroth, et al. (2002). "The respiratory complex I (NDH I) from *Klebsiella pneumoniae*, a sodium pump." J Biol Chem **277**(37): 33811-7.
- Gemperli, A. C., P. Dimroth, et al. (2003). "Sodium ion cycling mediates energy coupling between complex I and ATP synthase." Proc Natl Acad Sci U S A **100**(3): 839-44.
- Gemperli, A. C., C. Schaffitzel, et al. (2007). "Transport of Na<sup>+</sup> and K<sup>+</sup> by an antiporter-related subunit from the *Escherichia coli* NADH dehydrogenase I produced in *Saccharomyces cerevisiae*." Arch Microbiol **188**(5): 509-21.
- Gietz, D., A. St Jean, et al. (1992). "Improved method for high efficiency transformation of intact yeast cells." Nucleic Acids Res **20**(6): 1425.
- Giraud, M. F. and J. Velours (1994). "ATP synthase of yeast mitochondria. Isolation of the F1 delta subunit, sequence and disruption of the structural gene." Eur J Biochem **222**(3): 851-9.
- Glick, B. S. and G. Von Heijne (1996). "*Saccharomyces cerevisiae* mitochondria lack a bacterial-type sec machinery." Protein Sci **5**(12): 2651-2.
- Gonzalez-Halphen, D., A. Ghelli, et al. (2011). "Mitochondrial complex I and cell death: a semi-automatic shotgun model." Cell Death Dis **2**: e222.
- Grigorieff, N. (1998). "Three-dimensional structure of bovine NADH:ubiquinone oxidoreductase (complex I) at 2.2 Å in ice." J Mol Biol **277**(5): 1033-46.
- Guenebaut, V., A. Schlitt, et al. (1998). "Consistent structure between bacterial and mitochondrial NADH:ubiquinone oxidoreductase (complex I)." J Mol Biol **276**(1): 105-12.

- Guenebaut, V., R. Vincentelli, et al. (1997). "Three-dimensional structure of NADH-dehydrogenase from *Neurospora crassa* by electron microscopy and conical tilt reconstruction." J Mol Biol **265**(4): 409-18.
- Guse, A. H. (2004). "Biochemistry, biology, and pharmacology of cyclic adenosine diphosphoribose (cADPR)." Curr Med Chem **11**(7): 847-55.
- Guy, J., X. Qi, et al. (2002). "Rescue of a mitochondrial deficiency causing Leber Hereditary Optic Neuropathy." Ann Neurol **52**(5): 534-42.
- Hackett, C. S., W. B. Nova, et al. (1986). "Identification of the essential cysteine residue of NADH-cytochrome b5 reductase." J Biol Chem **261**(21): 9854-7.
- Hamamoto, T., M. Hashimoto, et al. (1994). "Characterization of a gene responsible for the Na<sup>+</sup>/H<sup>+</sup> antiporter system of alkalophilic *Bacillus* species strain C-125." Mol Microbiol **14**(5): 939-46.
- Hanahan, D. (1983). "Studies on transformation of *Escherichia coli* with plasmids." J Mol Biol **166**(4): 557-80.
- Häse, C. C. (2000). "Virulence and sodium bioenergetics." Trends Microbiol **8**(11): 490-1.
- Häse, C. C. and B. Barquera (2001). "Role of sodium bioenergetics in *Vibrio cholerae*." Biochim. Biophys. Acta **1505**: 169-178.
- Hayashi, M., Y. Nakayama, et al. (1996). "Existence of Na<sup>+</sup>-translocating NADH-quinone reductase in *Haemophilus influenzae*." FEBS Lett. **381**: 174-176.
- Hayashi, M., Y. Nakayama, et al. (2001). "Recent progress in the Na<sup>+</sup>-translocating NADH-quinone reductase from the marine *Vibrio alginolyticus*." Biochim. Biophys. Acta **1505**(1): 37-44.
- Hayashi, M., N. Shibata, et al. (2002). "Korormicin insensitivity in *Vibrio alginolyticus* is correlated with a single point mutation of Gly-140 in the NqrB subunit of the Na<sup>+</sup>-translocating NADH-quinone reductase." Arch. Biochem. Biophys. **401**(2): 173-7.
- Hiramatsu, T., K. Kodama, et al. (1998). "A putative multisubunit Na<sup>+</sup>/H<sup>+</sup> antiporter from *Staphylococcus aureus*." J Bacteriol **180**(24): 6642-8.
- Hirokawa, T., S. Boon-Chieng, et al. (1998). "SOSUI: classification and secondary structure prediction system for membrane proteins." Bioinformatics **14**(4): 378-9.
- Hirst, J. (2005). "Energy transduction by respiratory complex I--an evaluation of current knowledge." Biochem. Soc. Trans. **33**(Pt 3): 525-9.
- Hofhaus, G., H. Weiss, et al. (1991). "Electron microscopic analysis of the peripheral and membrane parts of mitochondrial NADH dehydrogenase (complex I)." J Mol Biol **221**(3): 1027-43.
- Hofmann, K. and W. Stoffel (1993). "TMbase - A database of membrane spanning protein segments." Biol. Chem. Hoppe-Seyler **374**: 166.
- Hore, P. J. (1989). "Nuclear magnetic resonance. Solvent suppression." Methods Enzymol **176**: 64-77.
- Hoult, D. I. (1976). "Solvent Peak Saturation with Single-Phase and Quadrature Fourier Transformation." Journal of Magnetic Resonance **21**(2): 337-347.
- Hunte, C., V. Zickermann, et al. (2010). "Functional modules and structural basis of conformational coupling in mitochondrial complex I." Science **329**(5990): 448-51.
- Hwang, T. L. and A. J. Shaka (1995). "Water Suppression That Works - Excitation Sculpting Using Arbitrary Wave-Forms and Pulsed-Field Gradients." Journal of Magnetic Resonance Series A **112**(2): 275-279.
- Infed, N., N. Hanekop, et al. (2011). "Influence of detergents on the activity of the ABC transporter LmrA." Biochim Biophys Acta **1808**(9): 2313-21.

- Jones, D. T., W. R. Taylor, et al. (1994). "A model recognition approach to the prediction of all-helical membrane protein structure and topology." Biochemistry **33**(10): 3038-49.
- Jones, E. W. (1991). Tackling the Protease Problem in *Saccharomyces cerevisiae*. Methods Enzymol. **194**: 428-453.
- Juárez, O., K. Athearn, et al. (2009). "Acid residues in the transmembrane helices of the Na<sup>+</sup>-pumping NADH:quinone oxidoreductase from *Vibrio cholerae* involved in sodium translocation." Biochemistry **48**(40): 9516-24.
- Juárez, O. and B. Barquera (2012). "Insights into the mechanism of electron transfer and sodium translocation of the Na<sup>+</sup>-pumping NADH:quinone oxidoreductase." Biochim Biophys Acta **1817**(10): 1823-32.
- Juárez, O., J. E. Morgan, et al. (2009). "The electron transfer pathway of the Na<sup>+</sup>-pumping NADH:quinone oxidoreductase from *Vibrio cholerae*." J. Biol. Chem. **284**: 8963–8972.
- Juárez, O., Y. Neehaul, et al. (2012). "The Role of Glycine Residues 140 and 141 of Subunit B in the Functional Ubiquinone Binding Site of the Na<sup>+</sup>-pumping NADH:quinone Oxidoreductase from *Vibrio cholerae*." J Biol Chem **287**(30): 25678-85.
- Juretic, D., L. Zoranic, et al. (2002). "Basic charge clusters and predictions of membrane protein topology." J Chem Inf Comput Sci **42**(3): 620-32.
- Kabsch, W. (2010). "XDS." Acta Crystallographica Section D **66**(2): 125-132.
- Kall, L., A. Krogh, et al. (2005). "An HMM posterior decoder for sequence feature prediction that includes homology information." Bioinformatics **21 Suppl 1**: i251-7.
- Karplus, P. A. and H. R. Faber (2004). "Structural Aspects of Plant Ferredoxin : NADP(+) Oxidoreductases." Photosynth Res **81**(3): 303-15.
- Kearney, E. B. and W. C. Kenny (1974). "Covalently bound Flavin Coenzymes." Horiz Biochem Biophys **1**: 62-96.
- Ken-Dror, S., J. K. Lanyi, et al. (1986). "An NADH:quinone oxidoreductase of the halotolerant bacterium Ba<sub>1</sub> is specifically dependent on sodium ions." Arch. Biochem. Biophys. **244**: 766-772.
- Kerscher, S. J. (2000). "Diversity and origin of alternative NADH:ubiquinone oxidoreductases." Biochimica et Biophysica Acta **1459**(2-3): 274-83.
- Kerscher, S. J., J. G. Okun, et al. (1999). "A single external enzyme confers alternative NADH:ubiquinone oxidoreductase activity in *Yarrowia lipolytica*." J Cell Sci **112 ( Pt 14)**: 2347-54.
- Khanna, G., L. Devoe, et al. (1984). "Relationship between ion requirements for respiration and membrane transport in a marine bacterium." J. Bacteriol. **157**(1): 59-63.
- Kikuno, R. and T. Miyata (1985). "Sequence homologies among mitochondrial DNA-coded URF2, URF4 and URF5." FEBS Lett. **189**: 85-88.
- Kinclova-Zimmermannova, O., H. Flegelova, et al. (2004). "Rice Na<sup>+</sup>/H<sup>+</sup>-antiporter Nhx1 partially complements the alkali-metal-cation sensitivity of yeast strains lacking three sodium transporters." Folia Microbiol (Praha) **49**(5): 519-25.
- Kinclova-Zimmermannova, O. and H. Sychrova (2006). "Functional study of the Nha1p C-terminus: involvement in cell response to changes in external osmolarity." Curr Genet **49**(4): 229-36.
- Kitamura, M., S. Kojima, et al. (1994). "Novel FMN-binding protein from *Desulfovibrio vulgaris* (Miyazaki F). Cloning and expression of its gene in *Escherichia coli*." J Biol Chem **269**(8): 5566-73.
- Klomsiri, C., P. A. Karplus, et al. (2011). "Cysteine-based redox switches in enzymes." Antioxid Redox Signal **14**(6): 1065-77.
- Kogure, K. (1998). "Bioenergetics of marine bacteria." Curr. Opin. Biotechnol. **9**: 278-282.



- Kosono, S., S. Morotomi, et al. (1999). "Analyses of a *Bacillus subtilis* homologue of the Na<sup>+</sup>/H<sup>+</sup> antiporter gene which is important for pH homeostasis of alkaliphilic *Bacillus* sp. C-125." Biochim Biophys Acta **1409**(3): 171-5.
- Kumar, V., A. K. Abbas, et al. (2004). Robbins and Cotran Pathologic Basis of Disease 7th edition. Philadelphia, W.B. Saunders Company.
- Kyte, J. and R. F. Doolittle (1982). "A simple method for displaying the hydropathic character of a protein." J Mol Biol **157**(1): 105-32.
- Land, E. J. and A. J. Swallow (1970). "One-electron reactions in biochemical systems as studied by pulse radiolysis: III. ubiquinone." J. Biol. Chem. **245**(8): 1890-1894.
- Leonard, J. V. and A. H. Schapira (2000). "Mitochondrial respiratory chain disorders I: mitochondrial DNA defects." Lancet **355**(9200): 299-304.
- Leonard, K., H. Haiker, et al. (1987). "Three-dimensional structure of NADH: ubiquinone reductase (complex I) from *Neurospora* mitochondria determined by electron microscopy of membrane crystals." J Mol Biol **194**(2): 277-86.
- Lin, P. C., A. Puhar, et al. (2008). "NADH oxidation drives respiratory Na<sup>+</sup> transport in mitochondria from *Yarrowia lipolytica*." Arch Microbiol **190**(4): 471-80.
- Lin, P. C., K. Türk, et al. (2007). "Quinone reduction by the Na<sup>+</sup>-translocating NADH dehydrogenase promotes extracellular superoxide production in *Vibrio cholerae*." J. Bacteriol. **189**: 3902-3908.
- Lin, S. J. and L. Guarente (2003). "Nicotinamide adenine dinucleotide, a metabolic regulator of transcription, longevity and disease." Curr Opin Cell Biol **15**(2): 241-6.
- Liolitsa, D., S. Rahman, et al. (2003). "Is the mitochondrial complex I ND5 gene a hot-spot for MELAS causing mutations?" Ann Neurol **53**(1): 128-32.
- Lippard, S. J. and J. M. Berg (1994). Principles of Bioinorganic Chemistry. Mill Valley, CA, University Science Books.
- London, R. E. (1999). "Theoretical analysis of the inter-ligand overhauser effect: a new approach for mapping structural relationships of macromolecular ligands." J Magn Reson **141**(2): 301-11.
- Loschen, G. and A. Azzi (1974). "Dibromothymoquinone: a new inhibitor of mitochondrial electron transport at the level of ubiquinone." FEBS Lett **41**(1): 115-7.
- Marley, J., M. Lu, et al. (2001). "A method for efficient isotopic labeling of recombinant proteins." J Biomol NMR **20**(1): 71-5.
- Marques, I., M. Duarte, et al. (2003). "The 9.8 kDa Subunit of Complex I, Related to Bacterial Na<sup>+</sup>-translocating NADH Dehydrogenases, is Required for Enzyme Assembly and Function in *Neurospora crassa*." J. Mol. Biol. **329**: 283-290.
- Massey, V. (2000). "The chemical and biological versatility of riboflavin." Biochem. Soc. Trans. **28**: 283-296.
- Massey, V. and G. H. Palmer (1966). "On the existence of spectrally distinct classes of flavoprotein semiquinones. A new method for the quantitative production of flavoprotein semiquinones." Biochemistry **5**: 3181-3189.
- Mathiesen, C. and C. Hägerhäll (2002). "Transmembrane topology of the NuoL, M and N subunits of NADH:quinone oxidoreductase and their homologues among membrane-bound hydrogenases and bona fide antiporters." Biochim Biophys Acta **1556**(2-3): 121-32.
- Mathiesen, C. and C. Hägerhäll (2003). "The 'antiporter module' of respiratory chain complex I includes the MrpC/NuoK subunit -- a revision of the modular evolution scheme." FEBS Lett **549**(1-3): 7-13.

- Mayer, M. and B. Meyer (1999). "Characterization of Ligand Binding by Saturation Transfer Difference NMR Spectroscopy." Angewandte Chemie International Edition **38**(12): 1784-1788.
- Mayorov, V., V. Biousse, et al. (2005). "The role of the ND5 gene in LHON: characterization of a new, heteroplasmic LHON mutation." Ann Neurol **58**(5): 807-11.
- Meisinger, C., N. Pfanner, et al. (2006). "Isolation of yeast mitochondria." Methods Mol Biol **313**: 33-9.
- Melo, A. M. P., T. M. Bandejas, et al. (2004). "New insights into type II NAD(P)H:quinone oxidoreductases." Microbiol. Mol. Biol. Rev. **68**(4): 603-616.
- Mitchell, P. (1961). "Coupling of phosphorylation to electron and hydrogen transfer by a chemi-osmotic type of mechanism." Nature **191**: 144-8.
- Mitchell, P. and J. Moyle (1967). "Respiration-driven proton translocation in rat liver mitochondria." Biochem J **105**(3): 1147-1162.
- Mitchell, P. and J. Moyle (1969). "Estimation of membrane potential and pH difference across the cristae membrane of rat liver mitochondria." Eur J Biochem **7**(4): 471-84.
- Moparthi, V. K., B. Kumar, et al. (2011). "Homologous protein subunits from *Escherichia coli* NADH:quinone oxidoreductase can functionally replace MrpA and MrpD in *Bacillus subtilis*." Biochim Biophys Acta **1807**(4): 427-36.
- Moras, D., K. W. Olsen, et al. (1975). "Studies of asymmetry in the three-dimensional structure of lobster D-glyceraldehyde-3-phosphate dehydrogenase." J Biol Chem **250**(23): 9137-62.
- Morgner, N., V. Zickermann, et al. (2008). "Subunit mass fingerprinting of mitochondrial complex I." Biochim Biophys Acta **1777**(10): 1384-91.
- Müller, F. (1987). "Flavin radicals: chemistry and biochemistry." Free Radic. Biol. Med. **3**: 215-230.
- Müller, V., F. Imkamp, et al. (2008). "Discovery of a Ferredoxin:NAD<sup>+</sup>-oxidoreductase (Rnf) in *Acetobacterium woodii*." Ann. N.Y. Acad. Sci. **1125**: 137-146.
- Mutafova-Yambolieva, V. N., S. J. Hwang, et al. (2007). "Beta-nicotinamide adenine dinucleotide is an inhibitory neurotransmitter in visceral smooth muscle." Proc Natl Acad Sci U S A **104**(41): 16359-64.
- Naini, A. B., J. Lu, et al. (2005). "Novel mitochondrial DNA ND5 mutation in a patient with clinical features of MELAS and MERRF." Arch Neurol **62**(3): 473-6.
- Nakamaru-Ogiso, E., M. C. Kao, et al. (2010). "The membrane subunit NuoL(ND5) is involved in the indirect proton pumping mechanism of *Escherichia coli* complex I." J Biol Chem **285**(50): 39070-8.
- Nakamaru-Ogiso, E., B. B. Seo, et al. (2003). "Amiloride inhibition of the proton-translocating NADH-quinone oxidoreductase of mammals and bacteria." FEBS Lett. **549**(1-3): 43-6.
- Nakayama, Y., Hayashi, M., Yoshikawa, K., Mochida, K., Unemoto, T. (1999). "Inhibitor studies of a new antibiotic, korormicin, 2-*n*-heptyl-4-hydroxyquinoline *N*-oxide and Ag<sup>+</sup> toward the Na<sup>+</sup>-translocating NADH-quinone reductase from the marine *Vibrio alginolyticus*." Biol. Pharm. Bull. **22**: 1064-1067.
- Nedergaard, J., D. Ricquier, et al. (2005). "Uncoupling proteins: current status and therapeutic prospects." EMBO Rep **6**(10): 917-21.
- Nicholls, D. G. (1974). "The influence of respiration and ATP hydrolysis on the proton-electrochemical gradient across the inner membrane of rat-liver mitochondria as determined by ion distribution." Eur J Biochem **50**(1): 305-15.
- Nicholls, D. G. and S. J. Ferguson (1992). *Bioenergetics 2*. London, Academic Press Limited.

- Nishida, F., M. Nishijima, et al. (2006). "Isoprenoid quinones in an aerobic hyperthermophilic archaeon, *Aeropyrum pernix*." FEMS Microbiol. Lett. **174**(2): 339 - 346.
- Nogues, I., J. Tejero, et al. (2004). "Role of the C-terminal tyrosine of ferredoxin-nicotinamide adenine dinucleotide phosphate reductase in the electron transfer processes with its protein partners ferredoxin and flavodoxin." Biochemistry **43**(20): 6127-37.
- Nolan, R. A. and W. G. Nolan (1972). "Elemental Analysis of Vitamin-Free Casamino Acids." Appl Microbiol **24**(2): 290-291.
- Oca-Cossio, J., L. Kenyon, et al. (2003). "Limitations of allotopic expression of mitochondrial genes in mammalian cells." Genetics **165**(2): 707-20.
- Oh, S., K. Kogure, et al. (1991). "Correlation between possession of a respiration-dependent Na<sup>+</sup> pump and Na<sup>+</sup> requirement for growth of marine bacteria." Appl. Environ. Microbiol. **57**(6): 1844-1846.
- Ohnishi, S. T., J. C. Salerno, et al. (2010). "Possible roles of two quinone molecules in direct and indirect proton pumps of bovine heart NADH-quinone oxidoreductase (complex I)." Biochim Biophys Acta **1797**(12): 1891-3.
- Ohnishi, T., J. Lim, et al. (1976). "Thermodynamic and EPR characteristics of a HiPIP-type iron-sulfur center in the succinate dehydrogenase of the respiratory chain." J Biol Chem **251**(7): 2105-9.
- Ohnishi, T., E. Nakamaru-Ogiso, et al. (2010). "A new hypothesis on the simultaneous direct and indirect proton pump mechanisms in NADH-quinone oxidoreductase (complex I)." FEBS Lett **584**(19): 4131-7.
- Ohnishi, T. and J. C. Salerno (1976). "Thermodynamic and EPR characteristics of two ferredoxin-type iron-sulfur centers in the succinate-ubiquinone reductase segment of the respiratory chain." J Biol Chem **251**(7): 2094-104.
- Ohnishi, T. and J. C. Salerno (2005). "Conformation-driven and semiquinone-gated proton-pump mechanism in the NADH-ubiquinone oxidoreductase (complex I)." FEBS Lett **579**(21): 4555-61.
- Orellano, E. G., N. B. Calcaterra, et al. (1993). "Probing the role of the carboxyl-terminal region of ferredoxin-NADP<sup>+</sup> reductase by site-directed mutagenesis and deletion analysis." J Biol Chem **268**(26): 19267-73.
- Orlean, P. (1990). "Dolichol phosphate mannose synthase is required in vivo for glycosyl phosphatidylinositol membrane anchoring, O mannosylation, and N glycosylation of protein in *Saccharomyces cerevisiae*." Mol Cell Biol **10**(11): 5796-805.
- Parker, W. D., Jr. and J. K. Parks (2005). "Mitochondrial ND5 mutations in idiopathic Parkinson's disease." Biochem Biophys Res Commun **326**(3): 667-9.
- Pauly, H. and L. Packer (1960). "The relationship of internal conductance and membrane capacity to mitochondrial volume." J Biophys Biochem Cytol **7**: 603-12.
- Peckham, G. D., R. C. Bugos, et al. (2006). "Purification of GFP fusion proteins from transgenic plant cell cultures." Protein Expr Purif **49**(2): 183-9.
- Pedelacq, J. D., S. Cabantous, et al. (2006). "Engineering and characterization of a superfolder green fluorescent protein." Nat Biotechnol **24**(1): 79-88.
- Pedersen, S. F., S. A. King, et al. (2007). "NHE1 inhibition by amiloride- and benzoylguanidine-type compounds. Inhibitor binding loci deduced from chimeras of NHE1 homologues with endogenous differences in inhibitor sensitivity." J Biol Chem **282**(27): 19716-27.
- Petrek, M., M. Otyepka, et al. (2006). "CAVER: a new tool to explore routes from protein clefts, pockets and cavities." BMC Bioinformatics **7**: 316.
- Pfanner, N. and M. Meijer (1997). "The Tom and Tim machine." Curr Biol **7**(2): R100-3.

- Pfenniger-Li, X. D. and P. Dimroth (1995). "The Na<sup>+</sup>-translocating NADH:ubiquinone oxidoreductase from the marine bacterium *Vibrio alginolyticus* contains FAD but not FMN." FEBS Lett. **369**: 173-176.
- Piubelli, L., A. Aliverti, et al. (2000). "Competition between C-terminal tyrosine and nicotinamide modulates pyridine nucleotide affinity and specificity in plant ferredoxin-NADP(+) reductase." J Biol Chem **275**(14): 10472-6.
- Pringle, J. R. (1991). Immunofluorescence methods for yeast. Methods Enzymol. **194**: 565-602.
- Prive, G. G. (2007). "Detergents for the stabilization and crystallization of membrane proteins." Methods **41**(4): 388-97.
- Radermacher, M., T. Ruiz, et al. (2006). "The three-dimensional structure of complex I from *Yarrowia lipolytica*: a highly dynamic enzyme." J Struct Biol **154**(3): 269-79.
- Ravanel, P., M. Tissut, et al. (1986). "Platanetin: A Potent Natural Uncoupler and Inhibitor of the Exogenous NADH Dehydrogenase in Intact Plant Mitochondria." Plant Physiol **80**(2): 500-4.
- Reid, G. A. (2002). Flavins, flavoproteins and flavoproteomics. Flavins and flavoproteins. S. Chapman, R. Perham and N. Scrutton, Rudolf Weber, Agency for Scientific Publications.
- Rich, P. R. (1984). "Electron and proton transfers through quinones and cytochrome bc complexes." Biochim Biophys Acta **768**(1): 53-79.
- Rich, P. R., S. A. Madgwick, et al. (1991). "The interactions of duroquinol, DBMIB and NQNO with the chloroplast cytochrome bf complex." Biochimica et Biophysica Acta (BBA) - Bioenergetics **1058**(2): 312-328.
- Rich, P. R., B. Meunier, et al. (1995). "Predicted structure and possible ionmotive mechanism of the sodium-linked NADH-ubiquinone oxidoreductase of *Vibrio alginolyticus*." FEBS Lett. **375**: 5-10.
- Ritchie, T. K., Y. V. Grinkova, et al. (2009). "Chapter 11 - Reconstitution of membrane proteins in phospholipid bilayer nanodiscs." Methods Enzymol **464**: 211-31.
- Roberts, A. G., M. K. Bowman, et al. (2004). "The inhibitor DBMIB provides insight into the functional architecture of the Qo site in the cytochrome b6f complex." Biochemistry **43**(24): 7707-16.
- Roberts, P. G. and J. Hirst (2012). "The Deactive Form of Respiratory Complex I from Mammalian Mitochondria is a Na<sup>+</sup>/H<sup>+</sup> Antiporter." J Biol Chem.
- Rodriguez-Navarro, A. (2000). "Potassium transport in fungi and plants." Biochim Biophys Acta **1469**(1): 1-30.
- Rosenthal, H. E. (1967). "A graphic method for the determination and presentation of binding parameters in a complex system." Anal Biochem **20**(3): 525-32.
- Rost, B., R. Casadio, et al. (1995). "Transmembrane helices predicted at 95% accuracy." Protein Sci **4**(3): 521-33.
- Sack, D. A., R. B. Sack, et al. (2004). "Cholera." Lancet **363**(9404): 223-33.
- Sanchez-Pedregal, V. M., M. Reese, et al. (2005). "The INPHARMA method: protein-mediated interligand NOEs for pharmacophore mapping." Angew Chem Int Ed Engl **44**(27): 4172-5.
- Sazanov, L. A. and P. Hinchliffe (2006). "Structure of the hydrophilic domain of respiratory complex I from *Thermus thermophilus*." Science **311**(5766): 1430-6.
- Scatchard, G. (1949). "The attractions of proteins for small molecules and ions." Annals of the New York Academy of Sciences **51**(4): 660-672.

- Schägger, H. and G. von Jagow (1987). "Tricine-sodium dodecyl sulfate-polyacrylamide gel electrophoresis for the separation of proteins in the range from 1 to 100 kDa." Anal Biochem **166**(2): 368-79.
- Schenk, B., J. S. Rush, et al. (2001). "An alternative cis-isoprenyltransferase activity in yeast that produces polyisoprenols with chain lengths similar to mammalian dolichols." Glycobiology **11**(1): 89-98.
- Schmidt, B., B. Hennig, et al. (1983). "Transport of the precursor to neurospora ATPase subunit 9 into yeast mitochondria. Implications on the diversity of the transport mechanism." J Biol Chem **258**(8): 4687-9.
- Schrödinger, LLC (2010). The PyMOL Molecular Graphics System, Version 1.3r1.
- Semeykina, A. L. and V. P. Skulachev (1990). "Submicromolar Ag<sup>+</sup> increases passive Na<sup>+</sup> permeability and inhibits the respiration-supported formation of Na<sup>+</sup> gradient in *Bacillus FTU* vesicles." FEBS Lett. **269**(1): 69-72.
- Sievers, F., A. Wilm, et al. (2011). "Fast, scalable generation of high-quality protein multiple sequence alignments using Clustal Omega." Mol Syst Biol **7**: 539.
- Sikorski, R. S. and P. Hieter (1989). "A system of shuttle vectors and yeast host strains designed for efficient manipulation of DNA in *Saccharomyces cerevisiae*." Genetics **122**(1): 19-27.
- Silver, S. (2003). "Bacterial silver resistance: molecular biology and uses and misuses of silver compounds." FEMS Microbiol Rev. **27**(2-3): 341-53.
- Simkovic, M. and F. E. Frerman (2004). "Alternative quinone substrates and inhibitors of human electron-transfer flavoprotein-ubiquinone oxidoreductase." Biochem J **378**(Pt 2): 633-40.
- Sistare, F. D. and R. C. Haynes, Jr. (1985). "The interaction between the cytosolic pyridine nucleotide redox potential and gluconeogenesis from lactate/pyruvate in isolated rat hepatocytes. Implications for investigations of hormone action." J Biol Chem **260**(23): 12748-53.
- Smith, P. K., R. I. Krohn, et al. (1985). "Measurement of protein using bicinchoninic acid." Anal Biochem **150**(1): 76-85.
- Sonnhammer, E. L., G. von Heijne, et al. (1998). "A hidden Markov model for predicting transmembrane helices in protein sequences." Proc Int Conf Intell Syst Mol Biol **6**: 175-82.
- Steffen, W., A. C. Gemperli, et al. (2010). "Organelle-specific expression of subunit ND5 of human complex I (NADH dehydrogenase) alters cation homeostasis in *Saccharomyces cerevisiae*." FEMS Yeast Res **10**(6): 648-59.
- Steuber, J. (2001). "The Na<sup>+</sup>-translocating NADH:quinone oxidoreductase (NDH I) from *Klebsiella pneumoniae* and *Escherichia coli*: implications for the mechanism of redox-driven cation translocation by complex I." J. Bioenerg. Biomembr. **33**: 179-185.
- Steuber, J. (2001). "Na<sup>+</sup> translocation by bacterial NADH:quinone oxidoreductases: an extension to the complex-I family of primary redox pumps." Biochim Biophys Acta **1505**(1): 45-56.
- Steuber, J. (2003). "The C-terminally truncated NuoL subunit (ND5 homologue) of the Na<sup>+</sup>-dependent complex I from *Escherichia coli* transports Na<sup>+</sup>." J Biol Chem **278**(29): 26817-22.
- Steuber, J., W. Krebs, et al. (1997). "The Na<sup>+</sup>-translocating NADH:ubiquinone oxidoreductase from *Vibrio alginolyticus*: redox states of the FAD prosthetic group and mechanism of Ag<sup>+</sup> inhibition." Eur. J. Biochem. **249**: 770-776.

- Steuber, J., C. Schmid, et al. (2000). "Na<sup>+</sup> translocation by complex I (NADH:quinone oxidoreductase) of *Escherichia coli*." Mol Microbiol **35**(2): 428-34.
- Stojanovski, D., A. J. Johnston, et al. (2003). "Import of nuclear-encoded proteins into mitochondria." Exp Physiol **88**(1): 57-64.
- Stolpe, S. and T. Friedrich (2004). "The *Escherichia coli* NADH:ubiquinone oxidoreductase (complex I) is a primary proton pump but may be capable of secondary sodium antiport." J Biol Chem **279**(18): 18377-83.
- Stuart, R. A. and W. Neupert (1996). "Topogenesis of inner membrane proteins of mitochondria." Trends Biochem Sci **21**(7): 261-7.
- Swartz, T. H., S. Ikewada, et al. (2005). "The Mrp system: a giant among monovalent cation/proton antiporters?" Extremophiles **9**(5): 345-54.
- Sychrova, H. (2004). "Yeast as a model organism to study transport and homeostasis of alkali metal cations." Physiol Res **53 Suppl 1**: S91-8.
- Takada, Y., N. Fukunaga, et al. (1988). "Respiration-dependent proton and sodium pumps in a psychrophilic bacterium, *Vibrio* sp. strain ABE-1 " Plant Cell Physiol. **29**(2): 207-214.
- Tao, M., M. S. Casutt, et al. (2008). "Oxidant-induced formation of a neutral flavosemiquinone in the Na<sup>+</sup>-translocating NADH:Quinone oxidoreductase (Na<sup>+</sup>-NQR) from *Vibrio cholerae*." Biochim Biophys Acta **1777**(7-8): 696-702.
- Tao, M., G. Fritz, et al. (2008). "The Na<sup>+</sup>-translocating NADH:quinone oxidoreductase (Na<sup>+</sup>-NQR) from *Vibrio cholerae* enhances insertion of FeS in overproduced NqrF subunit." J Inorg Biochem **102**(5-6): 1366-72.
- Tao, M., K. Türk, et al. (2006). "Crystallization of the NADH-oxidizing domain of the Na<sup>+</sup>-translocating NADH:ubiquinone oxidoreductase from *Vibrio cholerae*." Acta Crystallogr Sect F Struct Biol Cryst Commun **62**(Pt 2): 110-2.
- Tarr, J. B. and J. Arditti (1982). "Niacin Biosynthesis in Seedlings of *Zea mays*." Plant Physiol **69**(3): 553-6.
- Taylor, R. W., A. A. Morris, et al. (2002). "Leigh disease associated with a novel mitochondrial DNA ND5 mutation." Eur J Hum Genet **10**(2): 141-4.
- Thompson, J. D., D. G. Higgins, et al. (1994). "CLUSTAL W: improving the sensitivity of progressive multiple sequence alignment through sequence weighting, position-specific gap penalties and weight matrix choice." Nucleic Acids Res **22**(22): 4673-80.
- Thorburn, D. R., C. Sugiana, et al. (2004). "Biochemical and molecular diagnosis of mitochondrial respiratory chain disorders." Biochim Biophys Acta **1659**(2-3): 121-8.
- Tokuda, H. and K. Kogure (1989). "Generalized distribution and common properties of Na<sup>+</sup>-dependent NADH:quinone oxidoreductases in gram-negative marine bacteria." J. Gen. Microbiol. **135**: 703-709.
- Tokuda, H. and T. Unemoto (1981). "A Respiration-dependent Primary Sodium Extrusion System Functioning at Alkaline pH in the Marine Bacterium *Vibrio alginolyticus*." Biochem. Biophys. Res. Commun. **102**(1): 265-271.
- Tokuda, H. and T. Unemoto (1983). "Growth of a marine *Vibrio alginolyticus* and moderately halophilic *V. costicola* becomes uncoupler resistant when the respiration-dependent Na<sup>+</sup> pump functions." J. Bacteriol. **156**: 636-643.
- Tokuda, H. and T. Unemoto (1984). "Na<sup>+</sup> is translocated at NADH:quinone oxidoreductase segment in the respiratory chain of *Vibrio alginolyticus*." J. Biol. Chem. **259**: 7785-7790.
- Tran, Q. H., J. Bongaerts, et al. (1997). "Requirement for the proton-pumping NADH dehydrogenase I of *Escherichia coli* in respiration of NADH to fumarate and its bioenergetic implication." Eur. J. Biochem. **244**: 155-160.

- Treberg, J. R. and M. D. Brand (2011). "A model of the proton translocation mechanism of complex I." J Biol Chem **286**(20): 17579-84.
- Tsuchiya, T. and S. Shinoda (1985). "Respiration-driven Na<sup>+</sup> pump and Na<sup>+</sup> circulation in *Vibrio parahaemolyticus*." J. Bacteriol. **162**: 794-798.
- Türk, K., A. Puhar, et al. (2004). "NADH oxidation by the Na<sup>+</sup>-translocating NADH:quinone oxidoreductase from *Vibrio cholerae*: functional role of the NqrF subunit." J Biol Chem **279**(20): 21349-55.
- Tusnady, G. E. and I. Simon (2001). "Topology of membrane proteins." J Chem Inf Comput Sci **41**(2): 364-8.
- Uden, G., S. Achenbach, et al. (2002). "Control of FNR function of *Escherichia coli* by O<sub>2</sub> and reducing conditions." J. Microbiol. Biotechnol. **4**: 263-268.
- Unemoto, T., A. Akagawa, et al. (1992). "Distribution of Na<sup>+</sup>-dependent respiration and a respiration-driven electrogenic Na<sup>+</sup> pump in moderately halophilic bacteria." J. Gen. Microbiol. **138**: 1999-2005.
- Unemoto, T., M. Hayashi, et al. (1977). "Na<sup>+</sup>-dependent activation of NADH oxidase in membrane fractions from halophilic *Vibrio alginolyticus* and *V. costicola*." J. Biochem. **82**: 1389-1395.
- Unemoto, T., T. Ogura, et al. (1993). "Modifications by Na<sup>+</sup> and K<sup>+</sup>, and the site of Ag<sup>+</sup> inhibition in the Na<sup>+</sup>-translocating NADH-quinone reductase from a marine *Vibrio alginolyticus*." Biochim. Biophys. Acta **1183**: 201-205.
- Ushakova, A. V., V. G. Grivennikova, et al. (1999). "Triton X-100 as a specific inhibitor of the mammalian NADH-ubiquinone oxidoreductase (complex I)." Biochim. Biophys. Acta **1409**: 143-153.
- Vagin, A. and A. Teplyakov (2010). "Molecular replacement with MOLREP." Acta Crystallogr D Biol Crystallogr **66**(Pt 1): 22-5.
- Vgenopoulou, I., A. C. Gemperli, et al. (2006). "Specific modification of a Na<sup>+</sup> binding site in NADH:quinone oxidoreductase from *Klebsiella pneumoniae* with dicyclohexylcarbodiimide." J Bacteriol **188**(9): 3264-72.
- Voet, D. and J. G. Voet (2004). Biochemistry 3rd Edition. New York, John Wiley & Sons, Inc.
- Wackwitz, B., J. Bongaerts, et al. (1999). "Growth phase-dependent regulation of nuoA-N expression in *Escherichia coli* K-12 by the Fis protein: upstream binding sites and bioenergetic significance." Mol Gen Genet **262**(4-5): 876-83.
- Walker, J. E. (1992). "The NADH:ubiquinone oxidoreductase (complex I) of respiratory chains." Q Rev Biophys **25**(3): 253-324.
- Wallace, D. C. (1999). "Mitochondrial diseases in man and mouse." Science **283**(5407): 1482-8.
- Wallace, D. C. (2008). "Mitochondria as chi." Genetics **179**(2): 727-35.
- Weast, R. C. (1981). CRC Handbook of Chemistry and Physics. Boca Raton, CRC Press.
- Welihinda, A. A., R. J. Trumbly, et al. (1993). "On the regulation of Na<sup>+</sup>/H<sup>+</sup> and K<sup>+</sup>/H<sup>+</sup> antiport in yeast mitochondria: evidence for the absence of an Na<sup>+</sup>-selective Na<sup>+</sup>/H<sup>+</sup> antiporter." Biochim Biophys Acta **1144**(3): 367-73.
- White, H. B. and A. H. Merrill (1988). "Riboflavin-binding proteins." Ann. Rev. Nutr. **8**: 279-299.
- Wickerham, L. J. and K. A. Burton (1948). "Carbon Assimilation Tests for the Classification of Yeasts." J Bacteriol **56**(3): 363-71.
- Wickerham, L. J., M. H. Flickinger, et al. (1946). "A Modification of Henrici's Vegetable-Juice Sporulation Medium for Yeasts." J Bacteriol **52**(5): 611-2.

- Wierenga, R. K., P. Terpstra, et al. (1986). "Prediction of the occurrence of the ADP-binding beta alpha beta-fold in proteins, using an amino acid sequence fingerprint." J. Mol. Biol. **187**(1): 101-7.
- Wikstrom, M. (1984). "Two protons are pumped from the mitochondrial matrix per electron transferred between NADH and ubiquinone." FEBS Lett **169**(2): 300-4.
- Wilkinson, A., J. Day, et al. (2001). "Bacterial DNA ligases." Mol Microbiol **40**(6): 1241-8.
- Williamson, D. H., P. Lund, et al. (1967). "The redox state of free nicotinamide-adenine dinucleotide in the cytoplasm and mitochondria of rat liver." Biochem J **103**(2): 514-27.
- Wilson, D. F., M. Erecinska, et al. (1974). "Thermodynamic relationships in mitochondrial oxidative phosphorylation." Annu Rev Biophys Bioeng **3**(0): 203-30.
- Winn, M. D., C. C. Ballard, et al. (2011). "Overview of the CCP4 suite and current developments." Acta Crystallographica Section D **67**(4): 235-242.
- Wissenbach, U., D. Ternes, et al. (1992). "An *Escherichia coli* mutant containing only demethylmenaquinone, but no menaquinone: effects on fumarate, dimethylsulfoxide, trimethylamine N-oxide and nitrate respiration." Arch Microbiol **158**(1): 68-73.
- Wright, W. B. and G. S. D. King (1954). "The crystal structure of nicotinamide." Acta Crystallographica **7**(3): 283-288.
- Yadava, N., P. Potluri, et al. (2008). "Investigations of the potential effects of phosphorylation of the MWFE and ESSS subunits on complex I activity and assembly." Int J Biochem Cell Biol **40**(3): 447-60.
- Yaffe, M. P. and G. Schatz (1984). "Two nuclear mutations that block mitochondrial protein import in yeast." Proc Natl Acad Sci U S A **81**(15): 4819-23.
- Yagi, T. (1987). "Inhibition of NADH-ubiquinone reductase activity by *N,N'*-dicyclohexylcarbodiimide and correlation of this inhibition with the occurrence of energy-coupling site 1 in various organisms." Biochemistry **26**: 2822-2828.
- Yagi, T. (1991). "Bacterial NADH-quinone oxidoreductases." J. Bioenerg. Biomembr. **23**: 211-225.
- Yagi, T. and A. Matsuno-Yagi (2003). "The proton-translocating NADH-quinone oxidoreductase in the respiratory chain: the secret unlocked." Biochemistry **42**(8): 2266-74.
- Yagi, T., B. B. Seo, et al. (2001). "NADH dehydrogenases: from basic science to biomedicine." J. Bioenerg. Biomembr. **33**: 233-242.
- Yagi, T., T. Yano, et al. (1998). "Prokaryotic complex I (NDH-I), an overview." Biochim. Biophys. Acta **1364**: 125-133.
- Yamada, K., N. Hara, et al. (2006). "The simultaneous measurement of nicotinamide adenine dinucleotide and related compounds by liquid chromatography/electrospray ionization tandem mass spectrometry." Anal Biochem **352**(2): 282-5.
- Yano, T., L. S. Li, et al. (2006). "Steady-state kinetics and inhibitory action of antitubercular phenothiazines on *mycobacterium tuberculosis* type-II NADH-menaquinone oxidoreductase (NDH-2)." J. Biol. Chem. **281**(17): 11456-63.
- Yano, T., S. Magnitsky, et al. (2000). "Characterization of the complex I-associated ubisemiquinone species: toward the understanding of their functional roles in the electron/proton transfer reaction." Biochim. Biophys. Acta **1459**: 299-304.
- Yoshida, A., K. Imoto, et al. (1992). "An electric double-layer capacitor with high capacitance and low resistance." IEEE Transactions on Components, Hybrids, and Manufacturing Technology **15**(1): 133 - 138.



- Yoshikawa, K., Y. Nakayama, et al. (1999). "Korormicin, an antibiotic specific for gram-negative marine bacteria, strongly inhibits the respiratory chain-linked Na<sup>+</sup>-translocating NADH: quinone reductase from the marine *Vibrio alginolyticus*." J Antibiot (Tokyo) **52**(2): 182-5.
- Young, L. and C. B. Post (1996). "Catalysis by entropic guidance from enzymes." Biochemistry **35**(48): 15129-33.
- Zhadanov, S. I., E. Y. Grechanina, et al. (2007). "Fatal manifestation of a de novo ND5 mutation: Insights into the pathogenetic mechanisms of mtDNA ND5 gene defects." Mitochondrion **7**(4): 260-6.
- Zhou, B. P., D. A. Lewis, et al. (1995). "Mutagenesis at a highly conserved tyrosine in monoamine oxidase B affects FAD incorporation and catalytic activity." Biochemistry **34**(29): 9526-31.
- Zhou, Z. and R. P. Swenson (1995). "Electrostatic effects of surface acidic amino acid residues on the oxidation-reduction potentials of the flavodoxin from *Desulfovibrio vulgaris* (Hildenborough)." Biochemistry **34**(10): 3183-92.
- Zickermann, V., M. Bostina, et al. (2003). "Functional implications from an unexpected position of the 49-kDa subunit of NADH:ubiquinone oxidoreductase." J Biol Chem **278**(31): 29072-8.
- Zickermann, V., S. Kerscher, et al. (2009). "Architecture of complex I and its implications for electron transfer and proton pumping." Biochim Biophys Acta **1787**(6): 574-83.
- Ziegler, M. (2000). "New functions of a long-known molecule. Emerging roles of NAD in cellular signaling." Eur J Biochem **267**(6): 1550-64.
- Ziegler, M. and M. Niere (2004). "NAD<sup>+</sup> surfaces again." Biochem J **382**(Pt 3): e5-6.

## Acknowledgements

My sincere thanks go to my advisor, Prof. Julia Fritz-Steuber, who guided and supported me throughout my time in her group. Her scientific rigor and infectious optimism have been like a beacon to me.

Many thanks go to the collaboration partners of the research project P-LS-Meth/4 of the Baden-Württemberg Stiftung, Dr. Günter Fritz, Dr. Heiko Möller, Dr. Christiane Schaffitzel and to all of their co-workers on the project, for many exciting meetings, fruitful discussions and the resulting friendships.

Thank goes to Dr. Jens Pfannstiel and the Life Science Center of the University of Hohenheim for their support with mass spectrometric analysis and helpful discussion.

Dr. Urs Ziegler, Center for Microscopy and Image Analysis, University of Zürich, is gratefully acknowledged for his support with fluorescence microscopy and for providing us with the HCS CellMask stain.

I am very thankful to Dr. Marco Casutt, who introduced me to the work with NQR's. Thank you for all the good times, you'll always be the "Senior PhD" to me.

A huge thanks goes to all current and former members of the Steuber lab for their support and the unique atmosphere. In particular, I want to thank Hanna Grönheim, Petra Halang, Valentin Muras and Yasmin Kolar for all the invigorating coffee breaks, balcony- and other "meetings". Also acknowledged are the co-workers at the Department of Biochemistry in Zürich and at the Institute of Microbiology in Hohenheim for the great time.

Of course, I can't and won't omit Dr. Thomas Vorburger. Without him and Severin Wendelspiess, operation H.O.H. would not have been a success. Your friendship is invaluable to me.

I would like to thank Bea Kraft who helped me navigate the dire straits of my thesis and made Stuttgart a safe haven for me.

A very special thanks goes to my family, Ewa, Andreas and Astrid Steffen. They have always supported me and believed in me. I very much relish the visits at home.

## Financial Disclosure

The work featured in chapter 2 was supported by grants from the Swiss National Science Foundation (grant PP0033-118994), the Swiss Foundation for Research on Muscle Disease and Parkinson Schweiz. The work featured in chapter 3 was supported by contract research project P-LS-Meth/4 of the Baden-Württemberg Stiftung and by grant FR1321/3-1 from the Deutsche Forschungsgemeinschaft.

## *Curriculum vitae*

---

Surname	Steffen
First names	Wojtek Roman
Date and place of birth	23.05.1983 in Schlieren, Switzerland
Citizenship	Zurich, Switzerland
Nationalities	Swiss / Polish

### **Scientific Education**

April 2008 - Nov. 2012	Dissertation 'Structure and Function of Catalytic Subunits of Electrogenic NADH:Quinone Oxidoreductases' at the University of Zurich, since Oct. 2009 at the University of Hohenheim, Stuttgart, Germany. Completion of the degree of Dr. rer. nat. on the 15th of March 2013.
March 2008	Master of Science in Biochemistry, Chemistry/Biophysics track, at the Department of Biochemistry, University of Zurich. Degree 5.4 (German equivalent: 1.6).
Oct. 2002	Study of Chemistry and Biochemistry at the University of Zurich, Switzerland.

### **Employment**

Oct. 2009 - Nov. 2012	Employment in the group of Prof. Julia Fritz-Steuber, Department of Microbiology, University of Hohenheim.
Oct. 2009	Move to the Department of Microbiology, University of Hohenheim. Establishment of a new work group (head: Prof. Julia Fritz-Steuber).
April 2008 - Sep. 2009	Employment in the group of Prof. Julia Fritz-Steuber, Department of Biochemistry, University of Zurich.
March 2007 - Jan. 2008	Co-assistant at the practical course in Biochemistry for medical students, University of Zurich.
Aug. - Oct. 2005	Temporary employment at the cantonal department for consumer protection in Aarau, Switzerland.